Design, Fabrication, and Characterization of Flexible Electrodes for Recording Brain Electrical Activity

By

Olatoundji George GNONHOUE

MANUSCRIPT-BASED THESIS PRESENTED TO ÉCOLE DE TECHNOLOGIE SUPÉRIEURE IN PARTIAL FULFILLMENT FOR THE DEGREE OF DOCTOR OF PHILOSOPHY
Ph.D.

MONTREAL, APRIL 13, 2026

ÉCOLE DE TECHNOLOGIE SUPÉRIEURE
UNIVERSITÉ DU QUÉBEC

Olatoundji George GNONHOUE, 2026



The Creative Commons license allows readers to download this work and share it with others as long as the author is credited. The content of this work can't be modified in any way or used commercially.

BOARD OF EXAMINERS
THIS THESIS HAS BEEN EVALUATED
BY THE FOLLOWING BOARD OF EXAMINERS

Prof. Ilyass Tabiai, Thesis Supervisor
Department of Mechanical Engineering at École de technologie supérieure

Prof. Éric David, Thesis Co-supervisor
Department of Mechanical Engineering at École de technologie supérieure

Prof. Simon Joncas, President of the Board of Examiners
Department of Systems Engineering at École de technologie supérieure

Prof. Jérémie Voix, Member of the jury
Department of Mechanical Engineering at École de technologie supérieure

Prof. Nicole Demarquette, Member of the jury
Department of Mechanical Engineering at École de technologie supérieure

Prof. Jason Robert Tavers, External Evaluator
Department of Chemical Engineering at Polytechnique Montreal

THIS THESIS WAS PRESENTED AND DEFENDED ON FEBRUARY 23, 2026

IN THE PRESENCE OF A BOARD OF EXAMINERS AND PUBLIC

AT ÉCOLE DE TECHNOLOGIE SUPÉRIEURE

ACKNOWLEDGMENT

I would like to express my gratitude to my PhD thesis supervisor, Professor Ilyass Tabiai, for his support, guidance, and encouragement throughout my PhD journey. I extend my sincere thanks to my co-supervisor, Professor Eric David, and my co-advisor, Professor Jérémie Voix, for their continuous support and constructive feedback, which have been invaluable to my research.

I would also like to thank the members of the jury, Prof. Simon Joncas, Prof. Nicole Demarquette from École de technologie supérieure, and Prof. Jason Robert Tavares from Polytechnique Montreal, for agreeing to evaluate this work during the defense.

Certainly, I am also thankful to all the teachers and professors I had in my life. I would like to extend my gratitude to the technicians, Mohammad, Nabil, Xavier, Valentin, Radu and all the staff working in the Mechanical Engineering Department of ÉTS for their practical help whenever needed.

I am grateful to the following organizations for their support, which has enabled me to continue this work: Arbour Foundation, NSERC Alliance, MITACS and ÉTS-EERS Industrial Research Chair in In-Ear Technologies (CRITIAS), sponsored by EERS Global Technologies Inc.

I am profoundly grateful to Chris Gayee Wong Cho for her understanding, patience, and support whose presence brought immense joy and motivation to my life during this challenging journey. My sincerest appreciation goes to my parents, whose prayers and moral support have been a constant source of strength for me.

I also wish to acknowledge the supporting professionals and facilities at École de technologie supérieure for providing the necessary resources and a conducive environment for my research.

To all of you, thank you.

In memory of my sister Gloria Gnonhoue

Conception, fabrication et caractérisation d'électrodes flexibles pour l'enregistrement de l'activité électrique cérébrale

Olatoundji George GNONHOUE

RÉSUMÉ

L'électroencéphalographie (EEG) est une technique essentielle pour l'analyse de l'activité cérébrale, largement utilisée dans le diagnostic médical, les interfaces cerveau-machine et la neuroergonomie. Cependant, les électrodes conventionnelles, dites « humides », qu'elles soient rigides ou semi-flexibles, présentent des limitations en termes de confort, d'adaptabilité morphologique et de stabilité du signal. Cette thèse vise à concevoir, fabriquer et caractériser de nouvelles électrodes flexibles haute performance, optimisant à la fois la qualité des enregistrements EEG, la flexibilité, le confort et l'ergonomie.

Dans cette étude, plusieurs composites polymères conducteurs ont été explorés, notamment des matériaux à base de SEBS, SEBS-MA et EVA, intégrant des nanotubes de carbone et du noir de carbone. Ces matériaux ont été sélectionnés et optimisés afin de combiner conductivité électrique, flexibilité et stabilité mécanique. La fabrication des électrodes en configuration multibroches a été réalisée par dissolution chimique dans un solvant, suivie d'une compression mécanique, garantissant une intégration optimale à l'interface cuir-chevelu.

La caractérisation des électrodes s'est articulée autour de trois axes principaux :

- ❖ Propriétés mécaniques : Évaluation du module de stockage en fonction de la température afin de déterminer la souplesse et la résistance des composites.
- ❖ Propriétés électriques : Analyse de la conductivité et de l'impédance électrochimique pour optimiser la qualité du contact avec la peau.
- ❖ Performance EEG : Comparaison des signaux enregistrés avec ceux obtenus à l'aide d'électrodes flexibles commerciales afin d'évaluer la fidélité du signal.

Les résultats démontrent que les électrodes flexibles à base de SEBS-MA/8%wtCNT/2%wtCB constituent une alternative prometteuse aux électrodes classiques, offrant un équilibre optimal entre flexibilité et conductivité. De plus, l'analyse approfondie des signaux EEG met en évidence une meilleure flexibilité et une stabilité accrue du signal, notamment lors d'enregistrements prolongés.

Ces avancées ouvrent de nouvelles perspectives pour l'EEG portable, en particulier dans le cadre des applications de santé numérique et du suivi individualisé, en permettant le développement d'électrodes flexibles adaptées à l'enregistrement continu et personnalisé de l'activité cérébrale. Elles constituent également un levier important pour les interfaces cerveau–machine, en répondant aux exigences croissantes des neurosciences appliquées.

Mots-clés : Électroencéphalographie, Électrodes flexibles, Composites polymères conducteurs

Design, fabrication, and characterization of flexible electrodes for recording brain electrical activity

Olatoundji George GNONHOUE

ABSTRACT

Electroencephalography (EEG) is an essential technique for analyzing brain activity, widely used in medical diagnostics, brain-computer interfaces, and neuroergonomics. However, conventional electrodes, often wet, rigid or semi-flexible, have limitations in terms of comfort, morphological adaptability, and signal stability. This thesis aims to design, fabricate, and characterize new high-performance flexible electrodes that optimize EEG signal quality, flexibility, comfort, and ergonomics

In this study, several conductive polymer composites were explored, including SEBS, SEBS-MA, and EVA-based materials incorporating carbon nanotubes and carbon black. These materials were selected and optimized to combine electrical conductivity, flexibility, and mechanical stability. The fabrication of the multi-branched electrode configuration was carried out through chemical dissolution in a solvent, followed by mechanical compression, ensuring optimal integration at the scalp interface.

The characterization of the electrodes was structured around three main aspects:

- Mechanical properties: Evaluation of the storage modulus as a function of temperature to assess the flexibility and resistance of the composites.
- Electrical properties: Analysis of conductivity and electrochemical impedance to optimize the quality of skin contact.

❖ EEG performance: Comparison of recorded signals with those obtained using commercial flexible electrodes to evaluate signal fidelity.

The results demonstrate that SEBS-MA/8%wtCNT/2%wtCB-based flexible electrodes offer a promising alternative to conventional electrodes, providing an optimal balance between flexibility and conductivity. Furthermore, an in-depth analysis of EEG signals highlights improved flexibility and enhanced signal stability, particularly during prolonged recordings.

These advances open new perspectives for portable EEG, particularly in the context of digital health applications and individualized monitoring, by enabling the development of flexible electrodes suited for the continuous and personalized recording of brain activity. They also represent an important driver for brain–computer interfaces, by meeting the growing demands of applied neuroscience.

Keywords : Electroencephalography, Flexible electrodes, Conductive polymer composites

TABLE DES MATIÈRES

Page

INTRODUCTION 1

CHAPITRE 1 TECHNOLOGIES AND MATERIALS USED FOR THE MANUFACTURE OF DRY ELECTRODES 11
1.1 Introduction 11
1.2 Dry electrode technologies for EEG 13
1.2.1 Microneedle electrodes 13
1.2.2 Surface electrodes 15
1.2.3 Capacitive electrodes 16
1.3 Materials used for the manufacture of flexible dry electrodes 17
1.4 Applications of Flexible Dry Electrodes 22
1.5 Current challenges and future perspectives of flexible dry electrodes 23
1.6 Conclusion 25

CHAPITRE 2 PROPERTIES OF POLYMER MATERIALS FOR ELECTROENCEPHALOGRAPHY 27
2.1 Thermal properties 28
2.1.1 Glass transition temperature 28
2.1.2 Degradation temperature 29
2.1.3 block copolymers 30
2.1.4 Morphology of block copolymers and localization of conductive fillers 31
2.2 Mechanical properties 34
2.3 Electrical property 37
2.3.1 Dielectric behavior 37
2.3.1.1 Dielectric coefficient 37
2.3.1.2 Polarization Mechanisms 40
2.3.1.3 Dielectric dissipation factor 48
2.3.2 Electrical conductivity 50
2.3.3 Percolation theory 51
2.3.4 Skin/electrode contact impedance 52
2.4 Dispersion and Distribution 55
2.5 Electrophysiological activity: EEG and EMG signals 56
2.5.1 Brain activity and EEG frequency bands 56
2.5.2 EMG signals 57
2.5.3 Comparison of the characteristics of EEG and EMG signals 57
2.6 The concept of comfort in EEG electrodes 58
2.7 Summary of the literature review 60

CHAPITRE 3 FLEXIBLE DRY ELECTRODES BASED ON STYRENE-ETHYLENE-BUTYLENE-STYRENE/CARBON BLACK AND ETHYLENE-VINYL

ACETATE/CARBON BLACK FOR ELECTROENCEPHALOGRAPHY: ELECTRICAL, THERMAL AND MECHANICAL PROPERTIES 61
3.1 Introduction 62
3.2 Experimental testing 65
3.2.1 Materials 65
3.2.2 Preparation of SEBS/CB and EVA/CB Composites 66
3.2.2.1 Polymer dissolution 67
3.2.2.2 Filler incorporation 67
3.2.2.3 Solvent evaporation and film formation 67
3.3 Fabrication of Surface Multipin EEG Electrodes 68
3.4 Optimization and Reproducibility 69
3.5 Characterizations 69
3.5.1 Electrical characterization 69
3.5.2 Structural characterization 69
3.5.3 Thermal Characterization 70
3.5.4 Mechanical characterization 70
3.6 Experimental validation in vivo 71
3.7 Participants 72
3.8 Results 73
3.8.1 Electrical, structural and mechanical properties 73
3.8.1.1 Electrical properties 73
3.8.1.2 Structural properties 77
3.8.1.3 Thermal properties 78
3.8.1.4 Mechanical properties 79
3.9 Experimental validation in vivo 82
3.10 Discussion 86
3.11 Conclusion 92
3.12 Author credit statement 93
3.13 Author Declarations 93
3.14 Acknowledgements 93

CHAPITRE 4 ELECTRICAL AND THERMO-MECHANICAL PROPERTIES OF STYRENE-ETHYLENE-BUTYLENE-STYRENE/CARBON NANOTUBE AND STYRENE-ETHYLENE-BUTYLENE-STYRENE/CARBON BLACK MULTIPIN ELECTRODES FOR ELECTROENCEPHALOGRAPHY 95
4.1 Introduction 96
4.2 Materials and Methods 102
4.2.1 Materials 102
4.2.2 Electrode Preparation 102
4.2.3 Methods 104
4.2.3.1 Electrical Characterization 104
4.2.3.2 Structural Characterization 105
4.2.3.3 Thermo-Mechanical Characterization 105
4.2.3.4 Preliminary In Vivo Validation 106

4.2.3.5 Participants 108
4.3 Results 108
4.3.1 Electrical Properties 108
4.3.2 Structural Properties 112
4.3.3 Thermo-Mechanical Properties 113
4.3.4 In Vivo Validation 116
4.4 Discussion 119
4.5 Conclusion 124
4.6 Author credit statement 124
4.7 Author Declarations 125
4.8 Acknowledgements 125

CHAPITRE 5 HYBRID FLEXIBLE DRY ELECTRODES FOR ELECTROENCEPHALOGRAPHY: ELECTRICAL AND THERMO-MECHANICAL PROPERTIES 127
5.1 Introduction 128
5.2 Materials and Methods 131
5.2.1 Materials 131
5.2.2 Composite Preparation 131
5.2.3 Electrode Geometry 132
5.2.4 Composite Formulations 133
5.3 Characterization 134
5.3.1 Electrical Characterization 134
5.3.2 Structural Characterization 135
5.3.3 Thermo-Mechanical Characterization 135
5.3.4 Preliminary In Vivo Validation 136
5.3.4.1 Participants 138
5.4 Results 138
5.4.1 Electrical Properties 138
5.4.1.1 Frequency response and filler-morphology effects 139
5.4.2 Structural Properties 151
5.4.3 Thermo-Mechanical Properties 152
5.4.4 Dynamic Mechanical Thermal Analysis (DMTA) 156
5.4.5 Preliminary In Vivo Validation 158
5.5 Discussion 160
5.6 Conclusion 163
5.7 Author credit statement 164
5.8 Author Declarations 165
5.9 Acknowledgements 165

CHAPITRE 6 EXPLORATORY WORK 167
6.1 Influence of interphase thickness (matrix/reinforcement) on the percolation threshold in EVA/CB and SEBS/CB nanocomposites 168
6.1.1 Objective 168
6.1.2 Methodology 169

6.1.3 Results 169
6.1.3.1 Conductivity models as a function of reinforcement ratio and interphase 169
6.1.3.2 Characterization of dispersion and agglomeration 171
6.1.4 Conclusion 172
6.2 Experimental setup and EEG signal acquisition 173
6.2.1 Objective 173
6.2.2 Methodology 173
6.2.2.1 Laboratory designed EEG acquisition system 173
6.2.2.2 Commercial EEG Acquisition System 176
6.2.3 Résultats 180
6.2.4 Conclusion 181
6.3 Work on the artificial ear for the evaluation of EEG electrodes 182
6.3.1 Objective 182
6.3.2 Methodology 183
6.3.2.1 PDMS (RTV/615) and carbon black 184
6.3.2.2 Carbon fiber reinforced PDMS (RTV 615) 185
6.3.3 Results 187
6.3.3.1 PDMS (RTV/615) and carbon black 187
6.3.3.2 Carbon fiber reinforced PDMS (RTV 615) 194
6.3.3.3 Percolation study of RTV615/carbon fiber composites 196
6.3.4 Conclusion 200
6.4 Electrodes manufactured by 3D printing 201
6.4.1 Objective 201
6.4.2 Methodology 201
6.4.4 Conclusion 208
6.5 General conclusion 209
RECOMMENDATIONS 211
APPENDIX I RESEARCH ETHICS COMMITTEE APPROVAL 215

BIBLIOGRAPHY 219

LISTE DES TABLEAUX

Page

Table 3-1 SEBS/CB and EVA/CB nanocomposites at different carbon nanoparticle weight fractions.....67

Table 3-2 Comparison with relevant work in the application area.....85

Table 4-1 SEBS/CNT and SEBS/CB nanocomposites at different carbon nanoparticle weight fractions.....104

Table 5-1 Composition of styrene-ethylene-butylene-styrene (SEBS) nanocomposites with different weight fractions (%wt) of carbon nanotubes (CNT) and carbon black (CB).....133

Table 5-2 Composition of maleic anhydride-grafted styrene-ethylene-butylene-styrene (SEBS-MA) nanocomposites with different weight fractions of carbon nanotubes (CNT) and carbon black (CB).....134

Table 5-3 Electrical conductivity of SEBS and SEBS-MA composites with different CNT and CB loadings (see Figure 4.4 and 4.5).....141

Table 5-4 Electrical conductivity of SEBS composites (10 wt% reinforcement) with different CNT/CB ratios.....144

Table 5-5 Electrical conductivity and frequency-dependent behavior of SEBS composites with 20 wt% CNT/CB reinforcement (see Figure 4.9).....147

Table 5-6 Comparison of electrical conductivity between SEBS and SEBS-MA composites across different CNT/CB loadings (corresponding to Figure 4.10).....149

Table 5-7 Comparison of storage modulus (*E′*) for SEBS and SEBS-MA composites (24–36 °C, 1 Hz).....156

Table 6-1 Dispersion (D) and agglomeration (A) for SEBS-CB and EVA-CB composites.172

Table 6-2 Mechanical blending (RTV615/20%CB).....190

Table 6-3 Mechanical blend (RTV615/25%CB).....191

Table 6-4 Sonication dispersion of RTV/615 and carbon black (RTV615/20%CB).....193

Table 6-5 Composite made with RTV615/8wt%CF.....196

Table 6-6 Artificial ear made with RTV615/3%wtCF 198

Table 6-7 Artificial ear made with 3.5wt%CF.....198

Table 6-8 Artificial ear made with 4wt%CF.....199

Table 6-9 SEBS-MA parameters on the filament maker.....207

LISTE DES FIGURES

Page

Figure 2.1 : Schematic representations of different block copolymer architectures: (a) linear diblock copolymer AB, (b) linear triblock copolymer ABA, (c) linear triblock copolymer ABC, (d) star diblock copolymer AB , (e) branched diblock copolymer AB and (f) star triblock copolymer ABC.....31

Figure 2.2 : Circuit for measuring the capacitance of a capacitor 38

Figure 2.3: Illustration of the polarization charges in a capacitor: a) configuration without dielectric, b) configuration with a dielectric material between the plates .39

Figure 2.4 : Electric dipole.....41

Figure 2.5 Polarization process.....43

Figure 2.6: Equivalent circuit used to model losses in a dielectric material.....48

Figure 3.1. Schematic overview of the fabrication process for flexible multipin dry electrodes. The method includes (i) dissolving the SEBS or EVA polymer in toluene, (ii) dispersing conductive fillers (CB) to create a uniform suspension, (iii) evaporating the solvent to form composite films, and (iv) using compression molding to shape the films into multipin electrode structures.....66

Figure 3.2. Ultracortex "Mark IV" EEG headset used to install the electrodes on the head ...72

Figure 3.3. Electrodes installed in the system for the acquisition of electrical signals from the brain 72

Figure 3.4. Real part of the complex conductivity as a function of frequency of (a) SEBS/CB and (b) EVA/CB 74

Figure 3.5**.** Electrical conductivity as a function of mass fraction.....75

Figure 3.6. Micrograph of both electrodes: a) EVA/20wt%CB and b) SEBS/20%wtCB.....77

Figure 3.7. Differential scanning calorimetry (DSC) thermogram of EVA/20 wt% CB composite. The second heating (blue) and cooling (green) curves display a glass transition around −30 °C, a crystallization peak near 55–60 °C, and a melting endotherm at approximately 95–100 °C.....78

Figure 3.8**.** Differential scanning calorimetry (DSC) thermogram of the SEBS/20 wt% CB composite. The curve shows a glass transition of the ethylene–butylene

(EB) phase near −50 °C, a weak transition of the polystyrene domains at 90–100 °C 79

Figure 3.9. Stress-strain behavior of SEBS/20wt%CB and EVA/20wt%CB under compression tests 80

Figure 3.10. EEG signals of SEBS/20wt%CB, EVA/20wt%CB and commercial electrodes.83

Figure 4.1. Ultracortex “Mark IV” EEG headset for electrode placement.....107

Figure 4.2. EEG electrode placement and signal acquisition using the 10-20 system 107

Figure 4.3. Real part of the complex conductivity as a function of frequency of 110

Figure 4.4. Electrical conductivity of styrene-ethylene-butylene-styrene (SEBS) composites as a function of carbon nanotube (CNT) and carbon black (CB) filler loading (wt%).....111

Figure 4.5. Scanning electron microscopy (SEM) micrograph of a: (a) SEBS/16wt%CNT composite and (b) SEBS/20wt%CB composite.....113

Figure 4.6. TGA thermograms of SEBS/16wt%CNT and SEBS/20wt%CB 114

Figure 4.7. DMTA thermograms of polystyrene-block-poly(ethylene butylene)-block polystyrene (SEBS) polymer, SEBS/carbon nanotube (CNT), and SEBS/carbon black (CB) composites 115

Figure 4.8. Time-domain EEG recordings during eyes-open and blinking states, acquired using styrene-ethylene-butylene-styrene (SEBS)/20 wt% carbon black (CB) and styrene-ethylene-butylene-styrene (SEBS)/16 wt% carbon nanotube (CNT) composite electrodes, compared to a commercial flat dry flexible electrode.....118

Figure 4.9. Representative time-domain EEG signals during eyes-open and blinking states, demonstrating the performance of styrene-ethylene-butylene-styrene/20 wt% carbon black (SEBS/CB) composite, styrene-ethylene-butylene-styrene/16 wt% carbon nanotube (SEBS/CNT) composite, and commercial multipin electrodes. The signals illustrate the sensitivity and artifact rejection capabilities of each electrode type 119

Figure 5.1. Schematic overview of the fabrication process for flexible multipin dry electrodes. The method includes (i) dissolving the SEBS or SEBS-MA polymer in toluene, (ii) dispersing conductive fillers (CNT and CB) to create a uniform suspension, (iii) evaporating the solvent to form composite films, and (iv) using compression molding to shape the films into multipin electrode structures.....132

Figure 5.2. Schematic of electrode placement on the scalp using the Ultracortex “Mark IV” EEG headset 137

Figure 5.3. Photos of the electrodes used in this study. (Left) Commercial dry flexible electrode from OpenBCI (New York, NY, USA), used as a reference. (Right) Multipin flexible electrode developed in this work, side view. The built-in ruler shows the scale for electrode sizes 138

Figure 5.4. Electrical conductivities of SEBS/10 wt% CNT vs SEBS/10 wt% CB (σ′ vs frequency) 139

Figure 5.5. Electrical conductivity of SEBS/16 wt%CNT, SEBS/20 wt%CB, SEBS-MA/16 wt%CNT, and SEBS-MA/20 wt%CB (σ′ vs. frequency) 140

Figure 5.6. Hybrid SEBS composites with 5 wt% total reinforcement (σ′ vs. frequency) 142

Figure 5.7. Hybrid SEBS composites with 10 wt% total reinforcement showing CNT content-controlled transition to frequency-independent behavior (σ′ vs frequency) 143

Figure 5.8. Hybrid SEBS composites with 15 wt% total reinforcement (σ′ versus frequency) 145

Figure 5.9. Hybrid SEBS composites at 20 wt% total reinforcement (σ′ vs frequency) 146

Figure 5.10. Modifying with maleic anhydride reduces conductivity compared to SEBS at the same CNT/CB loadings (σ′ vs frequency), with no advantageous shift in percolation for these systems 148

Figure 5.11. Scanning electron micrograph of a multipin SEBS electrode reinforced with 10 wt% CNT and 5 wt% CB. Distinct regions are labeled: (i) particle-free SEBS matrix, (ii) CB+SEBS (agglomerated carbon black clusters), (iii) CNT+SEBS (fibrous nanotube networks), and (iv) CB+CNT+SEBS (mixed regions). The microstructure exhibits heterogeneous filler dispersion, with CNT networks forming conductive pathways and CB particles facilitating interfacial contacts, although some aggregation is observed 152

Figure 5.12. Thermogravimetric analysis (TGA) curves of SEBS and SEBS-MA composites reinforced with CNT and CB. All samples exhibit a single significant decomposition step, starting around 350–400 °C, which is typical of polymer matrix breakdown. The residual weights verify the intended CNT and CB loadings, with SEBS-MA/16 wt% CNT displaying a slightly higher residual percentage consistent with its reinforcement content 153

Figure 5.13. The differential scanning calorimetry (DSC) curve of pure SEBS exhibits a glass transition temperature (Tg) of approximately –60 °C, indicating its

elastomeric properties. No melting or crystallization transitions occur within the physiological range of 24–36 °C 155

Figure 5.14**.** Differential scanning calorimetry (DSC) curve of SEBS-MA. The glass transition temperature (Tg) occurs at about –60 °C, the same as in neat SEBS, confirming that maleic anhydride grafting does not alter the primary thermal transition of the matrix. No melting or crystallization transitions are observed within the physiological temperature range (24–36 °C) 155

Figure 5.15**.** Dynamic mechanical thermal analysis (DMTA) curves of SEBS and SEBS-MA composites (24–36 °C, 1 Hz). The storage modulus (E') increases with CNT and CB reinforcement, while SEBS-MA-based composites show a lower modulus than SEBS, confirming increased flexibility.....157

Figure 5.16**.** Time-domain EEG recording during eyes-open condition 159

Figure 5.17**.** Time-Domain EEG Recording During Eyes-Open with Blinking.....160

Figure 6.1: Comparison of the model by Mazaheri et al. . (Mazaheri et al., 2022) (in red) with the rewritten model (in blue and green).....171

Figure 6.2**:** EEG amplification circuit used for the first experimental tests. Adapted from Svard et al., (Svard et al., 2010).....174

Figure 6.3 : Circuit on the prototype board.....175

Figure 6.4: Experimental electrodes 176

Figure 6.5: OpenBCI Cyton board its main electronic components. 176

Figure 6.6**:** Configuration of electrode positions of the Ultracortex Mark IV helmet according to the international 10–20 system. 178

Figure 6.7**:** ThinkPulse active electrodes used as a reference. 178

Figure 6.8: Example of EEG signals visualized in OpenBCI GUI.....179

Figure 6.9: Ultracortex “Mark IV” EEG headset.....179

Figure 6.10: The complete Ultracortex EEG measurement system.....180

Figure 6.11: Signal measured at the output of the EEG amplification circuit observed on the oscilloscope.....181

Figure 6.12: Electrical properties of head tissues 183

Figure 6.13**:** Initial method decribed in the litterature 186

Figure 6.14: Modified procedure used in this work.....186

Figure 6.15: Real part of the complex conductivity as a function of frequency for RTV615/CB composites manufactured according to different dispersion processes: mechanical mixing and sonication. 188

Figure 6.16**:** Real part of the complex electrical conductivity as a function of frequency for RTV615/8 % CF composites obtained according to different manufacturing processes. 195

Figure 6.17**:** Real part of the complex electrical conductivity measured at 1 Hz as a function of the mass fraction of carbon fibers for RTV615/CF composites manufactured according to modified method 1 with autoclave. 197

Figure 6.18 : (a) Artificial ear made of silicone filled with 3.5% carbon fibers obtained after fabrication; (b) 3D model of the mold used for the production of the artificial ear. 199

Figure 6.19**:** Multipin electrodes fabricated by direct 3D printing from a commercially available carbon black 19- filled thermoplastic polyurethane (TPU/CB) conductive filament. The electrodes were produced using an additive manufacturing process. Surface irregularities and limited interlayer adhesion are observed, resulting in low mechanical robustness of the multi-tip microstructures.....203

Figure 6.20: Polymer molds manufactured by additive manufacturing from different printing materials (a) Nylon, b) High Temp resin and c) Rigid 10K resin) with the aim of exploring their use for compression molding of conductive polymer electrodes. 203

Figure 6.21**:** Thermal deformation and partial melting observed on additively printed nylon molds after use in a heat press during the compression molding process 204

Figure 6.22**:** SEBS (styrene-ethylene-butylene-styrene) granules used as a raw material for the manufacture of filaments for 3D printing. 205

Figure 6.23**:** 3devo Filament Maker machine used for extruding polymer filaments from thermoplastic granules. 205

Figure 6.24**:** Internal view of the 3devo Filament Maker machine showing the polymer filament extrusion process from SEBS granules. 206

Figure 6.25**:** SEBS filaments obtained after extrusion from granules using the 3devo Filament Maker machine, intended for use in 3D printing processes.....206

LIST OF ABREVIATIONS

Ag	Silver
AgCl	Silver chloride
Ag/AgCl	Silver/ silver chloride
Au	Gold
ASTM	American Society for Testing and Materials.
BCI	Brain-computer interfaces
BDS	Broadband dielectric spectrometer
Bi/In/Sn	Bismuth-indium-tin
CNT	Carbon nanotubes
CB	Carbon black
Cu	Copper
DC	Direct current
DSC	Differential scanning calorimetry
DSC/TG	Differential scanning calorimetry/thermogravimetry
DMA	Dynamic mechanical analysis
DMTA	Dynamic mechanical thermal analysis
EII	Electrode-skin interface impedance
EVA	Ethylene-vinyl acetate
EEG	Electroencephalography
Gr	Graphene
GF	Gauge factor
GUI	Graphical user interface
IrO_2	Iridium oxide
L/D	Length-to-Diameter
MA	Maleic anhydride
MWCNTs	Multi-walled carbon nanotubes
PDMS	Polydimethylsiloxane
PET	Polyethylene terephthalate

PI	Polyimide
Pt	Platinum
PPy	Polypyrrole
PMMA	Polymethyl methacrylate
PEDOT:PSS	Poly(3,4-ethylenedioxythiophene): polystyrene sulfonate
PU	Polyurethane
rpm	Rotation per minutes
SBS	Styrene–butadiene–styrene triblock copolymer
SEBS	Styrene-ethylene-butylene-styrene
SEBS-MA	Styrene-ethylene-butylene-styrene-maleic anhydride
SEM	Scanning electron microscopy
TGA	Thermogravimetric analysis
TPU	Thermoplastic polyurethane
Ti	Titanium
TPE	Thermoplastic elastomer
THF	Tetrahydrofuran

LIST OF SYMBOLS

cm^2	Square centimeter
Hz	Hertz
kΩ	Kilo-ohm
N	Newton
3D	Three-dimensional
wt%,	Weight percent
S/m	Siemens per meter
g	Gram
Ω	Ohm
S/cm	Siemens per centimeter
mm	Millimeter
%	Percent
MPa	Megapascal
J	Joule
µV	Microvolt
kHz	Kilohertz
min	Minute
m^2	Square meter
cm^3	Cubic centimeter
°C	Degrees celsius
kPa	Kilopascal
σ	Electrical conductivity

INTRODUCTION

Electroencephalography (EEG) is a non-invasive technique for measuring the brain's electrical activity and is widely used in both clinical practice and scientific research. EEG signals provide essential information for diagnosing and monitoring neurological and physiological conditions, including sleep disorders, anaesthesia depth, coma, encephalopathies, and brain death. Beyond clinical diagnostics, EEG has become increasingly important in research fields such as brain–computer interfaces, cognitive monitoring, and human–machine interaction, where reliable, stable, and repeatable signal acquisition is required.

Conventional EEG systems primarily rely on wet electrodes that use conductive gels to reduce the impedance at the skin–electrode interface. Although these electrodes are well established and capable of delivering high-quality signals, their use is associated with several practical limitations. Wet electrodes require time-consuming preparation procedures, including skin cleaning and impedance optimization, and may cause discomfort, skin irritation, or hair damage during prolonged recordings. In addition, the drying of the conductive gel over time limits the duration of EEG measurements and can lead to signal degradation, making wet electrodes poorly suited for long-term, wearable, or ambulatory monitoring applications.

In response to these limitations, dry EEG electrodes have been developed as an alternative to gel-based systems. By eliminating the need for conductive gels, dry electrodes significantly reduce preparation time and improve usability. However, many dry electrodes are fabricated from rigid materials, which limits their ability to conform to the curved and deformable surface of the human scalp. This lack of conformity often results in increased skin–electrode impedance, reduced signal stability, and discomfort, particularly during extended recording sessions or measurements performed on hairy regions of the scalp.

Flexible dry electrodes have therefore emerged as a promising solution to overcome the mechanical and comfort-related limitations of rigid electrode designs. Their mechanical compliance allows better adaptation to scalp morphology, leading to improved contact stability and potentially reduced impedance fluctuations. Flexible electrodes are commonly fabricated using polymeric materials, which offer advantages in terms of biocompatibility, processability,

and mechanical tunability. To achieve electrical conductivity, these polymers are typically combined with conductive fillers or coatings, including metallic layers and carbon-based nanomaterials such as carbon nanotubes and carbon black. Despite these advances, flexible dry EEG electrodes reported to date often still exhibit higher contact impedance than conventional wet electrodes, which remains a critical challenge for reliable and high-quality EEG acquisition.

Styrenic block copolymers, and in particular styrene–ethylene–butylene–styrene (SEBS), constitute an attractive class of materials for the development of flexible bioelectrodes due to their low elastic modulus, high flexibility, mechanical resilience, and chemical stability. These properties make SEBS well-suited for applications requiring intimate and durable contact with soft biological tissues. In parallel, ethylene–vinyl acetate (EVA), a thermoplastic elastomer widely used in biomedical and wearable applications, has also attracted interest owing to its flexibility, ease of processing, and tunable mechanical behavior through its vinyl acetate content. When combined with conductive carbon-based fillers, both SEBS- and EVA-based nanocomposites have demonstrated promising electrical and mechanical performance in flexible sensing and electronic applications. Nevertheless, despite their potential, the use of SEBS and EVA nanocomposites for dry EEG electrodes remains insufficiently explored, particularly with respect to a systematic and application-oriented characterization of their electrical, mechanical, and electromechanical behavior in the context of reliable biosignal acquisition.

The objective of this doctoral research is to design, fabricate, and characterize flexible dry EEG electrodes based on SEBS- and EVA-based nanocomposites reinforced with carbon black and carbon nanotubes. This work aims to establish structure–property–performance relationships linking material formulation, mechanical compliance, electrical conductivity, and electrode–skin impedance. By developing multipin flexible electrode architectures and evaluating their performance under realistic EEG recording conditions, this thesis seeks to contribute to the advancement of wearable, user-friendly, and reliable EEG technologies suitable for long-term brain activity monitoring.

0.1 Context of the research

Context and Challenges

This research aims to overcome the limitations of conventional gel-based EEG electrodes by developing dry, flexible electrodes suitable for long-term recordings. Unlike traditional wet electrodes, which require time-consuming preparation and suffer from gel degradation affecting signal quality and comfort, the proposed approach ensures stable skin–electrode contact, reliable signal acquisition, and improved usability. This work was conducted within the Industrial Research Chair in In-Ear Technologies (CRITIAS) at École de technologie supérieure, as part of Work Package 6 (WP6), focusing on innovative sensing solutions for intra-auricular applications. Emphasis is placed on flexible and conformable polymer materials to enable reliable physiological signal acquisition. Overall, this research contributes to the development of next-generation portable EEG systems for applications in health monitoring, neurotechnology, and smart in-ear devices.

Scientific Justification

The increasing demand for portable, wearable, and long-term EEG monitoring systems exposes the limitations of conventional electrode technologies and motivates the exploration of alternative material solutions. In this context, thermoplastic polymers constitute a particularly relevant class of materials for next-generation EEG electrodes, owing to their ease of processing, tunable mechanical properties, and compatibility with scalable and reproducible manufacturing techniques. Compared to thermoset elastomers, thermoplastics enable precise control over mechanical compliance and facilitate the fabrication of complex electrode geometries, which are essential for flexible and wearable bioelectronic devices.

Styrene–ethylene–butylene–styrene (SEBS) and ethylene–vinyl acetate (EVA) were selected as polymer matrices because they combine low elastic modulus, high flexibility, and mechanical resilience with good biocompatibility and environmental stability. These attributes promote intimate and durable contact with the scalp while minimizing discomfort during prolonged EEG recordings. Although SEBS and EVA are intrinsically electrically insulating, their use as matrix materials is intentional. In composite-based electrodes, the polymer phase

primarily governs mechanical compliance, skin conformity, and long-term comfort, which are critical to ensuring a stable and reliable electrode–skin interface.

Electrical conductivity is achieved through the incorporation of conductive carbon-based fillers, specifically carbon nanotubes (CNTs) and carbon black (CB). CNTs are particularly advantageous due to their high aspect ratio, excellent intrinsic conductivity, and ability to form percolated conductive networks at relatively low filler contents. When appropriately dispersed within thermoplastic matrices, CNTs enable efficient charge transport while preserving the flexibility of the composite. This design strategy effectively decouples mechanical and electrical functions, whereby the polymer matrix ensures compliance and durability, and the conductive fillers provide the electrical pathways required for EEG signal acquisition.

The combined use of thermoplastic matrices (SEBS and EVA) and conductive carbon-based fillers (CNTs and CB) thus represents a rational and scientifically grounded approach to addressing the competing requirements of flexibility, comfort, electrical performance, and manufacturability in dry EEG electrodes. A systematic investigation of these composite systems—encompassing their electrical, mechanical, and electromechanical behavior—is essential to establish structure–property–performance relationships relevant to EEG applications and to advance the development of reliable wearable bioelectronic technologies.

Technological and Applied Interest

- Improve user comfort by eliminating the need for gel.
- Facilitate long-term EEG use, making the technology more accessible for clinical and ambulatory applications.
- Contribute to the growth of portable neurotechnologies, promoting EEG use beyond laboratories and hospitals, particularly for home monitoring and brain-computer interfaces.

This PhD project presents a unique opportunity to drive innovation in biomedical sensors by integrating materials science, biomedical engineering, and EEG signal analysis. It will provide expertise at the intersection of fundamental research and clinical applications, opening perspectives in neuroengineering, medical devices, and brain-computer interfaces. The evolution of EEG technologies toward more comfortable, practical, and accessible solutions is

crucial for the future of neuroscience and medical devices. This PhD project addresses a growing need by developing innovative, flexible, and dry EEG electrodes, thus opening new avenues for research and healthcare.

0.2 Research Objectives

As discussed in Section 0.1, the growing demand for portable, wearable, and long-term EEG monitoring systems has revealed significant limitations in conventional wet electrode technologies. The need for conductive gels, combined with discomfort, signal degradation over time, and limited suitability for prolonged or ambulatory recordings, restricts their applicability in real-world settings. Recent advances in materials science and wearable bioelectronics offer new opportunities to address these challenges through the development of flexible dry EEG electrodes that ensure stable electrode–skin contact, mechanical compliance, and reliable signal acquisition without the use of gel.

In this context, the overarching objective of this thesis is to develop, fabricate, and validate flexible dry EEG electrodes based on conductive thermoplastic polymers, with a particular emphasis on optimizing the balance between electrical performance, mechanical flexibility, and long-term stability at the electrode–skin interface.
This thesis is organized into three studies, each addressing a distinct but complementary aspect of this objective.

Study 1 focuses on the development and material-level characterization of conductive polymer composites for dry EEG applications. In this study, styrene–ethylene–butylene–styrene (SEBS) and ethylene–vinyl acetate (EVA) are combined with carbon-based conductive fillers, namely carbon black (CB) and carbon nanotubes (CNT). Through a systematic investigation of electrical conductivity, contact impedance, mechanical compliance, and thermal stability, this study aims to identify the composite formulations that provide the most suitable balance of properties for flexible dry EEG electrodes. By establishing clear structure–property

relationships, this work lays the material foundation for subsequent electrode design and optimization.

Study 2 addresses the optimization of functional electrode properties through a comparative evaluation of SEBS/CB and SEBS/CNT composites implemented in flexible multipin EEG electrode architectures. This study examines how the choice of conductive filler influences key performance metrics, including electrode–skin contact impedance, scalp conformity, and mechanical stability under conditions relevant to prolonged EEG recordings. By linking material composition to electrode-level performance, this study provides design guidelines for achieving reliable and comfortable dry EEG electrodes suitable for practical use.

Study 3 focuses on the experimental validation of the developed electrodes under EEG recording conditions. In this study, the performance of the proposed dry EEG electrodes is benchmarked against commercial dry electrodes, with particular attention to signal quality and stability across different recording scenarios. Special emphasis is placed on hybrid SEBS/CNT/CB and SEBS-MA/CNT/CB nanocomposites, which are designed to exploit the complementary properties of CNT and CB while avoiding the high filler loadings and increased mechanical stiffness typically associated with single-filler systems. This study demonstrates the practical relevance of hybrid conductive networks for achieving low impedance, stable EEG signals, and improved user comfort.

Together, these three studies provide a comprehensive framework for the development of next-generation flexible dry EEG electrodes. By integrating material design, electrode optimization, and experimental validation, this thesis contributes to advancing dry EEG technology toward more comfortable, reliable, and scalable solutions for clinical, wearable, and long-term brain monitoring applications.

0.3 Structure of the Thesis

This thesis is organized into five chapters, followed by appendices containing supplementary material associated with the journal articles, where applicable.

Chapter 1 presents a comprehensive literature review that establishes the scientific and technological foundations necessary for this research. The chapter begins with an overview of EEG principles and the fundamentals of electrode–skin interfaces, with particular emphasis on contact impedance and signal quality. It then reviews existing EEG electrode technologies, including wet, semi-dry, and dry electrodes, and discusses their respective advantages and limitations. The chapter further examines materials and fabrication strategies used for dry EEG electrodes, focusing on conductive polymers, elastomers, and carbon-based fillers. Finally, different electrode geometries and design approaches are reviewed, and the key challenges associated with comfort, stability, and long-term EEG monitoring are identified.

Chapter 2 presents the material properties that are essential for understanding the articles included in this thesis. It provides a comprehensive overview of the electrical, mechanical, and thermal characteristics of the materials used, as well as their relevance to the development and performance of flexible dry EEG electrodes.

Chapter 3 presents the first journal article, which focuses on the development and characterization of flexible dry EEG electrodes based on styrene–ethylene–butylene–styrene (SEBS) and ethylene–vinyl acetate (EVA) filled with carbon black (CB). This chapter investigates the electrical, mechanical, and thermal properties of the proposed composites, evaluates electrode–skin contact impedance, and compares the EEG recording performance of the developed electrodes with that of commercial dry EEG electrodes.

Chapter 4 presents the second journal article, which examines the influence of conductive filler type and electrode geometry on dry EEG electrode performance. In particular, this chapter compares SEBS/CB and SEBS/carbon nanotube (CNT) composites implemented in flexible multipin electrode architectures. The electrical conductivity, thermo-mechanical behavior, and contact impedance of the electrodes are analyzed to identify key design parameters for improving signal quality and stability during prolonged EEG recordings.

Chapter 5 presents the third journal article, which investigates hybrid flexible dry EEG electrodes based on SEBS and maleic anhydride–modified SEBS (SEBS-MA) incorporating both CNT and CB fillers. This chapter explores how hybrid conductive networks influence filler dispersion, mechanical compliance, and electrical performance. The developed hybrid electrodes are benchmarked against those presented in previous chapters, and their ability to record stable EEG signals is experimentally validated.

Chapter 6 presents the exploratory work conducted as part of this thesis. It summarizes the main findings of these preliminary studies and highlights their contributions to the development and optimization of flexible dry EEG electrodes. This chapter also discusses the limitations of the exploratory approaches and outlines perspectives for future research.

0.4 Contributions

The contributions of this doctoral research consist primarily of peer-reviewed journal publications addressing the development, optimization, and validation of flexible dry EEG electrodes based on conductive thermoplastic polymer composites. This thesis incorporates three journal articles, each corresponding to a distinct stage of the research and collectively forming a coherent scientific contribution to the field of wearable EEG technologies.

The first article (Chapter 3) focuses on the development and characterization of flexible dry EEG electrodes based on SEBS/carbon black and EVA/carbon black composites, with an emphasis on their electrical, mechanical, thermal, and morphological properties, as well as preliminary EEG signal acquisition.

The second article (Chapter 4) investigates the influence of conductive filler type and electrode geometry through a comparative study of SEBS/carbon black and SEBS/carbon nanotube multipin electrodes, highlighting structure–property relationships relevant to contact impedance, flexibility, and thermo-mechanical stability.

The third article (Chapter 5) explores hybrid SEBS/CNT/CB and SEBS-MA/CNT/CB nanocomposites, demonstrating how hybrid conductive networks can achieve an improved balance between electrical conductivity and mechanical compliance, and providing in vivo EEG validation through benchmarking against commercial dry electrodes.

At the time of thesis submission, all three articles have been published in peer-reviewed international journals. Together, they constitute an original and integrated contribution to the advancement of flexible dry EEG electrodes, offering material-level insights, electrode design strategies, and experimental validation relevant to clinical, wearable, and long-term EEG applications. In addition to these scientific contributions, this doctoral work also involved the supervision of several graduate-level research projects, including master's theses and undergraduate capstone projects, through which students were trained in experimental design, materials characterization, and EEG electrode development.

CHAPITRE 1

TECHNOLOGIES AND MATERIALS USED FOR THE MANUFACTURE OF DRY ELECTRODES

Chapter outline: This chapter provides a comprehensive overview of the technologies and materials used in the fabrication of dry EEG electrodes. It begins by outlining the fundamental principles of dry electrode technology and its significance in EEG applications. The chapter then explores various fabrication techniques employed in the development of dry electrodes, including both traditional and emerging manufacturing methods. Following this, the discussion shifts to the materials commonly used in dry electrode fabrication. Special emphasis is placed on conductive polymers, elastomers, and carbon-based materials such as carbon nanotubes (CNTs), graphene, and carbon black (CB). The electrical and mechanical properties of these materials are examined in relation to their suitability for EEG applications. Additionally, the chapter explores the role of material processing techniques in optimizing the performance of dry electrodes. The advantages and limitations of different electrode materials are discussed, particularly in terms of contact impedance, flexibility, and durability. The chapter concludes by outlining the approach adopted in this study to evaluate and enhance the properties of flexible dry EEG electrodes, with a focus on material selection, structural design, and performance optimization strategies.

1.1 Introduction

Bioelectrical signals generated by cells or tissues during daily physiological activities are closely linked to the functional states of the body and its organs (Arai et al., 2015; Fu et al., 2020a). EEG is an essential technique for recording brain electrical activity. EEG plays a crucial role in research and diagnostics related to human brain function and is primarily used to diagnose neurological diseases (Zeydabadinezhad et al., 2024), such as epilepsy, Alzheimer's disease, Parkinson's disease, and sleep disorders. EEG detects abnormalities in

neuronal activity by measuring potential fluctuations on the scalp surface (H.-L. Peng, Jing-Quan Liu, et al., 2016). Thanks to technological advancements, EEG applications have expanded to include brain-computer interfaces (BCI), rehabilitation, mobile monitoring, and sports-related contexts (Das et al., 2020a; Fiedler et al., 2015; Palumbo et al., 2024). The conventional method for recording EEG signals typically involves using a conductive silver/silver chloride (Ag/AgCl) gel to ensure low-impedance contact with the skin (Y.-H. Chen et al., 2014). Additionally, these low-impedance values between the skin and the electrode contribute to the stability and reproducibility of EEG signals (Leach et al., 2020). The gel is necessary to maintain electrode stability on the skin and reduce contact resistance (Arai et al., 2015; de Camp et al., 2018; Fu et al., 2020a). However, this method presents several drawbacks, including the need for prior skin preparation (abrasion and shaving), the limited duration of recordings due to gel drying, risks of skin irritation and allergic reactions (Y. Li et al., 2021; H.-L. Peng, Liu, et al., 2016), and discomfort during electrode application and removal (S. M. Lee et al., 2014).

Gel drying causes an increase in skin-electrode impedance, which reduces EEG signal quality (Srivastava et al., 2015). Additionally, short circuits between adjacent electrodes, induced by gel spreading, can occur due to the skin's irregular surface (Wehrmann et al., 2013). These limitations restrict their use for long-term recordings and in ambulatory settings, rendering them unsuitable for extended applications (Arai et al., 2015; Baek et al., 2012; Chlaihawi et al., 2018; Cunha et al., 2009; Das et al., 2020a; de Camp et al., 2018; Fiedler et al., 2018a; Z. Wang et al., 2018). Moreover, gel residues may remain on the scalp, potentially causing irritation or skin rashes. These issues render wet electrodes impractical for portable or long-duration applications (Arai et al., 2015; Chlaihawi et al., 2018; Das et al., 2020a; de Camp et al., 2018; Fiedler et al., 2018a).

Given the limitations of wet electrodes, significant efforts have been made to develop dry electrodes that provide a more practical and comfortable alternative without compromising EEG signal quality (Al-Haidari et al., 2024). In recent years, researchers have developed dry electrodes using various conductive materials (Shad et al., 2020), and advancements in material science and electrode design have resulted in the creation of flexible dry EEG electrodes. These

electrodes offer greater comfort and adaptability to scalp contours while eliminating issues associated with conductive gels (Lopez-Gordo et al., 2014).

Dry electrodes utilize innovative materials, including conductive polymers, carbon-based composites, metal alloys, electrically conductive solutions, and hybrid materials, to improve signal quality and reduce skin-electrode impedance. However, challenges remain concerning the higher impedance of dry electrodes, their dependence on the pressure applied to the skin, and interference caused by hair (Habibzadeh Tonekabony Shad et al., 2020; Lopez-Gordo et al., 2014). The absence of gel in dry electrode configurations results in elevated contact impedance (Das et al., 2020a). Furthermore, dry electrodes composed of metallic materials that come into direct contact with the skin may lead to skin infections (G.-L. Li et al., 2020a). This section aims to present various manufacturing technologies for dry electrodes. We will explore different conductive polymers, composites, and nanomaterials combined with conductive fillers.

1.2 Dry electrode technologies for EEG

Dry electrodes can be categorized into three main types: microneedle electrodes, surface electrodes, and capacitive electrodes. This section aims to present the different manufacturing technologies for dry electrodes.

1.2.1 Microneedle electrodes

Microneedle electrodes consist of an array of miniaturized needles on the micrometer scale (Chang et al., 2017)**.** These electrodes can penetrate the outer insulating layer of the skin without requiring any skin preparation or conductive gel (K. Zheng et al., 2024). The absence of prior skin preparation, such as abrasive cleaning or the application of conductive gel, simplifies the installation process. Since no conductive gel is required, these electrodes facilitate long-term EEG recording (Arai et al., 2015). These electrodes exhibit low skin-contact impedance (Z. Chen et al., 2018; Griss et al., 2001; L. Ren et al., 2016; Ruffini et al., 2006) and reduce the presence of motion artifacts during EEG signal recording. Their design enables minimal penetration (Chang et al., 2017; Dabbagh et al., 2021; G. Lee et al., 2018; L. Ren et al., 2017).

Despite their numerous advantages, microneedle electrodes also have some drawbacks. Compared to wet electrodes, microneedle electrodes remain invasive due to their mode of operation (Krieger et al., 2019). The insertion of needles can cause discomfort or even mild pain, especially during prolonged use. Microneedles can be fragile and prone to breaking, which may compromise the safety and effectiveness of the electrodes (Z. Wang et al., 2024a). This complexity hinders their commercialization and large-scale production (Madden et al., 2020). Skin perforation increases the risk of infections, necessitating strict hygiene measures and biocompatible materials.

For the fabrication of this type of electrode, the height and thickness of the needle tips must be considered during the design and manufacturing process. Proper geometric design helps minimize user discomfort and ensures optimal EEG acquisition. Thicker tips allow for EEG recordings with less discomfort for the user (Krieger et al., 2019; Mansor et al., 2019). The needle height-to-width ratio influences the ease of insertion and mechanical integrity (Krieger et al., 2019). While higher height-to-width ratios facilitate insertion, lower ratios yield mechanically stronger needles. The tip radius is also a key parameter for ensuring proper skin penetration. Controlling these dimensional parameters is crucial to adapting microneedles to their intended functionality. The precision required for microneedle fabrication makes their production more expensive and technically demanding (L.-F. Wang et al., 2012a). Microneedle electrodes are currently not commercially available (Madden et al., 2020).

The manufacturing process for microneedle electrodes is complex and labor-intensive, involving techniques such as lithography, which is used to carve microscopic patterns on substrates (Arai et al., 2015; Z. Chen et al., 2018; G. Lee et al., 2018; L. Ren et al., 2017; Srivastava et al., 2015; R. Wang et al., 2017a), the KOH-dicing-KOH method (R. Wang et al., 2017b), self-assembly by magnetization, which is used to organize and assemble microstructures (K. Chen et al., 2016; Pan et al., 2016), thermal assembly (L. Ren et al., 2016), micromolding (M. Kim et al., 2015), injection molding for large-scale production (N. Yang et al., 2024), laser cutting for precise microstructure shaping, which is ideal for adjusting needle length and shape, laser patterning (W. Zhou et al., 2013, 2015, 2016), and 3D printing for customized electrodes (Dabbagh et al., 2021; Krieger et al., 2019; Mansor et al., 2019). These

processes enable the production of microneedle electrodes that integrate performance, compliance, and safety for advanced EEG applications.

1.2.2 Surface electrodes

Surface electrodes are designed to ensure direct contact with the skin without penetration, offering a compromise between comfort and signal quality. Less invasive than microneedle electrodes, they allow EEG signal acquisition while minimizing user discomfort. They only make direct contact with the outermost layer of the skin (Z. Wang et al., 2018). Their design makes them suitable for ambulatory applications and mobile environments, such as home health monitoring, wearable devices for sleep tracking or cognitive performance assessment, and sports-related EEG measurements for long-term monitoring (Iqbal et al., 2021).

Despite their advantages over microneedle electrodes, surface electrodes are sensitive to movement, leading to motion artifacts in EEG signals and affecting data quality. Strategies such as using adhesive structures or ergonomic designs aim to improve electrode stability and reduce motion-related artifacts. However, finding a balance between flexibility, conductivity, and user comfort remains a constant challenge in developing these electrodes.

Electrode stability on the skin is an important property to consider when designing and manufacturing surface electrodes. Poor stability can cause arbitrary displacement of the electrode during body movements, resulting in motion artifacts and poor-quality EEG acquisition (Cui et al., 2021; G. Li, Deng, et al., 2021). Sufficient adherence to the skin is crucial for long-term EEG recording and to prevent inflammation, irritation, and pain when removing the electrode from the skin (L. Cheng et al., 2023; W. Liu et al., 2022).

To improve comfort and efficiency, surface electrodes must be manufactured using flexible materials (L.-F. Wang et al., 2012a). The fabrication process for surface electrodes involves lithography and screen printing (Niu et al., 2021), plasma treatment (Pedrosa et al., 2016), laser prototyping (Leleux et al., 2014), dispersion of conductive reinforcements in a matrix (Jin et al., 2016; J. H. Lee et al., 2018, Stauffer et al., 2018), temporary tattoo-based application on the skin (Shustak et al., 2019), injection molding (Kaitainen et al., 2014), and spray coating (Fiedler et al., 2011a; Pedrosa et al., 2013). Additionally, electrode design must consider

breathability. Sweat accumulation can cause skin irritation (R. Xie et al., 2022; Y. Yang et al., 2022). A surface electrode should be designed to ensure reliable and stable skin-electrode contact and provide sufficient comfort for users (Symeonidou et al., 2018).

1.2.3 Capacitive electrodes

Capacitive electrodes function as a capacitor coupled to the skin surface, without direct contact (J. H. Kim et al., 2014; S. M. Lee et al., 2016b). EEG recording with capacitive electrodes relies on the capacitance formed between the electrode and the scalp, even in the presence of barriers such as air layers, hair, or fabrics (Babusiak et al., 2018; Wehrmann et al., 2013). These electrodes were developed to avoid the issue of lost physical contact with the scalp caused by the presence of hair (Bednar et al., 2021; H. Yuan et al., 2021). The absence of direct skin contact offers several significant advantages. It reduces the risks of infection and skin irritation and improves user comfort for prolonged use. Additionally, capacitive electrodes are ideal for portable applications, particularly in devices integrated into smart clothing, facilitating continuous brain activity monitoring without physical constraints. This principle enables EEG signal acquisition while maintaining a physical separation between the scalp and the electrode. Capacitive electrodes are less invasive than surface and microneedle electrodes. Eliminating skin contact removes the need for conductive gel for EEG acquisition, as required with wet electrodes (Hajare & Kadam, 2021). While this method is promising, some challenges remain. The high impedance between the electrode and the scalp results from the insulating layer, air gaps, and hair (S. M. Lee et al., 2016a; Shad et al., 2020; L. Yang et al., 2021). Signal amplitudes are low, making them unsuitable for high-quality EEG recordings. Although this technology avoids the risk of skin infections, further efforts are needed to develop amplifiers capable of acquiring higher-quality EEG signals.

The fabrication process for capacitive electrodes is simpler than that of microneedle or surface electrodes. They can be produced by applying a conductive solution onto polymers, then covering them with an insulating material (Baek et al., 2012, 2013; S. M. Lee et al., 2010; Lim et al., 2007; C.-T. Lin et al., 2011; Wartzek et al., 2011) or by using a metal plate covered with insulating materials (Fayyaz Shahandashti et al., 2019; S. M. Lee et al., 2013; Lim et al., 2014;

Portelli & Nasuto, 2017; Sullivan et al., 2007). Coating techniques such as spraying, dipping, and spin-coating are applied to ensure uniform material deposition.

Microneedle electrodes generally exhibit lower impedances due to their direct contact with subcutaneous tissues. In contrast, surface and capacitive electrodes tend to have higher impedances. The electrode-skin interface impedance (EII) is a key parameter for evaluating electrode performance, where lower values indicate better conduction efficiency and improved EEG signal quality (Xue et al., 2025).

1.3 Materials used for the manufacture of flexible dry electrodes

Conductive polymers and composites are the most commonly used materials for the fabrication of flexible EEG electrodes. Conductive polymers and their composites have emerged as promising solutions due to their ability to meet combined electrical, mechanical, and biocompatibility requirements. Flexible EEG electrodes are designed to ensure stable contact with the shape of the scalp. The stability of the scalp-electrode contact ensures a comfortable and reliable electrical connection for measuring brain activity. The choice of materials depends on specific design requirements, intended use, and manufacturer preferences.

To prevent signal loss during EEG measurements and ensure stable contact at the electrode-skin interface, it is recommended to develop electrodes using flexible materials (L. Cheng et al., 2023; E. K. Lee et al., 2021; B. Yao et al., 2022). Connectors are generally made from materials such as stainless steel or other metals that provide good conductivity and durability. Insulating materials are used to cover certain parts of the electrode to prevent unintended electrical contact. In some cases, electrodes need to be attached to the scalp, requiring an adhesive layer. The adhesive must securely maintain the connection to the skin without causing discomfort.

For the fabrication of flexible EEG electrodes, polydimethylsiloxane (PDMS), polyurethane (PU), polyimide (PI), polymethyl methacrylate (PMMA), polyethylene terephthalate (PET), polystyrene-block-poly(ethylene-ran-butylene)-block-polystyrene (SEBS), thermoplastic polyurethane (TPU), and poly(3,4-ethylenedioxythiophene): polystyrene sulfonate (PEDOT:PSS) are among the most suitable materials due to their flexibility and

biocompatibility (Hassan et al., 2022; Heng et al., 2022; B.-C. Kang et al., 2019; S.-J. Park et al., 2023; Sayyad et al., 2025a; T. Zeng et al., 2024; Zhuo et al., 2025). PDMS is the most commonly used material due to its flexibility, biocompatibility, and durability (Y. Li et al., 2022; Raspopovic et al., 2021). The combination of polymers with carbon reinforcements such as carbon nanotubes (CNTs), carbon black, carbon fibers, and graphene enables the fabrication of flexible electrodes for EEG measurements (Ai et al., 2024; Del Bosque et al., 2023; Hossain et al., 2022; Ruffini et al., 2006; Yun et al., 2023). Flexible polymer resins such as SU-8 are also used for manufacturing flexible electrodes (Srivastava et al., 2015). The choice of substrate depends on specific objectives and requirements (Sayyad et al., 2024). Advances in thin-film technologies allow for the deposition of metals such as silver/silver chloride (Ag/AgCl) and gold in ultra-thin layers on flexible polymers to improve electrical conductivity and reduce skin-electrode contact impedance.

A major challenge related to incorporating conductive additives into polymer matrices is the development of conductive blends with the lowest possible additive proportion to preserve the mechanical properties of the matrix while minimizing implementation and manufacturing costs (Kuester et al., 2016). The critical quantity of conductive additive in the mixture, at which the system's conductivity abruptly changes, is known as the electrical percolation threshold. This threshold depends on several factors, such as the volume fraction of the conductive filler, morphology, intrinsic properties of components, compatibility between the insulating polymer matrix and the conductive filler, particle shape, aspect ratio and orientation of the filler, interfacial tension between the conductive and insulating phases, and the dispersion and distribution of conductive fillers in the polymer matrix (Méndez et al., 2017; Mohd Radzuan et al., 2017). Several techniques exist to reduce the electrical percolation threshold, including the appropriate selection of system phases and the use of optimal manufacturing conditions (Azizi et al., 2018; Kuester et al., 2016). However, the fabrication method often has a dominant influence on achieving a low percolation threshold (J.-K. Yuan et al., 2011). Parameters such as temperature, mixer rotation speed, and mixing time (in molten or solvent state) tend to affect the electrical conductivity values of composites. Optimizing these parameters enables the most suitable combination for manufacturing conductive composites with low electrical percolation thresholds (Mondal et al., 2017; Yousefzade et al., 2016).

Electrodes made from a combination of different materials, called hybrid electrodes, optimize the electrical and mechanical properties of flexible EEG electrodes. Carbon-based reinforcements or metallic nanoparticles embedded in polymers are often used to fabricate hybrid electrodes (L. Yang, Liu, et al., 2022). The combination of metals and polymers allows the creation of hybrid electrodes that combine the flexibility of polymers with the electrical conductivity of metals. These hybrid electrodes improve conductivity and mechanical durability while reducing motion artifacts. Low-melting-point alloys, such as bismuth-indium-tin (Bi/In/Sn), gold (Au), silver (Ag), copper (Cu), and platinum (Pt), are widely used due to their excellent electrical conductivity and chemical stability. Carbon nanotubes, carbon black, and graphene are combined with metals to improve the electrical conductivity of flexible electrodes while maintaining acceptable mechanical flexibility. The use of each material presents promising prospects for improving EEG electrode performance, while requiring careful attention to sustainability and safety concerns for human health.

Extensive research has explored different geometries of dry polymer-based electrodes to reduce contact impedance and enhance user comfort. Harati & Jahanshahi (Harati & Jahanshahi, 2021) designed a 3D-shaped EEG electrode made of silicone with four legs to improve adaptation to the skin. To ensure optimal conductivity, copper (Cu) was chosen as the primary conductive layer. Each leg had dimensions of 4 mm × 4 mm, while the entire electrode measured 14 mm in width, 14 mm in length, and 13 mm in height. Flexible dry electrodes were mechanically and electrically characterized separately. Mechanical characterization included tensile strength measurements and a specific endurance test simulating running. Electrical characterization involved measuring contact impedance and recording EEG signals under open- and closed-eye conditions. The results indicate that the electrode can withstand over 50,000 impacts for approximately 11 hours without electrical failure. The maximum elongation at break was approximately 80%. The contact impedance at 10 Hz was 20 kΩ at FP1 and 70 kΩ at O1. Y. Zhao et al. (Y. Zhao et al., 2025) developed a flexible dry EEG electrode in the shape of a disc using polypyrrole (PPy). The results show that this electrode maintains a stable impedance of approximately 15 kΩ over an extended monitoring period while offering excellent breathability, optimal comfort, and good portability. At 10 Hz, the impedance of the PPy leather electrodes was comparable to that of commercial gel electrodes, both around 15

kΩ. To evaluate the relationship between skin interface impedance and applied pressure, tests were conducted under loads ranging from 0 N to 80 N. The results indicate that a pressure of 10 N results in an 8 kΩ decrease in interface impedance. Finally, the measured impedances at FP1 and FP2 were 12 kΩ and 13 kΩ, respectively. Fiedler et al. (Fiedler et al., 2018a) developed multi-pin EEG electrodes made of polyurethane (PU) coated with silver using a multi-step chemical coating process. Each electrode systematically contained 30 pins, each with spherical tips measuring 1 mm in diameter, a height of 6 mm, and a center-to-center spacing of 2.4 mm. Applying a normal force of at least 2 N resulted in reproducibly low skin-electrode impedance. Specifically, for a force of 2 N, all impedance measurements for electrodes with Shore hardness values of A98 and A90 remained below 250 kΩ. A normal force of 2 N, corresponding to a contact pressure of 0.9 kg/cm², combined with a Shore A90 substrate, ensured low and stable impedances while providing good wearing comfort for the multi-pin electrodes. Kappel et al. (Kappel et al., 2019) developed an auricular EEG electrode composed of a titanium (Ti) substrate coated with iridium oxide (IrO_2) and electrically protected by a silver (Ag) casing. To evaluate the quality of the EEG electrode, participants were instructed to keep their eyes open while watching a silent film and then relax with their eyes closed. A sound signal indicated the transition between conditions every 60 seconds. The impedance measured at approximately 50 Hz for electrodes placed in the ear canal was 435 kΩ for the IrO_2 electrode. D. Y. Kim et al. (D. Y. Kim et al., 2018) developed a nanoporous platinum electrode deposited in the L2 phase (L2-ePt). The L2-ePt electrodes were compared to commonly used clinical electrodes, including gold cup electrodes and flat platinum electrodes (FlatPt). Skin-electrode impedance was measured at 30 Hz using an impedance analyzer, as this frequency falls within the EEG spectrum and serves as a standard reference for monitoring the impedance of skin electrodes during EEG recordings. Signals were acquired using the L2-ePt electrode, alternating between open-eye and closed-eye cycles every 20 seconds for a total duration of two minutes. The impedance measurements obtained at 30 Hz were as follows: 10.0 ± 6.03 kΩ for the L2-ePt electrode, 26.10 ± 11.83 kΩ for the FlatPt electrode, and 12.23 ± 2.78 kΩ for the gold cup electrode.

K. Gao et al. (K. Gao et al., 2024a) developed a pin-shaped EEG electrode made of polyurethane (PU) that is capable of penetrating hair to establish good contact with the scalp.

The electrode's surface was covered with silver-plated conductive fabric to enhance its conductivity. The results showed that the electrode had an average contact impedance of 10.9 ± 2.7 kΩ and an EEG signal quality comparable to that of wet electrodes. The PU electrode structure was mounted on a circular base with a diameter of 17 mm and a thickness of 3 mm. Six columns were distributed on this base, each with a diameter of 2.5 mm at their base and 2 mm at their top. Zheng et al. (Y. Zheng et al., 2024) designed a two-channel EEG headband incorporating dry electrodes made of multilayer graphene doped with gold. For EEG signal recording, volunteers performed a sequence alternating between 5 seconds with their eyes closed and 5 seconds with their eyes open. Measurements revealed that the dry electrode had a contact resistance of approximately 20.7 kΩ with the scalp. De Camp et al. (de Camp et al., 2018) developed a dry, self-adhesive, non-metallic EEG electrode based on poly(3,4-ethylenedioxythiophene) (PEDOT). These PEDOT polymer electrodes had a round shape with a diameter of 3 mm and a thickness of 2 mm. Impedance was measured before and after polymerization at various frequencies. Before polymerization, the impedance values were 59 kΩ at 10 Hz, 20 kΩ at 100 Hz, and 11 kΩ at 500 Hz (standard deviation: 0.2 kΩ). After polymerization, the impedance values significantly decreased to 1.4 kΩ at 10 Hz, 1.4 kΩ at 100 Hz, and 1.4 kΩ at 500 Hz (standard deviation: 0.2 kΩ). These results demonstrated a significant reduction in impedance after polymerization, suggesting improved conductive properties of the electrode. K.-P. Gao et al. (K.-P. Gao et al., 2018) developed a pin-shaped dry EEG electrode, in which micro-bristles located at the top of the flexible pins were made from a composite of carbon fiber and polyurethane (PU) doped with carbon nanotubes (CNT). To reduce the contact impedance between the electrode and the scalp, the surfaces of the carbon fibers were coated with gold. The evaluation of the average skin-electrode contact impedance among five subjects revealed a value of 133 kΩ. In comparison, the wet electrode, secured with an adhesive gel, underwent an impedance check, ensuring a value below 5 kΩ before and after EEG measurements. During the recording, subjects alternated between open-eye and closed-eye periods according to specific instructions to assess the quality of the EEG signal captured by the dry electrode. J. H. Kim et al. (J. H. Kim et al., 2018) developed a carbon nanotube (CNT) and polydimethylsiloxane (PDMS) nanocomposite for wearable electronics applications. Increasing the CNT content improved electrical conductivity; however, electrical

resistance stabilized beyond 4 wt% CNT. EEG recordings were performed using alternating 60-second cycles of open and closed eyes. No noise artifacts resulting from body movements or external interference were detected. The contact impedance was not assessed in this study. To assess the electrical stability of the material, mechanical tensile cycling tests were performed on PDMS/CNT samples. The CNT/PDMS composites exhibited a surface resistance below 20 Ω/sq, a tensile strength of 3.65 MPa, an elastic strain of more than 45%, and a gauge factor reaching 10,000 cycles.

1.4 Applications of Flexible Dry Electrodes

Flexible dry electrodes have promising applications in the clinical field, particularly for long-term monitoring of patients with neurological disorders (S. Liu et al., 2024; Song et al., 2025; D. Yang et al., 2025). These electrodes are especially beneficial for sensitive populations, such as children and the elderly, due to their minimally invasive nature and reduced risk of skin irritation (Cioffi et al., 2024). The ease of use of flexible dry electrodes makes them ideal for telemedicine and remote monitoring. They enable continuous patient tracking in their daily environment, contributing to more accurate diagnoses and personalized care. The increasing adoption of flexible dry electrodes in these applications is supported by technological advancements, particularly in the development of flexible conductive materials, which offer an optimal balance between conductivity, flexibility, and comfort.

Dry electrodes play a crucial role in the development of wearable technologies and brain-computer interfaces (BCI), thanks to their ease of integration and ability to function without skin preparation (Ajel et al., 2024; Y. Cheng et al., 2025; Zhang et al., 2024). They are integrated into lightweight EEG headsets and smart headbands to monitor brain activity during daily activities, meditation sessions, or sports training (H. Zeng et al., 2024). Their portability enables real-time monitoring, which is useful for stress management or enhancing cognitive performance. Dry electrodes are increasingly being used in smart textiles for non-clinical applications, such as concentration tracking, mental fatigue detection, or even controlling electronic devices through thought (Sayyad et al., 2025b; Zare et al., 2025). This opens up

innovative prospects in the fields of gaming, virtual reality, and connected work environments (Ha et al., 2025; B.-H. Lee & Yin, 2024; S. Xu et al., 2024).

These applications highlight the potential of dry electrodes to transform not only the medical sector but also users' everyday lives by making EEG devices more accessible and adaptable to a wide range of contexts.

1.5 Current challenges and future perspectives of flexible dry electrodes

Flexible dry electrodes offer a promising alternative to traditional wet electrodes, particularly in terms of ease of use and comfort. Research into new composites with conductive fillers could help achieve an optimal balance between flexibility, conductivity, and biocompatibility (J. Zhao et al., 2024). Advances in technology using simple manufacturing processes could enable the development of electrodes better adapted to individual user morphology, thus improving both comfort and signal quality (X. Gao et al., 2024). The fabrication of electrodes using composite materials that offer an acceptable compromise between flexibility and electrical conductivity could pave the way for applications in dynamic environments, such as EEG measurements during movement, continuous home monitoring, and even brain-machine interfaces for sports activities (T. W. Kang et al., 2024; Y. Wang et al., 2025a).

The future of flexible EEG electrodes relies on material and technological innovations. The use of recyclable or biodegradable materials could represent a significant breakthrough in minimizing the environmental impact of disposable devices. Additionally, integrating advanced nanomaterials, such as hybrid nanocomposites, could enhance conductivity while maintaining the required flexibility and biocompatibility. The absence of standardized protocols and reference benchmarks in studies makes it difficult to compare and validate results across different research teams, thereby hindering the development of reliable and reproducible flexible dry electrodes (Beyrouthy et al., 2024; Ma, 2024; K. Yang et al., 2024). Corrosion is another major challenge for dry electrodes made of metallic materials intended for prolonged use in wearable healthcare devices. Despite numerous studies on these electrodes, the impact of corrosive environments, such as sweat, on their performance remains poorly documented.

Given that these electrodes are in direct contact with the skin and exposed to sweat, it is crucial to assess their corrosion resistance and surface stability over time (Camarinha et al., 2025).

One of the major challenges in the design of dry electrodes is finding a balance between ensuring sufficient electrical contact for high-quality signals and maintaining a mechanical force that does not cause excessive discomfort on the scalp (Sun et al., 2025). A painless flexible dry electrode would provide better softness and adaptability but would require a hairless scalp or specific skin preparation to ensure adequate contact. Hair-equipped electrodes with micro-spikes have been found to be an effective solution for establishing sufficient skin contact while ensuring comfortable wear for adults. This balance between mechanical force and comfort is particularly crucial in neonatal applications, where ensuring optimal contact without compromising skin integrity is a major challenge. Given that the skin of newborns is much more sensitive than that of adults, the development of flexible and mechanically less rigid electrodes could be a promising approach to facilitate their adoption in neonatal environments (Asayesh et al., 2025).

To ensure optimal functionality, materials used in EEG electrode fabrication must exhibit high biocompatibility to prevent immune reactions or inflammation, high conductivity for efficient signal transmission, and sufficient flexibility to adapt to movements and maintain stable skin contact (Z. Wang, 2025). Enhancing the manufacturing techniques for flexible EEG electrodes by combining precision with simplified processes, as well as optimizing characterization methods, is essential for their further development. Exploring new materials and integrating innovative manufacturing processes could open new perspectives in the design of these electrodes. Such advancements would promote better flexibility, increased comfort, and optimized performance, thus strengthening their adoption in various portable applications (Azeem et al., 2025). The impedance of dry electrodes in contact with the scalp can reach several hundred kΩ, which remains significantly higher than that of wet electrodes, typically around a few kΩ (Erickson et al., 2024; Luiz G. Ferreira & Pimenta, 2024). Optimizing EEG electrode geometry, combined with the integration of alternative materials, could represent a significant advancement in reducing contact impedance. These challenges and innovations will define the next steps toward more efficient, durable EEG electrodes that are suitable for daily

use in various environments. Despite its limitations, EEG remains a valuable and widely used tool for studying brain function across diverse applications.

1.6 Conclusion

Dry electrodes eliminate the limitations associated with conductive gels, particularly gel drying, which compromises signal stability during long-term recordings. In contrast, conventional wet electrodes require extensive preparation steps, including skin abrasion, gel application, impedance optimization, and post-measurement cleaning. These procedures are time-consuming, operator-dependent, and prone to variability. Moreover, gel drying can induce signal degradation, skin irritation, and artefacts such as gel bridging between electrodes, thereby limiting their suitability for prolonged and real-world monitoring conditions. These constraints highlight the need for alternative electrode technologies capable of ensuring stable electrical coupling without compromising usability.

Within this context, the development of dry electrodes relies on a set of quantitatively defined performance criteria established at the outset of this work. From an electrical standpoint, the electrode/skin contact impedance should remain below 5 kΩ, while the bulk electrical conductivity of the material should be on the order of 10^{-2} S/m or higher to ensure efficient signal transmission. From a mechanical perspective, the electrode must be as flexible as possible to ensure optimal conformability to the scalp. This requirement is assessed through the storage modulus (E′), which should remain as close as possible to that of the neat soft polymer matrix, thereby preserving the intrinsic flexibility of the material and ensuring effective electrode-scalp contact over time.

From a user perspective, comfort represents a key performance criterion that must be explicitly considered. The electrode should not induce any skin irritation, discomfort, or pain during use, even over prolonged recording periods. This requirement is directly linked to the mechanical compliance of the material and its ability to maintain gentle and stable contact with the scalp without generating localized stress concentrations.

Finally, cost considerations are explicitly integrated into the design strategy by aiming to minimize the use of high-cost conductive fillers while maintaining the targeted electrical and mechanical performance.

Existing electrode technologies only partially satisfy these requirements. Microneedle electrodes achieve low impedance but are limited by fabrication complexity, mechanical fragility, and potential risks associated with skin penetration. Capacitive electrodes enable non-contact measurements but remain highly sensitive to motion artefacts. Surface dry electrodes represent a promising alternative, although challenges related to motion sensitivity and long-term stability persist.

Overall, this work highlights the central role of material design in advancing EEG electrode technologies. The results demonstrate that flexible conductive polymer composites, particularly based on hybrid conductive networks, provide a robust solution to simultaneously meet the targeted performance criteria. This approach enables the development of dry, flexible, and cost-effective multipin electrodes compatible with scalable manufacturing processes, while ensuring a high level of user comfort. Ultimately, these advances facilitate the transition of EEG systems from controlled laboratory environments toward wearable, portable, and large-scale applications, thereby expanding their accessibility and impact.

CHAPITRE 2

PROPERTIES OF POLYMER MATERIALS FOR ELECTROENCEPHALOGRAPHY

The materials used to manufacture EEG electrodes can be classified according to their electrical, mechanical, and thermal properties. This chapter focuses primarily on dielectric materials used in the fabrication of conductive polymer composites. The concepts presented provide the theoretical foundation necessary for understanding and interpreting the physical and electrical properties of the composites studied, as observed during experimental measurements and analyzed using the models discussed in this thesis. Although these concepts are addressed in several reference works, this chapter aims to gather and organize them in a coherent, easily accessible manner.

To ensure reliable, stable operation of EEG electrodes, the materials used in their manufacture must have appropriate physical properties. Among these, the electrical properties of the conductive reinforcements and the dielectric properties of the polymer matrix play a crucial role, as they directly influence the composite's electrical conductivity, the skin/electrode contact impedance, and the quality of the measured EEG signal. However, the materials used in these electrodes are also subjected to thermal, mechanical, and environmental stresses during use. Consequently, the analysis of their performance generally relies on the study of their thermal, electrical, and mechanical properties.

This classification provides an important basis for analyzing the behavior of the conductive polymer composites studied in this thesis, particularly their dielectric properties, electrical percolation phenomena, and their influence on skin/electrode contact impedance and on the quality of EEG signals.

2.1 Thermal properties

The content of this section is based primarily on the concepts and models described in the scientific literature, particularly in (McCrum et al., 1997; Oswald & Mendes, 2012a).

2.1.1 Glass transition temperature

The glass transition temperature (T_g) is a fundamental thermal property of amorphous polymers as well as of amorphous regions present in semi-crystalline polymers. This parameter is particularly important for polymeric materials such as thermoplastic elastomers (TPU, SEBS, EVA) or certain thermosetting polymers, such as PDMS, since it corresponds to the transition of the material from a rigid glassy state to a rubbery state characterized by increased molecular mobility.

The glass transition temperature depends primarily on the polymer's chemical structure, particularly the flexibility of the macromolecular chain and the intermolecular interactions present in the material. It can also be influenced by the presence of additives, solvents, or plasticizers. Indeed, the introduction of these compounds generally tends to increase the segmental mobility of the polymer chains, which most often leads to a decrease in the glass transition temperature. This variation can be estimated using a thermodynamic mixing rule, expressed by the following equation:

$$T_{gm} = \frac{\Phi_p \alpha_{tp} T_{gp} - (1 - \Phi_p) T_{gs}}{\alpha_{tp} \Phi_p + (1 - \Phi_p) \alpha_{ts}} \qquad (2\text{-}1)$$

where T_{gm}, T_{gp}et T_{gs} are respectively the glass transition temperatures of the mixture, the polymer and the solvent or plasticizer; Φ_p the volume fraction of the polymer in the mixture; α_{tp} and α_{ts} are respectively the linear coefficients of thermal expansion of the polymer and the solvent.

In immiscible polymer blends, it is common to observe two distinct glass transition temperatures, each associated with the amorphous phase of a specific polymer. The presence

of these two transitions generally reflects phase separation within the material, indicating that the constituent polymers do not form a homogeneous system at the molecular level.

The glass transition temperature can be determined experimentally using Differential Scanning Calorimetry (DSC), a technique widely used to characterize the thermal transitions of polymer materials.

In the case of flexible polymer-based EEG electrodes, the glass transition temperature directly influences the material's mechanical properties. When the operating temperature exceeds the glass transition temperature (Tg), the polymer enters a rubbery state, characterized by greater mobility of the macromolecular chains. This state gives the material improved deformability and an increased ability to conform to the irregularities of the scalp surface, thus enhancing skin-electrode contact.

In the case of EEG electrodes applied to the scalp, human skin temperature is generally between 32 and 35°C, while the operating temperature is usually ambient temperature. Therefore, polymers with a glass transition temperature lower than the scalp temperature or the operating temperature remain in a rubbery state. This state gives the material better mechanical conformity, facilitating its adaptation to the irregular surface of the scalp and contributing to the stability of the electrode/skin contact, which is essential for reliable EEG signal acquisition. The operating condition can be expressed as:

$$T_{operation} > T_g \quad (2\text{-}2)$$

where $T_{operation}$ is the material's service temperature and T_g, the glass transition temperature of the polymer or mixture.

2.1.2 Degradation temperature

One property of the polymers used in EEG electrodes is their thermal stability, which prevents thermal degradation of the material, particularly when these polymers are used as copolymers or in polymer/solvent or polymer/conductive reinforcement mixtures. Thermal degradation of polymers refers to all the chemical and physical transformations that occur when the material is subjected to high temperatures. These transformations can lead to irreversible alterations of

the macromolecular structure, thus affecting the mechanical, thermal, and electrical properties of the polymer.

To assess the thermal stability of polymers and polymer composites, one of the most commonly used techniques is thermogravimetric analysis (TGA). This method involves measuring the mass change of a sample as a function of temperature or time in a controlled atmosphere. TGA allows for the determination of several important parameters, such as the degradation onset temperature, the different stages of thermal decomposition, and the residual fraction of the material after degradation. This information is particularly useful for evaluating the thermal stability of polymer composites containing solvents, plasticizers, or conductive reinforcements. In the case of materials used to manufacture EEG electrodes, TGA analysis verifies that the polymers and composites exhibit sufficient thermal stability for the manufacturing and operating conditions.

2.1.3 block copolymers

The concept of block copolymers is presented in this section based on references available in the literature (Demazy, s. d.-a; Lahittete, s. d.-a; Oswald & Mendes, 2012b). Copolymers are polymers composed of at least two different types of monomers incorporated within the same macromolecular chain. When the monomer units are grouped into distinct segments called blocks, they are referred to as block copolymers. In these materials, each block generally corresponds to a sequence of identical repeating units, and the different blocks are linked together by covalent bonds. Depending on the organization of the monomer units along the polymer chain, several architectures can be distinguished, including random, alternating, grafted, and block copolymers. Among these architectures, block copolymers occupy a special place due to their structural and functional properties. In these systems, the different blocks generally possess distinct chemical properties, which can lead to micro-phase separation and the formation of organized domains at the nanoscale.

Block copolymers can exhibit different molecular architectures depending on the number and arrangement of the blocks. The most common structures include diblock (AB), triblock (ABA or ABC) copolymers, as well as more complex architectures such as star, branched, or

multiblock copolymers. Schematic examples of these architectures are illustrated in figure 2.1. In the context of flexible EEG electrodes, certain block copolymers are of particular interest due to the chemical structure of their different domains. For example, SEBS (styrene-ethylene-butylene-styrene) is a triblock copolymer in which rigid polystyrene domains are dispersed in an ethylene-butylene elastomer matrix, giving the material good flexibility and mechanical stability, properties important for ensuring stable electrode-skin contact during EEG signal acquisition.

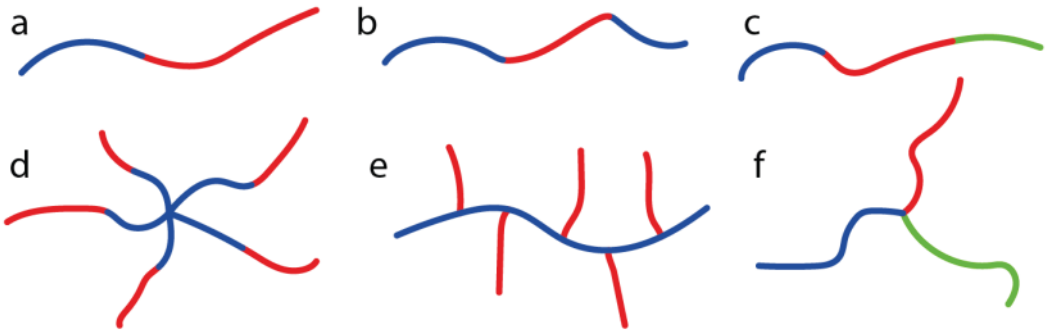


Figure 2.1 : Schematic representations of different block copolymer architectures: (a) linear diblock copolymer AB, (b) linear triblock copolymer ABA, (c) linear triblock copolymer ABC, (d) star diblock copolymer AB , (e) branched diblock copolymer AB and (f) star triblock copolymer ABC.

(Taken from (Demazy, s. d.-a))

2.1.4 Morphology of block copolymers and localization of conductive fillers

As introduced in the previous section, block copolymers (BCP) are macromolecules composed of two or more chemically distinct polymer chains covalently bonded together. Their structural organization and resulting morphologies are discussed in this section based on literature reports (Allahverdieva et al., 2023; Cabrini, s. d.; Chervanyov, 2023, 2025; Demazy, s. d.-b; Forcina, s. d.; Kakhramanov & Allahverdiyeva, 2023; Lahittete, s. d.-b; Sumita et al., 1991a; Wilkinson et al., 2022). Due to the thermodynamic incompatibility between these blocks, BCP systems exhibit microphase separation, leading to the formation of well-defined nanostructures or more complex morphologies. Unlike conventional polymer blends, the covalent linkage between blocks prevents macroscopic phase separation, confining the segregation to the nanoscale.

To better understand this behavior, it is useful to consider linear diblock copolymers of the AB type. Phase separation directly depends on the chemical affinity between the block species. Repulsive interactions between chemically distinct segments tend to minimize their contact, while the covalent bond between the blocks constrains this separation to the nanoscale. As a result, the system adopts a conformation that minimizes its free energy at thermodynamic equilibrium. The thermodynamics of this process can be described using the Flory–Huggins theory. The free energy of mixing (G_M) for a binary system is given by:

$$\frac{\Delta G_M}{K_B T} = \frac{f_A}{N_A}\ln(f_A) + \frac{f_B}{N_B}\ln(f_B) + \chi_{AB} f_A f_B \qquad (2\text{-}3)$$

where f_A and f_B are the volume fractions of blocks A and B (with $f_A + f_B = 1$), N_A and N_B are their respective degrees of polymerization, and χ_{AB} is the Flory–Huggins interaction parameter. This parameter, which represents the enthalpic contribution of the system and quantifies the incompatibility between A and B monomers, is defined as:

$$\chi_{AB} = (\frac{z}{K_B T})(\varepsilon_{AB} - \frac{1}{2}(\varepsilon_{AA} + \varepsilon_{BB})) \qquad (2\text{-}4)$$

where z is the coordination number, K_B is the Boltzmann constant, and T is the absolute temperature. The terms ε_{AB}, ε_{AA}, and ε_{BB} correspond to the interaction energies between A–B, A–A, and B–B monomer pairs, respectively.

The degree of microphase separation is governed by the product χ_N, where $N = N_A + N_B$ is the total degree of polymerization. When χ_N <10, entropic contributions dominate and the system remains disordered. As χ_N, approaches a critical value of approximately 10, the system undergoes an order–disorder transition (ODT), corresponding to the weak segregation limit (WSL). For χ_N >10, the system enters the strong segregation regime, characterized by well-defined and periodically ordered nanostructures. The equilibrium morphology depends strongly on the volume fraction of the blocks.

In addition to thermodynamic parameters, processing conditions such as thermal annealing, solvent vapor annealing, or external fields play a critical role in promoting self-assembly and driving the system toward equilibrium. These conditions influence domain orientation, periodicity, and long-range order, where interfacial effects become significant. Within this microphase-separated structure, the incorporation of conductive fillers such as carbon black

(CB) or carbon nanotubes (CNT) introduces an additional level of structural complexity. The spatial distribution of these fillers is not random but is governed by thermodynamic interactions and interfacial energies between the fillers and the polymer phases. Experimental observations, including transmission electron microscopy (TEM), reveal two main localization behaviors. First, fillers may preferentially disperse within a specific phase when their affinity for that phase is dominant, resulting in a relatively homogeneous distribution. Second, fillers may localize at the interface between the two phases when their interactions with both phases are comparable, often forming a continuous interfacial network. This localization behavior can be predicted using an interfacial energy approach based on the wetting coefficient, defined as:

$$\omega_A = \frac{\gamma_{f-B} - \gamma_{f-A}}{\gamma_{A-B}} \quad (2\text{-}5)$$

where γ_{f-A}, γ_{f-B}, and γ_{A-B} are the interfacial tensions between the filler and phases A and B, and between the two polymer phases, respectively. Depending on the value of the wetting coefficient, three localization regimes can be identified:

- $\omega_A > 1$: fillers preferentially localize within phase A
- $-1 < \omega_A < 1$: fillers localize at the A/B interface
- $\omega_A < 1$: fillers preferentially localize within phase B

These conditions demonstrate that filler distribution is governed by thermodynamic compatibility and interfacial energy minimization. In particular, interfacial localization is highly advantageous, as it promotes the formation of continuous conductive networks at lower filler loadings, thereby reducing the percolation threshold and enhancing electrical conductivity. Consequently, the spatial distribution of conductive fillers within block copolymer systems plays a crucial role in determining the final electrical properties of the composite. A controlled localization of fillers, especially at interfaces, enables the optimization of conductivity while preserving the mechanical integrity and flexibility of the material.

In the context of this thesis, these concepts are particularly relevant for SEBS-based composites filled with CB and CNT. The microphase-separated structure of SEBS, composed of rigid polystyrene domains dispersed within a soft elastomeric matrix, provides a favorable environment for selective filler localization, either within the elastomeric phase or at the interfaces between domains. Controlling this distribution represents a key strategy to achieve

an optimal balance between electrical conductivity, mechanical flexibility, and stable electrode/skin contact, which are essential requirements for the development of high-performance dry EEG electrodes.

2.2 Mechanical properties

This section is primarily based on the concepts reported in (McCrum et al., 1997).

The flexibility of the polymers used to manufacture EEG electrodes is a crucial parameter for ensuring proper electrode adaptation to the scalp surface and improving user comfort during signal acquisition. Using stress-strain curve analysis, several parameters describing the mechanical behavior of polymer materials can be experimentally determined.

Among these parameters, the modulus of elasticity E represents a fundamental quantity. It corresponds to the slope of the initial linear region of the stress-strain curve. In this region, the material exhibits elastic behavior, characterized by a proportional relationship between the applied stress and the resulting strain, in accordance with Hooke's law.

$$\sigma = E\varepsilon \qquad (2\text{-}6)$$

Or

σ : is the applied stress (Pa)

E : is the modulus of elasticity (Pa),

ε : is the relative deformation

Stress is the force applied per unit area to a material. Strain, on the other hand, is defined as the ratio of the material's elongation to its initial length. This parameter quantifies a material's ability to deform when subjected to mechanical stress.

The modulus of elasticity can be determined from various mechanical tests, such as tensile or compression tests. It can also be evaluated using dynamic mechanical analysis methods, notably Dynamic Mechanical Thermal Analysis (DMTA). This technique allows the

characterization of the viscoelastic behavior of materials by measuring the storage modulus E', associated with the elastic component of the material's response, as well as the loss modulus E'', which reflects the viscous component. These parameters can be studied as a function of temperature or frequency.

Dynamic mechanical analyses are of particular interest because they allow the mechanical behavior of materials to be characterized over time and frequency scales that are more representative of real-world operating conditions. These measurements are based on the principle that, during a dynamic mechanical stress applied to a viscoelastic material, the energy supplied to the system is distributed between two contributions: one part is stored elastically within the material, while another part is dissipated as heat due to internal viscous phenomena.

The calculation of mechanical parameters under dynamic conditions relies on the relationship between stress σ and strain ε. The stress generated in a polymer sample when subjected to a small-amplitude sinusoidal longitudinal strain ε, characterized by a frequency ω, also varies sinusoidally, but with a phase shift δ relative to the strain. The strain and stress at a given time t can be expressed as follows:

$$\varepsilon = \varepsilon_o \sin(\omega t) \tag{2-7}$$

$$\sigma = \sigma_o \sin(\omega t + \delta) \tag{2-8}$$

Where ε_o is the amplitude of the strain and σ_o is the amplitude of the stress. The stress equation can be transformed into the form:

$$\sigma = \sigma_o \sin\omega t cos\delta + \sigma_o \cos\omega t sin\delta \tag{2-9}$$

In the expression of constraint, the term $\sigma_o cos\delta$ is in phase with the deformation and corresponds to the stored elastic energy, and the term $\sigma_o sin\delta$ is phase-shifted by 90° with respect to the deformation and corresponds to the dissipated viscous energy. From the preceding equations, it is possible to define the storage modulus and the loss modulus. The storage modulus E'represents the elastic part of the mechanical response, associated with the energy stored in the material, and is given by the following equation:

$$E' = \frac{\sigma_o}{\varepsilon_o} cos\delta \quad (2\text{-}10)$$

The loss modulus E'' represents the viscous part of the response, associated with the energy dissipated as heat, and is given by the following equation:

$$E'' = \frac{\sigma_o}{\varepsilon_o} sin\delta \quad (2\text{-}11)$$

The ratio between the loss modulus and the storage modulus is defined as the loss factor, usually denoted by $tan\delta$. This parameter indicates the relative importance of viscous and elastic contributions to the viscoelastic behavior of the material. It thus allows us to assess a polymer's ability to dissipate energy as heat compared to the energy stored elastically during dynamic mechanical stress.

E' storage module is a particularly relevant parameter, as it provides a direct indication of the material's elastic stiffness. This parameter is closely linked to the polymer electrode's ability to adapt to the scalp surface while maintaining stable mechanical contact, an essential condition for ensuring the quality of EEG signal acquisition.

Dynamic modules can also be expressed as a complex module:

$$E^* = E' + iE'' \quad (2\text{-}12)$$

The complex modulus describes the dynamic mechanical behavior of polymers under small deformations. The absolute value of the complex modulus is given by:

$$E = \sqrt{E'^2 + E''^2} \quad (2\text{-}13)$$

In the case of flexible EEG electrodes, the mechanical properties of the polymers play a crucial role in device performance. The materials used must exhibit a relatively low modulus of elasticity or storage modulus to ensure good flexibility and mechanical conformity to the curved surface of the scalp. This mechanical conformity promotes better skin/electrode coupling, which helps reduce contact impedance and improve EEG signal stability. Therefore, evaluating the mechanical properties of the materials used in the manufacture of EEG electrodes is essential for optimizing the design of flexible dry EEG electrodes.

2.3 Electrical property

This section presents a synthesis of knowledge from the scientific literature and is based mainly on the work reported in (Gnonhoue, 2021; M. Guo, 2017; Heid, 2015; Helgeson, 2000; Kremer & Schönhals, 2003; Oswald & Mendes, 2012a).

2.3.1 Dielectric behavior

2.3.1.1 Dielectric coefficient

Dielectric materials are distinguished by the absence of free charges capable of moving over long distances within their structure. However, under the influence of an external electric field, local charge shifts can occur within the molecular chains of polymers.

To describe the dielectric behavior of materials, one of the most commonly used electrical properties is relative permittivity, denoted by ε_r. This dimensionless quantity characterizes a material's ability to become polarized when subjected to an electric field. Its value depends on several factors, including the nature of the material, the temperature, and the frequency of the applied electric field.

To introduce the concept of dielectricity, we can consider the case of a parallel plate capacitor consisting of two circular electrodes, connected to an electrical circuit as shown in figure 2.2. In this system, the accumulated electric charge Q on the electrodes is proportional to the voltage applied across its terminals U.

$$Q = CU \tag{2-14}$$

Or :

Q : stored electrical charge (C)

C : electrical capacitance of the capacitor (F)

U : applied voltage differential (V)

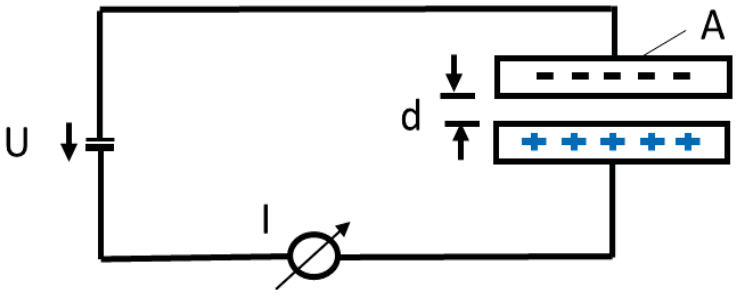


Figure 2.2 : Circuit for measuring the capacitance of a capacitor

The constant of proportionality C is called capacitance. The capacitance of an infinite capacitor with parallel plates under no-load conditions is defined by:

$$C_o = \varepsilon_o \frac{A}{d} \qquad (2\text{-}15)$$

Or :

C_o : capacitance of the capacitor in a vacuum (F)

ε_o : vacuum permittivity (8.85×10 −12 $F{\cdot}m$ −1)

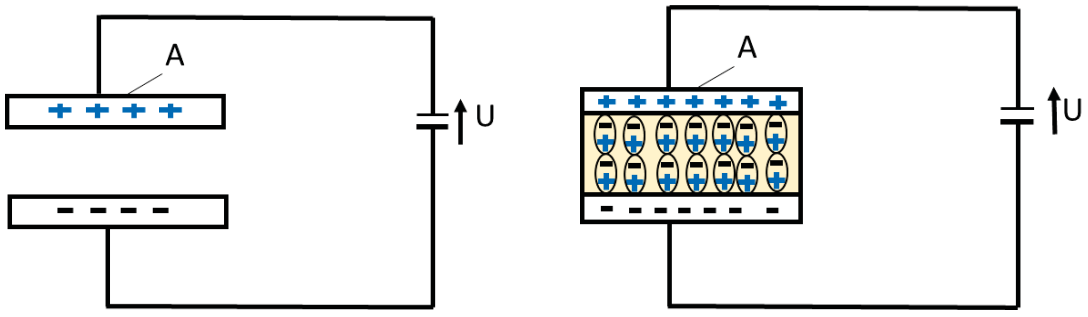
A : area of the capacitor plates (m²)

d : distance between the plates (m)

Thus, the electrical charge stored in the vacuum capacitor is given by:

$$Q_o = C_o U \qquad (2\text{-}16)$$

When a dielectric material is placed between the plates of a capacitor, the amount of charge stored in the capacitor changes. This change results from the action of the applied electric field, which causes the appearance of polarization charges within the dielectric material (figure 2.3). These charges arise from the local displacement of bound charges or the orientation of the dipoles present in the material. This polarization phenomenon is illustrated in figure 2.4.



a) b)

Figure 2.3: Illustration of the polarization charges in a capacitor: a) configuration without dielectric, b) configuration with a dielectric material between the plates

The new charges appearing between the metal plates of the capacitor are called Q_P. Thus, the total charge becomes:

$$Q = Q_o + Q_P \tag{2-17}$$

Or:

Q: total charge stored in the capacitor (C)

Q_o: charge in a vacuum (C)

Q_P : polarization charge induced in the dielectric (C)

In general, the load can be expressed per unit area:

$$\frac{Q}{A} = \frac{Q_o}{A} + \frac{Q_P}{A} = D \tag{2-18}$$

Or:

A: area of the capacitor plates (m^2)

D: electrical displacement density or electric flux ($C \cdot m^{-2}$)

By introducing the intensity of the electric field E, the previous equation can be rewritten as:

$$E = \frac{U}{d} = \frac{1}{\varepsilon_o}\frac{Q_o}{A} = \frac{1}{\varepsilon_o \varepsilon_r}\frac{Q}{A} \quad (2\text{-}19)$$

Or :

E: intensity of the electric field ($V \cdot m^{-1}$)

U: applied voltage differential (V)

d : distance between the capacitor plates (m)

ε_o : vacuum permittivity ($F \cdot m^{-1}$)

ε_r : relative permittivity of the material

The final result is:

$$\frac{Q_o}{A} = \varepsilon_o E \qquad \text{under a vacuum} \quad (2\text{-}20)$$

$$\frac{Q}{A} = \varepsilon_r \varepsilon_o E \qquad \text{with a dielectric} \quad (2\text{-}21)$$

These relationships show that the electric charge density is proportional to the applied electric field.

2.3.1.2 Polarization Mechanisms

When an electric field is applied to a dielectric material, the dipoles present in the material tend to align themselves with the field. However, this alignment does not occur instantaneously and is generally accompanied by a time delay related to the mobility of the bound charges within the material. This rearrangement of the dipoles results in the appearance of electric polarization.

Polarization thus corresponds to a change in the distribution of electric charges within the material under the influence of an external electric field. This phenomenon is associated with the orientation or displacement of bound charges within the molecular structure of the material.

An electric dipole consists of two charges of opposite signs, $+Q$ and $-Q$, separated by a certain distance. The electric dipole moment associated with this system is defined by the following relation:

$$\vec{p} = q\vec{l} \tag{2-22}$$

Figure 2.4 illustrates the structure of an electric dipole.

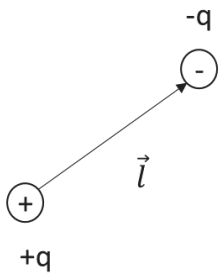


Figure 2.4 : Electric dipole

The polarization due to these dipoles corresponds to the vector sum of all the dipoles per unit volume. Therefore, the polarization P can be defined as:

$$\vec{P} = \frac{1}{\Omega}\sum_{i\in\Omega} \vec{P_i} \tag{2-23}$$

Polarization is expressed in coulombs per square meter C/m^2 . This physical quantity therefore represents the density of electric dipoles present in a given volume of material.

To illustrate this phenomenon, we can consider the case of a parallel-plate capacitor. Consider a capacitor initially charged and then disconnected from the voltage source before a dielectric material is introduced between its plates. The voltage measured across the capacitor decreases after the dielectric is inserted. This behavior is explained by the polarization of the material, which generates an internal electric field opposing the applied field. Consequently, the introduction of the dielectric results in an increase in the capacitor's capacitance.

In this context, it is possible to define the polarization charge density at the surface of the dielectric material by the following relationship:

$$P = \frac{Q_P}{A} \tag{2-24}$$

This results in the total load per unit area becoming:

$$D = \varepsilon_o E + P \tag{2-25}$$

This relationship can be rewritten as:

$$P = D - \varepsilon_o E \tag{2-26}$$

Using the previous relationships for the dielectric charge density per unit area, we obtain:

$$D = \varepsilon_o \varepsilon_r E \tag{2-27}$$

Substituting this relationship into the previous equation, we obtain:

$$P = \varepsilon_o \varepsilon_r E - \varepsilon_o E \tag{2-28}$$

$$P = \varepsilon_o(\varepsilon_r - 1)E = \varepsilon_o \chi E$$

In the case of a linear, homogeneous, and isotropic dielectric material, the induced polarization in the material is proportional to the applied electric field. In other words, when the material is subjected to an external electric field, the relationship between the polarization $\vec{P}$and the applied field $\vec{E}$is linear. Therefore, we can write:

$$\vec{P} = \varepsilon_o \chi \vec{E} \tag{2-29}$$

The quantity χ, called dielectric susceptibility, characterizes a material's ability to become polarized when subjected to an electric field. It represents a measure of a material's capacity to become polarized under the influence of an electric field.

At the microscopic level, several mechanisms can contribute to the polarization of a material subjected to an electric field. Among these, two molecular mechanisms play a particularly important role: displacement polarization, associated with the relative movement of positive and negative charges within atoms or molecules, and orientation polarization, which results from the alignment of permanent dipoles present in the material under the action of the electric field.

Under the influence of an applied electric field, the charges present in a material can undergo a relative displacement. This displacement can correspond either to a deformation of the electron cloud around the atomic nucleus, called electronic polarization, or to a relative displacement of positive and negative ions in ionic materials, known as ionic polarization.

These mechanisms result from the displacement of charges under the influence of the electric field and are generally grouped under the term displacement polarization. This phenomenon is illustrated in figure 2.5.

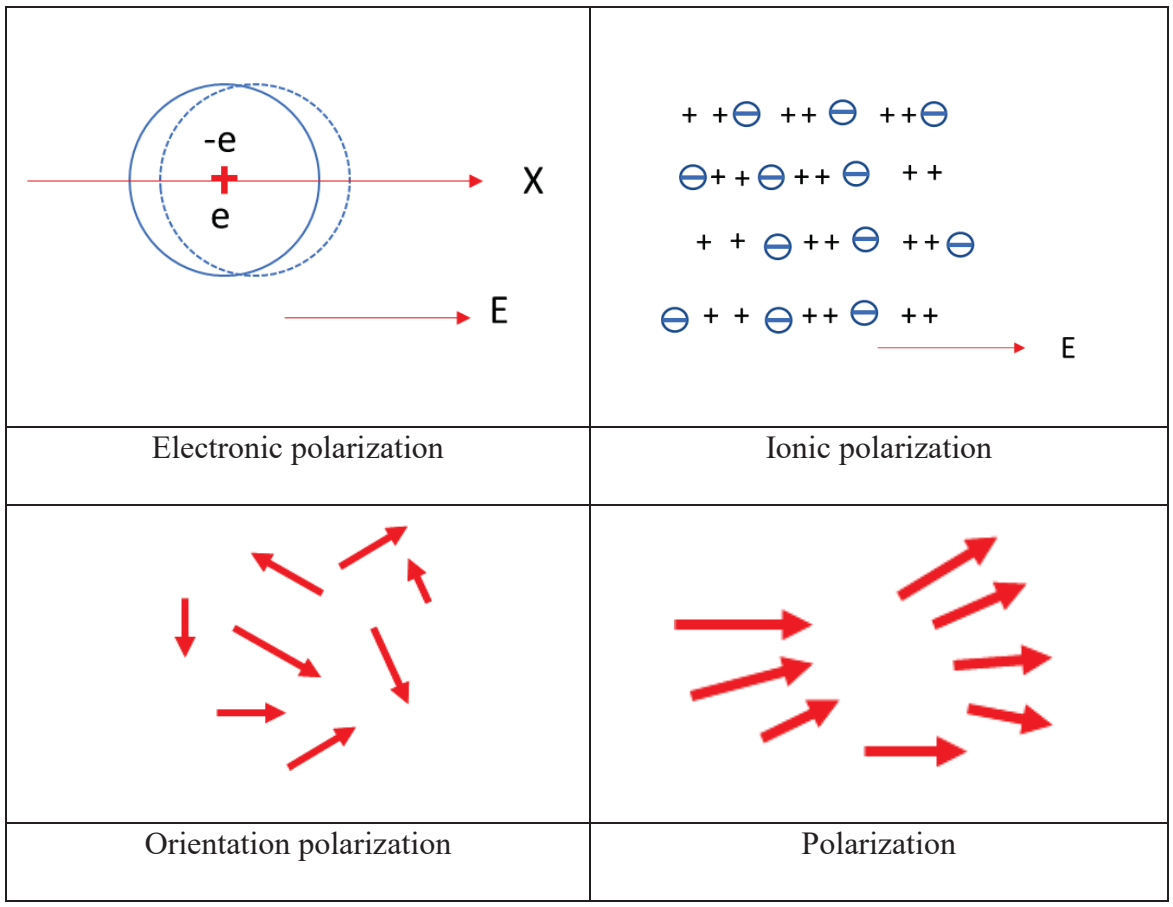


Figure 2.5 Polarization process

Due to their molecular structure, some molecules possess a permanent dipole moment even in the absence of an external electric field. When an electric field is applied, these permanent dipoles tend to gradually align themselves in the direction of the field. The degree of alignment

depends, in particular, on the intensity of the applied electric field. This mechanism is called orientational polarization and is also illustrated schematically in Figure 2.4.

The alignment or reorientation of molecular dipoles under the influence of an electric field is not instantaneous and requires a certain amount of time. Consequently, orientational polarization generally occurs more slowly than displacement polarization. The time required for this reorientation also increases when the viscosity of the surrounding medium is higher, because the mobility of the molecular dipoles is then more limited.

In the case of an alternating electric field applied at high frequency, the dipoles present in the material do not always manage to instantaneously follow the variations in the electric field. Beyond a certain characteristic frequency, the orientation of the dipoles exhibits a phase shift relative to the applied field. This phenomenon is known as dielectric relaxation.

Dielectric relaxation is generally associated with dielectric losses, which correspond to a dissipation of energy in the form of heat due to the internal movements of polar molecules.

When the electric field varies over time, it is often useful to describe this phase shift between the polarization and the electric field using complex algebra. In this context, the electric susceptibility is represented by a complex, dimensionless quantity. The expression for the complex susceptibility can then be written as follows:

$$\chi*(\omega) = \chi'(\omega) - j\chi''(\omega) \qquad (2\text{-}30)$$

When the polarization of a material is associated with a dipolar relaxation mechanism characterized by a time constant τ, the frequency dependence of the complex susceptibility can be described using the Debye model. This model provides a simplified approach to representing the dielectric relaxation phenomenon, although it does not always perfectly match experimental observations in real materials.

In this context, the variation of the complex susceptibility as a function of angular frequency can be expressed using Debye's equations, which allow us to describe the frequency behavior of materials exhibiting dipolar relaxation.

$$\chi'(\omega) = \chi_\infty + \frac{(\chi_s - \chi_\infty)}{1 + \omega^2\tau^2} \quad (2\text{-}31)$$

$$\chi''(\omega) = \frac{(\chi_s - \chi_\infty)\omega\tau}{1 + \omega^2\tau^2} \quad (2\text{-}32)$$

The Debye equations for complex permittivity as a function of frequency are:

$$\varepsilon'(\omega) = \varepsilon_\infty + \frac{(\varepsilon_s - \varepsilon_\infty)}{1 + \omega^2\tau^2} \quad (2\text{-}33)$$

$$\varepsilon''(\omega) = \frac{(\varepsilon_s - \varepsilon_\infty)\omega\tau}{1 + \omega^2\tau^2} \quad (2\text{-}34)$$

With ε_s, la permittivité électrique statique (pour $f = 0$); ε_∞, laelectrical permittivity at infinite frequency and ω, la electrical pulsation ($\omega = 2\pi f$).

The real and imaginary permittivities are influenced by temperature as well as frequency. The relaxation time depends on temperature, with a dependence that often follows the form of the Arrhenius law:

$$\tau = \tau_0 e^{e_a/kT} \quad (2\text{-}35)$$

With e_a,the activation energy; k, la Boltzmann constant.

The following equation describes the contribution associated with induced polarization. This component results primarily from electronic and ionic polarization mechanisms, which are characterized by very short response times. For frequencies below optical frequencies, the delay between induced polarization and the applied electric field can be considered negligible. Under these conditions, induced polarization can be assumed to be proportional to the applied electric field and is expressed by the following relationship:

$$\vec{P}_r = N_i \alpha_r \vec{E} \quad (2\text{-}36)$$

Where $P_{r,}$ denotes the rapid polarization, that is, the polarization that occurs very quickly after the application of an electric field. N_i represents the number of induced dipoles per unit volume, and α_r is the polarizability, which depends on the nature of the material. The total polarization, including the induced dipoles and the orientation of the permanent dipoles, can be expressed as:

$$\vec{P}_{tot} = \left(\frac{N_d \mu^2}{3kT} + N_i \alpha_r\right)\vec{E} \quad (2\text{-}37)$$

where μ is the dipole moment of the permanent dipole, N_d the number of these dipoles per unit volume, T the temperature in Kelvin and k the Boltzmann constant (k = 1.38 x 10^{-23} J/K).

In the time domain, the polarization phenomenon manifests itself in two forms: rapid polarization P_∞, which reacts quickly to the voltage demand, and polarization corresponding to dipolar relaxation phenomena P_d (t)(that which reacts with a delay).

The dipole polarization in the time domain, according to the Debye model, is:

$$P_d(t) = P_{ds}(1 - e^{-t/\tau}) \quad (2\text{-}38)$$

With $P_{ds}$the dipolar polarization at equilibrium and τ, the relaxation time

The total polarization P(t) in the time domain is the sum of the fast polarization and the dipolar polarization.

$$P(t) = P_\infty + P_{ds}(1 - e^{-t/\tau}) \quad (2\text{-}39)$$

One of the important parameters for evaluating the polarization mechanisms of a dielectric material is the relative permittivity, or dielectric constant. It is a physical property of dielectric materials. Like susceptibility, it is a complex number.

One of the essential parameters for analyzing polarization mechanisms in dielectric materials is the relative permittivity, also called the dielectric constant. Like electrical susceptibility,

permittivity can be described using a complex quantity. The relative permittivity, or dielectric constant, is described by the following expression:

$$\varepsilon_r = 1 + \chi = \frac{\varepsilon}{\varepsilon_0} \tag{2-40}$$

With ε_0, the permittivity of free space, and ε, the permittivity of the material.

Unlike orientational polarization, the variations associated with displacement polarization occur so rapidly that they can even follow a light wave. Therefore, the refractive index of light, n, is determined by the displacement contribution to the dielectric constant. The relationship between n and $\varepsilon_v$is given by:

$$n = \sqrt{\varepsilon_v} \tag{2-41}$$

This relationship allows us to measure polarization properties, because the polarization of electrons determines the refractive index of polymers.

A more comprehensive equation describing dielectric relaxation in heterogeneous materials can be described by the Maxwell–Wagner–Sillars (MWS) theory, which explains the interfacial polarization appearing in multiphase composites. This theory is based on a matrix/reinforcement model, in which a reinforcing phase (denoted *f*) is dispersed within a matrix (denoted *m*). Both phases are subjected to an external electric field and contribute to the overall dielectric behavior of the composite. Within this framework, the effective complex relative permittivity ε_r^* can be expressed as a function of the dielectric properties of the constituents and the average electric fields in each phase:

$$\varepsilon_r^*(\omega) = \frac{E_m \varphi_m \varepsilon_m^*(\omega) + E_f \varphi_f \varepsilon_f^*(\omega)}{E} \tag{2-42}$$

Where $\varphi_m$and $\varphi_f$represent respectively the volume fractions of the matrix and the reinforcement, while E_m, $E_f$and Ecorrespond to the average electric fields in the matrix, in the reinforcement particles and in the composite.

The electric field in the composite can be expressed as a weighted average of the electric fields of the constituents:

$$E = E_m\varphi_m + E_f\varphi_f \quad (2\text{-}43)$$

Materials containing air pockets have a dielectric permittivity $\varepsilon_{air} = 1$and metallic charges have a permittivity $\varepsilon_{metal} = \infty$.

2.3.1.3 Dielectric dissipation factor

The displacement or reorientation of molecules, particularly during dipolar or ionic polarization phenomena under the influence of an alternating electric field, leads to internal friction and, consequently, heating of the dielectric material. To describe this behavior and the associated losses, it is common to use an equivalent electrical circuit, such as the one shown in Figure 2.6, which allows for modeling the dielectric response of the material subjected to an alternating electric field.

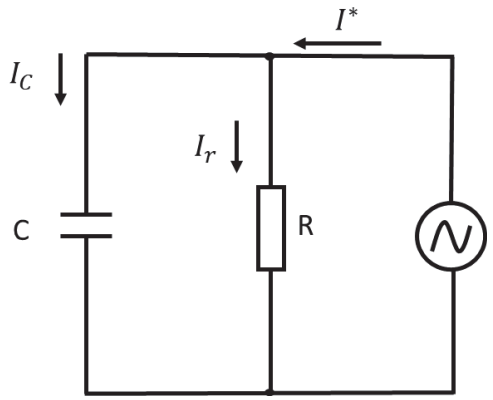


Figure 2.6: Equivalent circuit used to model losses in a dielectric material

Let us consider that an alternating current flows in this circuit, with an effective voltage *U* volt and an angular frequency defined by $\omega = 2\pi f$.

Where *f* is the frequency in hertz (Hz). In such a system, $I^*$the current phasor is either a complex number containing a real part (in phase with the voltage) and an imaginary part (out of phase by 90 ° with the voltage), or a resistive or lossy component.I_r and a capacitive component I_C.

In the frequency domain, the capacitor impedance, which is the inverse of a capacitor's admittance, is: $Y(\omega)$

$$Z^*(\omega) = \frac{U^*}{I^*} = \frac{1}{Y^*(\omega)} \tag{2-44}$$

In the case of the admittance and impedance relationships of the capacitor, *I* is the current phasor. It is usually a complex number.

In the case of an alternating current regime, capacitance can be described by a complex quantity, allowing for the simultaneous consideration of energy storage and dissipation phenomena. The complex capacitance is then related to the applied electric current and voltage by the following equation:

$$I^*(\omega) = j\omega C^*(\omega)U^*(\omega) \tag{2-45}$$

$$I^*(\omega) = \omega C_o[(\frac{\sigma}{\omega\varepsilon_o} + \varepsilon_r''(\omega)) + j\varepsilon_r'(\omega)]U^*(\omega)$$

The complex relative permittivity of a material can be expressed in the form:

$$\varepsilon_r^* = \varepsilon_r' - \varepsilon_r'' \tag{2-46}$$

Orε_r^* represents the complex relative permittivity, ε_r'corresponds to the real part of the permittivity, associated with the storage of electrical energy in the material, and ε_r'' represents the imaginary part of the permittivity, associated with dielectric losses.

The complex capacity is given by:

$$C^*(\omega) = C'(\omega) - jC''(\omega) = C_o[\varepsilon_r'(\omega) - j(\varepsilon_r''(\omega) + \frac{\sigma}{\omega\varepsilon_o})] \tag{2-47}$$

σ : is the conductivity of the dielectric material

It should be noted that during an experimental measurement of the imaginary part of the capacitance, the contribution of dielectric losses cannot be distinguished from that of conductivity, such that the measured imaginary permittivity corresponds to

$$\varepsilon_{r,exp}''(\omega) = \varepsilon_r''(\omega) + \frac{\sigma}{\omega\varepsilon_o}$$

The tangent of the loss angle or the dielectric dissipation factor is given by

$$\mathrm{tg}\delta(\omega) = \frac{C''(\omega)}{C'(\omega)} = \frac{\frac{\sigma}{\omega\varepsilon_o} + \varepsilon_r''(\omega)}{\varepsilon_r'(\omega)} \tag{2-48}$$

The current *I* flowing through a capacitor is not exactly in quadrature phase with the voltage *U* across its terminals. The loss angle δ is the complement of the phase angle θ φbetween the voltage and the current.

2.3.2 Electrical conductivity

Electrical conductivity is a key parameter for describing the transport of free charges in a material. It relates the electric current density to the applied electric field. Electrical conductivity σis given by:

$$\sigma = \frac{1}{R}\frac{A}{d} \tag{2-49}$$

The resistance to the passage of current, *R*, can be expressed by:

$$R = \frac{1}{\sigma}\frac{d}{A} \tag{2-50}$$

Resistance, like impedance, therefore depends on both the properties of the material and geometric parameters. Resistance is often described as the inverse of conductance *G* and can be expressed as:

$$R = \frac{1}{G} \tag{2-51}$$

Electrical conductivity, on the other hand, is defined as the inverse of resistivity ρ. It can also be expressed as:

$$\sigma = \frac{1}{\rho} \tag{2-52}$$

In the frequency domain, the expression for complex conductivity is given by:

$$\sigma^*(\omega) = \sigma'(\omega)+j\sigma''(\omega) \quad (2\text{-}53)$$

Or :

- $\sigma^*(\omega)$: conductivity (S m^{-1})
- $\sigma''(\omega)$: the imaginary part of the complex conductivity ($S\cdot m^{-1}$)
- $\sigma'(\omega)$: the real part of complex conductivity ($S\cdot m^{-1}$)

The relationship between complex conductivity and complex permittivity is as follows:

$$\sigma^*(\omega) = j\omega\varepsilon_o\varepsilon^*(\omega)= \sigma_{dc}+j\omega\varepsilon_o\varepsilon^*(\omega) \quad (2\text{-}54)$$

$$\varepsilon^*(\omega) = \varepsilon'(\omega)-j\varepsilon''(\omega) \quad (2\text{-}55)$$

The real part of the complex conductivity can therefore be expressed as follows:

$$\sigma'(\omega) = \sigma_{dc}+\omega\varepsilon_o\varepsilon''(\omega) \quad (2\text{-}56)$$

$$\sigma_{dc}=\lim_{\omega\to 0}\sigma'(\omega) \quad (2\text{-}57)$$

Where $\sigma'(\omega)$ represents the real part of the measured complex conductivity. Electrical conductivity is an intrinsic property of a material. σ_{DC} is the direct conductivity, which is equivalent to that defined in equations (1.51) and (1.53) and represents the value of $\sigma'(\omega)$at low frequencies. The component $\sigma_{AC}(\omega)$is a frequency-dependent component, which can generally be approximated by:

$$\sigma_{AC}(\omega) = C\omega^s \quad (2\text{-}58)$$

The exponent *s* in equation (2.55) is usually less than one, and *C* is a constant.

2.3.3 Percolation theory

In insulating matrices loaded with conductive particles, electrical conductivity increases sharply when the charge concentration exceeds the percolation threshold. This behavior is described by the percolation theory, according to which conductivity can be expressed as:

$$\sigma_{DC} = k(\varphi - \varphi_C)^t \quad (2\text{-}59)$$

Where k is a constant, *t* is the critical exponent, φis the volume fraction of conductive particles, and is $\varphi_C$the volume fraction at the critical concentration. Direct current (DC) conductivity is generally not equivalent to the real part of the complex alternating current (AC) conductivity. However, AC conductivity measurements are widely used because modern dielectric spectrometers allow accurate measurement of the electrical conductivity of conductive and insulating materials over a very wide range, from about 10^{-16} to several hundred S/m.

Volume fraction φ, of the conductive charges was calculated from equation (2.60).

$$\varphi = \frac{\omega/\rho_r}{\omega/\rho_r + (1-\omega)/\rho_m} \quad (2\text{-}60)$$

Where *ω* corresponds to the mass fraction, *ρ* to the density, and the indices *a* and *m* refer respectively to the reinforcement and the matrix.

These relationships are essential for understanding the influence of conductive fillers in the polymer composites used to manufacture EEG electrodes. The addition of fillers alters the effective dielectric permittivity at low concentrations and drastically changes the material's conductivity at higher concentrations. These phenomena have a direct impact on the composite's electrical properties, as well as on the electrode/skin contact impedance and, consequently, on the quality and stability of the recorded EEG signals.

2.3.4 Skin/electrode contact impedance

The content presented in this section is based primarily on the knowledge established in (Chi et al., 2010; Lim et al., 2007).

To understand the concept of skin-electrode contact impedance, we can consider that the skin, the electrode, and the skin-electrode interface are modeled by electrical impedances in series. The total impedance of the system then corresponds to the sum of the different contributions associated with the biological tissues ($Z_{tissues}$), the skin-electrode interface ($Z_{Skin/electrode}$), and the electrode ($Z_{electrode}$) itself:

$$Z_t = Z_{tissues} + Z_{Skin/electrode} + Z_{electrode} \quad (2\text{-}61)$$

In an EEG acquisition system, an internal differential amplifier measures the potential difference between a measuring electrode and a reference electrode placed on the scalp. The measurement system can be modeled as a voltage divider, where the source impedance Z_t corresponds to the total impedance of the electrode, the skin/electrode interface, and the biological tissues, while Z_{in} represents the input impedance of the amplifier.

The voltage measured at the amplifier output can then be expressed as:

$$V_{meas} = V_{bio} \frac{Z_{in}}{Z_{in} + Z_t} \quad (2\text{-}62)$$

Where V_{meas},is the voltage measured by the acquisition system, V_{bio} is the bioelectrical potential generated by brain activity.

In many cases, the electrical conductivity of biological tissues and the electrode material is relatively high, implying that their electrical resistances are relatively low. Consequently, the dominant contribution of the source impedance usually comes from the contact impedance at the skin/electrode interface. If we consider that the impedances associated with the electrode and the biological tissues remain approximately constant, the main variable influencing the total impedance becomes the contact impedance. This latter depends on several environmental and physiological factors, such as the presence of sweat, hair density, and the actual contact area between the electrode and the curved surface of the scalp.

The preceding equation thus shows that the quality of the measured signal depends strongly on the ratio between the amplifier's input impedance and the source impedance. To avoid any attenuation of the bioelectrical signal, the amplifier's input impedance must be much higher than the total system impedance.

$$Z_{in} >> Z_t \quad (2\text{-}63)$$

Under these conditions, the measured voltage becomes approximately:

$$V_{meas} \approx V_{bio} \quad (2\text{-}64)$$

This minimizes signal loss and improves the quality of EEG measurements. Therefore, reducing skin/electrode contact impedance is a key parameter in the design of high-performance EEG electrodes. In this context, the use of conductive polymer composites with both high electrical conductivity and good mechanical conformity to the scalp surface reduces contact impedance and improves the stability of recorded EEG signals.

One parameter to consider when acquiring EEG signals is the signal-to-noise ratio (SNR). EEG signals typically have an amplitude on the order of a few microvolts, which is significantly lower than that of electromyography (EMG) signals, and also operate in a lower frequency range. Under these conditions, the presence of noise can easily mask the useful signal, making it essential to maintain a high signal-to-noise ratio for reliable detection and interpretation of EEG signals. To properly visualize and analyze EEG signals, the amplitude of the biological signal must be greater than the noise present in the measurement system. In other words, the useful signal generated by brain activity must be sufficiently high relative to noise sources, such as electronic noise from the amplifier, electromagnetic interference, or fluctuations at the electrode-skin interface.

The signal-to-noise ratio can be expressed as:

$$\mathrm{SNR} = \frac{\mathrm{P_{signal}}}{\mathrm{P}_{noise}} \tag{2-65}$$

Where $\mathrm{P_{signal}}$ represents the EEG signal power and P_{noise}, the noise power. A high SNR is essential to ensure reliable detection of brain signals and improve the quality of EEG measurements. In this context, reducing the skin-electrode contact impedance and using electrodes with good electrical and mechanical properties helps improve the signal-to-noise ratio by reducing signal loss and disturbances associated with the electrode/skin interface.

A stable amplitude of the EEG signal is obtained when several key conditions are met:

- The electrical conductivity of the composite exceeds the percolation threshold, allowing the formation of continuous conductive paths within the material.
- The electrode material storage module ensures good mechanical conformity with the scalp surface, thus promoting better quality skin/electrode contact.
- The contact impedance (or total system impedance) remains significantly lower than the amplifier input impedance, allowing efficient voltage transfer without signal attenuation.
- The level of electrical noise remains low, ensuring a signal-to-noise ratio high enough for reliable detection and interpretation of EEG signals.

2.4 Dispersion and Distribution

The notion of dispersion and distribution is sometimes difficult to distinguish, and the following elements from the literature (Bisht et al., 2025; Bokobza, 2023; Griffin et al., 2022; X. Li et al., 2022; B. Luo et al., 2023; Mazitova et al., 2022; Olonisakin et al., 2022; Öztürkmen et al., 2023; Pavlyuchkova et al., 2024; Subramanian et al., 2022; Sumita et al., 1991b; Wen et al., 2022; Z. Xie et al., 2022) help clarify their differences. Dispersion refers to the state of deagglomeration of fillers within the polymer matrix. It describes the ability of particles to remain individualized and to limit the formation of agglomerates. In nanocomposites, dispersion occurs across multiple length scales, as primary nanoparticles may form submicron agglomerates that can further connect into larger networks when the filler volume fraction increases. Good dispersion enhances interfacial interactions and contributes to more uniform material properties, whereas poor dispersion leads to heterogeneities, local stress concentrations, and degradation of mechanical and functional performance. Distribution, in contrast, describes the spatial arrangement of fillers within the material, particularly in multiphase systems. The literature shows that fillers may either be predominantly localized within one phase or concentrated at the interface between two phases, depending on interfacial energies and processing conditions. This spatial distribution directly affects the formation of conductive networks and, consequently, the electrical properties of the composite.

Processing methods play a critical role in achieving adequate dispersion. Techniques such as melt mixing, high-shear mixing, ultrasonic dispersion, and solution processing are commonly used to reduce agglomeration. However, increasing filler content can increase viscosity and promote aggregation, making dispersion control more challenging. The evaluation of dispersion and distribution relies on morphological characterization techniques such as scanning electron microscopy (SEM) and transmission electron microscopy (TEM), often combined with statistical analysis. These approaches enable the observation of agglomeration states, identification of filler localization within different phases, and assessment of distribution uniformity. Complementary techniques such as energy-dispersive X-ray spectroscopy (EDS) mapping and X-ray diffraction (XRD) can further support this analysis.

In the context of this thesis, these concepts are particularly important for SEBS-based and EVA composites filled with CNTs and/or CB. Filler dispersion governs the formation of an effective conductive network at the local scale, while its distribution within the microstructure controls the global connectivity of this network. Both aspects are directly related to the electrical performance of the electrodes, particularly contact impedance and EEG signal stability, and are therefore key parameters in the development of flexible dry EEG electrodes.

2.5 Electrophysiological activity: EEG and EMG signals

The content presented in this section is primarily based on references available in the literature (Abdulhameed et al., 2025; Gougeh, s. d.; Karacan & Türker, 2025; Kushwah et al., 2025; Moumane, s. d.; S. Shi et al., 2025; Veronica et al., 2024) to briefly describe the main characteristics of the electrophysiological signals measured in this work, particularly electroencephalography (EEG) and electromyography (EMG) signals. The aim is to define the amplitude and frequency ranges of the signals studied, as well as the main frequency bands associated with brain activity.

2.5.1 Brain activity and EEG frequency bands

Electroencephalography (EEG) measures the electrical activity of cortical neurons using electrodes placed on the scalp. EEG signals are characterized by relatively low amplitudes, typically ranging from a few microvolts to a few hundred microvolts, and by a frequency band typically between 0.5 and 40 Hz in clinical applications, although some studies may analyze higher frequencies. The brain rhythms observed in EEG signals correspond to synchronized oscillations of neuronal populations and are generally classified into different frequency bands associated with specific physiological or cognitive states.

Delta waves correspond to the lowest frequency band, between 0.5 and 4 Hz, and generally exhibit the highest amplitudes among EEG rhythms. They are primarily observed during deep sleep and are associated with brain recovery and repair processes. Theta waves, with frequencies generally between 4 and 8 Hz, often appear during states of drowsiness, deep relaxation, or during certain cognitive activities involving memory and emotional processing.

Alpha waves, located in the frequency band of 8 to 12 Hz, are generally observed in an awake but relaxed individual, particularly when the eyes are closed. These oscillations are often more pronounced in the occipital regions of the brain. Beta waves, between 13 and 30 Hz, generally correspond to states of active wakefulness, concentration, or cognitive activity. They are frequently observed in the frontal and central regions of the brain. Finally, gamma waves, whose frequency is generally greater than 30 Hz, are associated with complex cognitive processes such as attention, perception, and sensory integration.

These different frequency bands allow for the interpretation of brain activity in various physiological and cognitive contexts and constitute an important reference for the analysis of EEG signals.

2.5.2 EMG signals

Electromyography (EMG) measures the electrical activity generated by muscle fibers during their activation. Unlike EEG signals, which originate primarily from cortical neuronal activity, EMG signals result from the action potentials of muscle motor units during muscle contraction. Intracellular recordings show that the action potentials of muscle fibers can reach amplitudes on the order of 100 mV. In terms of frequency content, the power spectrum of EMG signals is generally broader than that of EEG signals and can range from a few hertz to several hundred hertz, or even up to several kilohertz.

2.5.3 Comparison of the characteristics of EEG and EMG signals

EEG and EMG signals exhibit distinct characteristics in terms of biological source, amplitude, and frequency band. EEG signals originate primarily from the activity of cortical neurons and have relatively low amplitudes, typically between 10 and 100 μV, with a frequency band approximately between 0.5 and 40 Hz. Conversely, EMG signals, generated by the activity of muscle fibers, generally have higher amplitudes and a wider frequency band, extending up to several hundred hertz.

These differences are important in the context of bioelectrical signal acquisition, as they influence acquisition parameters, filtering techniques, and the design of electrodes used for signal recording.

In this thesis, the polymer electrodes developed are primarily intended for the acquisition of EEG signals, characterized by low amplitudes and a relatively narrow frequency band. Therefore, the quality of electrode-skin contact, mechanical stability, and electrical noise reduction are essential parameters for ensuring reliable acquisition of brain signals.

2.6 The concept of comfort in EEG electrodes

The content of this section is based on a comprehensive analysis of the literature on EEG electrodes, wearable neurotechnology, and user-centred device design (Fiedler et al., 2016, 2018b; Haueisen et al., 2020; Knight & Baber, 2005; Moumane, s. d.; Y. Peng et al., 2022; Rahman et al., 2023; H. Ren et al., 2024; Taji et al., 2018; Vasconcelos et al., 2021; Z. Wang et al., 2025; Warsito et al., 2023a; Yoon et al., 2024) including experimental and review studies addressing comfort, signal quality, and electrode/skin interaction. Comfort is a critical parameter in the evaluation of electroencephalography (EEG) systems, particularly in the context of wearable and long-term monitoring applications (Haueisen et al., 2020; Y. Peng et al., 2022; Rahman et al., 2023). Unlike electrical or mechanical properties, comfort cannot be defined as a single physical quantity, as it is inherently subjective and depends on individual perception, physiological conditions, and duration of use (Knight & Baber, 2005; H. Ren et al., 2024). Despite this limitation, several studies have attempted to operationalize comfort through experimental protocols, most commonly using subjective rating scales (Fiedler et al., 2016; Vasconcelos et al., 2021; Warsito et al., 2023a). In EEG research, comfort is typically quantified using self-reported numerical scales. For example, (H. Ren et al., 2024) evaluated comfort using a scale from -5 to 5, measured at multiple time points after electrode application. Their results demonstrated a progressive decrease in comfort over time, highlighting the strong dependence of comfort on wearing duration. In particular, hybrid headbands integrating flexible multipin showed significantly better comfort scores compared to systems requiring higher mechanical pressure, especially after prolonged. These findings are consistent with other experimental studies comparing dry electrode technologies, which also report that

comfort decreases as contact force and wearing time increase (Vasconcelos et al., 2021; Warsito et al., 2023a). Similarly, Fiedler et al. (Fiedler et al., 2018b) demonstrated that contact pressure is a key parameter governing both signal quality and comfort. While increasing the normal force improves electrode/skin contact and reduces impedance, it simultaneously increases local pressure on the scalp, leading to discomfort. This establishes a fundamental trade-off between electrical performance and user comfort, which is consistently reported across multiple studies on dry EEG electrodes (Fiedler et al., 2016, 2018b; Rahman et al., 2023; Yoon et al., 2024). More broadly, several experimental works have confirmed that parameters such as electrode geometry, stiffness, and contact conditions significantly influence both perceived comfort and signal stability (Y. Peng et al., 2022; H. Ren et al., 2024). Beyond subjective evaluation, comfort has been shown to correlate with measurable physical variables. These include contact force, pressure distribution, material compliance, and electrode design (Fiedler et al., 2016; Haueisen et al., 2020; Rahman et al., 2023). For instance, multipin electrodes are effective in ensuring stable contact through hair but may induce localized pressure points, whereas softer electrodes provide better comfort (Vasconcelos et al., 2021). These observations demonstrate that comfort emerges from a complex interaction between mechanical design and application conditions. The importance of comfort is further emphasized in the development of wearable EEG technologies. From a broader perspective, comfort must be considered a multidimensional concept. Studies in human device interaction, Knight and Baber (Knight & Baber, 2005), have shown that comfort is influenced not only by physical factors such as pressure and pain, but also by perceptual and cognitive components, including user expectations, emotional state, and attention. This multidimensional nature explains why comfort cannot be reduced to a single measurable parameter. Instead, it is generally assessed using a combination of subjective scores and indirect physical indicators, which limits direct comparison between different studies and electrode technologies (H. Ren et al., 2024; Warsito et al., 2023a). Across the literature, including experimental comparisons of dry electrodes, headbands, and wearable EEG systems (Fiedler et al., 2016, 2018b; Rahman et al., 2023; Vasconcelos et al., 2021), a consistent conclusion emerges: comfort results from a compromise between mechanical loading and electrical performance. Increasing contact pressure improves signal quality but reduces comfort, while reducing pressure improves

comfort but may degrade signal reliability. In addition, the duration of use plays a central role, with a study reporting a significant deterioration of comfort after 30 to 60 minutes of continuous wear (Vasconcelos et al., 2021). In this context, the development of flexible polymer-based electrodes represents a promising approach to improving comfort without compromising electrical performance. By reducing material stiffness and enhancing conformability to the scalp, these systems aim to minimize localized pressure and improve long-term wearability. This strategy is fully aligned with current trends in the literature, which emphasize the need to optimize the balance between electrode/skin impedance, mechanical stability, and user comfort in next-generation EEG systems (Y. Peng et al., 2022; Rahman et al., 2023; Yoon et al., 2024). In summary, the literature demonstrates that comfort in EEG systems can be partially quantified using subjective evaluation scales and indirectly related to measurable physical parameters such as contact force, pressure, and material properties. However, due to its inherently subjective and multidimensional nature, comfort cannot be defined as a universal physical quantity. Consequently, current research focuses on improving electrode design to enhance perceived comfort while maintaining acceptable signal quality. Within this framework, the present work contributes to the development of flexible conductive polymer electrodes, aiming to improve both user comfort and EEG acquisition reliability in dry-contact systems.

2.7 Summary of the literature review

This chapter established the theoretical framework governing the performance of flexible dry EEG electrodes based on conductive polymer composites. The mathematical relationships presented clarify how parameters such as the volume fraction of conductive charges, the storage modulus, and the skin/electrode contact impedance jointly influence voltage transfer efficiency and noise levels in the microvolt range characteristic of EEG signals. This theoretical framework forms the basis for interpreting the experimental results presented in subsequent chapters.

CHAPITRE 3

FLEXIBLE DRY ELECTRODES BASED ON STYRENE-ETHYLENE-BUTYLENE-STYRENE/CARBON BLACK AND ETHYLENE-VINYL ACETATE/CARBON BLACK FOR ELECTROENCEPHALOGRAPHY: ELECTRICAL, THERMAL AND MECHANICAL PROPERTIES

George Gnonhoue [a], Ilyass Tabiai [a*], Jérémie Voix [a], Éric David [a]

[a] École de technologie supérieure, 1100 Notre-Dame Street West, Montreal, Quebec, H3C 1K3, CANADA

Paper published in the *Journal of Applied Polymer Science*, November 2025

https://doi.org/10.1002/app.70163

Chapter outline: This chapter presents the article corresponding to the results of the project's first part. It emphasizes the dispersion and distribution of the conducting additives in the polymeric matrix, additive-matrix interactions, the formation of an electrically conducting network, and the properties of styrene-ethylene-butylene-styrene/carbon black (SEBS/CB) and ethylene-vinyl acetate/carbon black (EVA/CB) nanocomposites for EEG.

Abstract: EEG is an essential technique for monitoring brain electrical activity in clinical, sports, and wearable health settings. However, traditional wet electrodes face issues like gel drying and skin irritation, while coated dry electrodes tend to degrade over time, affecting long-term signal stability. This study explores flexible dry electrodes made from conductive polymer composites—poly(styrene-b-ethylene-ran-butylene-b-styrene) filled with carbon black (SEBS/CB) and ethylene-vinyl acetate filled with carbon black (EVA/CB)—as affordable and recyclable alternatives to standard materials such as PDMS and TPU. The electrodes were manufactured using solvent casting and compression moulding, ensuring

even filler distribution and consistent surface quality. Both composites reached an electrical conductivity of around 0.01 S/m with a percolation threshold close to 12 wt% CB. Contact impedance tests showed better performance for SEBS/CB electrodes (5.4 ± 0.9 kΩ) compared to EVA/CB (26.7 ± 4.4 kΩ), nearing the value of a commercial flexible electrode (4.2 ± 0.5 kΩ). Mechanical testing confirmed that SEBS/CB is softer and more elastic, facilitating stable, low-noise EEG signal collection. Overall, SEBS/CB composites provide a good balance of electrical performance, flexibility, and scalability, highlighting their potential for next-generation, long-term EEG monitoring systems.

Keywords: Dry EEG electrodes, conductive polymer composites, contact impedance, mechanical flexibility

3.1 Introduction

EEG measures brain electrical activity via scalp electrodes, reflecting physiological and cognitive states (Arai et al., 2015; Cunha et al., 2009; Fu et al., 2020a; Krachunov & Casson, 2016). EEG signals, classified into Delta (0.5–4 Hz), Theta (4–8 Hz), Alpha (8–12 Hz), Beta (12–30 Hz), and Gamma (30+ Hz) bands, are fundamental for diagnosing neurological disorders and for continuous brain–computer interface (BCI) and health monitoring applications. The reliability of EEG recordings strongly depends on maintaining low skin–electrode contact impedance, which ensures a stable signal-to-noise ratio and accurate measurements (Das et al., 2020a; Fiedler et al., 2015; Leach et al., 2020). Traditional wet electrodes, despite their low impedance and high signal quality, have notable drawbacks such as gel drying, skin irritation, and instability during extended use or movement. (Arai et al., 2015; Baek et al., 2012; Chlaihawi et al., 2018; Cunha et al., 2009; de Camp et al., 2018; Fiedler et al., 2018a; Fu et al., 2020a; Y. Li et al., 2021; H.-L. Peng, Liu, et al., 2016; Srivastava et al., 2015; Wehrmann et al., 2013). As a result, research has shifted towards dry flexible electrodes, which eliminate the need for electrolytic gels and are better suited for wearable and long-term applications. These gel-free electrodes need materials that are flexible, biocompatible, and electrically conductive to ensure signal quality under different mechanical deformations. (Iqbal et al., 2021; L.-F. Wang et al., 2012a).

Flexible polymers are commonly used as base materials, with material choices varying based on design, application, and user needs in clinical, research, or consumer settings. Dry flexible electrodes enhance comfort during long-term EEG by conforming to the scalp's curvatures, maintaining stable contact even during movement, and improving signal quality. While these electrodes present a higher impedance than wet ones, optimizing the surface texture and design can minimize contact impedance, enhance skin contact, and reduce motion artifacts. Effective designs, such as those using silver-coated electrodes (Leach et al., 2020; Stauffer et al., 2018b), ensure stable signals, comfort, and minimal irritation. These electrodes achieve impedance levels below 50 kΩ at 10 Hz, making them suitable for reliable and prolonged EEG recordings (Cui et al., 2021; G. Li, Deng, et al., 2021).

Over the past few years, various materials have been investigated to achieve this balance**.** PDMS (polydimethylsiloxane) and TPU (thermoplastic polyurethane) have been widely used due to their softness and skin compatibility, but their relatively high contact impedance and limited recyclability constrain their performance and scalability (TPU) (Hassan et al., 2022; Heng et al., 2022; B.-C. Kang et al., 2019; Y. Li et al., 2022; S.-J. Park et al., 2023; Raspopovic et al., 2021). For instance, Fiedler et al. (Fiedler et al., 2015) developed Ag/AgCl-coated polyurethane electrodes that reached ~150 kΩ impedance, while Heijs et al. (Heijs et al., 2021) reported 602 ± 401 kΩ using similar multipin electrodes. Recent efforts have explored conductive coatings and composite formulations—such as silver-filled TPU (Z. Wang et al., 2024b), carbon black (CB)/TPU (Xing & Casson, 2023a), graphene/PDMS composites (Das et al., 2020b), and multi-walled carbon nanotube (MWCNT)–PDMS mixtures (Oh et al., 2024a; Sharma et al., 2024a), achieving moderate improvements in flexibility and signal quality. Nevertheless, contact impedance typically remains in the 10–600 kΩ range, which is still considerably higher than that of wet electrodes.

To overcome these challenges, attention has increasingly turned toward thermoplastic elastomers (TPEs) that combine the softness of rubbers with the processability of plastics. Among them, Styrene-Ethylene-Butylene-Styrene (SEBS) and Ethylene-Vinyl Acetate (EVA) have emerged as promising alternatives. SEBS exhibits exceptional elasticity, softness, and chemical resistance, making it ideal for skin-interfacing biomedical devices.

EVA offers comparable flexibility, biocompatibility, and easy processing, with adjustable mechanical properties depending on its vinyl acetate content (Costa et al., 2015). Both materials are recyclable thermoplastics, contrasting with non-recyclable PDMS, and they are compatible with scalable manufacturing processes such as extrusion, injection molding, and 3D printing—key advantages for the mass production of wearable biosensors (Y.-J. Park et al., 2006; Tekay et al., 2023).

When combined with conductive fillers such as carbon black (CB), carbon fibers, or graphene, these matrices can form lightweight, low-cost conductive composites suitable for EEG electrodes. CB is particularly advantageous due to its high surface area, ease of dispersion, chemical stability, and significantly lower cost than CNTs or graphene. Recent works (J. Guo et al., 2020; Shafiee & Ramazani S.A., 2008) have shown that SEBS- and EVA-based composites exhibit tunable conductivity and mechanical properties, making them strong candidates for flexible bioelectronic applications. However, their use in EEG electrodes has not yet been thoroughly explored or benchmarked against established PDMS- and TPU-based designs, leaving a clear gap in the literature.

The present study addresses this gap by systematically investigating SEBS/CB and EVA/CB composites as alternative materials for flexible dry EEG electrodes. Using a chemical dissolution method for homogeneous filler dispersion, flexible electrodes were fabricated and characterized for their electrical conductivity, contact impedance, mechanical compliance, and EEG signal acquisition capability. The obtained results were directly compared with those of commercial dry electrodes and benchmarked against recent PDMS- and TPU-based designs from the literature.

This work highlights, for the first time, the comparative advantages of SEBS- and EVA-based carbon black composites in balancing low contact impedance, high flexibility, and scalable manufacturability. Beyond performance improvement, the use of thermoplastic matrices introduces sustainability and cost-efficiency benefits that are critical for the next generation of wearable EEG systems. The study thus contributes to expanding the material platform for bioelectronic interfaces by proposing recyclable, high-performance elastomeric composites

for durable and comfortable long-term EEG applications. Section 1 outlines the methodology for developing and characterizing SEBS/CB and EVA/CB electrodes, focusing on the surface morphology, compression testing, electrical properties, contact impedance, and brain signal acquisition. Results are compared with those of commercial dry flexible EEG electrodes. Section 2 details the experimental procedures used to prepare and characterize SEBS/CB and EVA/CB electrodes, including composite formulation, electrode fabrication, morphological analysis, mechanical testing, electrical characterization, and EEG signal acquisition methodology. The discussion addresses the study's limitations and suggests directions for future research. The objective is to determine the composite material that offers the optimal combination of electrical conductivity, low contact impedance, mechanical compliance, thermal stability, and scalp conformity. This work ultimately seeks to advance the development of durable, high-performance EEG electrodes designed for long-term, real-world applications.

3.2 Experimental testing

This section details the materials, preparation methods, and fabrication process used to develop SEBS/CB and EVA/CB flexible EEG electrodes. The main aim is to compare the performance of SEBS/CB and EVA/CB materials with that of a commercial dry flexible electrode, to identify which provides superior electrical conductivity and lower contact impedance for recording brain electrical signals. The methodology was designed to ensure reproducibility and facilitate other researchers in replicating the fabrication process. All experimental procedures were conducted under controlled conditions, with the purity and specifications of the materials used clearly outlined. A future clinical study involving long-term, multi-participant EEG recordings is planned.

3.2.1 Materials

Two thermoplastic matrices were selected: Styrene–ethylene–butylene–styrene (SEBS) and ethylene–vinyl acetate (EVA), chosen for their elasticity and mechanical resilience.

- SEBS, with a number-average molecular weight of 54,000 g/mol and a polystyrene content of 30 wt.%, was supplied by Kraton Polymers (Paulínia, Brazil) with a purity greater than 99%.
- EVA (vinyl acetate content 28 wt.%, density 0.950 g/cm³) was obtained from Repsol (Madrid, Spain), analytical grade, with a purity of over 98%.
- Carbon black nanoparticles (Carbon Lampblack C198-500, Lot 145509, average diameter approximately 50 nm, nominal conductivity around 400 S/m, density = 1.8 g/cm³) were sourced from Fisher Chemical (Ottawa, Canada), with a purity over 99%.
- Toluene (UN1294, Optima grade, Lot 234238) was used as a solvent and obtained from Fisher Chemical (Ottawa, Canada), with a purity of ≥ 99.8%.

All materials were used as received without further purification. The preparation steps were carried out in a fume hood to ensure solvent safety and process safety repeatability.

3.2.2 Preparation of SEBS/CB and EVA/CB Composites

The preparation process involved four main stages: dissolving the polymer, dispersing the filler, and removing the solvent, as shown schematically in Figure 3.1.

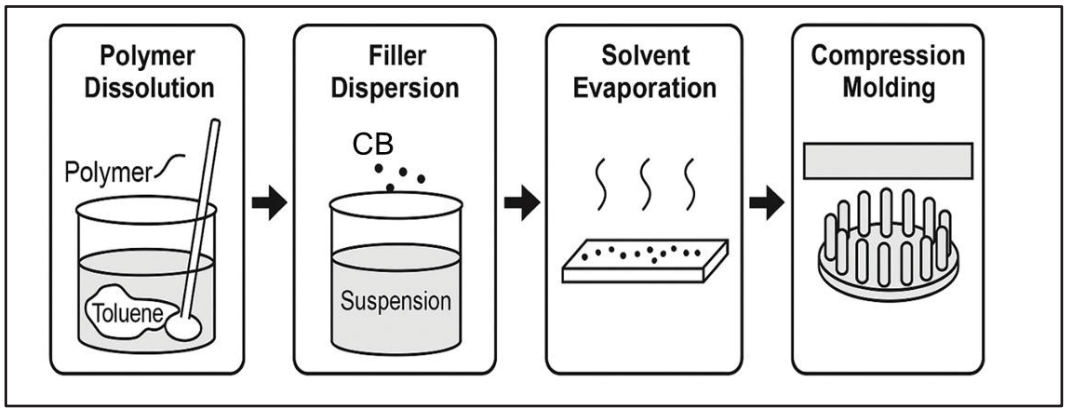


Figure 3.1. Schematic overview of the fabrication process for flexible multipin dry electrodes. The method includes (i) dissolving the SEBS or EVA polymer in toluene, (ii) dispersing conductive fillers (CB) to create a uniform suspension, (iii) evaporating the solvent to form composite films, and (iv) using compression molding to shape the films into multipin electrode structures

3.2.2.1 Polymer dissolution

Each polymer (SEBS or EVA) was dissolved separately in toluene at 100 °C with magnetic stirring (600 rpm) until a clear, homogeneous solution was achieved.

3.2.2.2 Filler incorporation

After complete dissolution, carbon black (CB) was gradually added to the polymer solution at various mass fractions ranging from 0 to 20 wt.% (see Table 3-1). The mixture was stirred for an extra 30 minutes at 100 °C to ensure uniform dispersion of CB within the matrix. The formation of the composite depended on the physical entanglement of polymer chains with the conductive CB network, enabling efficient electron transport after the solvent was removed.

SEBS, owing to its elastomeric block-copolymer architecture, accommodates higher filler loadings because of its greater chain mobility and tolerance to viscosity increases. In contrast, EVA exhibits a marked rise in viscosity at elevated CB contents, which restricts its processability under identical mixing and molding conditions.

3.2.2.3 Solvent evaporation and film formation

The resulting dispersions was cast and left to dry under a chemical fume hood at room temperature until all solvent evaporated, resulting in nanocomposite films.

Table 3-1 SEBS/CB and EVA/CB nanocomposites at different carbon nanoparticle weight fractions

SEBS/CB (wt%)		EVA/CB (wt%)	
Reinforcements	Matrix	Reinforcements	Matrix
0	100	0	100
3	97	5	95

Table 3-1 SEBS/CB and EVA/CB nanocomposites at different carbon nanoparticle weight fractions

SEBS/CB (wt%)		EVA/CB (wt%)	
Reinforcements	Matrix	Reinforcements	Matrix
5	95	8	92
6	94	12	88
7	93	16.5	83.5
8	92	18.5	81.5
10	90	20	80
12	88	-	
15	85	-	
20	80	-	

3.3 Fabrication of Surface Multipin EEG Electrodes

The solid composites were molded into surface multipin EEG electrodes using compression molding (Figure 3.1).

- Step 1: Pre-heating and low-pressure molding at 215 °C, 0.8 MPa, 5 min
- Step 2: High-pressure consolidation at 215 °C, 5 MPa, 15 min

Each electrode consisted of 19 cylindrical pins arranged in a circular pattern. The pins had an average height of 4.9 ± 0.09 mm and a diameter of 1.41 ± 0.01 mm. The center-to-center distance between neighboring pins was about 2.5 mm, which corresponds to an edge-to-edge spacing of approximately 1.1 mm at the electrode–skin interface.

3.4 Optimization and Reproducibility

Distinct CB loadings were explored for SEBS and EVA to identify the electrical percolation threshold and the conductivity plateau for each matrix. For both material systems, the composite exhibiting the highest electrical conductivity was selected for subsequent electrical, mechanical, and morphological characterizations. To ensure reproducibility, three independent batches of each selected formulation were fabricated and characterized under identical conditions.

3.5 Characterizations

3.5.1 Electrical characterization

The electrical conductivities of the different composites were not measured using conventional electrophysiological techniques (e.g., impedance at fixed frequencies or skin-contact methods), but rather using a frequency-domain dielectric spectrometer (Alpha-A Dielectric Analyzer, BDS – Novocontrol, Montabaur, Germany) to characterize their intrinsic bulk conductivity. For each formulation, measurements were performed on three independent samples to ensure reproducibility. Each sample was shaped into a 20 mm-diameter and 1.2 mm-thick disk and placed between two solid brass electrodes to form a planar electrode/composite/electrode sandwich. This setup allows for accurate determination of the real part of the complex conductivity over a wide frequency range (10^{-2} to 10^{5} Hz) at 30 °C. The aim was to assess percolation behavior and frequency dependence of conductivity in the bulk material, independently of contact with biological tissue.

3.5.2 Structural characterization

To study the distribution of the conductive particles in the host matrix, the morphology of the composites was investigated using a high-resolution scanning electron microscope (Hitachi SU-8230 field emission-SEM) at 5 kV. Cross-sections of the specimens were prepared using a cryogenic fracture technique, after which they were coated with a platinum layer of

approximately 2 nm under vacuum conditions using a turbo-pumped sputter coater/carbon coater (Q150T).

3.5.3 Thermal Characterization

Differential Scanning Calorimetry (DSC) was employed to investigate the thermal properties of the pure polymer matrices (SEBS and SEBS-MA). Tests were conducted in a nitrogen atmosphere to prevent oxidation. Approximately 10 mg samples were sealed in aluminum pans and heated at a rate of 10 °C/min. To avoid thermal degradation, the measurement ranges were tailored to the thermal stability of each material: –100 to 250 °C. These conditions facilitated the detection of key transitions, including the glass transitions of both the soft and hard phases, without interference from decomposition.

3.5.4 Mechanical characterization

Cyclic compression tests were conducted on SEBS/20wt% CB and EVA/20wt% CB composites using the ASTM D575-91 standard to define specimen geometry and test conditions. Standard cylindrical specimens measured 28.6 ± 0.1 mm in diameter and 12.5 ± 0.5 mm in thickness. A compressive load of 100 kN was applied using a universal testing machine (MTS Alliance RF/200, MTS Systems Corporation, Eden Prairie, Minnesota, United States). Each test involved three consecutive loading–unloading cycles to evaluate the flexibility, shape memory behavior, and mechanical repeatability of the materials. All measurements were carried out under ambient laboratory conditions, with a temperature of approximately 23 °C and relative humidity of 45–55%.

To characterize the mechanical performance, key parameters were extracted from the stress–strain curves, including the stress at 50% compression, the elastic modulus, the hysteresis loss (energy dissipated per cycle), the loading energy, and the energy ratios between cycles to assess energy retention and mechanical stability. Tests were performed on three independent samples per material to ensure repeatability and statistical reliability of the results.

3.6 Experimental validation in vivo

Multipin flexible EEG electrodes were selected to evaluate contact impedance and EEG artifacts associated with eye movements. These artifacts were wirelessly recorded using the OpenBCI™ 16-channel Cyton Biosensing Board (OpenBCI, NY, USA) in combination with the Ultracortex 'Mark IV' EEG headset (OpenBCI, NY, USA). Contact impedance was measured at 31 Hz using the same acquisition system, as shown in Figure 3.2.

To simulate practical conditions for wearable EEG applications, the skin was neither cleaned nor abraded before measurements. The headset, in which the electrodes were inserted, was comfortably positioned on the head without applying pressure to the electrode surfaces. A commercial dry flexible electrode (OpenBCI, NY, USA) was placed at position 2 (see Figure 3.2), while the multipin electrodes developed in this study were inserted at positions 1 and 3.

Figure 3.3 shows the custom-designed multipin electrode alongside the commercial flexible electrode used as a reference. Performance evaluation was based on comparisons of contact impedance and EEG signal amplitude between the developed and commercial electrodes. The measurement system consisted of a ground, a reference electrode, and the developed electrode, allowing impedance to be measured between the developed and reference electrodes. Figure 3.2 illustrates the Ultracortex 'Mark IV' EEG headset used for signal acquisition and impedance measurements.

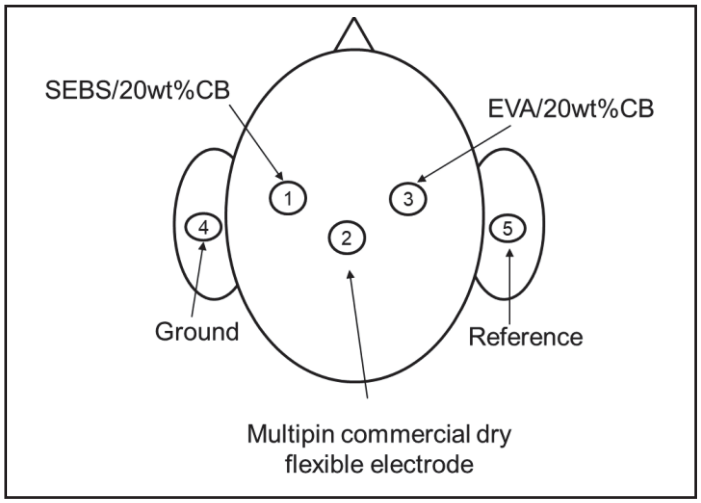


Figure 3.2. Ultracortex "Mark IV" EEG headset used
to install the electrodes on the head

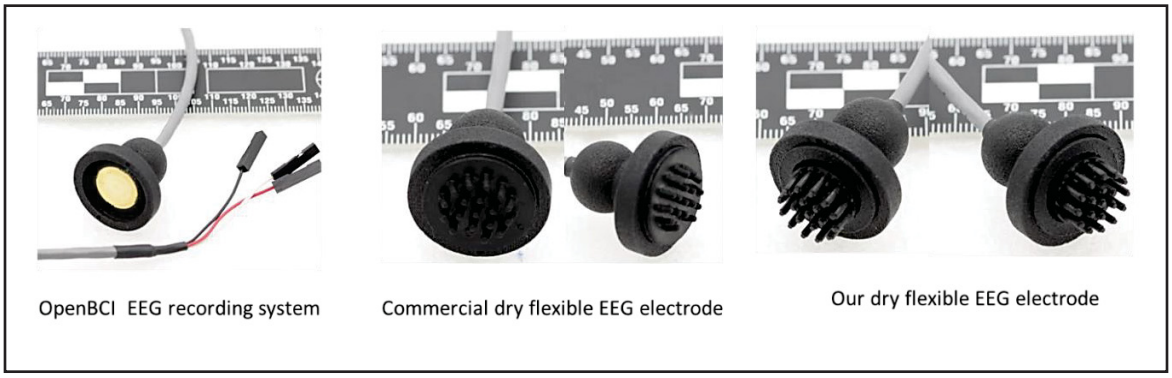


Figure 3.3. Electrodes installed in the system for the acquisition of electrical signals from
the brain

3.7 Participants

Participant testing validated the effectiveness of the developed electroencephalogram (EEG) electrodes under physiological conditions by assessing EEG signal quality and motion artifacts. Healthy adult participants (n = 4; 1 male and 3 females, aged between 21 and 35 years) were recruited for EEG measurements. All procedures were approved by the ÉTS Internal Review Board (« Comité d'éthique de la recherche », Approval No. H20230504) and conducted in accordance with the Declaration of Helsinki. Informed consent was obtained from all participants before the experiments.

To ensure a controlled environment, participants were comfortably seated in a quiet room during signal acquisition. EEG signals were recorded for 10 seconds. Following standard EEG protocols and the American Clinical Neurophysiology Society guidelines (Sinha et al., 2016), participants were instructed to minimize head and facial muscle movements and remain still to reduce motion artifacts. At designated time points—approximately at 1 s, 3 s, 8 s, and 10 s—they were asked to blink in response to a sound cue to evaluate the electrodes' ability to detect blink-related EEG activity.

3.8 Results

3.8.1 Electrical, structural and mechanical properties

3.8.1.1 Electrical properties

Figure 3.4 depicts the frequency dependence of the real part of the complex conductivity (σ') for SEBS and EVA composites with various carbon black loadings. Only the real part is shown here, as it directly reflects the conductive behavior associated with effective charge transport mechanisms within the composite materials. These measurements were performed across all tested formulations to determine the electrical percolation behavior. Once the percolation threshold is reached, σ' becomes almost frequency-independent, indicating that it closely approaches the true direct current (DC) conductivity. Figure 3.5 shows the electrical conductivity of the SEBS/CB and EVA/CB composites as a function of mass fraction, at a frequency of 1 Hz.

The percolation threshold for both SEBS/CB and EVA/CB composites was found to be ~12wt.%. Beyond this threshold, the electrical conductivity of both composites reached a plateau at about 0.01 S/m at 20wt.%. Below the percolation threshold, the measured conductivity is overestimated due to the influence of frequency-dependent mechanisms such as interfacial polarization and charge hopping, which do not reflect true DC conduction.

This behavior is visible in Figure 3.4-a for concentration below 15wt%CB for SEBS/CB composite, and below 16.5wt%CB, for EVA/CB composite in Figure 3.4-b. It can also be seen in the non-conductive domain (0 to 12wt%) that the value of the AC conductivity at a

given frequency is not well correlated with the CB concentration. The composites with the highest mass fraction (SEBS/20wt%CB and EVA/20wt%CB) were chosen for the fabrication of the electrodes to perform the EEG measurements since, as could be expected, they have the highest electrical conductivities (0.01 S/m).

The evolution of the electrical conductivity of the composites as a function of the frequency in Figure 3.4 confirms that the percolation threshold of the SEBS/CB composites is below 15wt%CB and that of the EVA/CB composites is below 16.5wt%CB.

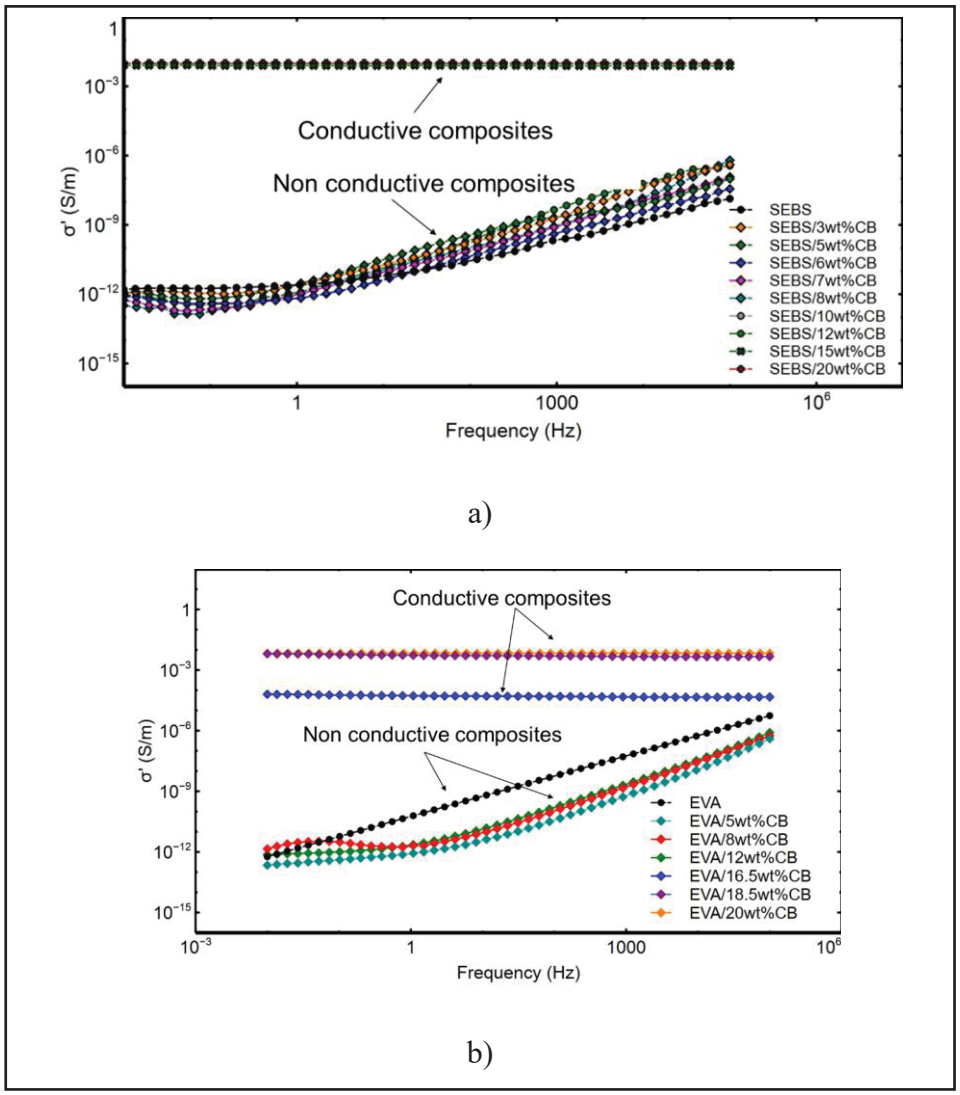


Figure 3.4. Real part of the complex conductivity as a function of frequency of (a) SEBS/CB and (b) EVA/CB

Figure 3.5 shows that the EVA/CB and SEBS/CB composites have the same percolation threshold (12wt%CB).

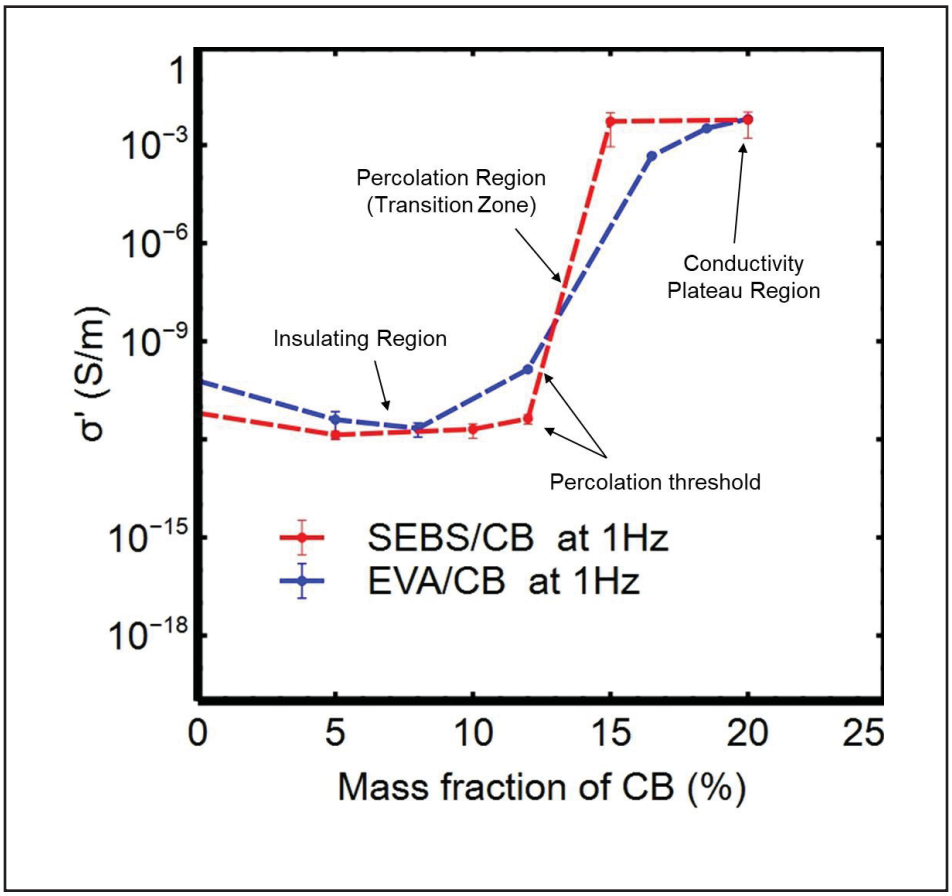


Figure 3.5**.** Electrical conductivity as a function of mass fraction

The graph of Figure 3.5 depicts the electrical conductivity of SEBS/CB composites as a function of carbon black (CB) mass fraction, measured at 1 Hz. At low CB mass fractions (0–12wt%), the conductivity remains extremely low, around 10^{-12} S/m, indicating an insulating behavior. This suggests that CB particles are insufficiently connected to form conductive paths within the SEBS matrix. Around 12wt% CB, there is a sharp increase in conductivity, spanning several orders of magnitude, reaching approximately 10^{-2} S/m. This marks the percolation threshold, where CB particles form a continuous network, enabling efficient electrical conduction. Beyond 15 wt% CB, the conductivity plateaus, showing no significant increase as the CB concentration increases further. This indicates that the conductive network has stabilized, and additional CB has a diminishing effect on further improving conductivity.

The percolation threshold is observed near 12wt% CB. The steepness of the conductivity increase at the percolation threshold demonstrates that CB particles form a well-distributed and interconnected network in the SEBS matrix, enhancing electrical properties efficiently. Below the percolation threshold, SEBS/CB composites are suitable for applications requiring insulating properties. Near or beyond the percolation threshold, the composites exhibit significant conductivity, making them suitable for EEG electrodes. The graph of Figure 3.4-a demonstrates the percolation behavior of SEBS/CB composites, with a critical threshold near 12wt% CB. Beyond this threshold, the material becomes conductive, suitable for flexible electronic applications. The results highlight the importance of achieving uniform filler dispersion and optimizing CB content for specific electrical properties.

The plot in Figure 3.4-b shows the variation of electrical conductivity of EVA/CB (Ethylene-Vinyl Acetate/Carbon Black) composites as a function of the carbon black (CB) mass fraction, measured at 1 Hz. From 0 to 12%, the conductivity remains extremely low, around 10^{-12} S/m, indicating that the material is electrically insulating. In this range, the carbon black particles are too sparsely distributed to form conductive pathways. The composite behaves like a dielectric material. From 12% CB content, a significant increase in conductivity is observed, reaching a plateau of 10^{-2} S/m. This sharp rise is attributed to the percolation threshold, where CB particles form a continuous conductive network within the EVA matrix. From 16.5 to 20%, beyond the percolation threshold, the conductivity stabilizes at 10^{-2} S/m. Further increases in CB concentration enhance the density of the conductive network but do not drastically improve the conductivity as saturation is approached. Below 12% CB, composites have an insulating behavior due to isolated CB particles whereas above 12% CB, they have a conductive behavior due to interconnected CB particles. For flexible electrodes, a CB content above the percolation threshold (12–20%) is necessary to ensure sufficient electrical conductivity for signal acquisition. Adjusting the CB content allows to tune the conductivity and mechanical properties in order to balance performance and flexibility. These findings confirm the need to carefully optimize the CB mass fraction to achieve the desired electrical properties in EVA/CB composites. A CB mass fraction of 12–20% is ideal for applications requiring conductivity, such as dry EEG electrodes.

3.8.1.2 Structural properties

Figure 3.6 presents the scanning electron microscope (SEM) micrograph of SEBS/CB and EVA/CB composites containing 20wt%CB. The results show that the CB particles appear to be well distributed at this concentration in both composites. The Figure 3.6 shows that due to the high concentration of carbon black (20wt%) in the nanocomposites, some agglomerated particles were observed in SEBS/20wt%CB and EVA/20wt%CB. The agglomerations are indicated in Figure 3.6 as large CB in the SEBS/20wt%CB and EVA/20wt%CB samples. The interaction of the reinforcement (CB) inside the different matrices is also apparent. The presence of agglomerates is primarily attributed to the high CB concentration. Despite this, these agglomerates contribute to the formation of conductive paths within the composites through CB-CB contacts. As the CB concentration increases, these agglomerates become more interconnected, enhancing the density of the conductive network.

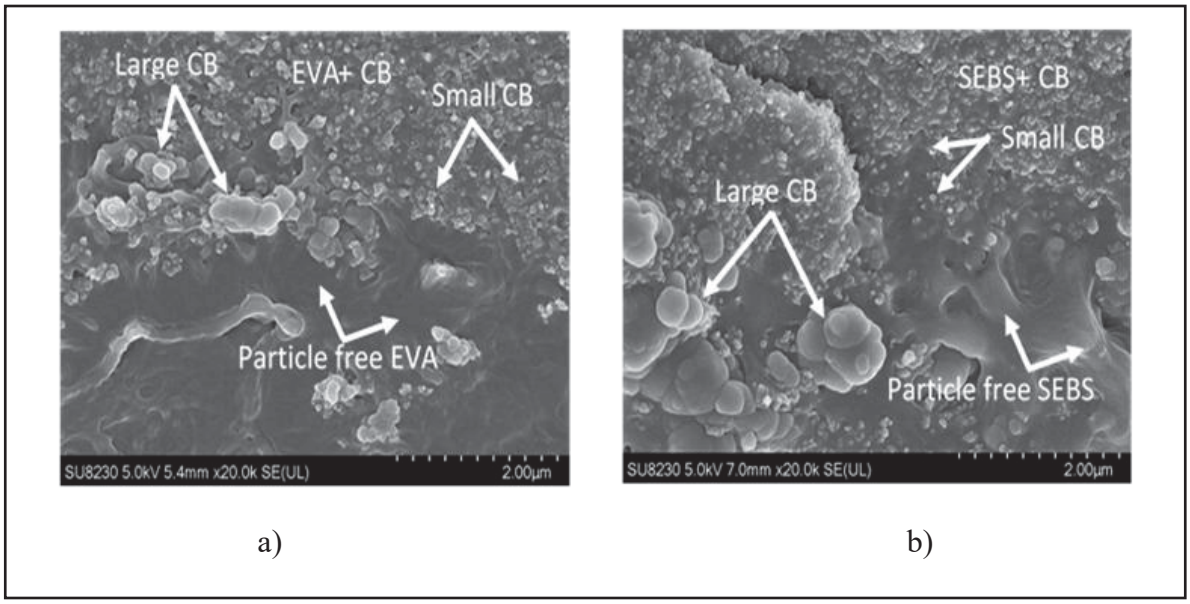


Figure 3.6. Micrograph of both electrodes: a) EVA/20wt%CB and b) SEBS/20%wtCB

3.8.1.3 Thermal properties

To support the development of flexible dry EEG electrodes, DSC analysis was performed to assess whether adding carbon black influences the thermal stability and segmental mobility of the SEBS and EVA matrices. As shown in Figures 3.7 and 3.8, both composites retain the characteristic thermal signatures of their respective elastomers.

The SEBS/CB composite exhibits a glass-transition temperature (Tg) near –50 °C, typical of the ethylene–butylene soft phase, with no melting or crystallization peaks across the heating and cooling cycles. This confirms the fully amorphous nature of SEBS and indicates that CB loading does not disturb its microphase-separated structure. The EVA/CB composite shows a Tg around - 35 °C, along with a broad endothermic transition above 80–90 °C corresponding to the softening of the vinyl-acetate–rich domains.

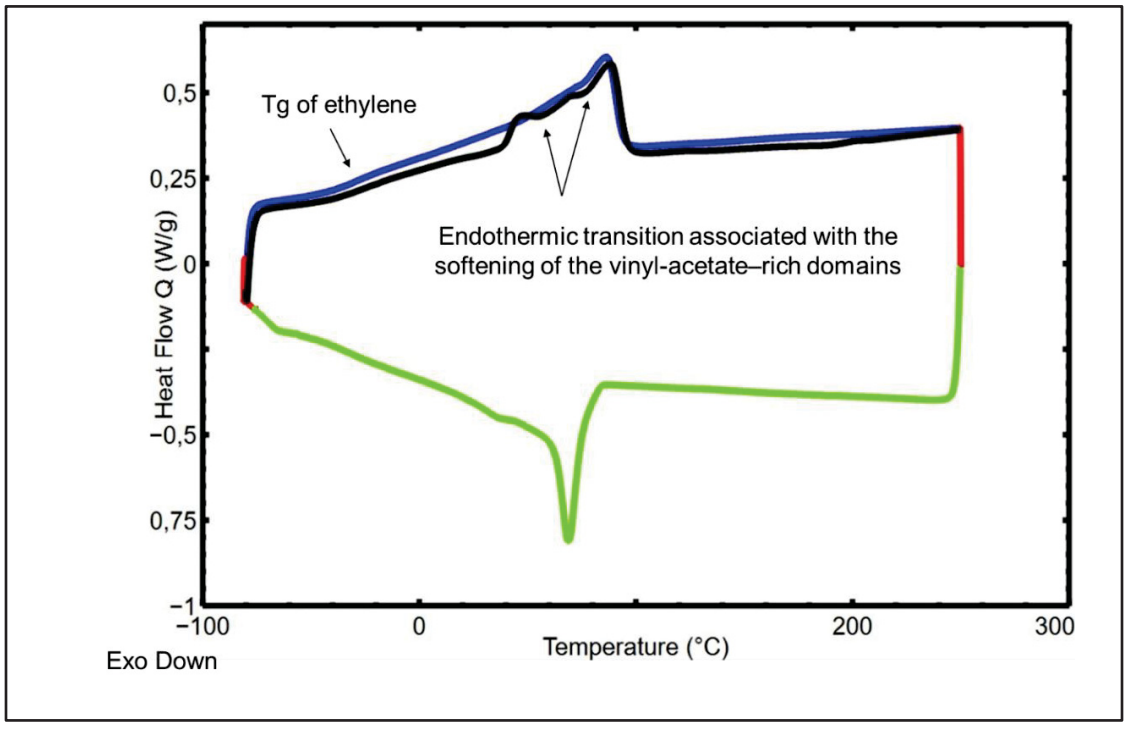


Figure 3.7. Differential scanning calorimetry (DSC) thermogram of EVA/20 wt% CB composite. The second heating (blue) and cooling (green) curves display a glass transition around −30 °C, a crystallization peak near 55–60 °C, and a melting endotherm at approximately 95–100 °C

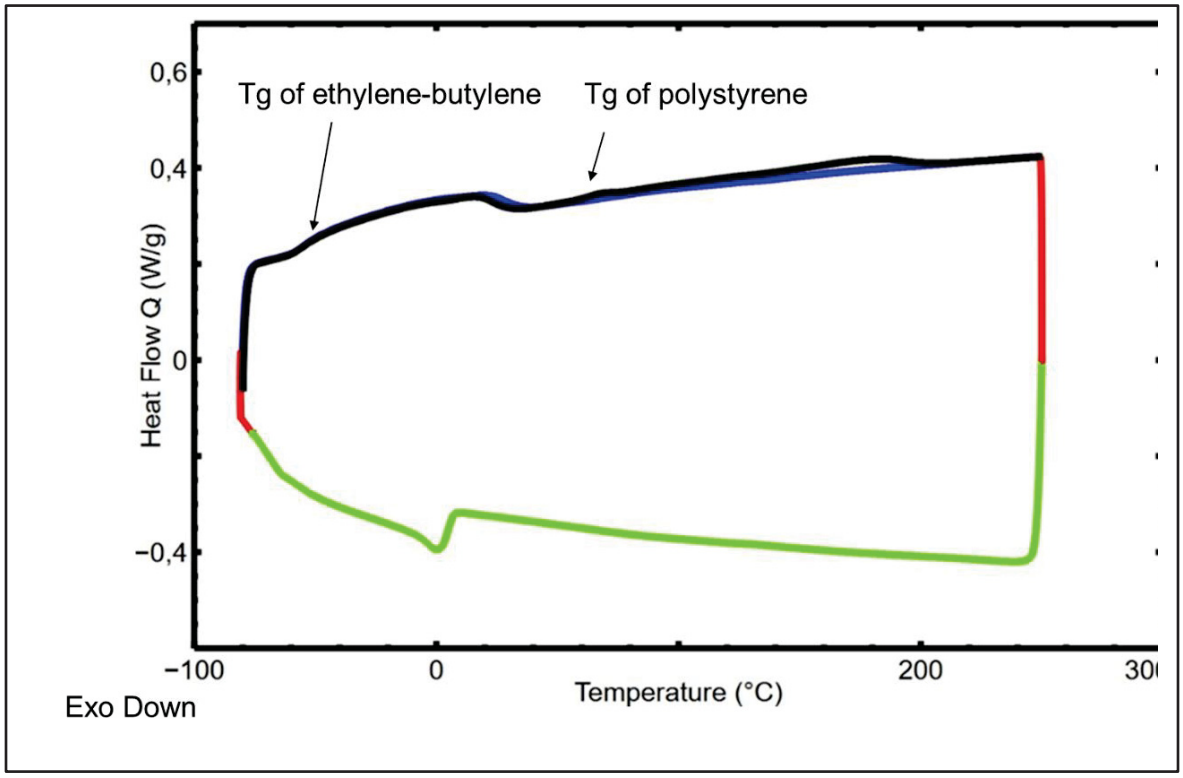


Figure 3.8. Differential scanning calorimetry (DSC) thermogram of the SEBS/20 wt% CB composite. The curve shows a glass transition of the ethylene–butylene (EB) phase near −50 °C, a weak transition of the polystyrene domains at 90–100 °C

These results demonstrate that the thermal transitions of both matrices remain essentially unchanged after CB incorporation. This is an important outcome for EEG electrode fabrication: the CB network enhances conductivity without compromising the thermal integrity or processing window of the elastomer. The composites, therefore, maintain the flexibility and thermal stability required for reliable, skin-conforming EEG electrodes while supporting improved electrical performance.

3.8.1.4 Mechanical properties

Figure 3.9 shows the results of cyclic compression tests performed on SEBS/20wt%CB (green curve) and EVA/20wt%CB (red curve).

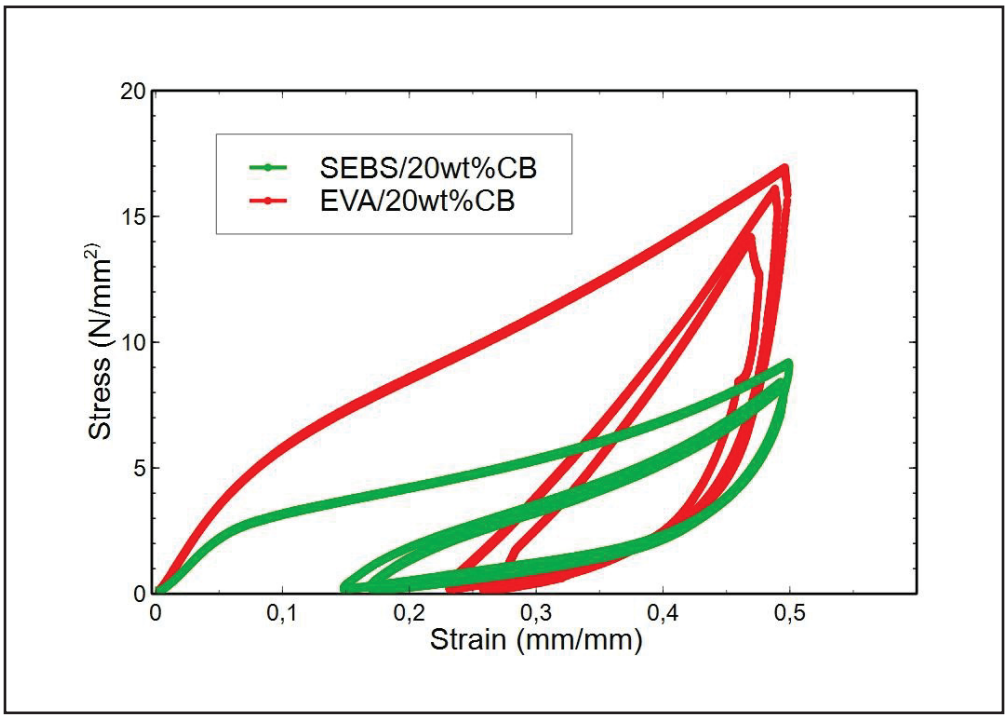


Figure 3.9. Stress-strain behavior of SEBS/20wt%CB and EVA/20wt%CB under compression tests

The steeper slope of the stress-strain curve at the initial linear region indicates stiffness. EVA/20wt%CB (red curve) shows a higher stiffness as compared to SEBS/20wt%CB, suggesting that EVA/20wt%CB is less deformable under compression. The loops in the curves indicate energy dissipation during loading and unloading (hysteresis). EVA/20wt%CB exhibits larger hysteresis loops as compared to SEBS/20wt%CB, indicating a greater energy loss, likely due to a greater internal friction or viscoelastic effects. SEBS/20wt%CB shows a narrower hysteresis loop, suggesting a better elastic recovery after compression as compared to EVA/20wt%CB, which retains more deformation after unloading. EVA/20wt%CB withstands a higher maximum stress at a given strain, showing greater resistance to deformation under load. However, SEBS/20wt%CB achieves a higher strain at lower stress, demonstrating greater flexibility. SEBS/20wt%CB is more flexible and better suited for applications requiring high deformation and recovery, such as wearable sensors or flexible electrodes. EVA/20wt%CB, being stiffer, might be preferred for applications demanding higher structural integrity under load. To manufacture dry flexible EEG electrodes, SEBS/20wt%CB is a better choice than

EVA/20wt%CB, based on the following key measured parameters, including: the stress at 50% extension, the elastic modulus, the hysteresis loss, the loading energy, and the energetic ratios across multiple cycles:

- The stress at 50% of EVA/20wt%CB is 16.2 MPa, and that of SEBS/20wt%CB is 9.35 MPa. EVA/20wt%CB exhibits a higher stress at a 50% extension, indicating a greater resistance to deformation as compared to SEBS. This suggests that EVA is more rigid, while SEBS/20wt%CB is more flexible, making SEBS potentially more suitable for applications where flexibility and adaptability (conforming to curved surfaces) are essential.
- The elastic Modulus EVA/20wt%CB is 63.8 MPa and that of SEBS/20wt%CB is 47.2 MPa. EVA/20wt%CB has a higher elastic modulus, confirming its greater rigidity. SEBS, with a lower elastic modulus, is softer and more elastic, which may provide better comfort and adaptability in flexible electrode applications such as EEG systems.
- The hysteresis Loss (Energy Dissipated as Heat) of EVA/20wt%CB is Cycle 1: 27.2 J → Cycle 3: 7.63 J, and that of SEBS/20wt%CB is Cycle 1: 13.3 J → Cycle 3: 5.17 J. EVA/20wt%CB dissipates significantly more energy as heat than SEBS in all cycles. This decrease in energy values corresponds to the reduction of the area enclosed by the stress–strain hysteresis loops between the first and third loading–unloading cycles, indicating that the material dissipates less mechanical energy as heat as its internal structure becomes stabilized after repeated deformation. Both materials stabilize after repeated cycles, with the hysteresis loss decreasing by approximately 72% (EVA/20wt%CB) and 61% (SEBS/20wt%CB) from Cycle 1 to Cycle 3. SEBS demonstrates a lower energy dissipation overall, indicating greater efficiency and mechanical resilience.
- The loading Energy (Total Energy Absorbed) of EVA/20wt%CB is Cycle 1: 32.79 J → Cycle 3: 12.78 J, and that of SEBS/20wt%CB Cycle 1: 18.93 J → Cycle 3: 10.19 J. EVA/20wt%CB absorbs more energy than SEBS/20wt%CB, consistent with its higher rigidity and resistance to deformation. Both materials show reduced loading energy over cycles, reflecting material stabilization under repeated loading.

- The energetic Ratio (Energy Returned/Stored) of EVA/20wt%CB is Cycle 1 = 82%, Cycle 2 = 63%, Cycle 3 = 59% and that of SEBS/20wt%CB is Cycle 1 = 70%, Cycle 2 = 53%, Cycle 3 = 50%. EVA/20wt%CB has higher energetic ratios in all cycles, meaning that it returns a higher proportion of absorbed energy. However, the ratio drops more significantly for EVA/20wt%CB (23% reduction) than for SEBS/20wt%CB (20% reduction) from Cycle 1 to Cycle 3. SEBS shows a more stable energy return behavior, although it is overall less efficient than EVA in energy restitution.

3.9 Experimental validation in vivo

The contact impedance of EVA/20wt%CB electrode is 26.8 ± 4.4 kΩ**.** This high impedance with significant variability (large standard deviation) indicates poor electrical contact with the skin, which leads to reduced signal quality and increased noise during EEG measurements. The large variability suggests inconsistent performance, likely caused by an inadequate interaction between the electrode and the skin. The same impedance of flexible commercial electrodes is 4.2 ± 0.5 kΩ. This is the lowest impedance, suggesting a highly consistent performance as compared to that of the EVA/20wt%CB electrode. The minimal impedance ensures an optimal signal quality, making it a benchmark for EEG applications. The contact impedance of the SEBS/20wt%CB electrode is 5.4 ± 0.9 kΩ. This value is much lower than that of EVA/20wt%CB, and close to that of the commercial electrode. The small standard deviation indicates consistent performance. The low impedance reflects a better electrode-skin interface and improved electrical conductivity, likely due to SEBS's flexibility and a better dispersion of conductive fillers. Its low contact impedance makes it suitable for reliable EEG signal acquisition. Figure 2.10. shows the eye movement-related artifacts of SEBS/20wt%CB, EVA/20wt%CB and commercial electrodes.

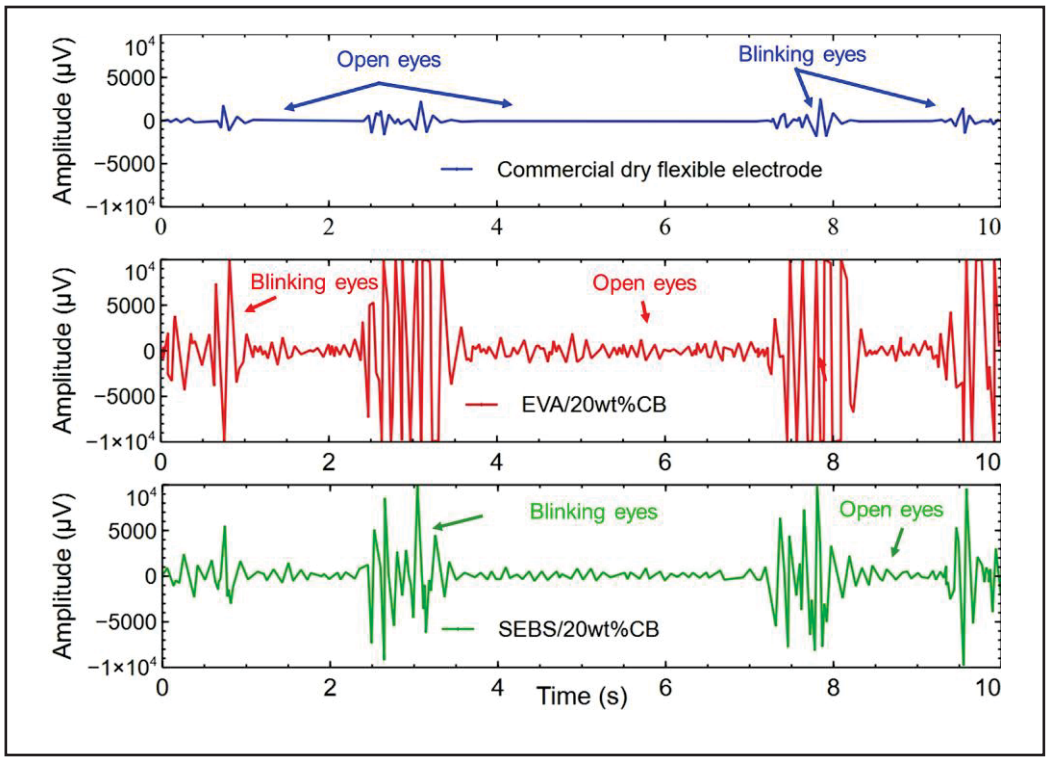


Figure 3.10. EEG signals of SEBS/20wt%CB, EVA/20wt%CB and commercial electrodes

The eye movement-related artifacts plots in Figure 3.10, which show a comparison of the commercial dry flexible electrode, EVA/20wt%CB, and SEBS/20wt%CB, reveal notable differences in signal quality and stability.

- Commercial Dry Flexible Electrode (Top Panel - Blue Line): The signal is stable and clear, with amplitudes of ~±2000 μV. The consistent patterns during eyes-open and eyes-closed periods indicate good sensitivity to changes in brain activity. The commercial electrode provides reliable signal quality, serving as a benchmark for comparison.
- EVA/20wt%CB Electrode (Middle Panel - Red Line): The signal shows amplitude spikes exceeding ±10000 μV, particularly during transitions between eyes-open and eyes-closed states. These spikes suggest poor contact impedance and suboptimal electrode-skin contact, compromising signal reliability. When comparing the signal amplitudes recorded during the eyes-open phases, significantly larger amplitude

fluctuations are observed with the EVA/20wt%CB electrode compared to SEBS/20wt%CB and PDMS (EVA/CB > SEBS/CB > Commercial Dry Flexible Electrode PDMS, with no fluctuations detected for the commercial electrode). These pronounced variations may account for the higher overall amplitude observed with EVA/CB.

- SEBS/20wt%CB Electrode (Bottom Panel - Green Line): The signal amplitude is well-controlled and remains within ~±10000 μV, reflecting a better contact impedance. The clear differentiation between eyes-open and eyes-closed states suggests that SEBS/20wt%CB electrodes are capable of effectively capturing EEG signals.

To better contextualize the contribution of this work, Table 3-2 summarizes the performance of the newly developed SEBS/CB and EVA/CB electrodes in comparison with recently reported flexible dry and wet EEG electrodes. The comparison includes parameters such as material composition, fabrication method, contact impedance, electrical conductivity, mechanical compliance, and electrode type.

Table 3-2 clearly shows that while most PDMS- and TPU-based dry electrodes exhibit contact impedance values ranging from tens to several hundred kilo-ohms, the SEBS/CB composite developed in this study achieves a remarkably low impedance of approximately 5 kΩ, approaching that of commercial flexible electrodes. Furthermore, SEBS/CB combines this electrical performance with superior softness and elasticity, resulting in stable EEG signal acquisition and enhanced user comfort. The recyclability and processability of thermoplastic matrices such as SEBS and EVA also provide an additional advantage over conventional thermoset-based systems, enabling scalable, cost-effective manufacturing for wearable biosensors.

Table 3-2 Comparison with relevant work in the application area

Electrode Material	**Fabrication Method**	**Contact Impedance**	**Reference**
PDMS/AgNWs	3D printing	10 kΩ at 1 kHz	(Z. Wang et al., 2018)
PDMS/CNT	Sonication	290 kΩ at 10 Hz	(Burgar, s. d.)
PDMS/CNT	Sonication + Magnetic stirring	9 kΩ	(Sanguantrakul et al., 2024)
PDMS/CB	Sonication + Magnetic stirring	18 kΩ at 10 Hz	(X. Cheng et al., 2019)
PDMS/Au	Coating	18 kΩ at 20 Hz	(L.-F. Wang et al., 2012a)
PDMS/Cu	Coating	600 kΩ at 31 Hz	(Meng et al., 2016)
PDMS/Cu	Coating	39.43 kΩ	(Han et al., 2025a)
PDMS/CNT	Tree-roll milling	19-38 kΩ at 1 kHz	(Oh et al., 2024b)
PDMS/MWCNTs	Sonication	250 kΩ at 30 Hz	(Sharma et al., 2024b)
PDMS/Ag/CNT-GO	Coating	6.4-7.2 kΩ	(P. Li et al., 2023)
PU/Ni/Cu	Coating	2000 kΩ	(Baek et al., 2013)
PU/Ag/AgCl	Coating	702 ± 219 kΩ	(Warsito et al., 2023a)
PU/CB	3D printing	70–90 kΩ at 30 Hz	(Xing & Casson, 2022)
PU/Ag/AgCl	Coating	264 ± 125 kΩ	(Vasconcelos et al., 2021)

Table 3-2 Comparison with relevant work in the application area

Electrode Material	**Fabrication Method**	**Contact Impedance**	**Reference**
PU/Ag/AgCl	Coating	601.5 ± 400.8 kΩ	(Heijs et al., 2021)
EVA/CB	Magnetic stirring	26.8 ± 4.4 kΩ at 31 Hz	This work
SEBS/CB	Magnetic stirring	5.4 ± 0.9 kΩ at 31 Hz	This work
Commercial flexible electrodes	-	4.2 ± 0.5 kΩ at 31 Hz	This work

3.10 Discussion

This study aimed to evaluate the electrical and mechanical performance of flexible dry electrodes based on SEBS/CB and EVA/CB for EEG signal acquisition, comparing them with commercial flexible dry electrodes. The results highlight several key findings regarding electrical conductivity, mechanical properties, contact impedance, and EEG signal quality. The percolation threshold for both SEBS/CB and EVA/CB composites was found to be identical, with both materials exhibiting comparable bulk electrical conductivity once a continuous carbon-black network is established. Below this threshold, incomplete pathways lead to high resistivity, while approaching it produces the expected sharp rise in conductivity associated with classical percolation behavior. Above the threshold, conductivity continues to improve as additional CB densifies the existing network; however, excessive loading increases mixture viscosity, promotes agglomeration, and restricts polymer chain mobility. These effects can limit conductivity gains and decrease elasticity by introducing stiffness. For flexible dry EEG electrodes, such stiffening is undesirable, as it reduces skin conformity and comfort. This highlights the need for an optimal CB concentration that provides a robust conductive network

without compromising the mechanical compliance required for wearable bioelectronic applications.

However, the electrical conductivity plateau achieved by the composites developed in this study is approximately one order of magnitude lower than that reported in similar studies using melt-mixed SEBS/CB composites, such as the work by Kuester et al. (Kuester et al., 2016). Similar effects of CB dispersion and network morphology on conductivity development have been reported by Jamatia et al. (Jamatia et al., 2023) reported an electrical conductivity of 0.01 S/m for SEBS/CB composites prepared via the toluene dissolution method with a very high filler content of 70 vol%. Conversely, SEBS-based composites containing 5 wt% of carbon black (CB) fabricated through extrusion, as reported by Lakto et al. (Latko et al., 2015), exhibited a significantly lower conductivity of 0.0001 S/m. These comparisons suggest that the processing method, filler dispersion, and polymer-filler interactions critically influence the final electrical performance of the composites. As reported in previous studies (Arjmand et al., 2014; Gonçalves et al., 2016; Jiang et al., 2009; Pavlovsky & Siegmann, 2009) and as confirmed by the findings of this work, the variation in electrical conductivity as a function of conductive filler concentration can be generally divided into three distinct regions. In the insulating region, corresponding to low filler content, the AC conductivity strongly depends on frequency. As the CB content increases and approaches the percolation threshold, a sharp rise in conductivity is observed. Beyond this threshold, the AC conductivity becomes almost frequency-independent, indicating the formation of a continuous conductive network within the polymer matrix. At this stage, the composite behaves as an electrically conductive material (Kausar, 2016). In addition, recent works on conductive polymer composites and EMI-shielding materials provide valuable insight into the structure–property relationship of similar systems. For example, hybrid and hierarchical composites based on MXene, CNTs, or π-conjugated polymers have been shown to enhance both conductivity and flexibility through synergistic filler dispersion and strong interfacial bonding (Gui et al., 2023a; C. Li et al., 2025; Y. Li et al., 2024; Y. Luo et al., 2025; J. Wang et al., 2025). Furthermore, MAX-phase-based and core–shell magnetic filler systems enhance electromagnetic absorption and mechanical resilience, highlighting the significance of filler architecture in energy dissipation and mechanical reinforcement. (Nath et al., 2021; Ugraskan et al., 2022; C. Xu et al., 2016).

SEM micrographs revealed a homogeneous dispersion of CB particles, but agglomerations were present at higher CB loadings (20wt%), particularly in both SEBS/CB and EVA/CB composites. Similar agglomerations were reported in (Latko et al., 2015; Pavlovsky & Siegmann, 2009) due to the high concentration of carbon black. While these agglomerations can lead to some variations in conductivity, they also contribute to the formation of percolating networks necessary for efficient charge transport. The presence of CB-CB contacts ensures that conductive paths are present inside the polymer matrix, supporting the electrical performance.

EVA/20wt%CB is stiffer and more resistant to deformation, with higher stress and modulus, whereas SEBS/20wt%CB is softer and more elastic, offering better adaptability and comfort. SEBS/20wt%CB dissipates less energy as heat, resulting in lower hysteresis loss, and is more mechanically resilient under repeated loading cycles. Both materials stabilise over cycles, but SEBS/20wt%CB demonstrates better overall consistency in energy absorption and dissipation. EVA/20wt%CB is suitable for applications requiring rigidity and higher energy restitution. However, its higher hysteresis losses and reduced stability may limit performance under repeated mechanical loads. SEBS/20wt%CB is better suited for applications where flexibility, comfort, and mechanical durability are essential, such as flexible EEG electrodes. Its lower hysteresis loss and higher resilience under repeated use make it a more reliable choice. SEBS/20wt%CB has a lower stiffness, indicated by the gentler slope of the stress-strain curve, making it more flexible and better able to conform to scalp contours, thus enhancing user comfort. The narrower hysteresis loop for SEBS/20wt%CB signifies better elastic recovery, ensuring the electrode maintains good skin contact after repeated compression, which is vital for long-term EEG monitoring. Known for its biocompatibility, SEBS is safer for direct skin contact, reducing the risk of irritation or discomfort. The lower stress at the same strain decreases the risk of discomfort or pressure-related issues during prolonged use. Conversely, EVA/20wt%CB's higher stiffness may limit its ability to conform to scalp curves, potentially leading to poor contact and increased impedance at the skin-electrode interface. Its larger hysteresis suggests less adaptability and greater discomfort over extended periods. Overall, SEBS/20wt%CB is the preferred material for dry, flexible EEG electrodes, as its superior flexibility ensures better skin-electrode contact, lower impedance, and more reliable signal

acquisition. Similar behaviour has been observed in other thermoplastic elastomer nanocomposites and EOC-based foams, which exhibited improved cyclic compression recovery and reduced hysteresis when reinforced with comparable filler content (Nayak et al., 2025). The current results also align with those of Wang et al. (Kausar et al., 2017), and Ugraskan et al. (Ponnamma et al., 2016), where carbon-based or SWCNT-reinforced polymer composites demonstrated improved conductivity and compressive recovery due to efficient filler–matrix adhesion. Similarly, PVDF- and polyurethane-based nanocomposites exhibit balanced conductivity and flexibility (Y.-H. Lee et al., 2025a; C. Xu et al., 2016), while hybrid systems integrating graphene, nanodiamond, or MXene phases show outstanding EMI shielding and mechanical durability (Ghosh et al., 2019; Katheria et al., 2025). Overall, these results confirm that the interplay between filler dispersion, interfacial adhesion, and matrix elasticity governs the electrical and mechanical response of SEBS/CB and EVA/CB composites. SEBS/20 wt% CB, in particular, provides an optimal balance of conductivity, softness, and resilience, making it an excellent candidate for durable and comfortable dry EEG electrodes. The superior flexibility of the SEBS/CB electrodes make them particularly suitable for EEG applications, ensuring better conformity to the scalp curvature and reducing motion artifacts.

The DSC thermograms of the SEBS/CB and EVA/CB composites provide additional insight into the thermal stability and segmental mobility of the elastomer matrices after the incorporation of carbon black. Both materials retain their characteristic thermal transitions, indicating that the filler does not alter the intrinsic thermal behavior of the polymers. SEBS/CB exhibits a glass transition near –50 °C, consistent with the soft ethylene–butylene phase, while EVA/CB shows a Tg around –35 °C followed by a mild endothermic transition associated with the softening of the vinyl-acetate-rich–rich domains. These observations confirm that the addition of 20 wt% carbon black does not disrupt the microphase structure or thermal relaxation mechanisms of either matrix. This is particularly relevant for EEG applications, as the preservation of the thermal transitions ensures that the composites maintain the elasticity, softness, and temperature resilience required for skin-conforming electrodes. The stable thermal behavior supports the conclusion that the improvements in electrical conductivity and mechanical response reported in this study arise primarily from the formation and densification

of the CB conductive network, rather than from modifications of the polymer thermal properties.

The comparative results highlight that the SEBS/CB electrode developed in this work offers the best trade-off between conductivity, impedance, flexibility, and manufacturability among polymer-based dry electrodes reported to date. Its performance is close to that of commercial reference electrodes, demonstrating the effectiveness of carbon black dispersion and the suitability of SEBS as a soft, recyclable matrix for EEG applications. EVA/CB electrodes, while less flexible, still outperform many PDMS- and TPU-based counterparts in terms of impedance and cost-effectiveness. These findings confirm the potential of SEBS- and EVA-based composites as sustainable alternatives for large-scale fabrication of comfortable and durable EEG electrodes.

The stability of flexible dry electrodes over time is vital for reliable EEG signal acquisition. In this study, measurements were taken over a 10-second recording period, which aligns with durations reported in previous research using the same timeframe (Mermi Dibek & Baykan, 2025; Qi et al., 2025; Triggiani et al., 2025; X. Zhong et al., 2026). During this period, both SEBS/CB and EVA/CB electrodes showed consistent impedance and signal amplitude, confirming their short-term stability. Although the in vivo evaluation provided useful insights into the real-world performance of the electrodes, certain limitations must be recognized. The study involved four participants, and the EEG recordings lasted only 10 seconds, which limits the statistical significance of the findings. Future research will involve larger participant groups, longer recording sessions, and additional analyses in both time and frequency domains to verify the robustness of the observed performance. These efforts will also assist in validating the long-term stability and clinical potential of SEBS-based electrodes for wearable and medical-grade EEG monitoring.

SEBS/CB electrodes exhibited significantly lower contact impedance than EVA/CB electrodes, as well as those made of TPU and PDMS discussed in this paper. The EEG signal analysis further supports the superiority of SEBS/CB electrodes over EVA/CB. SEBS/20wt%CB electrodes are preferred for flexible EEG applications due to their lower

contact impedance and more stable signal performance as compared to EVA/20wt%CB. The signal waveforms highlight the significant role of contact impedance in ensuring stable and high-quality signal acquisition. Contact impedance, a key parameter influencing EEG signal quality, is critical for evaluating electrode performance. Compared to the SEBS/CB and EVA/CB electrodes developed in this study, the active claw-shaped dry electrodes proposed by Wang et al. (Z. Wang et al., 2024c) exhibit significantly higher and less stable contact impedance, particularly over hairy scalp areas. Similarly, other flexible, low-cost dry electrodes reported in the literature (G. Li et al., 2020; Motiepor et al., 2025; Z. Shi et al., 2023a) also present higher contact impedance relative to the SEBS/CB electrodes developed in this work, further demonstrating the superior electrical performance of the latter. This superior performance is attributed to the improved skin-electrode interface stability and the lower impedance achieved with the SEBS/CB formulation, which is particularly beneficial for reliable and high-quality EEG signal acquisition. Furthermore, both SEBS/CB and EVA/CB electrodes outperform the silicone-based dry electrodes fabricated by Hang et al. (Han et al., 2025b) and Stauffer et al. (Stauffer et al., 2018c) in terms of contact impedance, underscoring their enhanced electrical properties and more stable skin-electrode coupling. These findings underscore that contact impedance, alongside bulk electrical conductivity, is a critical parameter in the design and fabrication of effective EEG electrodes. The results clearly demonstrate that contact impedance, rather than electrical conductivity alone, plays a dominant role in determining EEG signal quality. This study highlights the strong potential of SEBS/CB electrodes as a superior alternative to conventional materials such as EVA for flexible EEG applications. SEBS/CB electrodes exhibit low contact impedance, excellent flexibility, and deliver a stable EEG signal acquisition. Nevertheless, there remains room for further improvements, particularly in optimizing the electrode-skin interface, enhancing long-term stability, and refining manufacturing processes to scale production while maintaining performance. Further improvements can be explored:

- Optimizing SEBS/CNT composites: Carbon nanotube (CNT) reinforcements could enhance conductivity without significantly increasing stiffness.
- Evaluating long-term stability: Investigating the durability of SEBS/CB electrodes under prolonged use and repeated compression cycles.

- Improving skin adhesion: Future designs could incorporate self-adhesive materials or integrate the electrodes into EEG headsets for better stability and reduced motion artifacts.
- Exploring hybrid composites: Combining SEBS with additional conductive fillers (e.g., CB, graphene, CNT) could further reduce the impedance and enhance the signal quality.

3.11 Conclusion

This study provided a comprehensive comparison between flexible dry EEG electrodes fabricated from SEBS/CB and EVA/CB conductive polymer composites, emphasizing their electrical, mechanical, and functional performance. Both composites achieved a bulk electrical conductivity of approximately 0.01 S/m with a percolation threshold near 12 wt% carbon black. However, SEBS/CB electrodes exhibited significantly lower contact impedance (5.4 ± 0.9 kΩ) compared to EVA/CB (26.7 ± 4.4 kΩ), approaching the performance of a commercial flexible electrode (4.2 ± 0.5 kΩ).

From a mechanical perspective, SEBS/CB demonstrated greater softness, elasticity, and energy efficiency, leading to improved scalp conformity and reduced hysteresis loss during cyclic deformation. In contrast, EVA/CB exhibited higher rigidity and energy dissipation, consistent with its thermoplastic character. EEG recordings further confirmed that SEBS/CB electrodes produced more stable and higher-quality signals, whereas EVA/CB performance was limited by higher impedance and lower flexibility.

Overall, the results indicate that SEBS/CB composites provide the most balanced combination of electrical performance, mechanical compliance, and user comfort, making them promising materials for durable, high-performance, and comfortable dry EEG electrodes.

Nevertheless, some limitations should be acknowledged: the number of in vivo tests was limited, the measurements were restricted to short-term recordings, and long-term stability or large-scale reproducibility was not yet evaluated. These aspects will be addressed in future work through extended testing across multiple participants and under dynamic, real-world conditions to confirm the robustness and reliability of the developed electrodes.

3.12 Author credit statement

The authors of the published version of this study are George Gnonhoue (GG), Ilyass Tabiai (IT), Jérémie Voix (JV), and Éric David (ED).

GG conducted the investigation and performed the experiments, data processing, and formal analyses. He carried out the analytical calculations, contributed to the interpretation of the results, and prepared the figures. GG drafted the original version of the manuscript and incorporated all revisions following peer review.

IT contributed to the conceptualization of the project and the development of the experimental methodology. He participated in the scientific validation of the proposed approaches, the acquisition of funding, and the critical review of the manuscript, and provided overall supervision of the work.

JV contributed to the investigation and formal analysis, as well as to funding acquisition. He participated in the review and editing of the manuscript and co-supervised the project throughout its execution.

ED contributed to the conceptualization of the project and the development of the methodology. He was involved in formal analysis, funding acquisition, and critical review of the manuscript, and provided scientific co-supervision of the work.

IT and ED jointly supervised the project.

3.13 Author Declarations

The authors declare that they have no known competing financial interests or personal relationships that could have appeared to influence the work reported in this paper. The data of this study are available upon request.

3.14 Acknowledgements

The authors would like to acknowledge the financial support received from NSERC Alliance (ALLRP 566678-2021), MITACS IT26677 (SUBV-2021-168), and PROMPT (#164_Voix-

EERS 2021.06) for the ÉTS-EERS Industrial Research Chair in In-Ear Technologies, which is sponsored by EERS Global Technologies Inc.

CHAPITRE 4

ELECTRICAL AND THERMO-MECHANICAL PROPERTIES OF STYRENE-ETHYLENE-BUTYLENE-STYRENE/CARBON NANOTUBE AND STYRENE-ETHYLENE-BUTYLENE-STYRENE/CARBON BLACK MULTIPIN ELECTRODES FOR ELECTROENCEPHALOGRAPHY

George Gnonhoue [a], Ilyass Tabiai [a*], Jérémie Voix [a], Éric David [a]

[a] École de technologie supérieure, 1100 Notre-Dame Street West, Montreal, Quebec, H3C 1K3, CANADA

Paper published in the *journal Sensors and Actuators: A. Physical*, December 2025

https://doi.org/10.1016/j.sna.2025.117446

Chapter outline: This chapter presents the article corresponding to the results of the third part of the project. It emphasizes the dispersion and distribution of conducting additives in the polymeric matrix, the interactions between additives and the matrix, the formation of an electrically conductive network, and the properties of flexible styrene-Ethylene-Butylene-Styrene/Carbon Black (SEBS/CB) and styrene-Ethylene-Butylene-Styrene/Carbon Nanotubes (SEBS/CNT) electrodes for EEG.

Abstract: Flexible EEG electrodes have attracted increasing attention due to their potential applications in mobile health monitoring. However, balancing electrical conductivity, flexibility, stretchability, and EEG signal recording remains challenging. Here, we fabricated polystyrene-block-poly(ethylene butylene)-block-polystyrene (SEBS) composites with carbon nanotubes (CNT) and carbon black (CB) via solvent dissolution. The percolation threshold was approximately 12wt% for SEBS/CB composites and approximately 2wt% for SEBS/CNT composites. At 20wt%, SEBS/CB composite conductivity plateaued at 0.01 S/m, whereas SEBS/CNT composite conductivity reached 1.26 S/m at 16 wt%. Contact impedance was

4.2 ± 0.45 kΩ for SEBS/16wt%CNT and 5.4 ± 0.9 kΩ for SEBS/20wt%CB. SEBS/CNT was slightly stiffer than SEBS/CB. The electrodes reliably recorded EEG signals, demonstrating their potential for health monitoring and long-term EEG measurements.

4.1 Introduction

The development of wearable electronics has transformed electroencephalogram (EEG) electrode technology (Huang et al., 2024; Palumbo et al., 2024; Xiong et al., 2024). EEG electrodes are sensors that detect brain activity, and traditional EEG systems typically employ rigid, wet electrodes with conductive gel to ensure stable contact and low impedance at the skin-electrode interface However, wet electrodes can be uncomfortable, cause skin irritation or hair damage with prolonged use, and necessitate application by skilled personnel, who may perform skin abrasion to optimize contact impedance (Di Flumeri et al., 2019). The conductive gel dries out, limiting measurement duration and impacting signal quality, making gel-based EEG systems less than ideal for non-laboratory settings (H.-L. Peng et al., 2015; Petrossian et al., 2023; Zeydabadinezhad et al., 2024).

To address the limitations associated with wet electrodes, semi-dry electrodes have recently emerged as a promising alternative. These systems deliver a minimal amount of electrolyte to the scalp via porous or absorbent media, forming a hydrated interface that effectively stabilizes contact impedance. Despite their advantages, electrolyte-based interfaces, including semi-dry configurations, still pose a risk of skin irritation or infection (S. Lin et al., 2019). Moreover, semi-dry electrode technology continues to face technical challenges such as precise control over electrolyte release (G. Li et al., 2018), prevention of short circuits between neighboring electrodes, and maintaining structural integrity under mechanical pressure during use (P. Li et al., 2022). Recent advances have highlighted the potential of hydrogel-based materials to support controlled electrolyte release in semi-dry configurations. In particular, flexible hydrogels such as polyvinyl alcohol/polyacrylamide (PVA/PAM) and Fe^{3+}-doped gelatin/poly(acrylate-co-acrylamide) have demonstrated acceptable electrochemical properties, with contact impedance values of 18 ± 8.9 kΩ and 17.8 ± 3.69 kΩ at 10 Hz, respectively (G. Li et al., 2023, 2025). These materials exhibit strong signal correlation with

conventional wet electrodes during standard EEG paradigms (eyes closed/open) and ensure better moisture retention, mechanical resilience, and long-term comfort. Studies (G. Li, Wang, et al., 2021; G.-L. Li et al., 2020b) emphasize that semi-dry electrodes combine the mechanical flexibility of dry systems with the signal stability of wet electrodes, making them suitable for continuous, high-fidelity EEG monitoring in wearable and brain-computer interface applications. The high conductivity of the electrodes enabled reliable acquisition of cortical electrical activity, essential for exploring complex cognitive processes and higher-order consciousness. In this context, the recent work by Sidheekha et al. (Sidheekha et al., 2023) provides valuable insights into multifunctional conductive polymer-based electrodes. They introduced polyaniline/chitosan (PANI/CS) hybrid hydrogels that act as both energy storage devices and self-sensing elements. These electrodes utilize the redox-driven faradaic properties of polyaniline to detect variations in current, temperature, and electrolyte concentration through changes in potential and energy consumption. This integrated sensing-storage approach, requiring no additional connectivity, highlights the potential of conductive polymer composites for next-generation bioelectronic interfaces.

Despite their advantages, semi-dry electrodes are not a definitive solution. Their reliance on hydrated interfaces introduces limitations such as electrolyte evaporation, limited shelf life, and potential material degradation. Furthermore, skin irritation risks, manufacturing complexity, and maintenance requirements may hinder their widespread adoption for daily or long-term EEG monitoring. These drawbacks have sustained interest in the development of fully dry electrodes, which aim to simplify use while maintaining high signal fidelity and comfort. This work focuses on designing dry and flexible EEG electrodes based on Polystyrene-block-poly(ethylene butylene)-block polystyrene (SEBS) and carbon-based conductive fillers. These electrodes are a gel-free, user-friendly alternative that maintains stable performance over hair-covered regions, addressing challenges in wearable neurotechnology.

Recent efforts have focused on next-generation EEG systems that eliminate the need for any gel or liquid interface. Dry electrodes, especially those based on flexible materials, provide stable contact with the skin’s curved surface, unlike rigid electrodes, which do not conform to

scalp contours and limit EEG signal acquisition (Veronica et al., 2024; F. Wang et al., 2024; Zeydabadinezhad et al., 2024). Consequently, recent studies have been exploring flexible, multifunctional composite materials to enhance EEG electrode performance and user comfort (Dadjou et al., 2024; Zeydabadinezhad et al., 2024). Multifunctional composite materials are being developed to create EEG electrodes with optimal flexibility, conductivity, and comfort for long-term use (K. Gao et al., 2024b; Kaveh et al., 2024; O. Lee & Lee, 2024; Y. Peng et al., 2024; Van Der Heijden et al., 2024). Ergonomic, flexible multipin geometries have improved EEG signal quality and user comfort, enhancing the potential for diagnostics and neuroscience research (Abdullah & Al-Neami, 2021; Damalerio et al., 2023; Fiedler et al., 2023; Haueisen et al., 2020; Heijs et al., 2021; S. Lin et al., 2023; Q. Liu et al., 2023; Z. Shi et al., 2023b; Warsito et al., 2023b; Xing & Casson, 2022, 2023b). Thermoplastic polyurethane (TPU) and polydimethylsiloxane (PDMS), combined with carbon reinforcements, show promise for fabricating flexible electrodes (K. Chen et al., 2024; Hong et al., 2024; X. Zhao et al., 2024). Carbon black (CB) and carbon nanotubes (CNTs) are commonly incorporated into polyurethane (PU) and PDMS to produce multipin EEG electrodes (Fu et al., 2020b; B.-S. Lin et al., 2021; S. Lin et al., 2023; Lozano & Stoeber, 2019; J. Wang et al., 2023; Xiao et al., 2021). These materials achieve electrical conductivity through a conductive surface coating or by embedding carbon reinforcements to enhance volume conductivity, enabling stable signal acquisition in dry conditions. Fiedler et al. (Fiedler et al., 2015) developed a 24-pin dry EEG electrode made of polyurethane and coated with Ag/AgCl for ergonomic and flexible multipin EEG electrodes. Integrated into a textile cap, the system can accommodate up to 97 multipin electrodes. In tests comparing this 97-channel dry EEG cap with a conventional 128-channel wet EEG cap, parameters such as resting-state EEG, alpha activity, eye blinks, and visual evoked potentials were evaluated. The wet electrodes-maintained impedance values below 20 kΩ, while the dry electrodes exhibited average impedances below 150 kΩ for 92 of the 97 channels. Despite the higher impedance, the system reliably recorded EEG signals. Heijs et al. (Heijs et al., 2021) also validated flexible multipin dry electrodes against a commercial wet system. Their dry electrode setup consisted of 32 AgCl-coated polyurethane electrodes fabricated via electroless plating, whereas the wet system employed 32 Ag/AgCl gel electrodes. EEG signal acquisition was evaluated using auditory stimuli and tasks involving

eyes-open and eyes-closed conditions. The mean impedance of the wet electrodes was 6.8 ± 5.6 kΩ, whereas the dry electrodes exhibited a higher mean impedance of 602 ± 401 kΩ. Wand et al. (Z. Wang et al., 2024b) designed a dry, claw-shaped EEG electrode for detecting signals in both hairy and non-hairy areas. This electrode, fabricated entirely from 3D-printed TPU, features a conductive coating created by blending TPU with a silver (Ag) solution. Its performance was evaluated against that of a traditional wet electrode through contact impedance tests and EEG signal acquisition during tasks involving eye-opening and eye-closing conditions. The wet electrode exhibited contact impedance values of 5 kΩ at 1 Hz in hairless areas and 10 kΩ in hairy areas, while the TPU electrode exhibited higher impedances of 18.6 kΩ and 122 kΩ in hairless and hairy regions, respectively. Xing and Casson (Xing & Casson, 2023a) also developed flexible, 3D-printed TPU multipin electrodes, which exhibited a typical contact impedance in the 100–200 kΩ range, demonstrating their suitability for flexible electrodes with moderate impedance for EEG signal capture.

Recent studies have explored PDMS and innovative designs for flexible, long-wear EEG electrodes to enhance user comfort and signal reliability in both hairy and non-hairy scalp areas. Das et al. (Das et al., 2020b) developed electrodes that combine CNT, PDMS, and graphene, highlighting the affordability, biocompatibility, and robustness of graphene. These electrodes performed comparably to traditional silver/silver chloride (Ag/AgCl) electrodes. Oh et al. (Oh et al., 2024a) fabricated multi-walled carbon nanotube (MWCNT) and PDMS composites using paste mixing and three-roll milling, producing a series of composites with varying CNT content (0.5–10 wt%). As CNT concentration increased, the conductivity of the composite rose, peaking at 100 S/m beyond 5 wt%. The contact impedance of these composites was evaluated, with wrinkled electrodes achieving 19 kΩ and unwrinkled electrodes achieving 38 kΩ at 1 kHz. These electrodes were validated with eye movement and cognitive tasks. Sharma et al. (Sharma et al., 2024a), prepared MWCNT-PDMS composites using a solution-based method, creating electrodes with an impedance comparable to that of silver/silver chloride (Ag/AgCl) across the 20 Hz–1 kHz spectrum. For example, MWCNT-PDMS dry electrodes exhibited an impedance ranging from 626 kΩ at 20 Hz to 124 kΩ at 1 kHz, closely matching that of silver/silver chloride (Ag/AgCl) electrodes. Wang et al. (L.-F. Wang et al., 2012b) designed flexible PDMS-based multipin dry electrodes coated with a gold layer and

fabricated using manual and ultrasonic methods. These electrodes, having either 13 or 21 pins, recorded EEG signals effectively through hair without the use of conductive gel. In non-hairy areas, the silicone dry electrodes exhibited impedance levels of 8.0 kΩ at 20 Hz and 5.0 kΩ at 10 kHz without skin preparation, while in hairy areas, they yielded 18 kΩ at 20 Hz and 10 kΩ at 10 kHz. Stability testing over 5.5 hours revealed that the dry electrodes maintained a consistent impedance of around 3.8 kΩ, while those of the wet electrodes increased from an initial 1.8 kΩ to over 8 kΩ within the same period. EEG electrode technology has shifted toward dry, flexible, and user-friendly alternatives to rigid wet electrodes, which are often uncomfortable, complex to apply, and exhibit signal instability during prolonged use. Flexible polymers such as PDMS and TPU, combined with conductive fillers like carbon nanotubes (CNTs) and carbon black (CB), have demonstrated significant potential for the fabrication of multipin electrodes capable of maintaining reliable skin contact, including on hairy scalp regions. Despite these advantages, challenges remain, including high contact impedance, limited scalability of fabrication, and mechanical properties that may hinder long-term comfort and durability. Conductive polymer composites such as polystyrene-block-poly(ethylene butylene)-block-polystyrene (SEBS)/CB and SEBS/CNT are not restricted to EEG applications. Compared with conventional PDMS- and TPU-based flexible electrodes, SEBS/CB composites provide clear benefits in processing simplicity, cost, and scalability. SEBS is a thermoplastic elastomer that can be easily processed by melt-mixing, hot pressing, or extrusion without the need for curing or vacuum-degassing steps, allowing for swift production. (Robertson et al., 2023; Y. Xu et al., 2020) . Recent studies have demonstrated that SEBS-based materials can also be engineered into porous, breathable, and recyclable structures suitable for wearable and thermal-management applications while maintaining excellent flexibility and mechanical robustness (R. Wang et al., 2025; M. Xu et al., 2025; W. Zhong et al., 2025) . Furthermore, both SEBS and carbon black are low-cost, recyclable materials that can be reprocessed using standard thermoplastic routes, providing a sustainable and environmentally friendly alternative for large-scale manufacturing of flexible EEG electrodes (Bidiyasar et al., 2024). Their combination of electrical conductivity, mechanical softness, and long-term durability makes them promising for bioelectronic interfaces, including electrocardiography (ECG), electromyography (EMG), and other skin-mounted sensors.

Nevertheless, EEG electrodes impose more stringent functional requirements. They must ensure low contact impedance without conductive gel, maintain skin contact through hair-covered scalp regions, and provide stable signal acquisition over extended periods, even with micro-movements (Das et al., 2020a; de Camp et al., 2018; Habibzadeh Tonekabony Shad et al., 2020; L. Yang et al., 2021). Meeting these challenges requires elastomeric materials that are conductive, compliant, biocompatible, and conform closely to the scalp's complex geometry (Fu et al., 2020a). SEBS-based composites are strong candidates for next-generation dry EEG electrodes and versatile for broader biomedical sensing platforms. SEBS, a thermoplastic elastomer known for its flexibility, softness, and skin compatibility, has attracted attention in piezoresistive sensors and ECG devices (Cetin & Karahan Toprakci, 2021a; M. Liu et al., 2023a; Y. Peng et al., 2024; Tekay, 2020; Tekay et al., 2023; X. Wang et al., 2018; X. Yang et al., 2019a; B. Zhou et al., 2022). However, its application in EEG systems, particularly in composite configurations incorporating carbon nanotubes (CNTs) or CB, remains insufficiently explored. To address this gap, this study comparatively evaluates SEBS/CB and SEBS/CNT composites for flexible multipin EEG electrodes. This investigation builds on our previous comparative work with SEBS/CB and ethylene-vinyl acetate (EVA)/CB composites, which identified SEBS/CB as promising due to its superior electrical, mechanical, and stability properties. We extend that approach by integrating CNTs and systematically characterizing the composites' electrical performance (via impedance spectroscopy and conductivity), mechanical flexibility (via dynamic mechanical analysis), and thermal stability. This study does not aim to validate the electrodes in terms of EEG signal decoding or clinical performance. Instead, we focus on evaluating material properties critical for designing reliable, comfortable dry EEG electrodes. A dedicated clinical study assessing long-term recording quality and usability across multiple users and conditions is outside this paper's scope and will be considered in future work. The goal is to identify the composite material that best balances electrical conductivity, low contact impedance, mechanical compliance, thermal stability, and scalp conformity. Ultimately, this research aims to support the development of durable, high-performance EEG electrodes suitable for extended, real-world use.

4.2 Materials and Methods

This section investigates the use of polystyrene-block-poly(ethylene butylene)-block polystyrene (SEBS)-based materials to enhance EEG measurements. It compares SEBS/carbon black and SEBS/CNT composites with a commercial dry flexible electrode to identify the formulation with superior electrical conductivity and lower contact impedance. This study does not evaluate clinical efficacy or brain-signal decoding performance. The focus is on assessing critical material properties—electrical behavior, mechanical compliance, and electrode-skin contact stability—that determine the suitability of these composites for flexible dry EEG electrodes. A follow-up clinical study involving long-term and multi-subject EEG recordings will be considered in future work.

4.2.1 Materials

Polystyrene-block-poly(ethylene butylene)-block polystyrene (SEBS), with a number average molecular weight of 54,000 g/mol and a polystyrene content of 30 wt%, was supplied by Kraton (Kraton, Paulínia – SP, Brazil). SEBS was selected as the base material for fabricating flexible EEG electrodes. Multiwalled Carbon Nanotubes (MWCNTs), specifically NC 7000™ from Nanocyl S.A. (Sambreville, Belgium), were used as conductive fillers. These nanotubes have an average diameter of 9.5 nm, an average length of 1.5 μm, a surface area of 250-300 m^2/g, a nominal electrical conductivity of 100 S/m, a density of 1.30-2.00 g/cm^3, and a carbon purity of 90%. Carbon Lampblack nanoparticles (C198-500, Lot 145509), purchased from Fisher Chemical (Fisher Scientific Company, Ottawa (ON), Canada), were also used. These particles have a diameter of 50 nm, a nominal conductivity of 400 S/m, and a density of 1.8 g/cm^3. For the dissolution, UN1294 toluene Optima (T291-4, Lot 234238), also from Fisher Chemical, was used.

4.2.2 Electrode Preparation

The composites were prepared by dissolving pure SEBS in toluene at a fixed solvent-to-polymer ratio of 10 mL g^{-1} (i.e., 100 mL of toluene for 10 g of total composite). Solvent

blending was selected to achieve nano-scale dispersion of conductive fillers while preserving the anisotropic structure of carbon nanotubes, which is essential for efficient electrical percolation. When properly recovered, the solvent does not introduce environmental concerns and enables more uniform filler distribution and stable conductivity compared with dry mechanical mixing (Alam et al., 2021, 2024). The dissolution was carried out at 100 °C under magnetic stirring at 600 rpm until a homogeneous polymer solution was obtained. Subsequently, carbon nanotubes (CNT, 0–16 wt%) and carbon black (CB, 0–25 wt%), as summarized in Table 1, were gradually added to the solution. The mixture was maintained under the same stirring conditions (600 rpm, 100 °C) for an additional 30 min to promote uniform filler dispersion and minimize agglomeration.

After casting, the mixture was placed under a fume hood and dried at room temperature for at least 24 hours to ensure complete solvent evaporation. This extended drying period was chosen to facilitate the full removal of toluene before moulding. The resulting composite was molded by compression to manufacture multipin-shaped EEG electrodes at a temperature of 215 °C, with an initial pressure of 0.8 MPa for 5 minutes, followed by an increase to 5 MPa for an additional 15 minutes while maintaining the temperature. During the subsequent hot-pressing process used to form the multipin electrode geometry, the material was processed at 215°C, well above the boiling point of toluene (110°C), adding an extra thermal step for solvent removal. These combined ventilated drying and high-temperature moulding steps help reduce the chances of residual toluene in the final electrodes. Each electrode consisted of 19 pins, with each pin measuring 4.9 ± 0.09 mm in height and 1.41 ± 0.01 mm in diameter. The pins were arranged in a circular configuration with a center-to-center spacing of approximately 2.5 mm, resulting in an inter-electrode edge-to-edge spacing of approximately 1.1 mm on the contact surface. This multipin layout is designed to improve contact performance on hairy scalp regions by allowing the pins to gently part the hair and establish multiple low-impedance contact points on the skin. This configuration enhances signal quality and reduces motion artifacts during EEG acquisition.

The nanocomposites fabricated using this procedure are listed in Table 4-1. Three samples of each nanocomposite were used for characterization

Table 4-1 SEBS/CNT and SEBS/CB nanocomposites at different carbon nanoparticle weight fractions

SEBS/CNT		SEBS/CB	
Reinforcements (wt%)	Matrix (wt%)	Reinforcements (wt%)	Matrix (wt%)
0	100	0	100
4	96	5	95
6	94	10	90
8	92	12	88
10	90	15	85
12	88	20	80
14	86	25	75
16	84	-	

4.2.3 Methods

4.2.3.1 Electrical Characterization

Electrical characterization assesses the electrical performance and conductivity of composite electrodes, crucial for EEG signal acquisition with minimal distortion. The electrical conductivities of the composites were measured using a frequency-domain broadband dielectric spectrometer (BDS) (Alpha-A Dielectric Analyzer, Novocontrol, Germany). Circular samples with a diameter of 20 mm and a thickness of 1.2 mm were mounted between two solid brass electrodes, forming a typical plane-plane electrode/composite/electrode sandwich configuration. Measurements were performed from 10^{-2} Hz to 10^{5} Hz at 30°C. This

setup accurately determines complex impedance, providing insights into the material's conductive behavior, frequency-dependent response, and electrochemical stability—critical parameters for high-performance EEG electrodes.

4.2.3.2 Structural Characterization

Structural characterization examines the composite's internal morphology and evaluates the dispersion of conductive particles within the polymer matrix, factors influencing electrical performance and mechanical integrity. We used a high-resolution scanning electron microscope (SEM) (Hitachi SU-8230 field emission) at an accelerating voltage of 5 kV. To prepare the samples, composite cross-sections were obtained via cryogenic sectioning to preserve the internal structure. These cross-sections were coated with a ~2 nm layer of platinum under vacuum using a turbo-pumped sputter/carbon coater (Q150T) to enhance surface conductivity and image resolution. This technique enables high-contrast imaging of the conductive filler network and assesses dispersion homogeneity, impacting the composite's functional properties.

4.2.3.3 Thermo-Mechanical Characterization

Thermo-mechanical characterization confirms conductive particle weight fractions, assesses thermal stability via decomposition temperatures, and evaluates mechanical behavior as a function of temperature. These properties are essential for material integrity during processing and use in biomedical applications such as EEG acquisition. To assess the thermal stability and validate the filler content, thermogravimetric analysis (TGA) was performed using a Diamond TG/differential thermal analysis (DTA) instrument (Perkin Elmer). Samples weighing approximately 10–13 mg were heated from 20°C to 500°C at a rate of 3°C/min under a nitrogen atmosphere flowing at 100 mL/min. The temperature was held at 500°C for 2 minutes to ensure complete decomposition. This technique determines the decomposition onset, residual mass (used to verify the filler content), and the composites' thermal degradation profiles. To investigate the viscoelastic behavior of the composites, dynamic mechanical thermal analysis (DMTA) was conducted using a DMTA Q800 (TA Instruments Inc.). Tests were performed on polystyrene-block-poly(ethylene butylene)-block polystyrene (SEBS) and nanocomposites

containing 16 wt% CNT and 20 wt% CB. A double cantilever clamp with a 22 mm frame size and a 2 mm center clamp was used. Rectangular specimens (8 mm width × 2 mm thickness) were tested at a constant strain of 0.4%, a frequency of 1 Hz, and a heating rate of 2 °C/min over the 25 °C to 35 °C temperature range. All measurements were carried out under ambient laboratory conditions, with a temperature of approximately 23 °C and relative humidity of 45–55%. Only the storage modulus was measured, providing insights into the stiffness and elastic behavior of the composites across the tested temperature range.

4.2.3.4 Preliminary In Vivo Validation

Preliminary in vivo validation was performed to assess the real-world performance of the developed flexible multipin EEG electrodes in terms of contact impedance and EEG signal acquisition quality. To reflect realistic application conditions, measurements were performed on hairy regions of the scalp. This step is crucial for determining their effectiveness and comfort compared to commercial solutions. Flexible multipin EEG electrodes were selected to evaluate contact impedance and EEG artifacts associated with eye blink reflex. These artifacts were wirelessly recorded using the OpenBCI™ 16-channel Cyton Biosensing Board (OpenBCI, New York (NY), USA) coupled with the Ultracortex 'Mark IV' electroencephalogram headset (OpenBCI, New York (NY), USA). Contact impedance was measured at 31 Hz using the same acquisition system, as illustrated in Figure 4.1. To simulate conditions for wearable EEG applications, the skin was neither cleaned nor abraded before measurements. The electrodes were securely inserted into the headset, which was comfortably positioned on the subject's head without applying pressure to the electrode surfaces, ensuring a user-friendly testing environment. Commercial dry flexible electrodes from OpenBCI were used as references at positions 1, 2, and 5 on the headset, and the flexible multipin electrodes developed in this work were inserted at positions 3 and 4. Figure 4.2 displays both the developed electrode and the commercial reference for visual comparison. Performance was evaluated by measuring contact impedance and EEG signal amplitude for both the developed electrodes and reference electrodes. For statistical reliability, three measurements were performed for each configuration, and the mean and standard deviation were calculated to quantify variability and repeatability. This in vivo validation provides insights into electrode-

skin interface quality, signal integrity, and usability, and compares the developed and commercial EEG electrodes under real-world conditions.

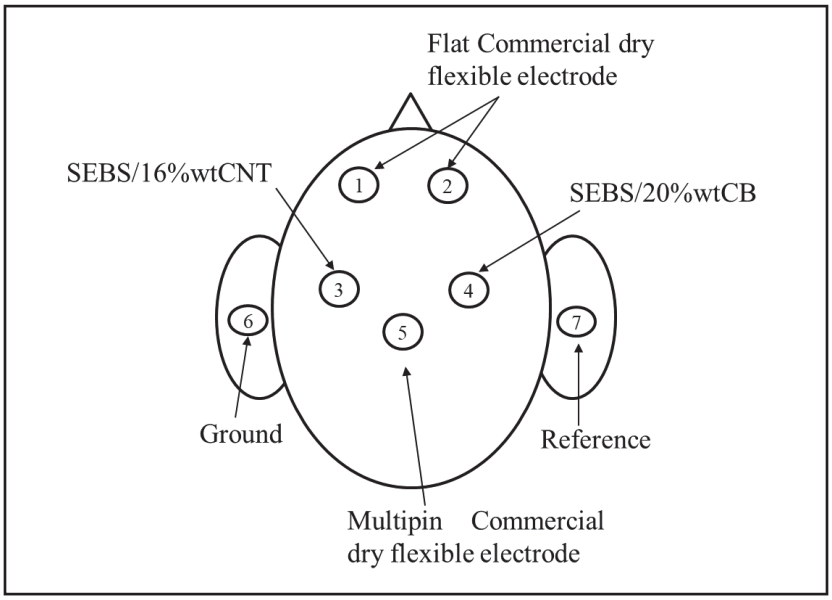


Figure 4.1. Ultracortex “Mark IV” EEG headset for electrode placement

The headset ensures consistent and accurate positioning of EEG electrodes on the scalp to facilitate reliable EEG data acquisition



Figure 4.2. EEG electrode placement and signal acquisition using the 10-20 system

EEG measures electrical activity reflecting neuronal activity related to cognitive processes.

4.2.3.5 Participants

Participant testing validated the effectiveness of the developed EEG electrodes under physiological conditions by assessing EEG signal quality and motion artifacts. Healthy adult participants (n = 4; 1 male and 3 females, aged between 21 and 35 years) were recruited for EEG measurements. All procedures were approved by the ÉTS Internal Review Board (Approval No. H20230504) and conducted according to the Declaration of Helsinki. Informed consent was obtained from all participants prior to the experiments. To ensure a controlled environment, participants were comfortably seated in a quiet room during signal acquisition. EEG signals were recorded for 10 seconds. Following standard EEG protocols and the American Clinical Neurophysiology Society guidelines (Sinha et al., 2016), participants minimized head and facial muscle contractions and remained still to minimize motion artifacts. At a designated moment, participants were asked to blink in response to a sound cue in order to assess the ability of the electrodes to capture characteristic blink-related EEG activity.

4.3 Results

4.3.1 Electrical Properties

Figure 3.3 depicts the real part of the complex conductivity of polystyrene-block-poly(ethylene butylene)-block-polystyrene (SEBS)/carbon nanotube (CNT) and SEBS/carbon black (CB) composites as a function of frequency. Above the percolation threshold, this value approximates the true direct current (DC) conductivity, and below this threshold, it overestimates conductivity because of a frequency-dependent term. As shown in Figure 4.3, once the mass fraction of the composites exceeds 2wt% of CNT and 12wt% of CB, which are the respective percolation thresholds of SEBS/CNT and SEBS/CB composites, the electrical conductivity of the composites becomes independent of frequency. The variation in the real part of the complex conductivity of a composite material as a function of the concentration of the conductive filler can be divided into three regions. In the insulating region, at low conductive particle contents, the complex or AC conductivity is a function of frequency. This behavior is visible in Figure 4.3 for concentrations below 12wt%CB for the SEBS/CB

composite and below 3wt%CNT for the SEBS/CNT composite. With further increases in CB and CNT loading, the electrical conductivity becomes almost independent of frequency, and at this point, the composite material can be considered electrically conductive (Kausar, 2016). Figure 4.3 also shows the non-conductive domain (0-12wt% for SEBS/CB and 0 to 2wt% for SEBS/CNT) that the value of the electrical conductivity at a given frequency is not monotonically correlated with the CB and CNT concentrations due to the contribution of the relaxation mechanisms. SEBS/20wt%CB and SEBS/16wt%CNT were chosen for the fabrication of the multipin electrodes to be used to perform the EEG measurements since they exhibit the highest electrical conductivities. The dotted curves in Figure 4.3 represent the non-conductive composites, while the solid lines represent the conductive ones.

For SEBS/CNT composites:

- Conductivity increases with the CNT content.
- The percolation threshold occurs around 3–4 wt% of CNT.
- Composites containing ≥ 6wt% CNT as reinforcement exhibited stable electrical conductivity across a wide frequency range.

For SEBS/CB composites:

- Conductivity increases with the CB content.
- The percolation threshold occurs around 12–15 wt%of CB.
- Only composites containing ≥ 20 wt% CB exhibited high and stable electrical conductivity.

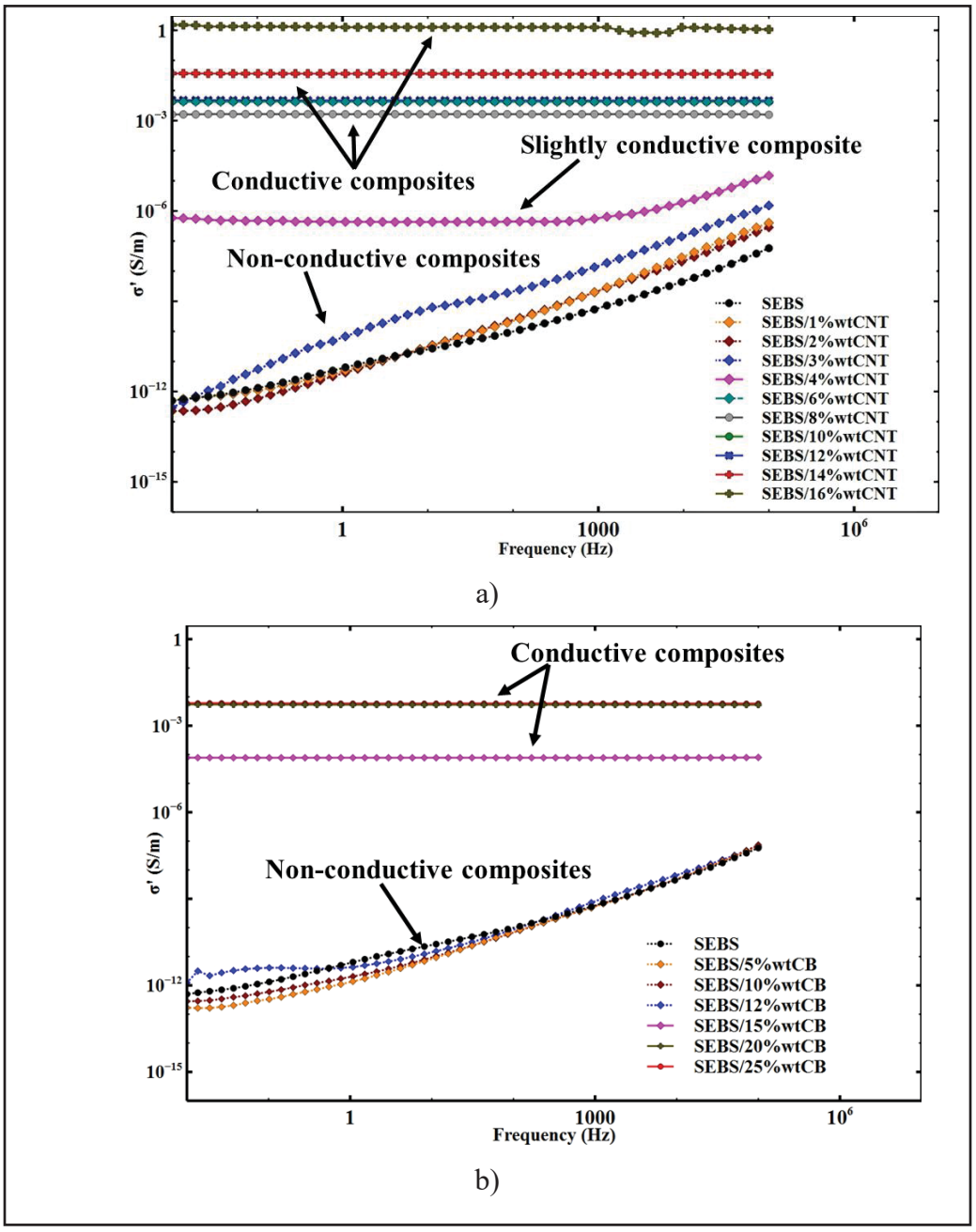


Figure 4.3. Real part of the complex conductivity as a function of frequency of (a) SEBS/CNT and (b) SEBS/CB

Figure 4.4 shows the real part of the complex electrical conductivity of SEBS/CB and SEBS/CNT composites as a function of mass fraction at 1 Hz. The percolation thresholds for SEBS/CB and SEBS/CNT composites were approximately 12 wt% and 2wt%, respectively. In Figure 4.4, it can be observed that beyond the percolation threshold, the electrical conductivity of SEBS/CB composites reached a plateau at 0.01 S/m at 20wt%, while that of the SEBS/CNT composite is 1.26 S/m at 16wt%. Figure 4.4 shows that the percolation threshold of SEBS/CNT composites is lower than that of SEBS/CB. At a mass fraction of 2wt% of CNT within the matrix, SEBS/CNT composites begin to exhibit electrical conductivity, while the SEBS/CB counterparts start to be electrically conductive at a mass fraction of 12wt% of CB.

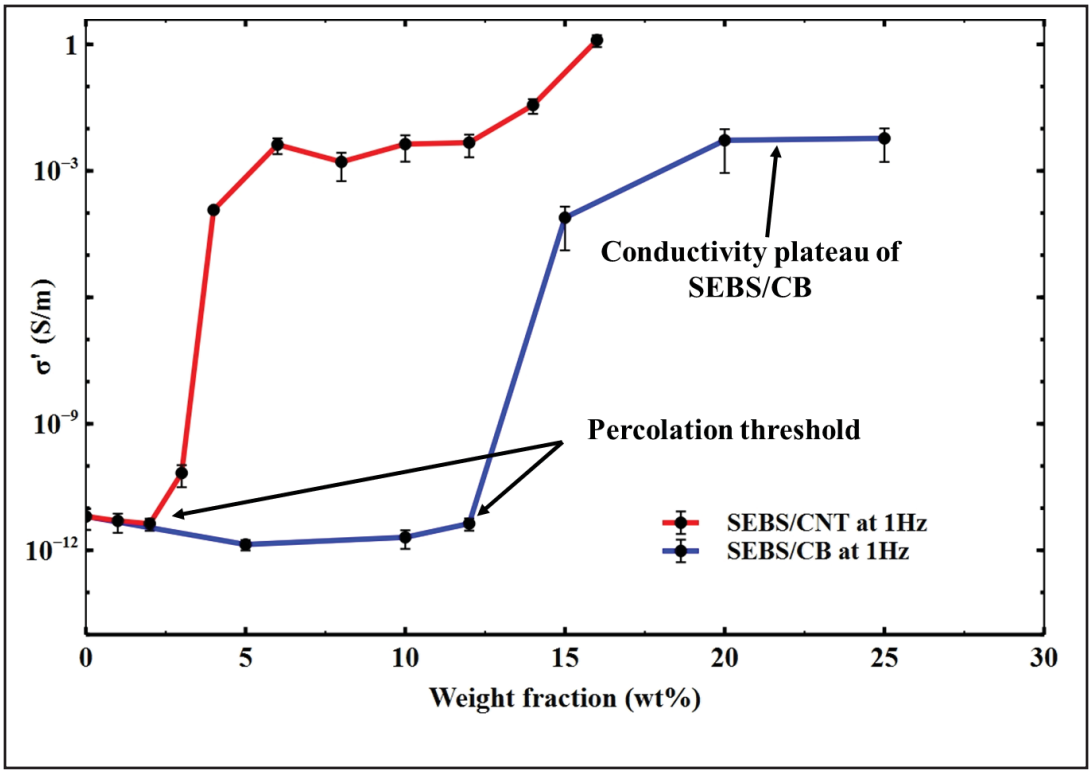


Figure 4.4. Electrical conductivity of styrene-ethylene-butylene-styrene (SEBS) composites as a function of carbon nanotube (CNT) and carbon black (CB) filler loading (wt%)

Increasing the mass fraction of conductive reinforcements significantly enhances the electrical conductivity of the composites. A distinct percolation threshold was observed at approximately 12 wt% for SEBS/CB and 2 wt% for SEBS/CNT, indicating the formation of continuous conductive networks at lower filler contents in the CNT-based composites. Beyond the percolation threshold, SEBS/CB composites exhibit conductivity stabilization near 20 wt% CB due to network saturation and particle aggregation, while SEBS/CNT composites maintain a steady conductivity increase owing to the superior dispersion and high aspect ratio of CNTs. This contrast highlights the greater efficiency of CNTs in forming continuous conductive networks and mitigating the percolation–saturation effect observed in CB-filled systems. This difference highlights the superior efficiency of CNTs in establishing conductive pathways as compared to carbon black.

4.3.2 Structural Properties

Figure 4.5 presents the SEM micrograph of polystyrene-block-poly(ethylene butylene)-block polystyrene (SEBS)/CNT composites containing 16wt% and SEBS/CB composites containing 20wt%CB. The results show that CNT particles appear to be well distributed in the polystyrene-block-poly(ethylene butylene)-block polystyrene (SEBS)/16wt%CNT composites. Figure 4.5(b) shows that some aggregates were observed in the SEBS/20wt%CB composite due to the high concentration of CB (20 wt%). Figure 4.5 illustrates the interaction of the reinforcing agents, CB and CNT, within the different matrices. The morphology of SEBS/16wt%CNT composites revealed that, compared to SEBS/20wt% CB, carbon black (CB) exhibited a greater aggregation in the matrix, whereas carbon nanotubes (CNTs) were more evenly distributed. A uniform dispersion of CB in SEBS may still pose challenges, especially at high concentrations. From an electrical properties standpoint, the presence of aggregates does not negatively impact the composite conductivity, as it facilitates the formation of conductive paths via CB-CB contacts (Cetin & Karahan Toprakci, 2021b; Kouediatouka et al., 2023; H. Lin et al., 2024). Due to their geometric structure and large specific surface area, CNTs also promote CNT-CNT contacts within the SEBS/16wt%CNT composite, enabling conductive pathways throughout the matrix.

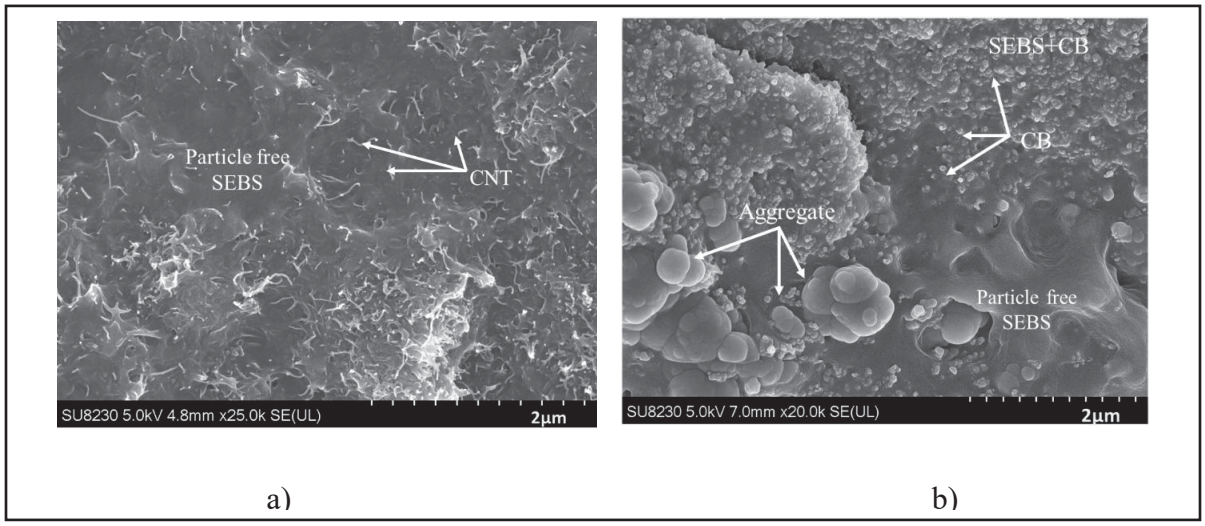


Figure 4.5. Scanning electron microscopy (SEM) micrograph of a: (a) SEBS/16wt%CNT composite and (b) SEBS/20wt%CB composite

4.3.3 Thermo-Mechanical Properties

A TGA was performed on the composites for which micrographic views were taken, as shown in Figure 4.6. The TGA results compare the thermal stability and filler contents of SEBS/16wt%CNT (red curve) and SEBS/20wt% CB (blue curve). Both composites remain thermally stable with no significant weight loss in this range, indicating a good thermal resistance of the polymer-filler systems up to ~370°C. A sharp weight loss begins at around 370–400°C, corresponding to the thermal degradation of the SEBS matrix. The temperature at which decomposition starts is similar for both composites, suggesting a comparable thermal stability. After the complete degradation of the SEBS matrix (~500°C), the SEBS/20wt%CB composite leaves about a 20% residue, matching its carbon black content. The SEBS/16wt%CNT composite leaves about a 16% residue, consistent with its CNT content.

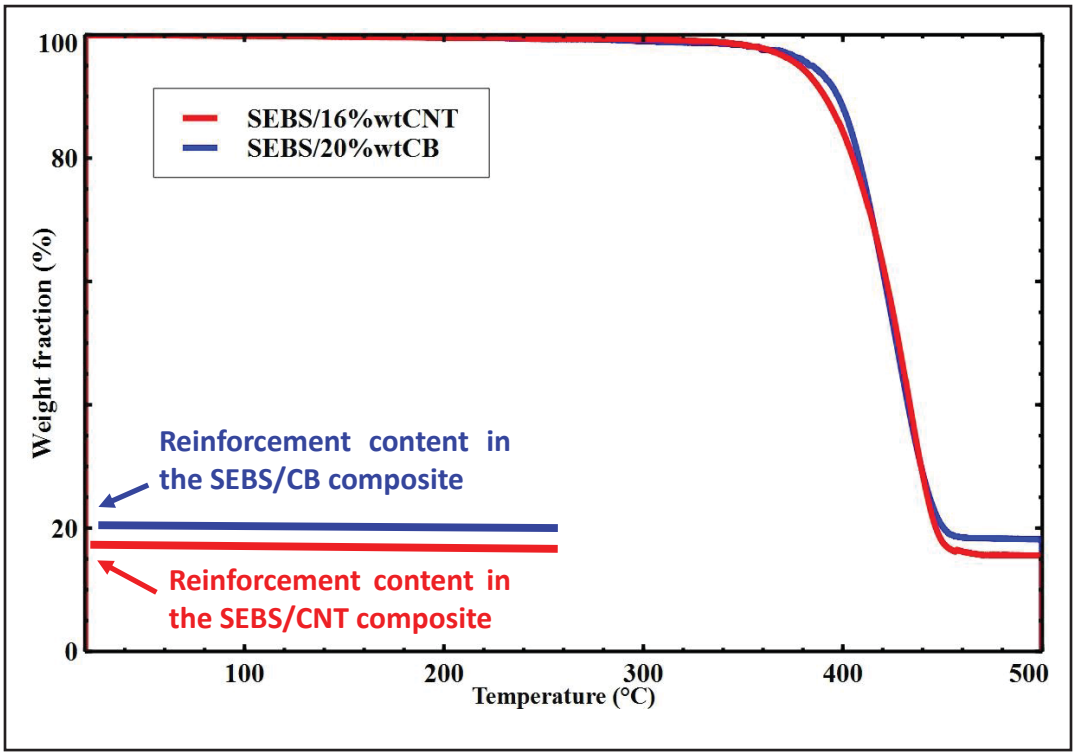


Figure 4.6. TGA thermograms of SEBS/16wt%CNT and SEBS/20wt%CB

Figure 4.7 presents a dynamic mechanical thermal analysis of neat polystyrene-block-poly(ethylene butylene)-block-polystyrene (SEBS), and SEBS/16wt%CNT, and SEBS/20wt%CB composites. It can be observed that the storage modulus of the SEBS/16wt%CNT composite is higher than that of the SEBS/20wt%CB composite, and that the storage modulus of pure SEBS is lower than those of the SEBS/16wt%CNT and SEBS/2wt%CB composites. It can be concluded that the presence of reinforcements within the matrices adds to the mechanical stiffness of the latter.

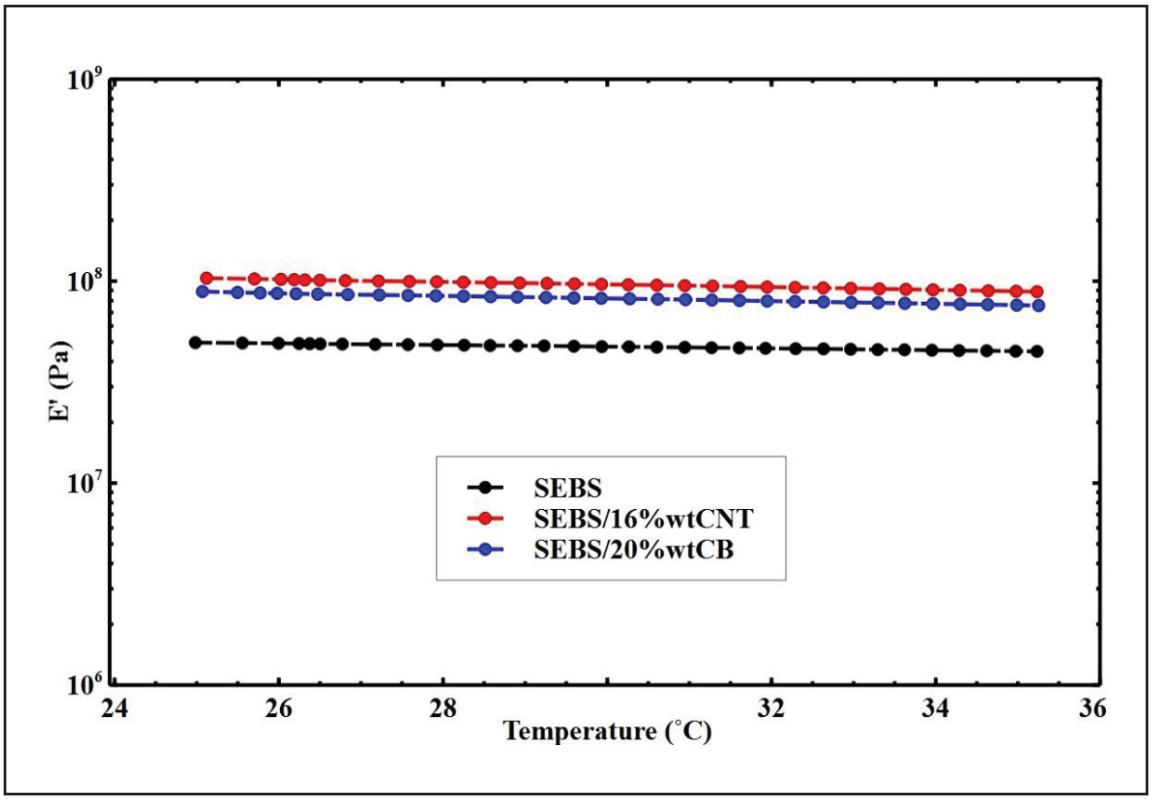


Figure 4.7. DMTA thermograms of polystyrene-block-poly(ethylene butylene)-block polystyrene (SEBS) polymer, SEBS/carbon nanotube (CNT), and SEBS/carbon black (CB) composites

The addition of carbon nanotubes (CNTs) increases the storage modulus (E') because CNTs reinforce the polymer matrix, increasing stiffness as compared to the pure polymer. The addition of CB to polystyrene-block-poly(ethylene butylene)-block polystyrene (SEBS) also increases E', but less so than CNTs, even at a loading of 20%, which is in good agreement with the conductivity measurements.

4.3.4 In Vivo Validation

This section discusses the comparative analysis of the quality of multipin electrodes obtained from polystyrene- block- poly(ethylene butylene)- block- polystyrene (SEBS)/ 16wt%CNT and SEBS/20wt%CB composites versus commercial flexible electrodes at positions 1, 2, and 5, as presented in Figure 4.1. The results provide insights into the performance of the various composites used in this work for EEG signal capture. Contact impedance is a key factor in EEG signal quality, varying with the electrode material. The higher electrical conductivity of the SEBS/16wt%CNT composite as compared to the SEBS/20wt%CB composite improved the quality of EEG signals by reducing the contact impedance between the electrode and the skin. The contact impedance

reduction resulted in more stable signals, as shown in Figure 4.8, under conditions of open and blinking eyes, where detecting subtle variations in the amplitude of EEG signals is important. The contact impedance of polystyrene-block-poly(ethylene butylene)-block polystyrene (SEBS)/16wt% CNT electrodes with pins at position 3 is 4.2 ± 0.45 kΩ, as compared to commercial electrodes without pins at positions 1 and 2, whose impedances are 3.6 ± 0.6 kΩ and 3.8 ± 0.45 kΩ, respectively. The contact impedance of the flexible commercial electrode with pins at position 5 is 4.2 ± 0.45 kΩ. The optimal electrical conductivity and low contact impedance of the SEBS/16 wt% CNT electrode allowed to capture electrical activity from the brain.

As discussed in the previous sections, CB also improves the electrical conductivity of SEBS, but to a lesser extent than CNTs. This may result in a lower EEG signal-to-noise ratio compared to SEBS/16wt%CNT electrode, as shown in Figures 4.8 and 4.9. The contact impedance of polystyrene block poly(ethylene butylene) block polystyrene (SEBS)/20wt%CB electrodes with pins at position 4 is 5.4 ± 0.9 kΩ, compared to commercial electrodes without pins at positions 1 and 2, whose impedances are 3.6 ± 0.6 kΩ and 3.8 ± 0.45 kΩ, respectively. The contact impedance of the flexible commercial electrode with pins at position 5 is 4.2 ± 0.45 kΩ.

Figure 4.8 presents EEG time-domain recordings of the commercial flat dry flexible electrode at positions 1 and 2, compared to polystyrene-block-poly(ethylene butylene)-block-

polystyrene (SEBS)/16 wt%CNT and SEBS/20wt%CB at positions 3 and 4, when the subject's eyes were open and blinking. Figure 4.9 presents EEG time-domain recordings of the commercial multipin dry flexible electrode at position 5, compared to SEBS/16wt%CNT and SEBS/20wt%CB at positions 3 and 4, when the subject's eyes were open and blinking.

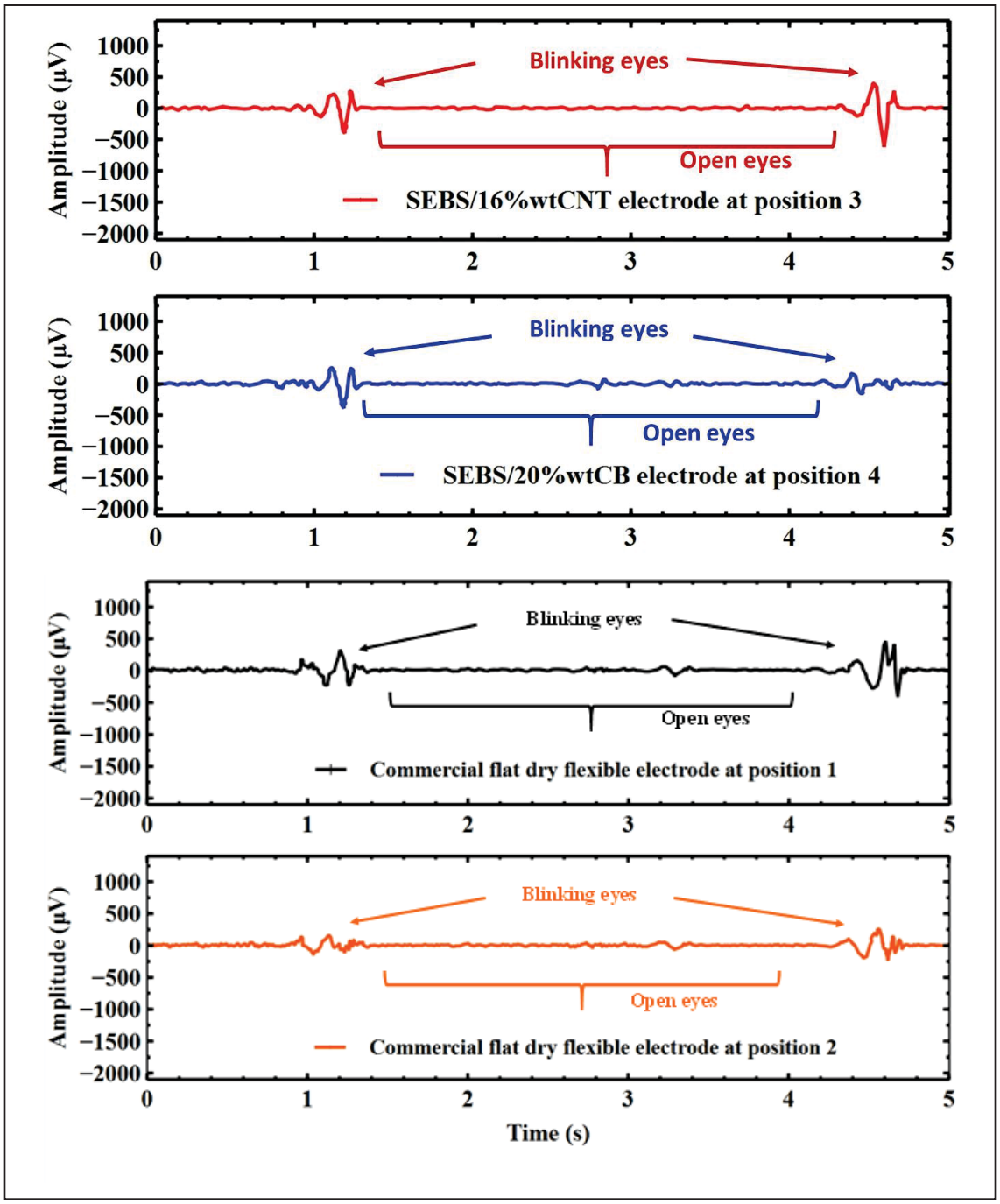


Figure 4.8. Time-domain EEG recordings during eyes-open and blinking states, acquired using styrene-ethylene-butylene-styrene (SEBS)/20 wt% carbon black (CB) and styrene-ethylene-butylene-styrene (SEBS)/16 wt% carbon nanotube (CNT) composite electrodes, compared to a commercial flat dry flexible electrode

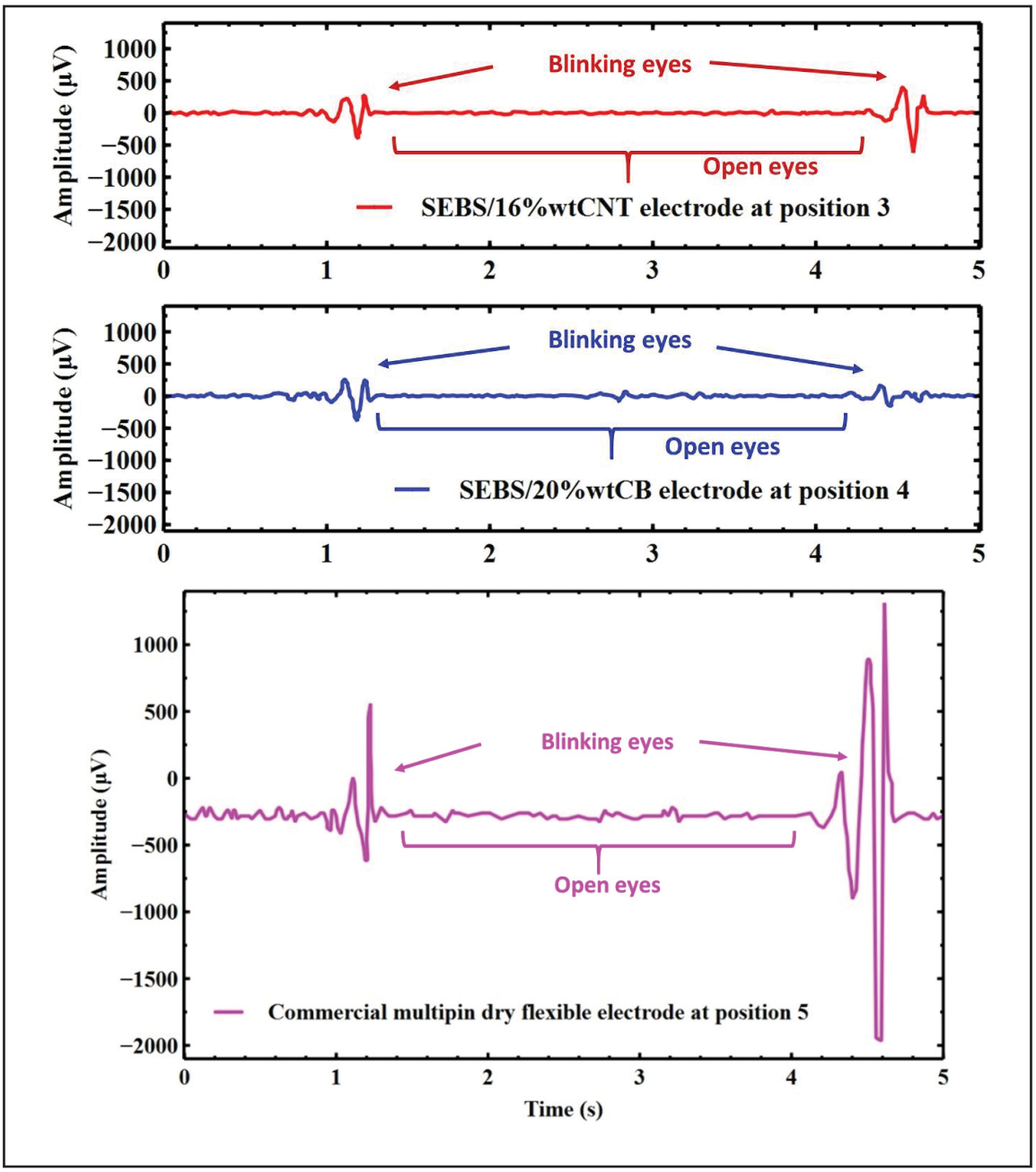


Figure 4.9. Representative time-domain EEG signals during eyes-open and blinking states, demonstrating the performance of styrene-ethylene-butylene-styrene/20 wt% carbon black (SEBS/CB) composite, styrene-ethylene-butylene-styrene/16 wt% carbon nanotube (SEBS/CNT) composite, and commercial multipin electrodes. The signals illustrate the sensitivity and artifact rejection capabilities of each electrode type

The SEBS/16wt%CNT and SEBS/20wt%CB electrode pins help maintain stable contact with the scalp, which is essential for minimizing motion-related artifacts and ensuring a contact impedance comparable to that of flexible commercial electrodes.

The SEBS/CNT electrodes, although slightly stiffer than the SEBS/CB counterparts, provide an impedance similar to that of commercial electrodes due to their low contact impedance. These electrodes may be suitable for long-term EEG recordings.

4.4 Discussion

This study evaluated the electrical and mechanical performance of flexible dry SEBS/CB and SEBS/CNT electrodes for EEG signal acquisition, comparing them with commercial flexible dry electrodes. The results highlight key findings regarding electrical conductivity, mechanical properties, contact impedance, and EEG signal quality.

The multipin architecture of the electrodes developed in this work improved electrode–skin contact and mechanical stability, thereby enabling reliable time-domain EEG signal acquisition. The contact impedance measured for SEBS/16 wt% CNT electrodes was 4.2 ± 0.45 kΩ, whereas SEBS/20 wt% CB electrodes with pins exhibited a slightly higher impedance of 5.4 ± 0.9 kΩ. Although SEBS/CNT multipin EEG electrodes were marginally stiffer than their SEBS/CB counterparts, both systems provided stable and reproducible electrode–skin coupling suitable for EEG measurements.

From an electrical perspective, the percolation threshold of SEBS/CB composites was approximately 12 wt%, whereas SEBS/CNT composites reached percolation at around 2 wt%. Beyond percolation, the electrical conductivity of SEBS/CB composites plateaued at ~0.01 S m^{-1} at 20 wt%, while SEBS/16 wt% CNT composites achieved a substantially higher conductivity of 1.26 S m^{-1}. These values are consistent with the work of Yang *et al.* (X. Yang et al., 2019b), who reported percolation thresholds of 2.07 wt% for SEBS/CNT and 5.22 wt%

for SEBS/CB nanocomposites using ultrasonic dispersion followed by magnetic stirring, with conductivity plateaus of approximately 1 S m^{-1} and 0.1 S m^{-1}, respectively. The relatively high conductivity achieved in the present electrodes is critical for efficient charge transport and reduced interfacial impedance, thereby enabling reliable detection of cortical electrical activity.

More broadly, previous studies have demonstrated that the performance of sensing and functional electrodes is strongly governed by nanocomposite architecture and interfacial charge-transfer phenomena. NiO/MWCNT-based electrodes reported in (Shahmiri et al., 2013) exhibited reduced oxidation overpotentials, improved selectivity, and lower detection limits, highlighting the key role of CNT/oxide interfaces in facilitating charge transfer and minimizing interfacial resistance. Similarly, Mo-doped VS_2/CNT nanocomposites investigated in (Moradbeigi et al., 2023), showed increased electroactive surface area and reduced charge-transfer resistance due to synergistic interactions between CNT conductive networks and chemically doped chalcogenide phases, as confirmed by electrochemical impedance spectroscopy. Beyond electrochemical systems, CNT-based polymer nanocomposites reported in (Litkohi et al., 2021) exhibited unconventional electrical responses governed by filler dispersion, interfacial polarization, and percolative network formation, further underscoring the dominant influence of interfacial phenomena on macroscopic electrical behavior. In this context, the present SEBS-based CNT and CB composites follow analogous structure–property relationships, where electrode performance is primarily dictated by conductive network morphology and interfacial impedance.

The high electrical conductivity achieved in the electrodes developed in this work enabled reliable recording of brain electrical activity. Owing to their excellent intrinsic conductivity, CNT-based networks provided SEBS/CNT electrodes with low interfacial impedance, resulting in EEG waveforms comparable to those obtained using commercial flexible conductive polymer electrodes and ensuring efficient signal transmission from the scalp to the acquisition system. In contrast, carbon black, while an effective conductive filler, exhibits lower electrical conductivity than CNTs, leading to slightly higher interfacial impedance in SEBS/CB electrodes compared with both SEBS/CNT and commercial electrodes.

SEM micrographs revealed that, compared to SEBS/20wt%CB, carbon black (CB) exhibited a greater aggregation in the matrix, whereas carbon nanotubes (CNTs) were more evenly distributed. A uniform dispersion of CB in SEBS still poses challenges, especially at high concentrations. The remaining weights obtained through TGA tests confirmed the nominal concentrations used when compounding composites. The more homogeneous dispersion of CNTs in SEBS/16 wt% CNT composites compared with the CB aggregation observed in SEBS/20 wt% CB composites is attributed to differences in filler geometry, interfacial interactions, and processing viscosity. The high aspect ratio and conjugated structure of CNTs favor uniform network formation at lower concentrations, while π–π interactions between CNTs and the styrene domains of SEBS enhance compatibility and dispersion stability. Similar π–π interfacial effects have been reported in CNT-based nanocomposites and conjugated organic frameworks, where they facilitate charge transport and structural uniformity (Jing et al., 2025; Qin et al., 2025; Yan et al., 2025; Zhu et al., 2025). In contrast, the quasi-spherical morphology and higher required loading of CB increase compound viscosity, limit shear dispersion, and promote micro-scale agglomeration (Atif et al., 2013; Gómez Martín et al., 2024).

DMTA tests showed that the SEBS/CNT electrode is stiffer than the SEBS/CB electrode. CB and CNT offer distinct solutions for EEG applications, each having its advantages and disadvantages. CB is an economical choice with acceptable electrical conductivity at high mass concentrations, while CNTs provide acceptable electrical conductivity at low mass concentrations and high mechanical stiffness, but at a higher cost. Besides improving conductivity, CNTs increase material stiffness more than CB, potentially affecting user comfort. However, a good compromise between stiffness and flexibility would allow for stable electrodes with optimal performance. Hybrid electrodes containing SEBS, CNT, and CB could provide EEG electrodes with optimal flexibility, electrical conductivity, and contact impedance.

Recent advancements have highlighted the growing interest in hybrid nanocomposites incorporating graphene, carbon nanotubes (CNTs), and polymer matrices for the development of high-performance electrochemical sensors. For example, Bakytkarim et al. (Bakytkarim et al., 2024) reported a sensitive electrochemical sensor for chlorogenic acid detection based on

a ternary composite consisting of multi-walled carbon nanotubes (MWCNTs), reduced graphene oxide (r-GO), and platinum nanoparticles (Pt nanoparticles (NPs)), deposited on a glassy carbon electrode (Pt/r-GO/MWCNTs/glassy carbon electrode (GCE)). The system demonstrated excellent reproducibility and sensitivity, attributed to the synergistic interaction between the high electrical conductivity of r-GO, the large surface area of MWCNTs, and the catalytic activity of Pt NPs.

Similarly, Parthasarathy (P, 2023) developed a biosensor for Escherichia coli detection using a PVA/r-GO/polyethylenimine (PEI) nanocomposite. In this case, the combination of functionalized polymers with carbon-based nanomaterials improved both electrical performance and biocompatibility, enabling a stable and selective electrochemical response suitable for biological sensing. Moreover, Biswas et al. (Biswas et al., 2025) reviewed the potential of graphene-based hybrid nanomaterials in energy storage, particularly in supercapacitor applications. Their findings emphasize the importance of synergistic interactions between conductive fillers and polymeric hosts to achieve high surface area, efficient charge transport, and mechanical robustness. Although electrical conductivity measurements were not always reported, the observed improvements in electrochemical performance clearly demonstrate the functional benefits of hybrid material architectures. These insights support our approach in employing SEBS-based composites filled with CNTs and CB for the development of flexible dry EEG electrodes. By leveraging the mechanical flexibility and skin compatibility of SEBS, along with the high conductivity of CNTs and the low percolation threshold of CB, our hybrid electrodes achieve a balanced combination of electrical performance, mechanical stability, and low contact impedance, essential features for next-generation bioelectronic interfaces.

The functioning of the developed electrodes is based on a piezoresistive sensing mechanism, in which the electrical resistance varies in response to mechanical deformation or displacement at the electrode–skin interface. This behavior resembles that of strain or displacement sensors, where signal fluctuations correspond to subtle mechanical movements. For instance, Wan et al. (Wan et al., 2025) demonstrated this concept in structural health monitoring by using a functionalized conductive elastomer that exhibited high sensitivity and long-term stability in detecting strain through resistance variations. In our case, the resistance changes recorded

during muscle activity—such as eye blinks—can be attributed to micro-displacements and variations in contact pressure between the elastomeric pins and the scalp. These effects are closely linked to the mechanical compliance of the material and the quality of the skin–electrode contact. As such, our electrodes effectively operate as soft displacement sensors, whose performance depends on the integrity of the conductive network and the material's capacity to conform to scalp morphology under minimal applied force. In addition, Wang et al. (H. Wang et al., 2023) explored how thermo-mechanical properties influence the performance of piezo-electrets made from cyclic olefin copolymers with varying stiffness and thermal resistance. Based on the inverse relationship between the piezoelectric coefficient and the elastic modulus, their study showed that careful material selection and structural design can offset the limitations of high stiffness. These observations highlight the importance of optimizing the reinforcement ratio in elastomeric composites to ensure sufficient flexibility. Adequate flexibility is essential for maintaining stable electrode–skin contact, enabling reliable EEG signal acquisition, accommodating scalp curvature and subject motion, and improving long-term user comfort. Accordingly, this balance was a key design criterion in the development of the SEBS-based EEG electrodes.

While the current results demonstrate the potential of SEBS-based composites—particularly those reinforced with CNTs or CB—for use in flexible dry EEG electrodes, it is important to highlight that this study was deliberately limited to the characterization of material properties. Our objective was not to assess the electrodes' capacity to decode complex brain signals or validate clinical performance across different use scenarios. A more comprehensive evaluation of signal quality, stability over long-term recordings, and inter-subject reproducibility will require a dedicated clinical study involving repeated EEG acquisitions under realistic conditions. Such a study will be considered in a subsequent phase of this research. Future investigations should include comprehensive impedance characterization, including both impedance magnitude and phase angle (tan δ), performed before and after scalp cleaning to quantitatively assess the influence of scalp conditions and further validate the robustness of SEBS-based electrodes under varying conditions relevant to wearable and clinical EEG applications.

4.5 Conclusion

This study demonstrated the potential of SEBS-based nanocomposites as flexible dry electrodes for EEG signal acquisition. Among the tested formulations, SEBS/16wt%CNT composite exhibited superior electrical conductivity (1.26 S/m) and the lowest contact impedance (4.2 ± 0.45 kΩ), enabling EEG signal acquisition comparable to commercial multipin electrodes. In contrast, SEBS/20 wt% CB electrodes reached a conductivity plateau of 0.01 S/m and a contact impedance of 5.4 ± 0.9 kΩ. SEM analysis confirmed a more uniform dispersion of CNTs compared to CB, which tended to agglomerate at higher concentrations. Thermogravimetric analysis validated the filler content, while DMTA results indicated that SEBS/CNT composites were stiffer than SEBS/CB ones, which may influence long-term comfort. EEG recordings from both materials revealed reliable signal detection, including blink artifacts, though SEBS/CB electrodes exhibited slightly more signal noise.

These findings suggest that SEBS/CNT composites are better suited for applications requiring high signal fidelity, whereas SEBS/CB may be favored when comfort and softness are prioritized. The ergonomic multipin design contributed to improved contact stability across the scalp, particularly in hairy areas, supporting robust EEG acquisition without conductive gel.

Future work will focus on the development of hybrid SEBS/CNT/CB electrodes to optimize the trade-off between electrical performance and mechanical compliance. Additional investigations will involve long-term user testing, analysis of motion artifacts, and performance assessment under varying physiological and environmental conditions (e.g., sweat, temperature, hair density). These efforts aim to advance the design of next-generation dry, flexible EEG systems that are biocompatible, reliable, and suitable for extended wear in real-world settings.

4.6 Author credit statement

The authors of the published version of this study are George Gnonhoue (GG), Ilyass Tabiai (IT), Jérémie Voix (JV), and Éric David (ED).

GG conducted the investigation and performed the experiments, data processing, and formal analyses. He carried out the analytical calculations, contributed to the interpretation of the results, and prepared the figures. GG drafted the original version of the manuscript and incorporated all revisions following peer review.

IT contributed to the conceptualization of the project and the development of the experimental methodology. He participated in the scientific validation of the proposed approaches, the acquisition of funding, and the critical review of the manuscript, and provided overall supervision of the work.

JV contributed to the investigation and formal analysis, as well as to funding acquisition. He participated in the review and editing of the manuscript and co-supervised the project throughout its execution.

ED contributed to the conceptualization of the project and the development of the methodology. He was involved in formal analysis, funding acquisition, and critical review of the manuscript, and provided scientific co-supervision of the work.

IT and ED jointly supervised the project.

4.7 Author Declarations

The authors declare that they have no known competing financial interests or personal relationships that could have appeared to influence the work reported in this paper. The data of this study are available upon request.

4.8 Acknowledgements

The authors would like to acknowledge the financial support received from NSERC Alliance (ALLRP 566678-2021), MITACS IT26677 (SUBV-2021-168), and PROMPT (#164_Voix-EERS 2021.06) for the ÉTS-EERS Industrial Research Chair in In-Ear Technologies, which is sponsored by EERS Global Technologies Inc.

CHAPITRE 5

HYBRID FLEXIBLE DRY ELECTRODES FOR ELECTROENCEPHALOGRAPHY: ELECTRICAL AND THERMO-MECHANICAL PROPERTIES

George Gnonhoue [a], Ilyass Tabiai [a*], Jérémie Voix [a], Éric David [a]

[a] École de technologie supérieure, 1100 Notre-Dame Street West, Montreal, Quebec, H3C 1K3, CANADA

Paper published in the *Journal of Applied Polymer Science*, November 2025

DOI: https://doi.org/10.1002/app.70099

Chapter outline: This chapter presents the article corresponding to the results of the third part of the project. It emphasizes the dispersion and distribution of the conducting additives in the polymeric matrix, additive-matrix interactions, the formation of an electrically conducting network, and the properties of flexible styrene-Ethylene-Butylene-Styrene/Carbon Nanotubes/Carbon Black (SEBS/CNT/CB) and Maleic Anhydride-Grafted styrene-Ethylene-Butylene-Styrene/Carbon Nanotubes/Carbon Black (SEBS-MA/CNT/CB) Electrode for EEG.

Abstract: This study evaluates styrene-ethylene-butylene-styrene (SEBS) composites modified with carbon nanotubes (CNT) and carbon black (CB) for flexible EEG electrodes. Maleic anhydride-grafted styrene-ethylene-butylene-styrene (SEBS-MA) with 8%wt carbon nanotubes (CNT) and 2 %wt carbon black (CB) provides an optimal balance of conductivity and flexibility, a storage modulus comparable to styrene-ethylene-butylene-styrene (SEBS), and yields a highly flexible conductive material. SEBS and SEBS-MA composites with 8%wtCNT/2%wtCB produced stable, low-noise signals, suggesting responsiveness to brain activity. The contact impedance of the elastomeric thermoplastic

polymer (SEBS)/8%wtCNT/2%wtCB electrode is 4.25 ± 0.5 kΩ, and 4.5 ± 0.6 kΩ for SEBS-MA/8%wt CNT/2%wtCB, comparable to a commercial electrode (4.75 ± 1.5 kΩ). SEBS/8%wtCNT/2%wt CB and SEBS-MA/8%wtCNT/2%wtCB produced stable, low-noise EEG signals. In vivo EEG recordings demonstrated that SEBS-MA with 8%wtCNT/2%wt CB effectively captured transitions between the eyes-open and eyes-closed states, yielding clear and stable signals. These findings suggest that SEBS-MA/8%wtCNT/2%wtCB is a promising material for flexible, high-performance EEG electrodes due to its balance of electrical conductivity, mechanical stability, and signal clarity.

Keywords: flexible electrodes; electroencephalography; electrical properties; mechanical properties

5.1 Introduction

EEG is a non-invasive technique that records brain electrical activity through electrodes placed on the scalp (Arai et al., 2015; Cunha et al., 2009; Fu et al., 2020a; Krachunov & Casson, 2016). Conventional EEG systems rely on wet electrodes, which use a conductive gel to reduce electrode–skin impedance to values typically in the range of 5–10 kΩ (Hinrichs et al., 2020; G. Li et al., 2018). This ensures high-quality signal acquisition; however, gel electrodes present significant drawbacks. The gel dries out over time, causing impedance to rise and signal degradation, and their application and removal are inconvenient and uncomfortable for the user (Petrossian et al., 2023). These limitations restrict their suitability for long-term and portable EEG applications.

To overcome these challenges, research has focused on the development of dry electrodes, which operate without the need for gel (R. Wang et al., 2017b). Three main categories exist: microneedle electrodes, which penetrate the stratum corneum and can achieve impedances as low as 10–50 kΩ (Arai et al., 2015; J. Li et al., 2022), but may cause discomfort and biocompatibility concerns; capacitive electrodes, which record signals through an insulating layer and allow non-contact acquisition, but often suffer from impedances above 200 kΩ and are highly sensitive to motion artifacts (Babusiak et al., 2018; Baek et al., 2012; Y. Gao et al., 2020; S. M. Lee et al., 2013, 2016a); and surface electrodes, which contact the skin

directly and offer a more user-friendly solution with relatively simple fabrication steps, though they typically present impedances above 20 kΩ range (X. Cheng et al., 2019; L. Yang, Gan, et al., 2022).

Most modern surface dry electrodes depend on thin conductive coatings applied to a polymer substrate. These coatings can deteriorate or peel off after repeated use, reducing performance (Asayesh et al., 2025; Fiedler et al., 2011b, 2015, 2016, 2018b, 2023; Warsito et al., 2023a). To address this limitation, bulk conductive composites have been developed, in which electrical conductivity is embedded throughout the electrode rather than only at the surface (Hoon Lee et al., 2014). Conductivity is generally achieved by incorporating carbon-based fillers such as carbon black (CB) or carbon nanotubes (CNTs) (Heo et al., 2020). CB and CNTs each present distinct advantages and limitations when used individually as conductive fillers. CB is low-cost and widely available, but requires high loadings to reach percolation (Y. Wang et al., 2025b), which increases stiffness. CNTs enable high conductivity at lower loadings and can reduce contact impedance below, but their addition tends to stiffen the polymer matrix and reduce flexibility (Oh et al., 2024a).

To overcome these trade-offs, several studies have proposed the development of hybrid electrodes, in which two or more fillers are incorporated into the same polymer matrix. The rationale is that the complementary properties of different fillers can be exploited. This synergistic effect has been shown to lower the overall percolation threshold, improve electrical stability, and reduce the need for excessively high filler loadings (Alavi et al., 2023; Aravinth et al., 2024; Cai et al., 2024; He et al., 2024; J.-W. Li et al., 2024; Y. Yao et al., 2024). Nevertheless, the primary challenge remains optimizing the fabrication process. Achieving the right balance between filler fraction, dispersion quality, and electrical performance is critical to ensuring that electrodes are both conductive and mechanically compliant. Excessive filler loading leads to stiffness and discomfort, while insufficient loading compromises conductivity and increases impedance.

The choice of polymer matrix also plays a central role. Blends of polydimethylsiloxane (PDMS) and thermoplastic polymer (TPU), reinforced with materials such as CNT and CB, graphene, and silver nanowires, are commonly used to fabricate hybrid composites for flexible sensors that detect human movements (Cai et al., 2024; He et al., 2024; Kumar et

al., 2024; Lv et al., 2023; Mahato et al., 2024; Paul et al., 2023; Promsung et al., 2024; Shajari et al., 2022; J. Wang et al., 2024; Warsito et al., 2023a; S. Xu et al., 2020). PDMS offers softness and biocompatibility; however, its excessive flexibility leads to unstable electrode–skin contact, resulting in impedance fluctuations (L.-F. Wang et al., 2012a; Z. Wang et al., 2018). TPU, on the other hand, offers mechanical robustness but can sometimes be too rigid for comfortable long-term wear (Fiedler et al., 2023; Heijs et al., 2021; Vasconcelos et al., 2021). Consequently, alternative matrices such as styrene–ethylene–butylene–styrene (SEBS) have attracted attention. SEBS is a thermoplastic elastomer that combines soft and hard phases: the soft phase provides skin conformity and comfort, while the complex domains stabilize contact under mechanical pressure at the surface of the electrodes (Alavi et al., 2023; T. Chen et al., 2022; M. Liu et al., 2023b; Y. Yao et al., 2024; B. Zhou et al., 2022). Furthermore, maleic anhydride-grafted SEBS (SEBS-MA) enhances filler dispersion and interfacial adhesion, potentially reducing the high stiffness of composites (Alikhani & Mohammadi, 2023; Grigorescu et al., 2016).

To develop flexible, comfortable EEG electrodes with stable, low impedance, we explore SEBS/CNT/CB and SEBS-MA/CNT/CB hybrid nanocomposites, designed to leverage the complementary properties of CNT and CB while avoiding the high filler loadings and mechanical stiffness typically associated with single-filler systems. In this study, we investigate these hybrid nanocomposites as bulk conductive materials for dry surface EEG electrodes. Previous research on SEBS/CB and SEBS/CNT composites has shown low contact impedance at high filler loadings—specifically 20 wt% CB (despite a percolation threshold above ~12 wt%) and 16 wt% CNT (despite a percolation threshold near ~3 wt%). However, such high filler levels can reduce flexibility and comfort. By combining CNT and CB, synergistic conductive networks can form, allowing for reduced filler content while maintaining conductivity and lowering electrode–skin impedance below clinically relevant levels (<5 kΩ). The addition of maleic anhydride into SEBS (SEBS-MA) enhances filler dispersion and polymer–nanoparticle interactions, potentially alleviating stiffness. These hybrid nanocomposites were prepared through solvent dissolution and systematically evaluated for morphology, dispersion, electrical conductivity, and EEG performance, to

create durable, flexible, low-impedance electrodes that address the limitations of traditional wet and coated dry electrodes.

5.2 Materials and Methods

5.2.1 Materials

The materials used in this study were chosen for their suitability in flexible EEG electrode applications. Styrene–ethylene–butylene–styrene (SEBS), an elastomeric thermoplastic polymer with a number-average molecular weight of 54,000 g/mol and a polystyrene content of 30 wt%, was supplied by Kraton (Paulínia – SP, Brazil). Maleic anhydride-grafted SEBS (SEBS-MA), also obtained from Kraton, was used to improve the interaction between the polymer matrix and conductive fillers.

Multiwalled carbon nanotubes (MWCNTs), NC 7000™ grade, were obtained from Nanocyl S.A. (Sambreville, Belgium). These nanotubes have an average diameter of 9.5 nm, an average length of 1.5 μm, a surface area ranging from 250 to 300 m^2/g, a nominal electrical conductivity of 100 S/m, a density between 1.30 and 2.00 g/cm^3, and a carbon purity of at least 90%.

Carbon black (CB), Lampblack type C198-500 (Lot 145509), was obtained from Fisher Chemical (Fisher Scientific, Ottawa, ON, Canada). It consists of nanoparticles approximately 50 nm in size, with a nominal electrical conductivity of 400 S/m and a density of 1.8 g/cm^3.

For solution processing, toluene (UN1294, Optima, T291-4, Lot 234238) was purchased from Fisher Chemical (Fisher Scientific Company, Ottawa, ON, Canada).

5.2.2 Composite Preparation

Electrode composites were created using a solution-casting and compression-molding process (see schematic in Figure 5.1).

Polymer dissolution: SEBS or SEBS-MA pellets were dissolved in toluene at 100 °C with magnetic stirring at 600 rpm until a clear, homogeneous solution formed.

Filler incorporation: CNT and CB were added to the polymer solution at specified weight fractions (Tables 5-1 and 5-2). Dispersion was maintained through continuous stirring at 100 °C for 30 minutes to ensure uniform distribution of the filler.

Solvent evaporation: The suspension was cast and left to dry under a fume hood at room temperature until all solvent evaporated, resulting in nanocomposite films.

Electrode molding: The dried films were compression molded into multipin electrode geometries using a heated press at 215 °C. The process involved an initial pressure of 0.8 MPa for 5 minutes, followed by a pressure of 5 MPa for 15 minutes.

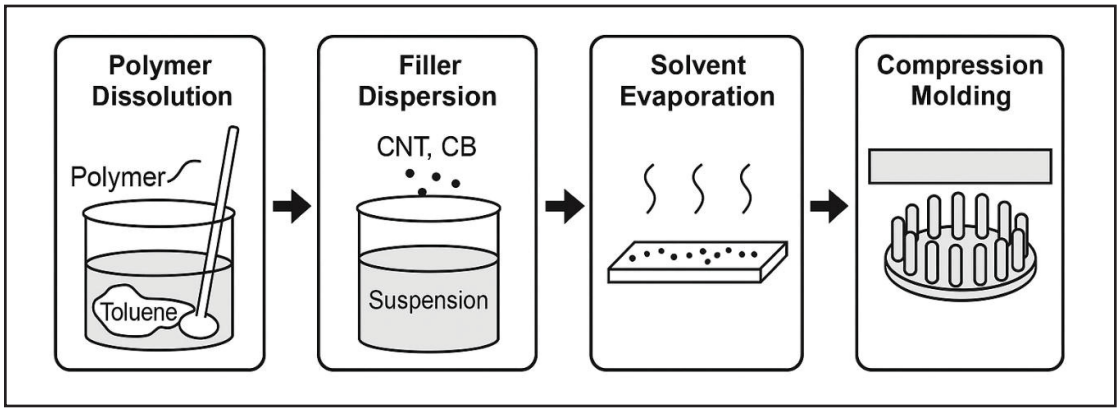


Figure 5.1. Schematic overview of the fabrication process for flexible multipin dry electrodes. The method includes (i) dissolving the SEBS or SEBS-MA polymer in toluene, (ii) dispersing conductive fillers (CNT and CB) to create a uniform suspension, (iii) evaporating the solvent to form composite films, and (iv) using compression molding to shape the films into multipin electrode structures

5.2.3 Electrode Geometry

Each electrode consisted of 19 cylindrical pins arranged in a circular pattern. The pins had an average height of 4.9 ± 0.09 mm and a diameter of 1.41 ± 0.01 mm. The center-to-center distance between neighboring pins was about 2.5 mm, which corresponds to an edge-to-edge spacing of approximately 1.1 mm at the electrode–skin interface.

5.2.4 Composite Formulations

The compositions of the prepared composites are summarized in Tables 5-1 and 5-2. For each formulation, three independent samples were fabricated and characterized to ensure reproducibility. Comparative analyses were conducted between SEBS/CNT/CB and SEBS-MA/CNT/CB composites at equivalent filler loadings to determine the most suitable material for EEG applications.

Table 5-1 Composition of styrene-ethylene-butylene-styrene (SEBS) nanocomposites with different weight fractions (%wt) of carbon nanotubes (CNT) and carbon black (CB)

Reinforcements		Matrix
CNT	CB	
-	-	100
3	2	95
8	2	90
10	-	90
-	10	90
10	5	85
16	-	84
15	5	80
-	20	80

Table 5-2 Composition of maleic anhydride-grafted styrene-ethylene-butylene-styrene (SEBS-MA) nanocomposites with different weight fractions of carbon nanotubes (CNT) and carbon black (CB)

Reinforcements		Matrix
CNT	CB	
-	-	100
3	2	95
8	2	90
10	-	90
-	10	90
10	5	85
16	-	84
15	5	80
-	20	80

5.3 Characterization

5.3.1 Electrical Characterization

Electrical conductivities of the composites were measured using a frequency-domain broadband dielectric spectrometer (Alpha-A Dielectric Analyzer, Novocontrol, Montabaur, Germany). Disks with a 20 mm diameter and a thickness of 1.2 mm were placed between two solid brass electrodes, creating a plane-plane electrode/composite material/electrode

sandwich. The measurements were performed over a frequency range from 10^2 Hz to 10^5 Hz at 30 °C.

5.3.2 Structural Characterization

The composite morphology was examined with a high-resolution scanning electron microscope (SEM, Hitachi SU-8230 field-emission SEM) operated at 5 kV to evaluate the dispersion of conductive fillers within the matrix. Cross-sections were prepared using a microtome and sputter-coated with approximately 2 nm of platinum using a turbo-pumped sputter/carbon coater (Quorum Technologies Q150T).

5.3.3 Thermo-Mechanical Characterization

Thermogravimetric analysis (TGA) was performed using a Diamond TG/Differential Thermal Analysis (DTA) system (PerkinElmer) to determine the filler weight fractions and decomposition temperatures of the composites. Approximately 10–13 mg of material was heated from 20 to 500 °C at a rate of 3 °C/min under a nitrogen flow of 100 ml/min, followed by a 2-minute isothermal hold at 500 °C.

Differential Scanning Calorimetry (DSC) was used to examine the thermal properties of the pure polymer matrices (SEBS and SEBS-MA). Tests were carried out in a nitrogen atmosphere to prevent oxidation. Approximately 10 mg samples were sealed in aluminum pans and heated at a rate of 10 °C/min. To prevent thermal degradation, the measurement ranges were adjusted based on the thermal stability of each material: –100 to 220 °C for SEBS and –100 to 320 °C for SEBS-MA. These conditions allowed for the detection of key transitions, including the glass transitions of both the soft and hard phases, without interference from decomposition.

Dynamic mechanical thermal analysis (DMTA) of SEBS-MA/CNT/CB and SEBS/CNT/CB composites was performed using a Q800 instrument (TA Instruments Inc.) with a double cantilever clamp (22 mm frame, 2 mm center clamp). Rectangular specimens (8 mm wide, 2 mm thick) were tested at a strain of 0.4%, a frequency of 1 Hz, and a heating rate of 2 °C/min across 25–35 °C. Measurements were conducted under laboratory conditions

(~23 °C, 45–55% relative humidity). The storage modulus was solely evaluated to assess stiffness and elastic behavior within this temperature range.

5.3.4 Preliminary In Vivo Validation

Multipin flexible EEG electrodes were tested for contact impedance and EEG recording on hairy scalp areas to mimic real-world application conditions. This method was selected to evaluate both the electrode's performance and that of commercial alternatives.

Recordings were wirelessly collected using an OpenBCI™ 16-channel Cyton Biosensing Board embedded in the Ultracortex “Mark IV” EEG headset (OpenBCI, New York, NY, USA). This headset allows for comfortable electrode placement with minimal pressure, ensuring consistent positioning according to the international 10–20 system.

Contact impedance and EEG signal amplitude from the newly developed multipin electrodes at positions 1 and 3 (Figure 5.3) were compared to those from a commercial dry flexible electrode (OpenBCI, New York, NY, USA) placed at site 2. Measurements were taken on a healthy volunteer using a setup that included the developed electrode, a reference, and a ground, with impedance recorded between the test and reference electrodes.

To evaluate EEG signal quality, participants sat in a quiet room while recordings were taken for 10 seconds. Following standard protocols and the recommendations of the American Clinical Neurophysiology Society (Sinha et al., 2016), participants were instructed to minimize head and facial muscle activity and remain still to reduce movement artifacts. This method enabled reliable detection of eye-blink reflex artifacts and neural oscillations.

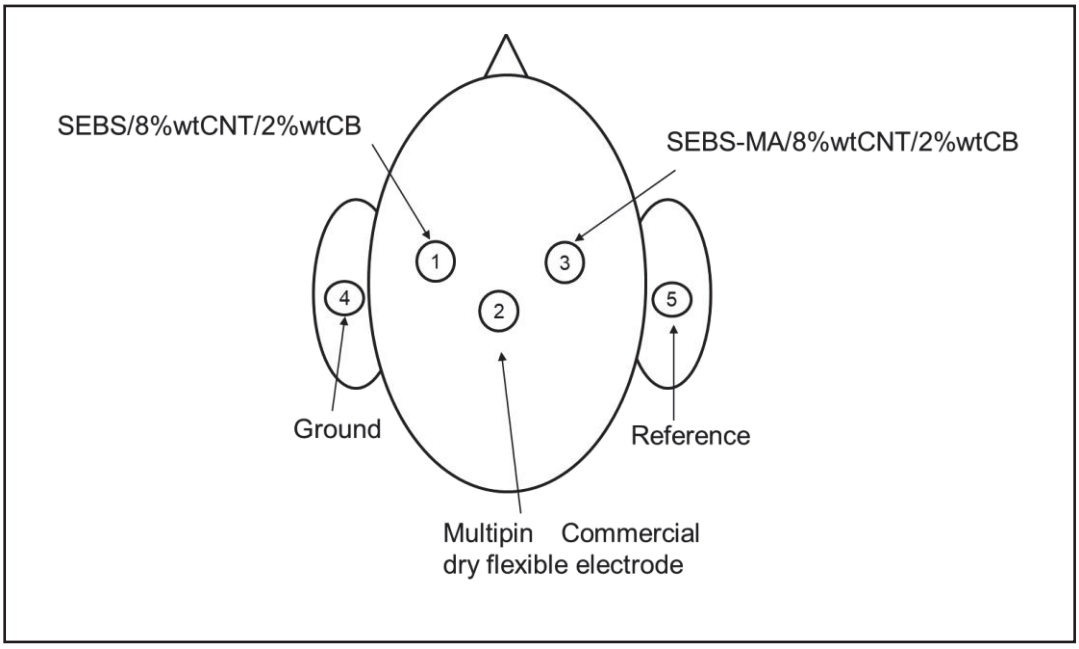


Figure 5.2**.** Schematic of electrode placement on the scalp using the Ultracortex "Mark IV" EEG headset

Multipin flexible electrodes developed in this work were positioned at sites 1 (left) and 3 (right), while a commercial dry flexible electrode (OpenBCI, USA) was placed at site 2 for comparison. Electrodes 4 and 5, located near the ears, served as ground references.

The Ultracortex "Mark IV" headset is designed to ensure consistent and precise electrode placement on the scalp, thereby improving the reliability of EEG measurements and reducing variability in data collection. The headset features adjustable arms and labeled slots that align electrodes according to the international 10–20 system. Figure 4.3 shows the electrodes developed in this work alongside the commercial flexible electrode from OpenBCI, which was used as a performance benchmark.

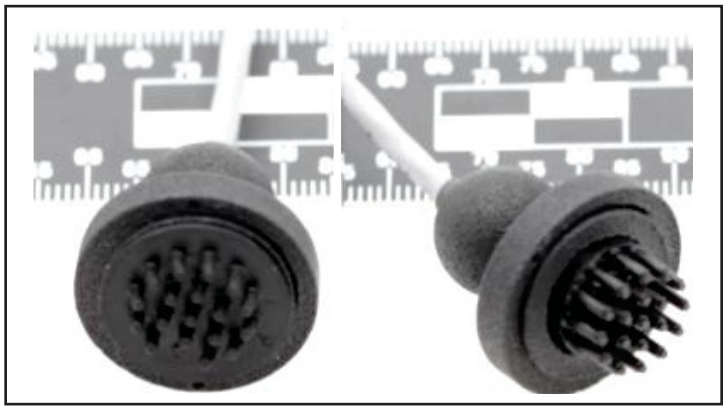


Figure 5.3. Photos of the electrodes used in this study. (Left) Commercial dry flexible electrode from OpenBCI (New York, NY, USA), used as a reference. (Right) Multipin flexible electrode developed in this work, side view. The built-in ruler shows the scale for electrode sizes

5.3.4.1 Participants

Participant testing was conducted to evaluate the performance of the developed EEG electrodes under physiological conditions, with a focus on signal quality and motion artifacts. Healthy adult volunteers (n = 4; 1 male, three females; age range 21–35 years) participated in EEG measurements.

All procedures were approved by the ÉTS Internal Review Board (Comité d'éthique de la recherche, Approval No. H20230504) and conducted in accordance with the principles outlined in the Declaration of Helsinki. Written informed consent was obtained from all participants before the experiments.

5.4 Results

5.4.1 Electrical Properties

Figures 5.4 – 5.10 summarize the real part of the complex conductivity, $\sigma'(f)$, for SEBS and SEBS-MA composites filled with CNT, CB, and CNT/CB hybrids.

5.4.1.1 Frequency response and filler-morphology effects

Figure 5.4 shows that SEBS/10wt%CNT is already a conductive composite ($\sigma' \approx 10^{-2}$ - 10^{-3} $S \cdot m^{-1}$, with a frequency-independent plateau), whereas SEBS/10 wt% CB remains insulating ($\sigma' \approx 10^{-12}$ $S \cdot m^{-1}$ at 1 Hz with strong dispersion). The higher aspect ratio of CNT encourages the formation of a connected network at much lower loadings than quasi-spherical CB. The differences highlight how filler shape influences charge transport pathways. CNTs, due to their high aspect ratio and intrinsic conductivity, tend to form more efficient percolation networks at lower loadings compared to CB, which comprises nearly spherical particles with a lower surface area-to-volume ratio. In this context, σ' refers to the real part of the complex electrical conductivity (σ), which measures the material's ability to conduct electricity through ion movement. It excludes the imaginary part (σ''), which accounts for capacitive or inductive responses related to energy storage. Therefore, σ' provides a direct measure of the composite's effective electrical performance, which is crucial for applications like dry EEG electrodes, where both high conductivity and long-term stability are essential.

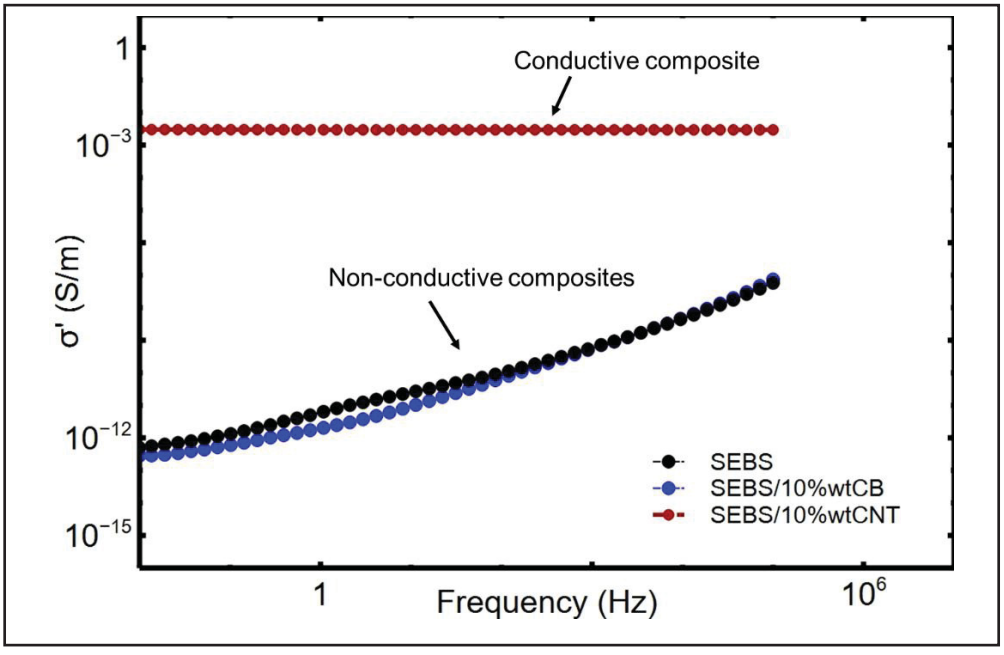


Figure 5.4. Electrical conductivities of SEBS/10 wt% CNT vs SEBS/10 wt% CB (σ' vs frequency)

Figure 5.5 compares high-loading systems: SEBS/16 wt% CNT reaches about 1 $S \cdot m^{-1}$ with a flat plateau, SEBS/20 wt% CB reaches roughly 10^{-2} $S \cdot m^{-1}$, and the SEBS-MA counterparts are consistently lower at the same filler levels (see below). The electrical conductivity data in Figure 5.5 demonstrate how reinforcement loading affects the conductivity of both SEBS and SEBS-MA matrices, offering insights into the percolation threshold and electron transport mechanisms within the composites. The electrical conductivity of SEBS and SEBS-MA composites with reinforcement weight fractions of 10%, 16%, and 20% is shown in Figures 5.4 and 5.5, illustrating distinct conductivity behaviors based on filler type and concentration.

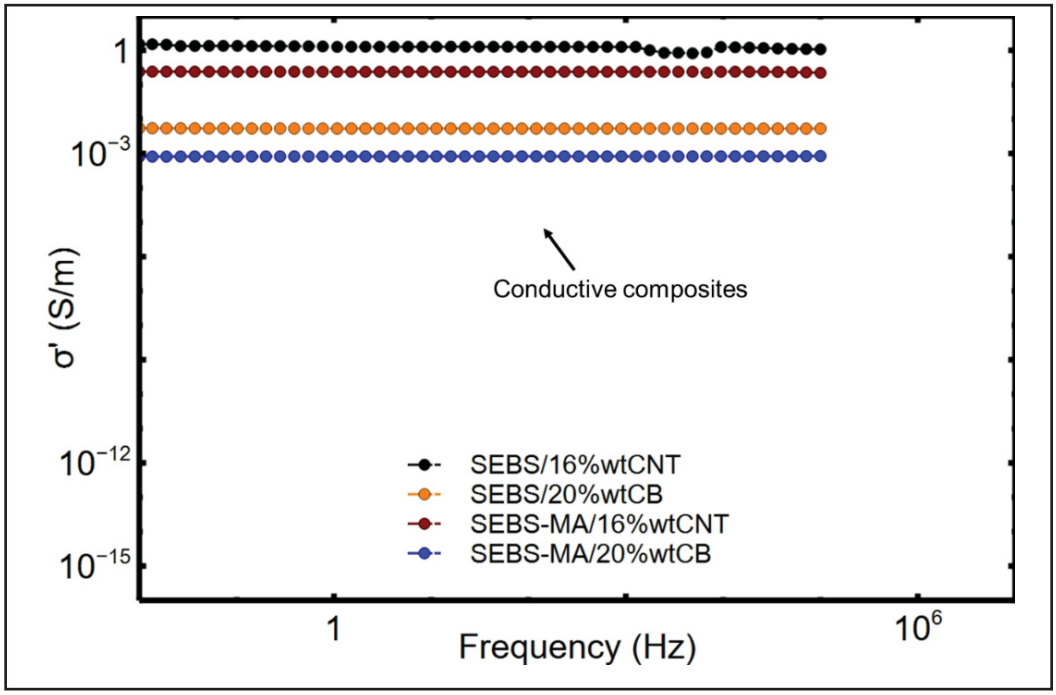


Figure 5.5. Electrical conductivity of SEBS/16 wt%CNT, SEBS/20 wt%CB, SEBS-MA/16 wt%CNT, and SEBS-MA/20 wt%CB (σ′ vs. frequency)

Table 5-3 summarizes the electrical conductivity of SEBS and SEBS-MA composites at different reinforcement loadings, complementing Figures 5.4 and 5.5 by highlighting the role of CNT and CB in determining conductive network formation.

Table 5-3 Electrical conductivity of SEBS and SEBS-MA composites with different CNT and CB loadings (see Figure 4.4 and 4.5)

Composite Formulation	Conductivity at 1 Hz (S/m)	Frequency Dependence	Interpretation
Neat SEBS (unfilled)	$\sim 10^{-12}$	Strong increase with frequency	Typical insulating behavior
SEBS/10%wtCB	$\sim 10^{-12}$	Increases significantly with frequency	CB is insufficient to form a conductive network at 10 wt%
SEBS/10%wt CNT	$10^{-3} – 10^{-2}$	Frequency-independent	Stable conductive network from CNTs
SEBS/16%wt CNT	~1	Frequency-independent	A strong CNT network guarantees reliable conduction.
SEBS/20%wtCB	$\sim 10^{-2}$	Frequency-independent	Continuous CB network established at 20 wt%
SEBS-MA/16%wtCNT	$10^{-1} – \sim 1$	Frequency-independent	Slightly lower conductivity than SEBS/16% CNT; CNT network is somewhat less efficient.
SEBS-MA/20%wtCB	$\sim 10^{-3}$	Frequency-independent	Lower than SEBS/20% CB; MA modification does not improve conduction

Hybrid series (Figure 5.6 – 5.9) confirm that CNT-rich blends control network formation and flatten the frequency response; in contrast, CB alone or CB-rich blends require significantly higher total loadings and still exhibit lower plateaus. For dry electrodes, $\sigma' \geq 10^{-2}$ $S \cdot m^{-1}$ with minimal frequency dependence around 31 Hz is desirable. CNT-rich SEBS (≥7–8 wt% CNT with a small CB fraction) meets this target, while CB-rich systems do not. Figure 5.6 compares the conductivity of SEBS composites with reinforcement weight

fractions of 5%. It illustrates the conductivity of SEBS composites with 5% reinforcement weight fractions as a function of frequency.

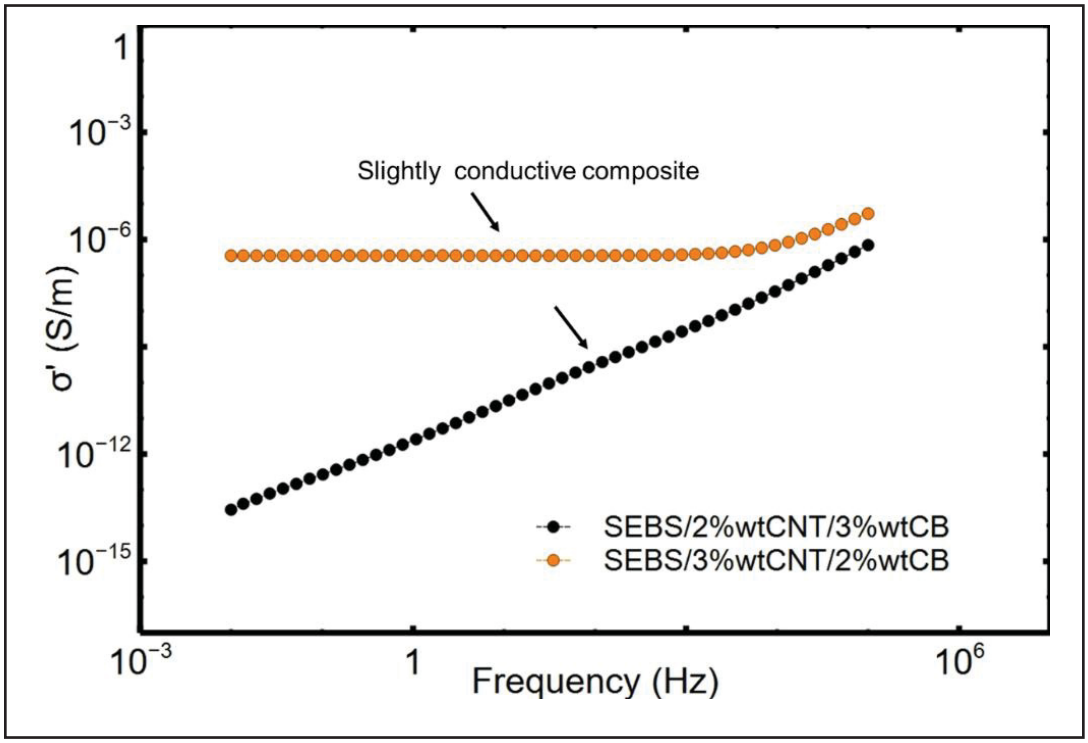


Figure 5.6. Hybrid SEBS composites with 5 wt% total reinforcement (σ′ vs. frequency)

The data show the baseline conductivity achieved at this low reinforcement loading, serving as a reference to compare with higher reinforcement concentrations. Figure 5.7 compares the conductivity of SEBS composites with 10% reinforcement weight fractions. It presents the conductivity of SEBS composites with 10% reinforcement as a function of frequency.

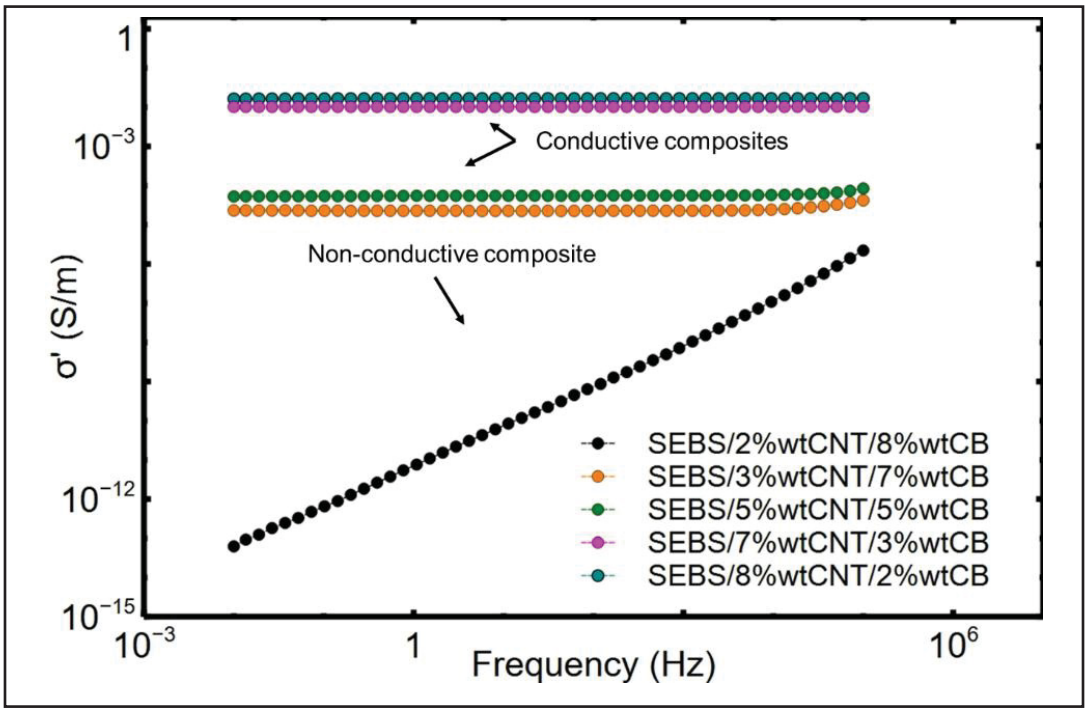


Figure 5.7. Hybrid SEBS composites with 10 wt% total reinforcement showing CNT content-controlled transition to frequency-independent behavior (σ′ vs frequency)

Figure 5.7 shows the electrical conductivity of SEBS composites containing 10% by weight of reinforcement. This concentration shows a significant increase in conductivity compared to lower concentrations, indicating the formation of conductive pathways within the composite material.

Table 5-4 summarizes the electrical conductivity values and frequency-dependent behavior of SEBS composites containing a total of 10 wt% reinforcement with different CNT/CB ratios, complementing the results shown in Figure 5.7.

Table 5-4 Electrical conductivity of SEBS composites (10 wt% reinforcement) with different CNT/CB ratios

Composite Formulation	Conductivity at 1 Hz (S/m)	Frequency Dependence	Interpretation
2% CNT / 3% CB	$\sim 10^{-12}$	Strong increase with frequency	Weak network, CB-dominated; poor continuous paths
3% CNT / 2% CB	$\sim 10^{-6}$	Slight increase after 10^3 Hz	CNT-dominated robust network; significantly higher conductivity than 2% CNT/3% CB
3% CNT / 7% CB	$\sim 10^{-5}$	Slight increase	Moderate network, improved vs 2% CNT/3% CB
5% CNT / 5% CB	$\sim 10^{-4}$	Slight increase	Higher conductivity than 3% CNT/7% CB
7% CNT / 3% CB	$\sim 10^{-2}$	Stable (frequency-independent)	Strong CNT-dominated network; robust conduction
8% CNT / 2% CB	$>10^{-2}$	Stable (frequency-independent)	Highly efficient CNT network; minimal CB contribution

Figure 5.8 displays SEBS composites with a 15% weight fraction, comparing their conductivity as a function of frequency across different amounts of carbon nanotubes (CNT) and carbon black (CB).

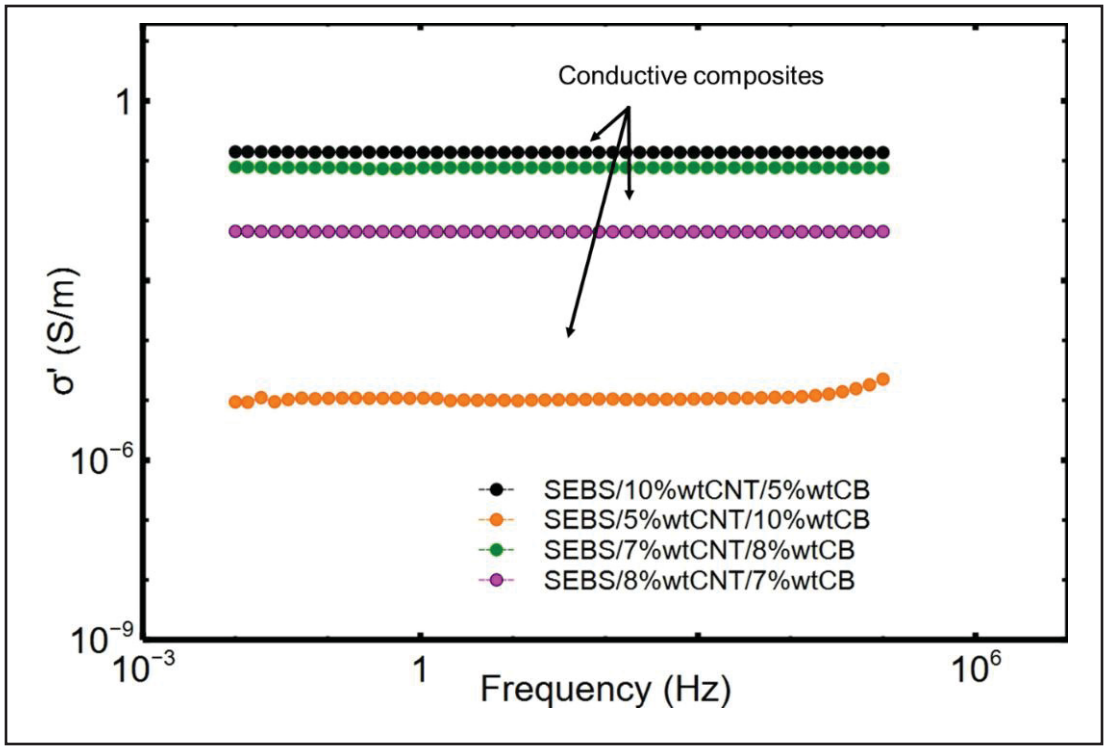


Figure 5.8. Hybrid SEBS composites with 15 wt% total reinforcement (σ′ versus frequency)

The electrical conductivity of SEBS composites with a 15% weight fraction of reinforcement at this level indicates a well-connected conductive network within the SEBS matrix. Figure 5.9 shows SEBS composites with 20% weight reinforcement, comparing the conductivity of SEBS composites with different amounts of carbon nanotubes (CNT) and carbon black (CB) as a function of frequency.

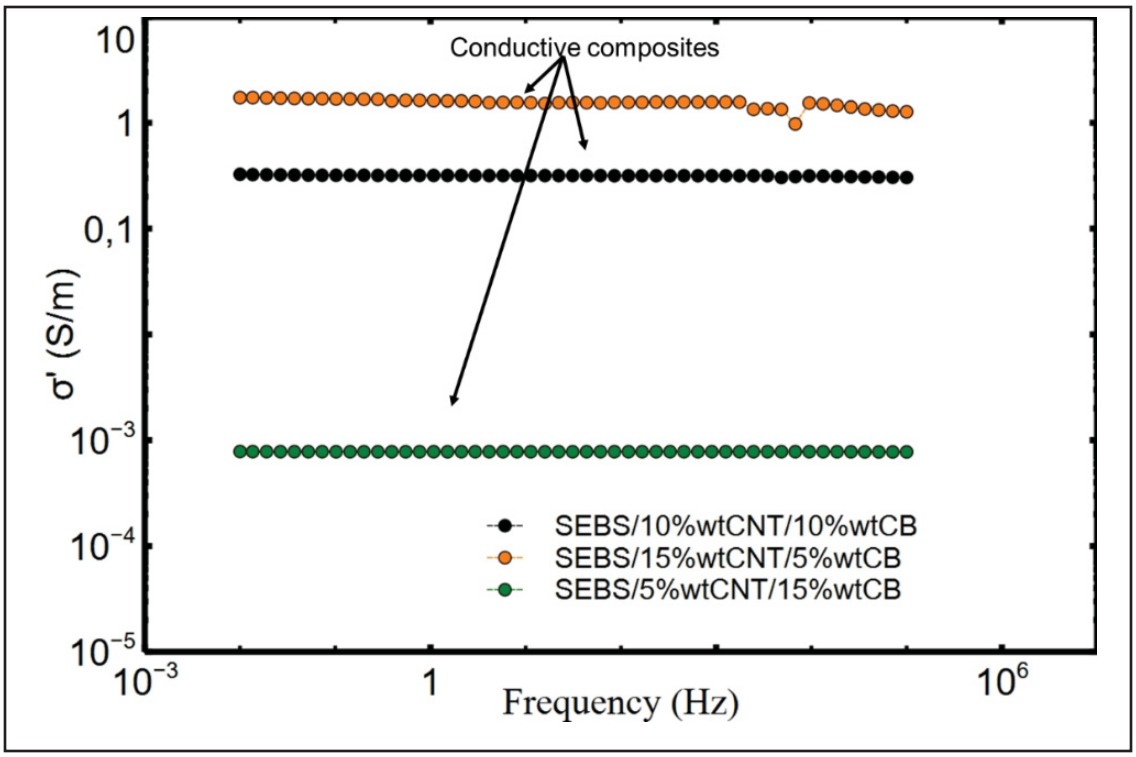


Figure 5.9. Hybrid SEBS composites at 20 wt% total reinforcement (σ′ vs frequency)

The electrical conductivity of SEBS composites with 20% weight of reinforcement exhibits a high level of conductivity, confirming the formation of a continuous and effective conductive network throughout the material. Table 5-5 summarizes the electrical conductivity and frequency-dependent behavior of SEBS composites with 20 wt% total reinforcement, highlighting the influence of CNT/CB ratios as shown in Figure 4.9.

Table 5-5 Electrical conductivity and frequency-dependent behavior of SEBS composites with 20 wt% CNT/CB reinforcement (see Figure 4.9)

Composite Formulation	Conductivity at 1 Hz (S/m)	Frequency Dependence	Interpretation
10% CNT / 5% CB	$>10^{-1}$	Stable (frequency-independent)	High CNT forms a robust network; CB adds extra contribution
5% CNT / 10% CB	$\sim10^{-5}$	Slight increase at high frequencies	Less efficient network due to lower CNT content
7% CNT / 8% CB	$\sim10^{-1}$	Stable across the range	Balanced CNT–CB contribution; effective network
8% CNT / 7% CB	$\sim10^{-2}$	Stable (frequency-independent)	CNT stabilizes the network; CB contribution is secondary
10% CNT / 10% CB	$\sim3\times10^{-1}$	Stable across the range	Well-formed conductive network; minimal frequency dependence
15% CNT / 5% CB	~2	Stable (frequency-independent)	Very robust CNT-dominated network; highest conductivity
5% CNT / 15% CB	$\sim10^{-3}$	Stable across the range	High CB but insufficient CNT; limited network efficiency

The greater effectiveness of CNT in forming a conductive network, compared to CB, results in higher conductivity and less frequency dependence. Combining CNT and CB can be fine-tuned to achieve specific electrical properties. A higher carbon black content, without sufficient carbon nanotubes to form synergistic networks, results in lower overall conductivity in SEBS composites. This maintains consistent conductivity across

frequencies, highlighting the efficiency of CNTs in creating a conductive network compared to CB. Although CB contributes to conductivity, its effect is less significant than that of CNTs, especially at higher concentrations. Excess CB without sufficient CNT can cause lower overall conductivity. The conductivity of SEBS composites is heavily influenced by the ratio of carbon nanotubes to carbon black; CNTs are crucial for establishing effective conductive networks, while CB plays a secondary role. Figure 5.10 compares the electrical conductivities (in S/m) of Maleic anhydride-grafted styrene-ethylene-butylene-styrene (SEBS-MA) composites with those of highly conductive styrene-ethylene-butylene-styrene (SEBS) composites across different frequencies. The data highlight the impact of varying carbon nanotube and carbon black concentrations in SEBS and SEBS-MA composites. Each line in the graph represents a specific combination of SEBS/SEBS-MA, CNT concentration, and CB concentration.

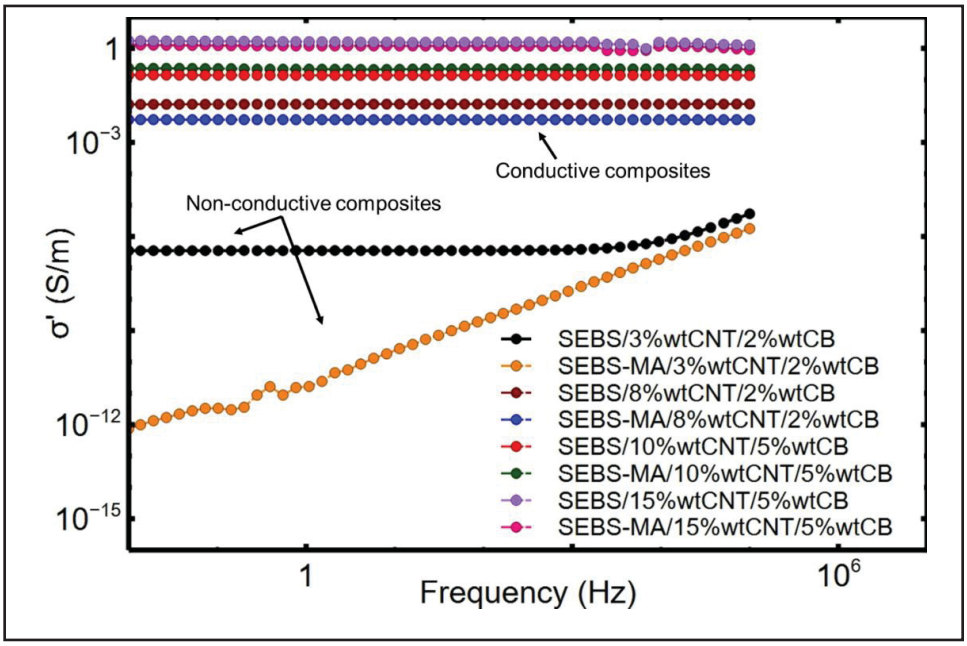


Figure 5.10. Modifying with maleic anhydride reduces conductivity compared to SEBS at the same CNT/CB loadings (σ′ vs frequency), with no advantageous shift in percolation for these systems

The electrical conductivity data in Figure 5.10 illustrates how both matrix type and reinforcement loading influence overall conductivity, providing insights for designing

composites with better electrical properties. Table 5-6 compares the electrical conductivity of SEBS and SEBS-MA composites, showing that maleic anhydride modification generally reduces conductivity across various CNT/CB loadings, as demonstrated in Figure 5.10.

Table 5-6 Comparison of electrical conductivity between SEBS and SEBS-MA composites across different CNT/CB loadings (corresponding to Figure 4.10)

Composite Formulation	Conductivity (S/m)	Comparison (SEBS-MA vs SEBS)	Interpretation
SEBS-MA /3%CNT/2% CB	Lower than SEBS/3% CNT/2% CB	SEBS-MA < SEBS	Maleic anhydride reduces conductivity at low loading.
SEBS-MA / 8% CNT / 2% CB	$<10^{-2}$	SEBS-MA < SEBS ($>10^{-2}$)	SEBS shows higher network efficiency
SEBS-MA / 10% CNT / 5% CB	$\sim 1\times10^{-1}$	SEBS-MA < SEBS ($\sim 2\times10^{-1}$)	CNT-rich SEBS is more conductive.
SEBS-MA / 15% CNT / 5% CB	~1	SEBS-MA < SEBS (~2)	SEBS forms a more robust network at high loading

Maleic anhydride-grafted styrene-ethylene-butylene-styrene (SEBS-MA) composites show lower conductivity than elastomeric thermoplastic polymer (SEBS) composites, indicating that maleic anhydride modification does not improve the interaction between carbon nanotubes (CNTs) and the polymer matrix. Increasing CNT and carbon black (CB) concentrations, along with modifying elastomeric thermoplastic polymer (SEBS) to maleic anhydride-grafted styrene-ethylene-butylene-styrene (SEBS-MA), positively affect electrical conductivity, especially at higher frequencies. The balance between carbon nanotubes and carbon black can be optimized to achieve the desired conductivity and frequency response characteristics.

As the CNT content increases, the overall conductivity of the composites rises, and the frequency dependence decreases, indicating a shift toward a more stable, efficient

conductive network dominated by CNTs. Conversely, higher carbon black content tends to lower the overall conductivity, reflecting less efficient network formation compared to CNTs. Increasing the proportion of CNTs significantly enhances overall conductivity and reduces frequency dependence, highlighting the role of CNTs in forming stable, efficient conductive networks within SEBS composites. The combination of carbon nanotubes and carbon black greatly influences the conductivity behavior of both SEBS and elastomeric thermoplastic polymer (SEBS) composites. Higher CNT content enhances conductivity and decreases frequency dependence, highlighting the importance of CNTs in establishing effective conductive networks. By adjusting the proportions of CNT and CB, the electrical properties of the composite can be tailored to specific requirements.

The electrical conductivity of filled SEBS and SEBS-MA composites follows the percolation scaling law for filler fractions above the critical threshold (ϕc). For CNT composites, loadings above approximately 3 wt% show a sharp increase in conductivity. SEBS/10 wt% CNT exhibits a stable plateau around 10^{-2} to 10^{-3} $S \cdot m^{-1}$, while 16 wt% CNT reaches about 1 $S \cdot m^{-1}$. For CB, the percolation threshold is much higher: composites with 10 wt% CB remain insulating, and only at 20 wt% does conductivity approach about 10^{-2} $S \cdot m^{-1}$. These results confirm that the percolation threshold of CNT (>3 wt%) is significantly lower than that of CB (>12 wt%), highlighting the greater efficiency of CNT networks for electron transport. Figures 4.4 – 4.10 consistently support these threshold estimates.

Hybrid CNT/CB systems primarily function as CNT-controlled composites when the CNT content exceeds approximately 3 wt% of the total load. For instance, 7/3 and 8/2 wt% CNT/CB formulations already reach $\geq 10^{-2}$ $S \cdot m^{-1}$ with only 8–10 wt% total filler. CB alone does not reduce the percolation threshold independently. Matrix chemistry also affects conductivity. SEBS-MA consistently shows lower σ' than SEBS at the same loadings (e.g., 8/2, 10/5, and 15/5 wt% CNT/CB), implying either a slightly higher effective ϕc or lower network efficiency due to less favorable filler–matrix interactions. Therefore, maleic anhydride grafting does not positively shift the percolation threshold, though it may still enhance mechanical or interfacial properties. From a design standpoint, to achieve EEG-grade conductivity ($\sigma' \geq 10^{-2}$ $S \cdot m^{-1}$ with minimal dispersion), CNT loadings should be kept

at ≥7–8 wt%, with 2–3 wt% CB as a secondary filler. Formulations with high CB alone are not advised because their percolation threshold is well above 12 wt%, and conductivity gains are limited.

5.4.2 Structural Properties

Scanning electron microscopy (SEM) was used to examine the morphology of the electrodes and the distribution of conductive fillers within the SEBS matrix. Figure 4.11 shows a micrograph of a multipin SEBS-based electrode reinforced with 10 wt% CNT and 5 wt% CB. Distinct regions are labeled to highlight filler dispersion: particle-free SEBS, CB+SEBS, CNT+SEBS, and CB+CNT+SEBS.

The particle-free SEBS areas represent the pure polymer matrix, characterized by smooth surfaces without filler inclusions. In contrast, the CB+SEBS regions display clusters of small, spherical, or irregularly shaped particles, indicating partial agglomeration of carbon black and suggesting limited uniformity in its dispersion. The CNT+SEBS regions show fibrous, entangled networks typical of carbon nanotubes, confirming the presence of extended conductive pathways that significantly contribute to percolation and charge transport. Finally, the CB+CNT+SEBS regions exhibit a combination of CB particles embedded within CNT entanglements, implying synergistic interactions where CB may bridge CNT bundles or improve filler–matrix interfacial contact. Overall, the micrograph shows a varied distribution of fillers within the SEBS matrix. While CB tends to form clusters, CNTs create interconnected fibrous networks, and their co-localization indicates some synergy between the two fillers. These structural observations directly relate to the electrical behavior discussed in Section 4.1, where CNT-dominated systems showed better conductivity and consistent performance across frequencies, while CB contributed less.

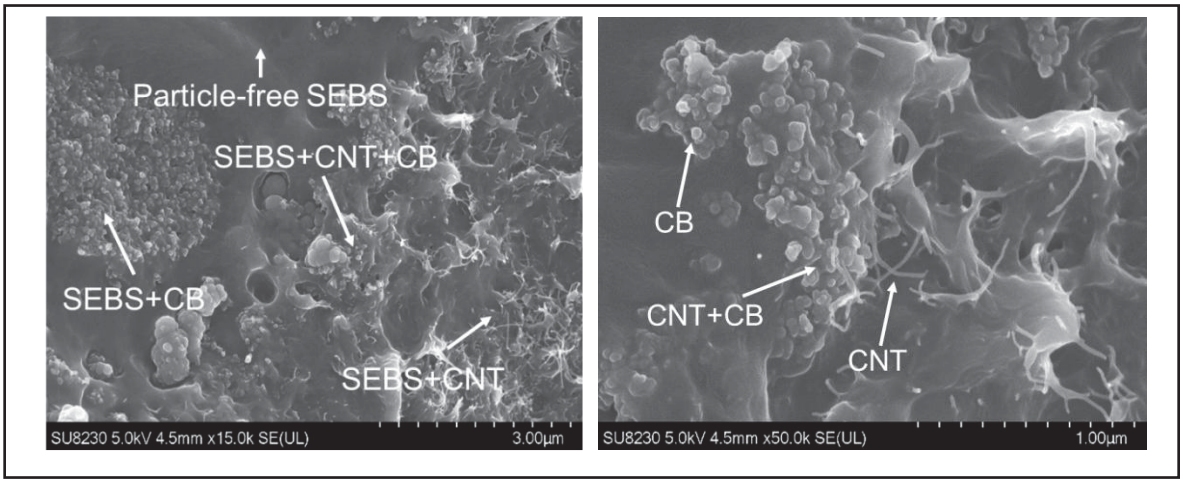


Figure 5.11**.** Scanning electron micrograph of a multipin SEBS electrode reinforced with 10 wt% CNT and 5 wt% CB. Distinct regions are labeled: (i) particle-free SEBS matrix, (ii) CB+SEBS (agglomerated carbon black clusters), (iii) CNT+SEBS (fibrous nanotube networks), and (iv) CB+CNT+SEBS (mixed regions). The microstructure exhibits heterogeneous filler dispersion, with CNT networks forming conductive pathways and CB particles facilitating interfacial contacts, although some aggregation is observed

The scanning electron microscope (SEM) image in Figure 5.11 shows distinct phases within the SEBS/CB/CNT composite. Carbon nanotubes (CNTs) appear as tangled, fibrous networks that create conductive pathways, which are vital for their electrical performance. In contrast, carbon black (CB) appears as clumped, spherical, or irregular particles, indicating limited dispersion within the matrix. While the CNT network supports efficient percolation, excessive entanglement can raise viscosity during processing. The hybrid CNT–CB regions suggest some synergistic interactions, where CB particles may enhance contact between CNT bundles. However, CB aggregation could reduce both electrical conductivity and mechanical strength. Overall, the SEM analysis shows an uneven distribution of fillers, with CNTs mainly contributing to conductivity and CB playing a smaller yet supportive role.

5.4.3 Thermo-Mechanical Properties

Thermogravimetric analysis (TGA) and differential scanning calorimetry (DSC) were performed to assess the thermal stability of SEBS and SEBS-MA composites reinforced

with CNT and CB. The TGA verified the filler content and examined the decomposition behavior, while the DSC detected thermal transitions relevant to EEG operating conditions.

As shown in Figure 5.12 (TGA curves), all composites underwent a sharp weight loss starting around 350–400 °C, which is typical of organic polymer degradation. After 400 °C, the rate of mass loss increased sharply, indicating the beginning of the main decomposition phase of the polymer matrix. Both SEBS/16 wt% CNT and SEBS-MA/16 wt% CNT exhibited very similar degradation patterns, with weight loss starting within the same temperature range. After complete degradation, the remaining weights closely matched the expected CNT and CB loadings, confirming the proper addition of fillers.

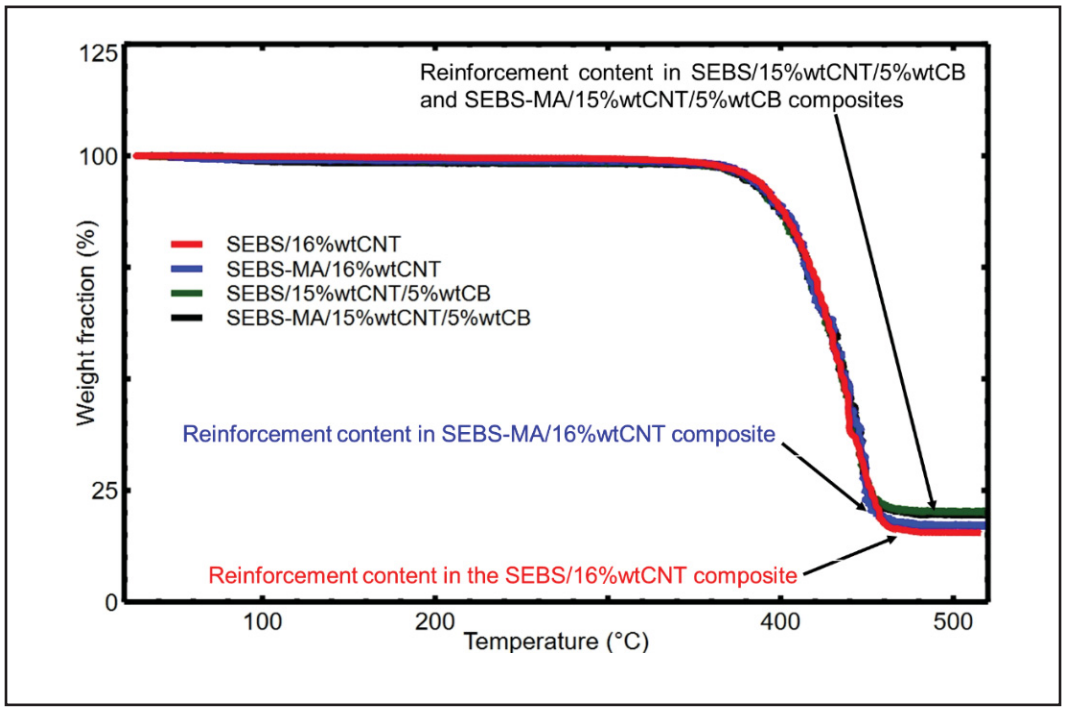


Figure 5.12**.** Thermogravimetric analysis (TGA) curves of SEBS and SEBS-MA composites reinforced with CNT and CB. All samples exhibit a single significant decomposition step, starting around 350–400 °C, which is typical of polymer matrix breakdown. The residual weights verify the intended CNT and CB loadings, with SEBS-MA/16 wt% CNT displaying a slightly higher residual percentage consistent with its reinforcement content

Complementary DSC analyses (Figures 5.13 and 5.14) revealed a glass transition temperature (Tg) of approximately –60 °C for both SEBS and SEBS-MA, indicating their elastomeric properties. No melting or crystallization transitions occur within the physiological temperature range (24–36 °C). The polystyrene (PS) phase exhibits a slightly higher transition range in SEBS (~90–100 °C). The consistent Tg and degradation onset confirm that grafting maleic anhydride does not alter the core thermal behavior of the SEBS matrix.

Overall, the TGA and DSC results show that composites based on SEBS and SEBS-MA undergo a single main decomposition process, demonstrating high thermal stability with degradation starting only above 350 °C. This temperature is well above the physiological range, ensuring that electrode performance remains unaffected during everyday EEG use or extended skin contact.

Importantly, confirming the filler content with TGA enhances the reliability of the electrical and mechanical properties reported in this study. While this work focused on the temperature range relevant to EEG, future studies could extend thermal analysis to assess behavior in other challenging environments.

These results confirm that grafting does not alter the core elastomeric transition of the material; however, it can improve resistance at high temperatures while maintaining flexibility within the range relevant to EEG applications

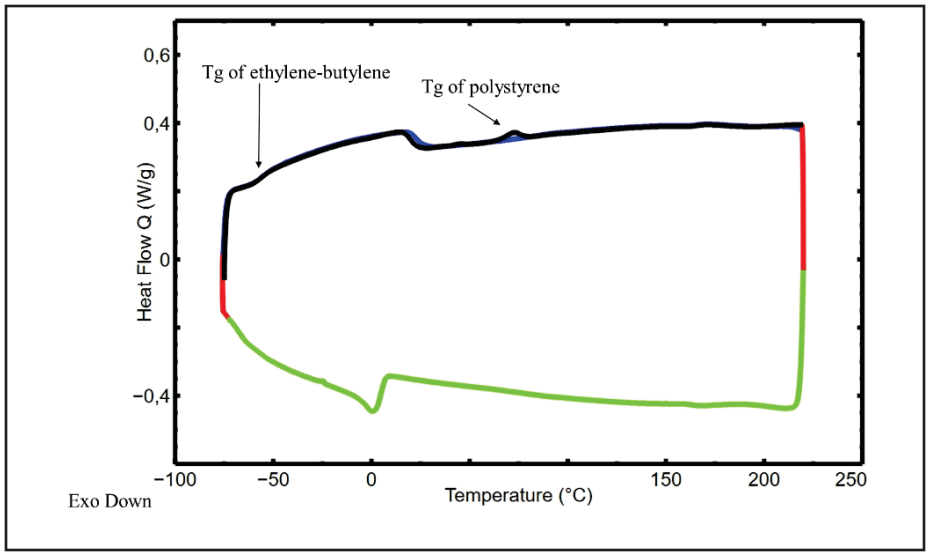


Figure 5.13. The differential scanning calorimetry (DSC) curve of pure SEBS exhibits a glass transition temperature (Tg) of approximately –60 °C, indicating its elastomeric properties. No melting or crystallization transitions occur within the physiological range of 24–36 °C

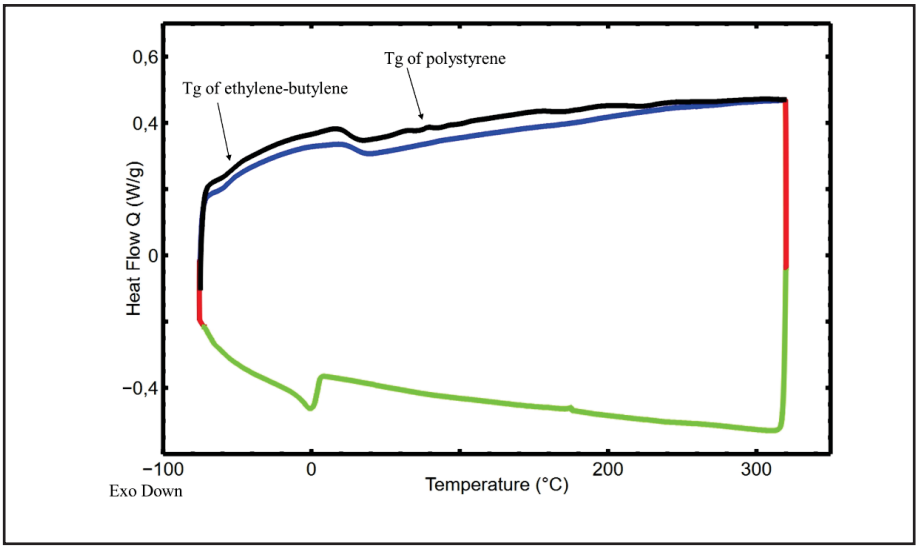


Figure 5.14**.** Differential scanning calorimetry (DSC) curve of SEBS-MA. The glass transition temperature (Tg) occurs at about –60 °C, the same as in neat SEBS, confirming that maleic anhydride grafting does not alter the primary thermal transition of the matrix. No melting or crystallization transitions are observed within the physiological temperature range (24–36 °C)

5.4.4 Dynamic Mechanical Thermal Analysis (DMTA)

Dynamic mechanical thermal analysis (DMTA) was conducted to assess the storage modulus (E') of SEBS and SEBS-MA composites within the physiological temperature range (24–36 °C) at 1 Hz. This range was selected because the electrodes are designed for use at room and scalp temperatures. The storage modulus indicates the elastic response of the materials under dynamic loading, with higher values reflecting greater stiffness.

The results (Figure 5.15) show that neat SEBS has a higher storage modulus than SEBS-MA, confirming that grafting maleic anhydride improves the material's flexibility. Reinforcing with CNT and CB significantly increases the modulus in both matrices, and the storage modulus generally rises with more reinforcement content. Notably, all curves remain nearly flat across the tested range, indicating stable, solid-like behavior under EEG-relevant conditions. A detailed comparison of the relative storage modulus across formulations is summarized in Table 5-7.

Table 5-7 Comparison of storage modulus (*E′*) for SEBS and SEBS-MA composites (24–36 °C, 1 Hz)

Material	Relative Storage Modulus (*E′*)
SEBS	Higher than SEBS-MA; Stiffer base polymer
SEBS-MA	Lower than SEBS; More flexible, softer base polymer
SEBS/20wt% CB	Slightly lower than SEBS-MA/20 wt% CB; MA-modified version slightly stiffer
SEBS/16wt%CNT	Slightly higher than SEBS-MA/16 wt% CNT
SEBS/8 wt%CNT/2wt%CB	Higher than SEBS-MA/8 wt%CNT/2wt%CB
SEBS-MA/8 wt%CNT/2wt%CB	Similar to SEBS; Most flexible conductive composite; optimal balance of properties
SEBS/10 wt%CNT/5wt%CB	Higher than SEBS-MA/10wt% CNT/5wt% CB
SEBS-MA/10wt%CNT/5wt%CB	Similar to SEBS/8wt% CNT/2wt%CB
SEBS/15 wt%CNT/5wt%CB	Higher than SEBS-MA/15 wt%CNT/5wt% CB

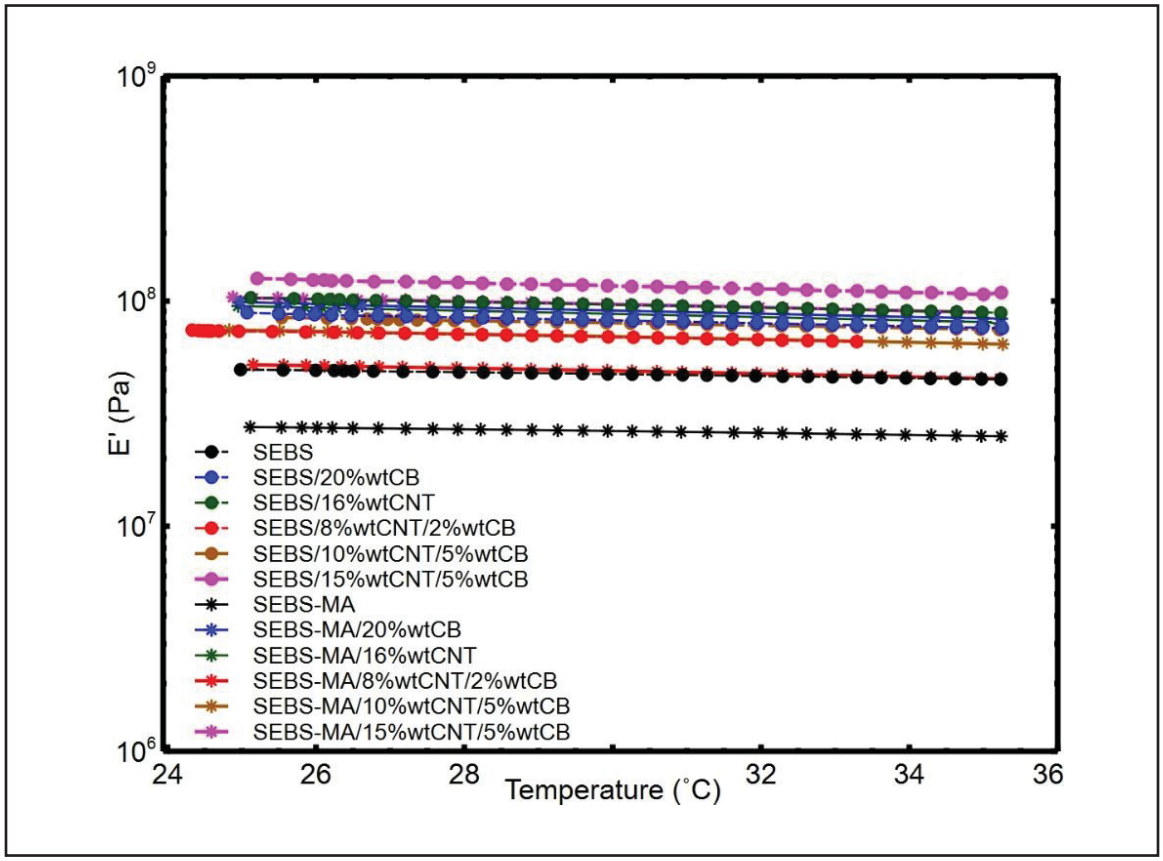


Figure 5.15**.** Dynamic mechanical thermal analysis (DMTA) curves of SEBS and SEBS-MA composites (24–36 °C, 1 Hz). The storage modulus (E') increases with CNT and CB reinforcement, while SEBS-MA-based composites show a lower modulus than SEBS, confirming increased flexibility

Overall, maleic anhydride modification improves flexibility, while CNT and CB reinforcements increase stiffness. Among all formulations, SEBS-MA/8wt%CNT/2wt%CB emerges as the most promising for EEG electrodes, offering high conductivity combined with a low storage modulus similar to that of neat SEBS. This balance of softness and electrical performance is ideal for ensuring both comfort and reliable scalp contact during long-term EEG applications. Importantly, when considering the DSC and TGA results, these findings confirm that the composites not only stay mechanically stable across the

physiological range but also have excellent thermal stability well above typical operating conditions, reaffirming their suitability for safe and reliable EEG use.

5.4.5 Preliminary In Vivo Validation

The contact impedance of the styrene-ethylene-butylene-styrene (SEBS)/8% wt CNT/2% wt CB electrode is 4.25 ± 0.5 kΩ, slightly lower than that of commercial flexible electrodes (4.75 ± 1.5 kΩ). The SEBS-MA/8% wt CNT/2% wt CB electrode shows a contact impedance of 4.5 ± 0.6 kΩ, placing it between the SEBS-based electrode and the commercial option. Based on these results, we can conclude that both SEBS-based electrodes are suitable for EEG applications, as they have contact impedance values comparable to those of commercial flexible electrodes (4.75 ± 1.5 kΩ), indicating their potential for similar electrical performance. The SEBS/8% wt CNT/2% wt CB electrode exhibits the lowest impedance (4.25 ± 0.5 kΩ), likely due to its higher electrical conductivity, which improves the electrode-skin interface and may reduce signal loss, thereby enhancing quality. The SEBS-MA/8% wt CNT/2% wt CB electrode has a slightly higher impedance (4.5 ± 0.6 kΩ), possibly because maleic anhydride modification affects composite dispersion or interfacial properties. Since EEG electrodes need low and stable contact impedance to prevent signal degradation, both SEBS-based electrodes show promise as alternatives to commercial flexible electrodes.

Figure 5.16 displays EEG time domain recordings of a commercial dry flexible electrode a t position 2, compared to SEBS-MA/8%wtCNT/2%wtCB and SEBS/8%wtCNT/2%wtCB at positions 1 and 3, respectively, when the subject's eyes were open.

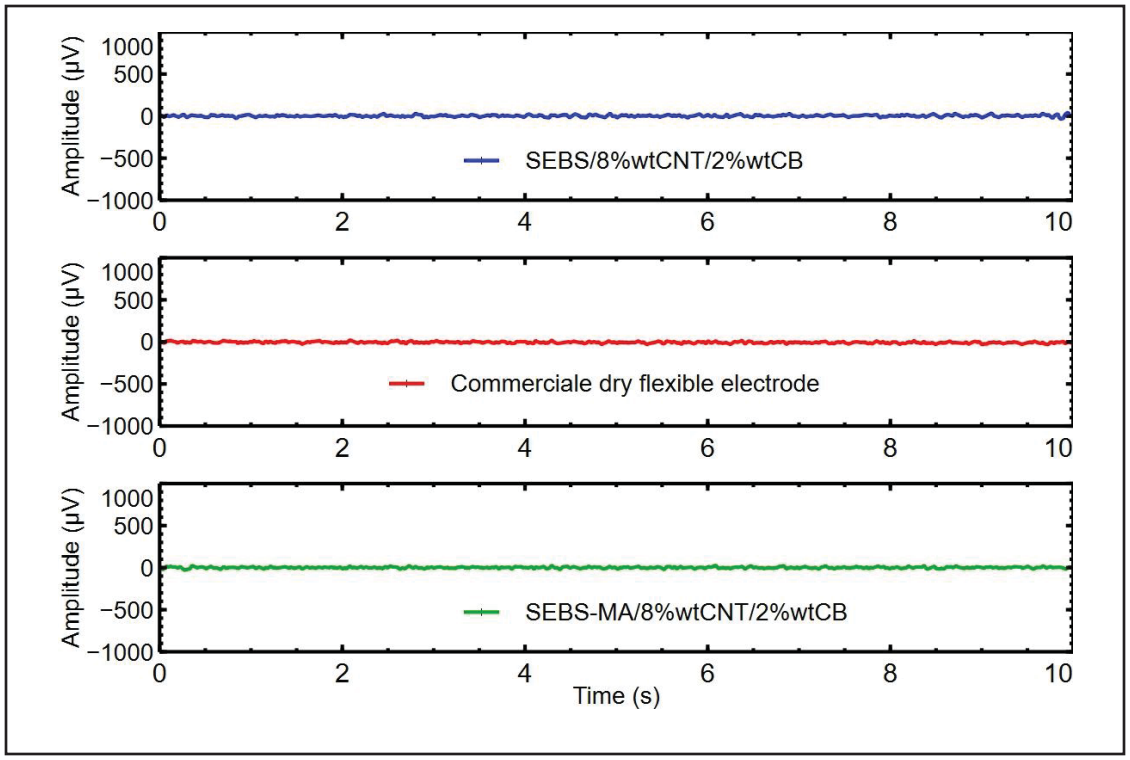


Figure 5.16. Time-domain EEG recording during eyes-open condition

Figure 5.17 shows a typical EEG time-domain recording captured while the subject's eyes were open and blinking. The data highlights characteristic artifacts caused by eye blinks, which are essential to identify and manage during EEG data processing. The signal from the SEBS/8%wtCNT/2%wtCB electrode exhibits moderate amplitude fluctuations but remains relatively stable, indicating that it records EEG data of acceptable quality. The signal from the commercial electrode is also stable, showing similar performance. Additionally, the signal from the SEBS-MA/8%wtCNT/2%wtCB electrode remains stable with minimal noise and fluctuations.

The transitions between different states (eyes open and closed) are clearly visible, indicating the electrode's sensitivity to changes in mental state. The signal from the commercial electrode remains stable during these transitions, showing consistent performance. Meanwhile, the signal from the SEBS-MA/8%wtCNT/2%wtCB electrode is clear and effectively handles the transitions between open and closed states. This performance further

confirms that SEBS-MA/8%wtCNT/2%wtCB is a promising choice for flexible, high-performance EEG electrodes, offering an ideal balance of conductivity and flexibility.

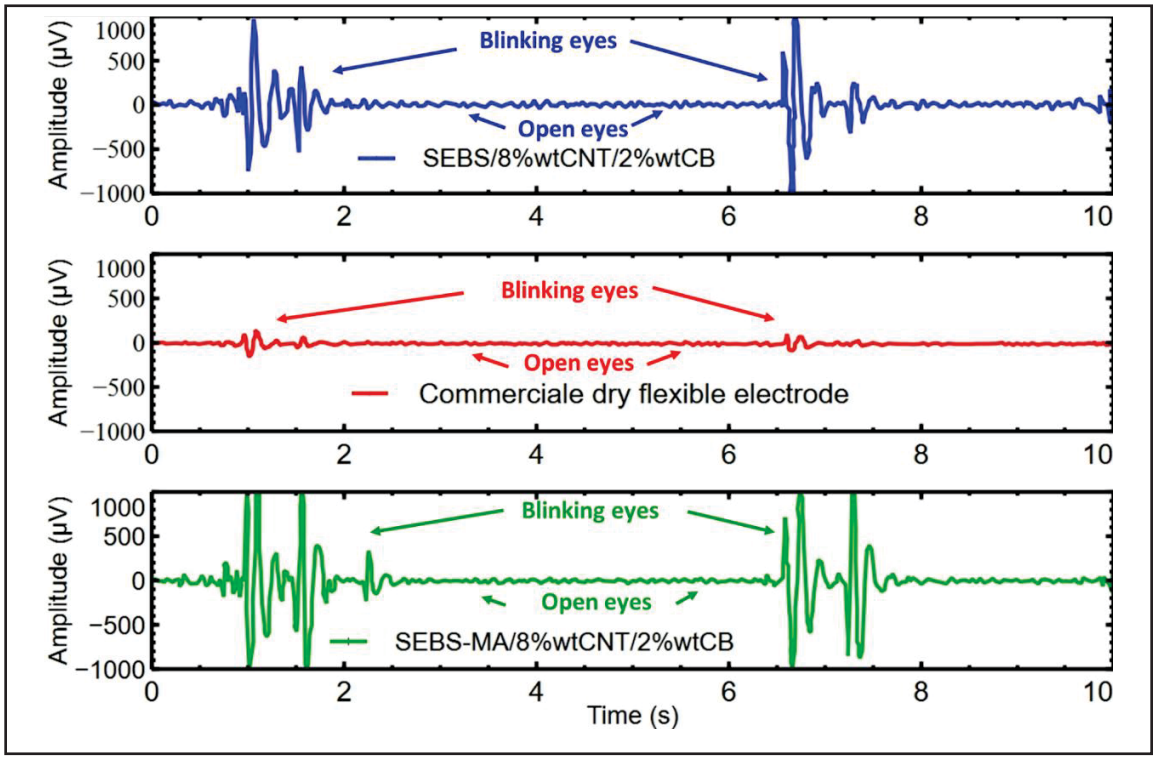


Figure 5.17**.** Time-Domain EEG Recording During Eyes-Open with Blinking

5.5 Discussion

This study demonstrates that composites based on SEBS and SEBS-MA are promising options for flexible dry EEG electrodes, offering a new alternative to PDMS- and TPU-based matrices. SEBS and SEBS-MA maintain a favourable balance of conductivity, flexibility, and stability, illustrating the innovative application of these materials in EEG devices.

The role of CNTs in increasing conductivity was clearly observed. Their high aspect ratio enables the efficient formation of a percolated network, significantly reducing impedance

once the percolation threshold is reached. However, adding more CNTs has disadvantages: excessive amounts can lead to agglomeration, poor dispersion, and higher processing viscosity, which can make the composite stiffer and decrease electrode comfort. Additionally, improvements in conductivity often plateau at higher CNT levels, indicating that network density, not just the amount of CNTs, is the critical factor. The addition of CB further boosts network connectivity by bridging gaps between nanotubes, creating a synergistic effect at optimal CNT/CB ratios. Recent literature has reported significant progress in conductive polymer composites, with a focus on multifunctional performance and interfacial optimization. For example, Liu et al. (C. Liu et al., 2025) and Liu et al. (Y. Liu et al., 2025) demonstrated self-healing CNT-based elastomers and PDMS-CNT composites with ultralow percolation thresholds, respectively. Gui et al. (Gui et al., 2023b) and Lee et al. (Y.-H. Lee et al., 2025b) reported hierarchical CNT/MXene and π-conjugated polymer/CNT systems with improved conductivity and EMI shielding. Likewise, Ye et al. (Ye et al., 2024) revealed how amorphous/crystalline heterophase structures enhance fatigue resistance. Together, these findings support the current results by demonstrating that continuous hybrid networks and optimized filler–matrix interactions are crucial for achieving simultaneous electrical conductivity, flexibility, and mechanical resilience. The hybrid SEBS-MA/CNT/CB composites in this study align with this design philosophy, demonstrating stable conductivity and flexibility suitable for wearable EEG applications.

SEBS-MA composites showed lower conductivity than their SEBS counterparts, likely due to changes in filler–matrix interactions caused by maleic anhydride grafting. However, the SEBS-MA/8%wt CNT/2%wt CB formulation exhibited stable conductivity and mechanical flexibility, as confirmed by DMTA results, which revealed a consistent storage modulus across the physiological temperature range. These properties are crucial for EEG electrodes that must remain flexible and reliable during long-term recordings. Notably, the transition temperatures found in this study closely match those reported in the literature for SEBS and SEBS-MA systems (Aouissi et al., 2025; Davidyants et al., 2025; X. Li et al., 2025).

Additionally, the compression properties of SEBS-based composites have been thoroughly characterized in our previous work, providing complementary insights into their mechanical

response under load. Cyclic compression tests conducted according to ASTM D575-91 on SEBS/20 wt% CB and EVA (ethylene-vinyl acetate)/20 wt% CB composites showed distinct behaviors: while EVA, a thermoplastic copolymer of ethylene and vinyl acetate, exhibited higher stiffness (elastic modulus ≈ 63.8 MPa; stress at 50% strain ≈ 16.2 MPa), the SEBS/20 wt% CB composite displayed lower stiffness (elastic modulus ≈ 47.2 MPa; stress ≈ 9.35 MPa) and greater deformability. These results confirm the inherent softness and elasticity of the SEBS matrix, key advantages for wearable and skin-contact sensors. Based on these findings and the DMTA results for pristine SEBS and SEBS-MA presented in Section 5.4, SEBS-MA is unlikely to differ substantially in compressive behavior from SEBS, as maleic anhydride grafting mainly improves polymer–filler interfacial adhesion and slightly enhances flexibility without significantly altering the bulk modulus. Consequently, the compressive mechanical performance of SEBS-MA composites can be reliably inferred from the SEBS data obtained in our previous study.

Regarding storage modulus, most past studies have analyzed these materials at temperatures well above those relevant to EEG operation. In contrast, this study specifically examined the physiological range (24–36 °C), the same range used in many other studies (Honda & Nishiyama, 2025; H. Wang et al., 2025; Z. Wang et al., 2025), providing more realistic insights into electrode behavior under actual use conditions.

Together, the DSC and TGA results confirm that SEBS and SEBS-MA composites stay thermally stable under EEG-relevant conditions (room and scalp temperatures). The degradation begins at around 400 °C, providing a large safety margin, which ensures that electrode performance is not affected by physiological heating or prolonged skin contact. The TGA profiles also confirmed filler incorporation and showed consistent thermal stability across all formulations. The minor differences in storage modulus between SEBS and SEBS-MA suggest that maleic anhydride functionalization may slightly improve flexibility without sacrificing thermal stability. Although this study focused on the physiological temperature range relevant to EEG, additional thermal analyses could further clarify how the materials behave during sterilization, storage, and processing, which will be explored in future work.

Preliminary in vivo EEG validation showed that SEBS/8%wt CNT/2%wt CB and SEBS-MA/8%wt CNT/2%wt CB electrodes provided clearer transitions and more stable signals compared to a commercial dry electrode, with the latter demonstrating the most consistent performance. Although promising, these results should be regarded as initial, given the small number of participants, and further validation with larger groups is necessary before making broader claims.

The contact impedance achieved in this study is significantly lower than that of most PDMS- and TPU-based dry electrodes reported in the literature. Commercial and experimental electrodes using these soft matrices typically show impedance values between 10 kΩ and 600 kΩ, depending on fabrication and testing conditions (Fiedler et al., 2015; Heijs et al., 2021; Oh et al., 2024a; Z. Wang et al., 2024d; Xing & Casson, 2023b). In contrast, the SEBS/CNT/CB and SEBS-MA/CNT/CB hybrid electrodes developed here achieved impedance values below 5kΩ, demonstrating a significant improvement in electrical performance. This result highlights the efficiency of the hybrid conductive network and the SEBS-based matrix in ensuring intimate skin contact, effective charge transfer, and stable EEG signal acquisition while preserving flexibility and comfort.

Despite promising results, this study has some limitations. The in vivo validation was preliminary, involving a small sample size of participants and only time-domain analysis. Future research should include larger groups, frequency-domain assessments, and long-term testing for comfort, durability, and electrode–skin interactions. Additionally, improving CNT dispersion methods could reduce agglomeration at higher loadings, enabling better conductivity without sacrificing flexibility. Addressing these issues will be crucial for establishing SEBS- and SEBS-MA-based composites as reliable next-generation materials for dry EEG electrodes.

5.6 Conclusion

This study shows that composites based on SEBS- and SEBS-MA, reinforced with CNT and CB, are promising options for flexible dry EEG electrodes. Notably, SEBS-MA/8%wt CNT/2%wt CB achieved a low contact impedance of 4.5 ± 0.6 kΩ, similar to commercial

flexible electrodes and close to SEBS/8%wt CNT/2%wt CB, which measured 4.25 ± 0.5 kΩ. The composite maintained a storage modulus comparable to that of pure SEBS, confirming high flexibility while providing enough stiffness for stable scalp contact. Initial in vivo EEG tests further demonstrated that both SEBS and SEBS-MA composites generated stable signals with accurate detection of brain state changes, outperforming EVA/CB electrodes in terms of noise reduction and stability.

Although these results are encouraging, some limitations need to be acknowledged. The in vivo validation was preliminary, involving a small sample size and limited to time-domain analysis. Larger studies and frequency-domain assessments are necessary to establish broader clinical relevance. SEBS-MA composites also showed a slight decrease in conductivity compared to SEBS, indicating a compromise between electrical performance and increased stiffness. Furthermore, large-scale reproducibility might be influenced by the dispersion and agglomeration of CNTs, which require careful optimization of processing conditions.

In summary, SEBS- and SEBS-MA-based nanocomposites demonstrate strong potential as next-generation EEG electrodes, offering a better balance of conductivity, flexibility, and stability compared to PDMS- or TPU-based options. However, further validation and process improvements are necessary to turn these materials into reliable, scalable devices for practical EEG applications.

A comprehensive quantitative percolation modeling study will be conducted in future research for each hybrid system to quantify the percolation thresholds better and understand the relationship between filler content, network formation, and electrical conductivity.

5.7 Author credit statement

The authors of the published version of this study are George Gnonhoue (GG), Ilyass Tabiai (IT), Jérémie Voix (JV), and Éric David (ED).

GG conducted the investigation and performed the experiments, data processing, and formal analyses. He carried out the analytical calculations, contributed to the interpretation of the results, and prepared the figures. GG drafted the original version of the manuscript and

incorporated all revisions following peer review.

IT contributed to the conceptualization of the project and the development of the experimental methodology. He participated in the scientific validation of the proposed approaches, the acquisition of funding, and the critical review of the manuscript, and provided overall supervision of the work.

JV contributed to the investigation and formal analysis, as well as to funding acquisition. He participated in the review and editing of the manuscript and co-supervised the project throughout its execution.

ED contributed to the conceptualization of the project and the development of the methodology. He was involved in formal analysis, funding acquisition, and critical review of the manuscript, and provided scientific co-supervision of the work.

IT and ED jointly supervised the project.

5.8 Author Declarations

The authors declare that they have no known competing financial interests or personal relationships that could have appeared to influence the work reported in this paper. The data of this study are available upon request.

5.9 Acknowledgements

The authors would like to acknowledge the financial support received from NSERC Alliance (ALLRP 566678-2021), MITACS IT26677 (SUBV-2021-168), and PROMPT (#164_Voix-EERS 2021.06) for the ÉTS-EERS Industrial Research Chair in In-Ear Technologies, which is sponsored by EERS Global Technologies Inc.

CHAPITRE 6

EXPLORATORY WORK

The work presented in the preceding chapters of this thesis has led to the development and characterization of flexible EEG electrodes based on conductive polymer nanocomposites, particularly those using SEBS, EVA, and SEBS-MA matrices reinforced with conductive fillers such as carbon nanotubes (CNTs) and carbon black (CB). This work has primarily focused on optimizing the electrical, mechanical, and electrochemical properties of the materials, as well as evaluating their performance in acquiring electroencephalographic signals.

In parallel with the main studies that led to the scientific publications presented in this thesis, several exploratory studies were conducted to investigate different approaches that could improve the design, fabrication, and evaluation of polymer EEG electrodes. These studies investigated complementary aspects not included in the scientific articles, but which provide additional insights and open up perspectives for the future development of flexible EEG devices. These exploratory studies focused in particular on:

- the development of PDMS-based conductive composites for the manufacture of an artificial ear to simulate the electrode-skin interface for the evaluation of EEG electrodes;
- the establishment of an experimental setup for the acquisition and visualization of EEG signals, including the use of open electronic platforms;
- the exploration of new manufacturing methods, such as the production of conductive filaments for 3D printing, with the aim of simplifying the manufacture of polymer electrodes;
- the analysis of certain fundamental aspects of conductive nanocomposites, including the influence of interphase and agglomeration of conductive charges on electrical properties.

Although this work has not yet reached the level of full experimental validation or scientific publication, it contributes to a better overall understanding of the behavior of conductive polymer nanocomposites and EEG acquisition systems. It also identifies several promising avenues of research for improving the performance of flexible EEG electrodes and for developing new manufacturing methods.

The following sections present the main approaches explored, the preliminary results obtained, and the associated research perspectives.

6.1 Influence of interphase thickness (matrix/reinforcement) on the percolation threshold in EVA/CB and SEBS/CB nanocomposites

6.1.1 Objective

The interphase formed between the polymer matrix and the reinforcing particles constitutes a key region in conductive polymer nanocomposites, as it directly influences the mechanical and electrical properties of the material. In particular, this interfacial region plays a crucial role in the formation of the conductive network and in determining the electrical percolation threshold. Among the parameters characterizing this interphase, its thickness is an important factor likely to affect the interactions between the conductive particles as well as the electrical conduction mechanisms in the nanocomposites.

Despite its importance, the experimental characterization of the interphase in polymer nanocomposites remains relatively limited in the literature, primarily due to the difficulty of accessing this region at the nanoscale and reliably quantifying its properties. A better understanding of the interphase characteristics is therefore essential for optimizing the electrical and mechanical properties of these materials.

In this context, a complementary study was conducted to evaluate the influence of all nanocomposite components, including the polymer matrix, the conductive reinforcement, and the matrix/reinforcement interphase, on the material's properties. The main objective of this work is to better understand the role of the interphase in conductive polymer nanocomposites, particularly its influence on the electrical percolation threshold.

The systems studied are polymer composites reinforced with carbon black (CB) particles, specifically SEBS/CB and EVA/CB composites. The development of this study and the execution of some of the analyses were carried out with the contribution of an intern recruited within the framework of the project and supervised by the author of this thesis.

6.1.2 Methodology

To evaluate the influence of the interphase on the structure of the nanocomposites, the degree of agglomeration of carbon black (CB) was compared in the different composites developed in article 1. To ensure the comparability of the results, all the composites were developed according to the same manufacturing process, based on the dissolution of the polymer matrix in toluene followed by the incorporation of the conductive reinforcement.

The contact thickness was also estimated numerically using the model proposed by Mazaheri et al. (Mazaheri et al., 2022). In the context of this study, a simplified reformulation of this model was developed to facilitate its application to the analysis of the nanocomposites studied.

Microscopic observations were carried out on all samples in order to identify the presence of agglomerates and to evaluate the distribution of carbon black within the different polymer matrices.

6.1.3 Results

6.1.3.1 Conductivity models as a function of reinforcement ratio and interphase

A recently developed model (Mazaheri et al., 2022), described by the equations (6.1), (6.2)and (6.3) is more complete. Indeed, the modeling takes into account the interphase thickness *t* forming uniformly around each nanoparticle.

$$\left(1-\frac{\Phi}{\alpha}\right)\frac{\sigma_e-\sigma_m}{2\sigma_e+\sigma_m}+\frac{\Phi}{\alpha}\frac{\sigma_e-\sigma_{com}}{2\sigma_e+\sigma_{com}}=0 \qquad (6.1)$$

σ_e, σ_m and σ_{com} are respectively the conductivities of the nanocomposite, the matrix and the CB complex (CB/interphase assembly).

$\alpha=\frac{r^3}{(r+t)^3}$ is the ratio between the volume of CB and the volume of complex CB.

$$\sigma_{com} = \frac{3\sigma_f\sigma_{int}r^3 + \sigma_{int}(2\sigma_{int} + \sigma_f)[(r+t)^3 - r^3] - 6\sigma_{int}(\sigma_{int} - \sigma_f)ln\frac{r+t}{r}}{3\sigma_{int}r^3 + (2\sigma_{int} + \sigma_f)[(r+t)^3 - r^3] - 6(\sigma_{int} - \sigma_f)ln\frac{r+t}{r}} \quad (6.2)$$

σ_f and σ_{int} are respectively the conductivities of the CB and the interphase.

$$\sigma_{int} = \frac{e^2\sqrt{2m\lambda}}{\hbar^2}\exp\left(-\frac{4\pi d_c\sqrt{2m\lambda}}{\hbar}\right) \quad (6.3)$$

With $e = 1.602176565 \times 10^{-19}$C, the charge of an electron, $m == 9.10938291 \times 10^{-31}$ C the mass of an electron, $\hbar = 1.054571817 \times 10^{-34}$ Planck's constant divided by 2π, d_c the tunneling distance and λ, the potential barrier.

Equations (6.1) to (6.3) can be simplified by neglecting certain terms based on their order of magnitude. This gives us the following equations:

$$\sigma_{com} \approx \sigma_{int} \quad (6.4)$$

$$\phi_c = \frac{r^3}{3(r+t)^3} \quad (6.5)$$

$$t = r\left(\frac{1}{\sqrt[3]{3\phi_c}} - 1\right) \quad (6.6)$$

It should be noted that equation (6.4) shows that the conductivity of the reinforcement σ_f is negligible. Equations (6.5) and (6.6) establish a relationship between the percolation threshold and the interphase thickness. According to these equations, the percolation threshold depends on two main geometric parameters: the interphase thickness and the radius of the carbon black (CB) particles. Thus, a decrease in the percolation threshold can be induced either by increasing the interphase thickness or by reducing the radius of the CB particles. Plotting the initial model and the rewritten model, the two resulting curves overlap (figure 6.1), which confirms the validity of the model simplification.

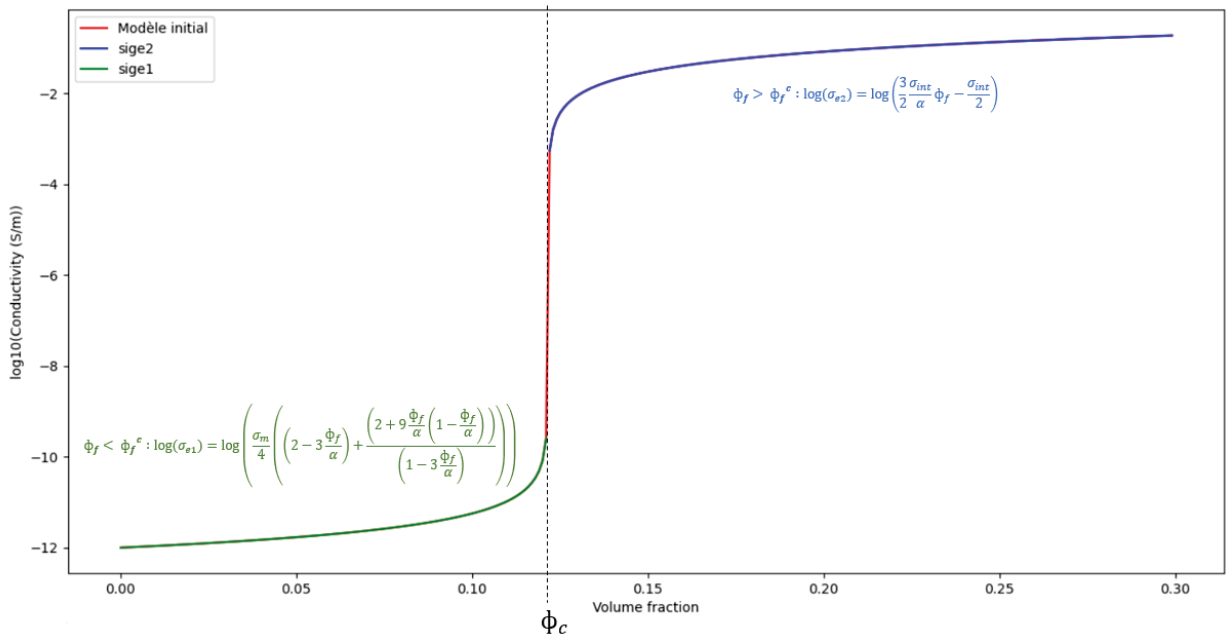


Figure 6.1: Comparison of the model by Mazaheri et al. . (Mazaheri et al., 2022) (in red) with the rewritten model (in blue and green)

6.1.3.2 Characterization of dispersion and agglomeration

The dispersion and agglomeration rates are shown in Table 6-1. The different parameters used for the comparison of the two matrices show that the dispersion of carbon black (CB) and the level of agglomeration are of the same order of magnitude for the composites studied.

More specifically, the results obtained indicate a dispersion rate of approximately 18% and an agglomeration rate of approximately 81% for the SEBS/CB and EVA/CB composites, which suggests a relatively similar distribution of conductive particles in both polymer matrices.

These results are consistent with the micrographs of the SEBS/CB and EVA/CB composites presented in articles 1 and 2, which highlight a heterogeneous dispersion of carbon black in both matrices at a mass fraction of 20%. The presence of CB agglomerates observed in these microstructures indicates that electrical conductivity in these nanocomposites is primarily associated with the formation of a conductive network consisting of aggregates and percolation pathways between the conductive particles.

Thus, despite partial dispersion of carbon black in the polymer matrix, agglomeration zones can contribute to the formation of continuous conductive paths, promoting the appearance of the electrical percolation threshold in these conductive polymer composites.

Table 6-1 Dispersion (D) and agglomeration (A) for SEBS-CB and EVA-CB composites

	SEBS-CB	EVA-CB
D	18%	18%
A	81%	81%

Ideally, the interphase thickness should be measured experimentally by atomic force microscopy (AFM) using a Veeco Nanoscope AFM V5.30 system equipped with a custom FM-AFM module, allowing for nanoscale characterization of the interfacial region between the polymer matrix and the reinforcing particles. However, due to experimental organization and time constraints within the scope of this doctoral project, this part of the study could not be completed.

Nevertheless, the approach proposed in this work highlights the importance of considering the interphase as a key parameter in analyzing the properties of conductive polymer nanocomposites. Future work could complement this study with experimental measurements of the interphase thickness to better understand the role of matrix/reinforcement interphase interactions on the electrical, mechanical, and thermal properties of nanocomposites. Such an analysis would contribute, in particular, to a better understanding of the mechanisms of conductive network formation and the influence of the interphase on the percolation threshold in these materials.

6.1.4 Conclusion

This study analyzed the influence of matrix/reinforcement interphase thickness on the electrical percolation threshold in EVA/CB and SEBS/CB-based conductive polymer nanocomposites. The results show that increasing the interphase thickness alters the interactions between the polymer matrix and the carbon black particles. This modification directly influences the effective distance between conductive charges and, consequently, the formation of conductive pathways responsible

for electrical conduction. A thicker interphase can promote the establishment of conductive contacts or tunneling mechanisms, thus contributing to a decrease in the percolation threshold.

These results highlight the importance of considering the interphase as a key parameter in the design of conductive nanocomposites. A better understanding and control of this interfacial region could optimize the electrical properties of materials while reducing the amount of conductive fillers required, which is a significant challenge for the development of conductive polymer composites for electronic and sensor applications.

Finally, future work could include more in-depth experimental investigations, including nanoscale characterization techniques and advanced modeling approaches, to better understand the physical mechanisms governing the influence of the interphase on electrical percolation in polymer nanocomposites.

6.2 Experimental setup and EEG signal acquisition

6.2.1 Objective

The aim of this section is to present the experimental setups developed to facilitate the acquisition of electroencephalographic (EEG) signals and to evaluate the performance of the conductive polymer electrodes developed within the framework of the work presented in this thesis. To this end, a comparison is made between a laboratory-designed acquisition system and a commercial system dedicated to EEG signal acquisition. This approach allows us to identify the most appropriate experimental conditions for the reliable recording of EEG signals and to optimize the acquisition method used for evaluating the developed electrodes.

6.2.2 Methodology

6.2.2.1 Laboratory designed EEG acquisition system

Initially, an EEG acquisition system was designed and assembled in the laboratory with the participation of an intern recruited for the project, under the supervision of the author of this thesis.

The setup was built on a prototyping board to explore different electronic configurations for amplifying electroencephalographic signals, the amplitude of which is generally on the order of a

few microvolts. The system is based on an analog amplification circuit, shown in Figure 6.2 below, whose architecture is inspired by a setup described in the literature by Svard et al. (Svard et al., 2010).

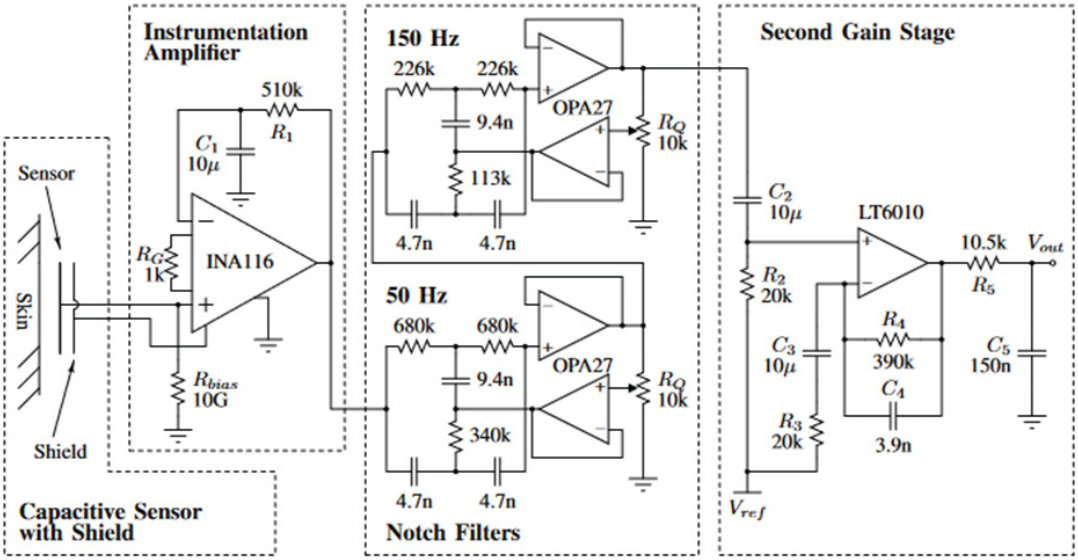


Figure 6.2**:** EEG amplification circuit used for the first experimental tests. Adapted from Svard et al., (Svard et al., 2010)

The decision to build the circuit on a prototyping board was quickly made, as this type of platform allows for quick and easy modifications to the electronic assembly. This approach is particularly advantageous during the exploratory phase of a project, where the circuit is not yet fully validated and may require several adjustments. Using a prototyping board thus facilitates the addition, replacement, or reconfiguration of electronic components to progressively optimize the circuit's performance.

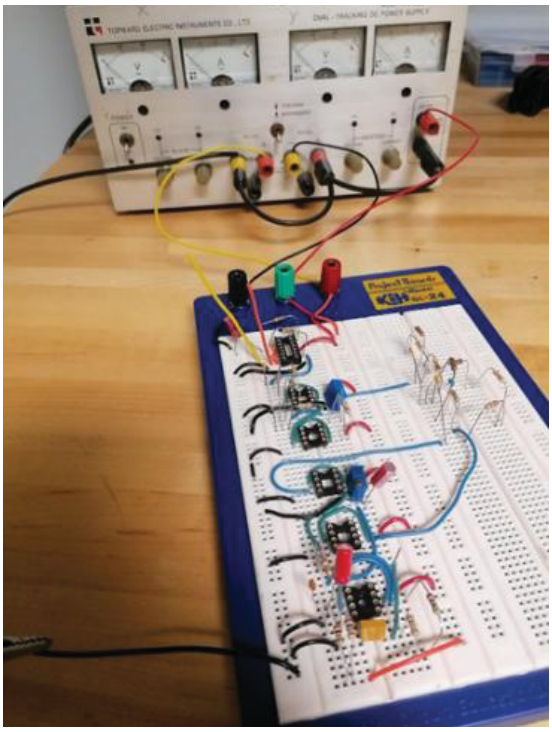


Figure 6.3 : Circuit on the prototype board

To perform the initial experimental measurements, a sensor capable of detecting electroencephalographic signals was required. An experimental electrode was therefore constructed using a 25-cent coin as a conductive support.

Initially, one face of the part was abrasive to facilitate soldering a conductive wire with tin, thus ensuring a stable electrical connection between the electrode and the acquisition circuit. Subsequently, the other face of the part was sanded to obtain the smoothest possible surface, in order to improve contact between the metal surface and the conductive polymer material used in this study, namely a thermoplastic urethane (TPU). Finally, the edges of the thermoplastic material were heated to allow for its permanent adhesion to the metal part, thus avoiding the use of adhesives such as tape. The resulting experimental electrode was then used for the initial signal acquisition tests.

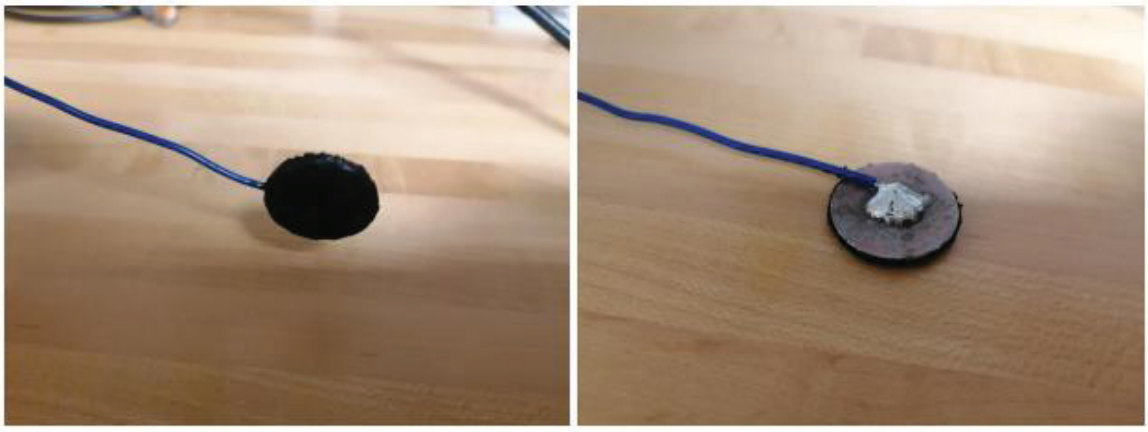


Figure 6.4: Experimental electrodes

6.2.2.2 Commercial EEG Acquisition System

The commercial EEG acquisition system used in this study is from the manufacturer OpenBCI and includes an OpenBCI Cyton Biosensing Board (8-Channel), a biopotential acquisition platform designed for recording physiological signals such as electroencephalography (EEG), electromyography (EMG), and electrocardiography (ECG). Data acquired by the board is transmitted to the computer via an OpenBCI USB dongle , enabling visualization and recording of the signals using the OpenBCI GUI software.



Figure 6.5: OpenBCI Cyton board its main electronic components.
Taken from (OpenBCI, s. d.-a)

The Cyton board uses the ADS1299 analog-to-digital converter, an integrated circuit developed by Texas Instruments and specifically designed for EEG applications and biopotential measurements. According to the technical documentation for this component, the input amplifier has an input impedance of approximately 500 MΩ–1 GΩ. Electrode placement on the scalp was performed using the OpenBCI EEG headset. The Ultracortex Mark IV EEG Headset is designed using the international 10–20 electrode positioning system. OpenBCI provides the STL and CAD design files for 3D printing this headset. This modular architecture allows for adapting the configuration and position of the electrodes to suit experimental needs. The Ultracortex Mark IV headset accommodates various types of EEG electrodes. In this study, the performance of the developed conductive polymer electrodes was compared to that of commercially available electrodes. The reference electrodes used were those from OpenBCI. ThinkPulse Active Electrode Kits are active electrodes that integrate a preamplifier directly at the electrode. The electrode-skin contact impedance was measured using the impedance check function built into the OpenBCI GUI software. This measurement involves injecting a low alternating current through the electrode and measuring the resulting voltage to estimate the electrode-skin contact impedance. This procedure allows for verification of the electrode-skin contact quality, identification of electrodes with excessively high impedance, and improvement of the quality of recorded EEG signals.

The EEG signals were acquired by connecting the electrodes to the differential analog inputs of the OpenBCI board. Cyton Biosensing Board . In this configuration, each channel measures the electrical potential difference between an active electrode and a reference electrode. The active electrodes correspond to the conductive polymer electrodes developed in articles 1 to 3 of this thesis, which are placed on the scalp.

The reference electrode is positioned on one ear, while an additional electrode, placed on the other ear, serves as a ground electrode. This configuration stabilizes the measurement and reduces the influence of interference. The recorded EEG signals are visualized in real time using the OpenBCI GUI software, which also allows for data logging and export for subsequent analysis. This experimental setup enables the evaluation of electrode-skin contact quality and the stability of the EEG signals obtained with the conductive polymer electrodes developed in this study.

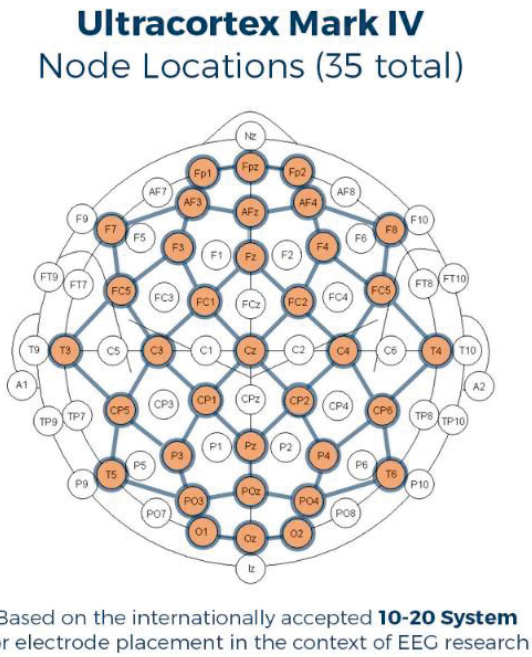


Figure 6.6**:** Configuration of electrode positions of the Ultracortex Mark IV helmet according to the international 10–20 system.

Taken from (OpenBCI, s. d.-d)



Figure 6.7**:** ThinkPulse active electrodes used as a reference.

Taken from (OpenBCI, s. d.-c)



Figure 6.8: Example of EEG signals visualized in OpenBCI GUI



Figure 6.9: Ultracortex “Mark IV” EEG headset

Taken from (OpenBCI, s. d.-d)

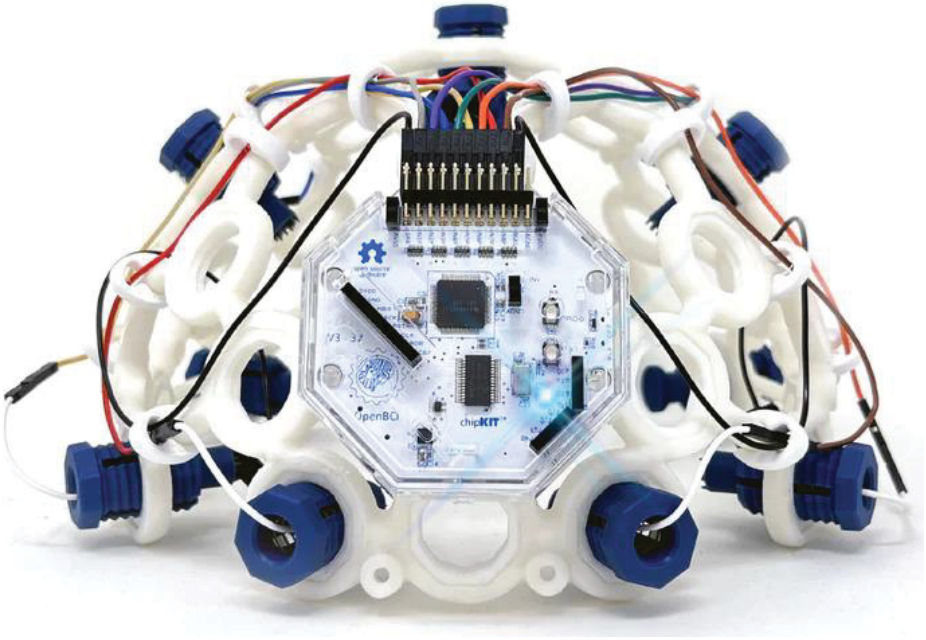


Figure 6.10: The complete Ultracortex EEG measurement system
Taken from (OpenBCI, s. d.-b)

6.2.3 Résultats

The signals obtained by touching the electrode of the laboratory-fabricated system with fingers were visualized using an oscilloscope to observe the circuit output. The measurements show that the output signal is highly noisy, making it difficult to distinguish between the signal generated by finger contact and the noise present in the system.

At this stage, the study of this setup was interrupted because the industrial partner involved in this part of the project did not wish to invest in manufacturing a new EEG measurement system. Nevertheless, the readings obtained show the presence of signal variations, which is an encouraging result. However, the significant amplitude of the observed noise makes it difficult to clearly identify the signal associated with finger contact.

Several factors can explain the presence of this noise in the experimental setup. In particular, the use of a breadboard for prototyping the circuit can introduce electrical interference and increase the system's sensitivity to environmental noise. Furthermore, the lack of electromagnetic shielding

and the high impedance of the skin/electrode interface can amplify the influence of external disturbances. Further work would require the use of a suitable data acquisition system, as well as the implementation of an appropriate filtering and shielding system, to allow for the recording and analysis of signals over time. The experimental result of the circuit, as observed using the oscilloscope, is shown in figure 6.11 below.

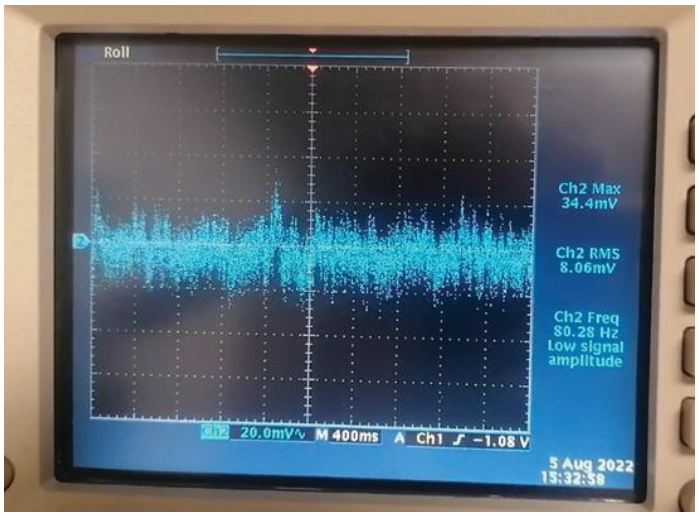


Figure 6.11: Signal measured at the output of the EEG amplification circuit observed on the oscilloscope

The experimental setup based on the commercial system enabled the stable acquisition of the EEG signals presented in Articles 1 to 3 of this thesis, as well as the measurement of the skin/electrode contact impedance and the comparison of the performance of polymer electrodes with that of commercial electrodes. The OpenBCI platform also offers great flexibility for integrating different electrode geometries, including the multi-tip electrodes developed in this work.

6.2.4 Conclusion

In this section, two experimental approaches for acquiring electroencephalographic signals were presented. First, a laboratory-designed EEG acquisition system was developed to explore different electronic configurations for amplifying EEG signals. Although this setup allowed observation of signal variations, the measurements obtained exhibited a high noise level, limiting the ability to clearly identify the signals of interest. These results highlight the challenges associated with

measuring very low- amplitude EEG signals and the need to use suitable acquisition systems, including appropriate filtering and shielding devices.

Subsequently, a commercial EEG acquisition system based on the OpenBCI platform was used to further the experimental evaluation of the conductive polymer electrodes developed in this thesis. This system enabled the stable acquisition of the EEG signals presented in articles 1 to 3, as well as the measurement of the electrode-skin contact impedance and the comparison of the performance of the polymer electrodes with that of the electrodes.

commercial. The OpenBCI platform also offers great flexibility for the integration of different electrode geometries, including the multi-tip electrodes developed in this work, making it a suitable tool for the study and evaluation of flexible EEG electrodes.

6.3 Work on the artificial ear for the evaluation of EEG electrodes

6.3.1 Objective

Skin/electrode impedance is a key parameter in EEG signal acquisition. This impedance can vary considerably from one individual to another depending on several physiological factors, including hair density, perspiration levels, skin hydration, and the intrinsic resistance of the skin tissue. These variations make systematic comparison of electrode performance difficult when measurements are taken directly on human subjects, as observed in the studies presented in Articles 1 to 3 of this thesis.

To provide a reproducible experimental environment for evaluating the performance of the electrodes developed in this work, a silicone artificial ear was designed and manufactured. Silicone was chosen as the base material due to its biocompatibility and widespread use in the medical field, particularly for the manufacture of implants and biomedical devices. The objective of this artificial model was to reproduce, as closely as possible, certain physical and electrical properties of human skin.

With this in mind, the material constituting the artificial ear was formulated to have a target electrical conductivity of around $4.4*10^{-1}$ S/m. This value was chosen as a reference since a

study report that the electrical conductivity of human skin is generally in this order of magnitude, although it can vary depending on physiological and environmental conditions.

The creation of such an artificial ear thus makes it possible to have a stable experimental model allowing: the evaluation of the performance of the EEG electrodes developed in this study; the measurement of the skin/electrode contact impedance under controlled conditions and the comparison of the performance of the conductive polymer electrodes with those of commercial electrodes.

The work carried out on this artificial ear includes the implementation of various manufacturing processes, including silicone polymerization, autoclave curing, and the exploration of other experimental methods aimed at controlling the electrical properties of the model.

Table 1 | Human head tissue resistivity and conductivity values.

Tissue	Mean Resistivity with lower/upper bounds (Ohm cm)	Mean Conductivity (S/cm)
Air Internal	50,000 (50,000 to 100,000)	2E-5
Air External	100,000	1E-6
Basal Ganglia	700	1.42E-3
Blood	160 (80 to 240)	6.25E-3
Brain White Matter	700 (350 to 1,050)	1.42E-3
Brain Gray Matter	300 (150 to 450)	3.334E-3
Cerebellum	650 (325 to 975)	1.54E-3
Cerebrospinal Fluid	65 (32.5 to 97.5)	1.54E-2
Corpus Callosum	834	1.199E-3
Dura	1,667 (1,000 to 5,000)	6E-4
Eye	200 (100 to 400)	5E-3
Fat	2,500 (1,250 to 5,000)	4E-4
Muscle	1,000 (200 to 1,800)	1E-3
Salivary Glands	576	1.74E-3
Scalp and Skin	230 (115 to 345)	4.35E-3
Skull Hard Bone	16,000 (8,000 to 40,000)	6.25E-5
Skull Soft Bone	2,500 (1,250 to 3,750)	4E-4
Soft Tissue	500 (250 to 750)	2E-3
Thalamus	112	8.93E-3

Mean values and lower and upper bounds of some of the tissues are included.

Figure 6.12: Electrical properties of head tissues
Taken from (Ramon et al., 2014)

6.3.2 Methodology

Two main approaches were investigated: mechanical mixing and sonication-assisted dispersion. Both fabrication processes were explored to evaluate their influence on reinforcement dispersion

and the final material properties. The mixtures were made using PDMS as the polymer matrix, reinforced with carbon black (CB) and, in some exploratory tests, with carbon fiber. The carbon black used is identical to that employed in the work presented in Articles 1 to 3 of this thesis. For the PDMS/CB mixtures, two reinforcement mass fractions, 20% and 25%, were selected for composite fabrication. This choice is based on the results obtained in Articles 1 to 3, which show that these concentrations allow the electrical percolation threshold to be reached and electrically conductive nanocomposites to be obtained.

6.3.2.1 PDMS (RTV/615) and carbon black

1- Mechanical mixture

In the case of mechanical mixing, PDMS and carbon black were mixed using a mechanical mixer to ensure the reinforcement was incorporated into the polymer matrix. After homogenization, the mixtures were poured into molds and then subjected to a thermal curing step. To assess the influence of the manufacturing process on the quality of the resulting composite, some preparations were made without an autoclave, while others were cured in an autoclave. This comparison aimed to determine the effect of the pressure and temperature applied in the autoclave on the dispersion of the reinforcement and the final properties of the material.

2- Dispersion by sonication

For the sonicated mixtures, a modified procedure was implemented to improve the dispersion of carbon black within the polymer matrix. Since PDMS does not dissolve in toluene and consists of two liquid components (base and crosslinking agent), an intermediate step involving solvent dispersion of the reinforcement was performed. First, the carbon black was dispersed in toluene and then sonicated to reduce agglomeration and improve dispersion homogeneity. The two PDMS components were then incorporated into the carbon black suspension to form the composite. After toluene evaporation, the resulting mixture was placed in an oven for PDMS crosslinking. Autoclaving was not feasible in this case, as the toluene would have damaged the device's rubber seals. This approach aimed to promote a more uniform distribution of the conductive

reinforcement within the polymer matrix before PDMS crosslinking, in order to improve the formation of the conductive network within the composite.

6.3.2.2 Carbon fiber reinforced PDMS (RTV 615)

For the fabrication of carbon fiber reinforced (CF) PDMS composites, three manufacturing processes inspired by the literature were explored to evaluate the influence of the mixing method on fiber dispersion within the polymer matrix and on the final properties of the composite. The objective of this comparative approach was to identify a manufacturing method that would achieve homogeneous dispersion of carbon fibers within the PDMS matrix, an essential condition for ensuring the formation of efficient conductive pathways and improving the electrical properties of the material.

1- Method 1: Mechanical mixing with autoclave cooking

The first method is based on the process described in the literature (Wei et al., 2020). . In this approach, PDMS and carbon fibers are mixed using a mechanical mixer to ensure the reinforcement is incorporated into the polymer matrix. In the original procedure, a vacuum degassing step is performed after mixing to remove air bubbles trapped in the composite. In this work, this step was replaced by autoclave curing, as the pressure and temperature conditions applied in the autoclave also promote the removal of air bubbles and improve material compaction.

Figure 6.13 presents the initial method described in the literature, while Figure 6.14 illustrates the modified procedure used in this work, including the use of the autoclave and the absence of a degassing step.

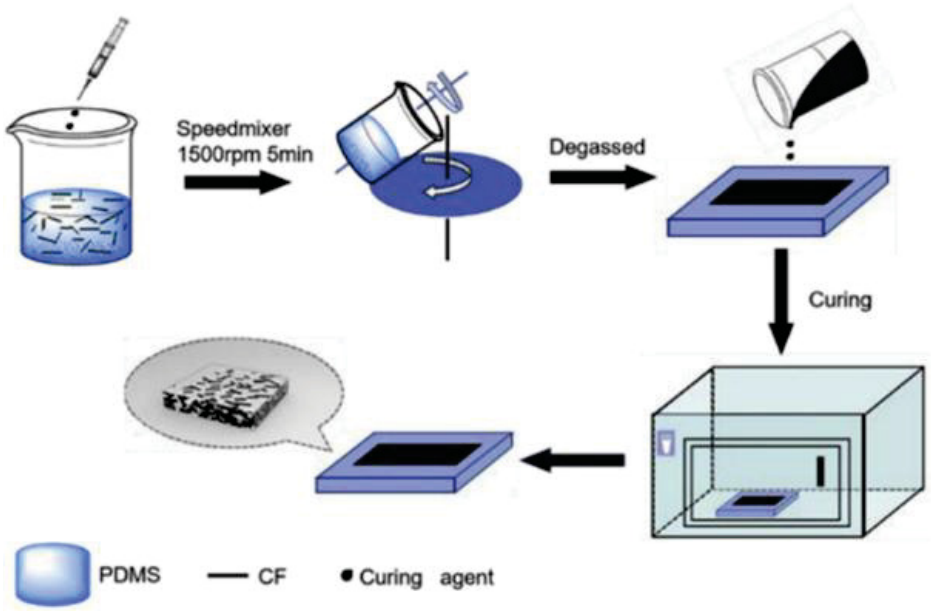


Figure 6.13: Initial method decribed in the litterature
Taken from (Wei et al., 2020)

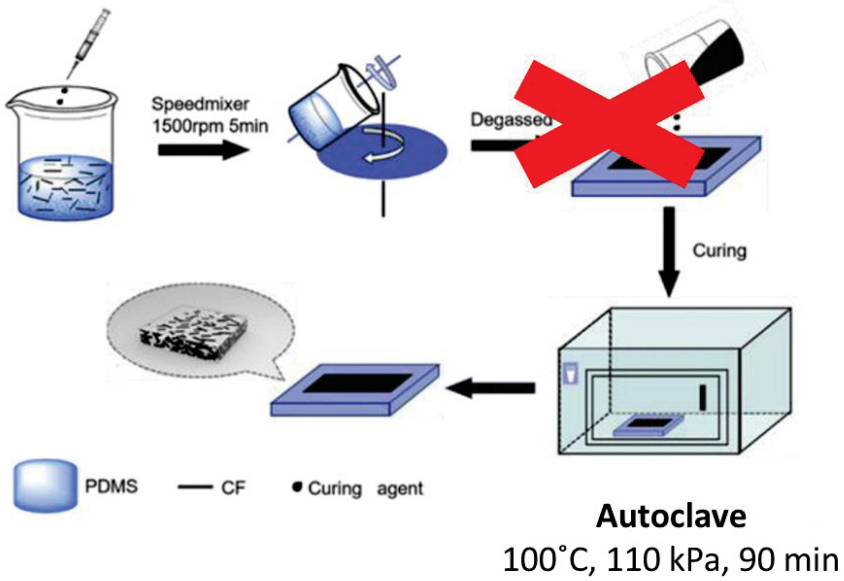


Figure 6.14: Modified procedure used in this work
Adapted from (Wei et al., 2020)

1- **Method 2:** Prolonged manual mixing

The second method is inspired by the process described in the study of Khosla et al (Khosla et al., 2018). In this case, the PDMS and carbon fibers were manually mixed for approximately 30 minutes to promote fiber dispersion within the polymer matrix. This approach relies on prolonged mixing to limit the formation of fiber agglomerates and improve their distribution within the composite.

2- **Method 3:** Rapid manual mixing

The third method is based on the process proposed in the study of Bensalah et al., (Bensalah et al., 2021). In this approach, the PDMS and carbon fibers are mixed manually for approximately 10 minutes, followed by molding and crosslinking of the composite. This method aims to simplify the manufacturing process while allowing the reinforcement to be incorporated into the polymer matrix. The different manufacturing processes presented above were then evaluated to analyze their influence on carbon fiber dispersion, the composite structure, and its electrical properties. The results obtained are presented in the following section.

6.3.3 Results

6.3.3.1 PDMS (RTV/615) and carbon black

The measurement of the real part of the complex conductivity as a function of frequency is shown in Figure 6.15. The results show a significant difference between the composites manufactured by sonication and those obtained by mechanical mixing.

The sonicated RTV615/20% CB composites exhibit relatively high and stable electrical conductivity across the entire frequency range studied. This behavior is characteristic of materials above the percolation threshold, where a continuous conductive network is formed within the polymer matrix. In contrast, the mechanically blended composites exhibit significantly lower conductivity values and a more pronounced frequency dependence. This behavior is typical of a semi-insulating material, indicating that the dispersion of carbon black within the PDMS matrix remains insufficient to allow the formation of an efficient conductive network. Even with a higher mass fraction of 25% carbon black, the mechanically blended composites do not exhibit

conductivity comparable to that obtained by sonication. This result suggests that the quality of the conductive reinforcement dispersion plays a crucial role in the formation of the conductive network, sometimes even more so than increasing the reinforcement mass fraction.

These observations confirm that sonication is a more efficient method for dispersing carbon black in the PDMS matrix, thereby promoting the formation of conductive pathways and improving the electrical properties of the composite.

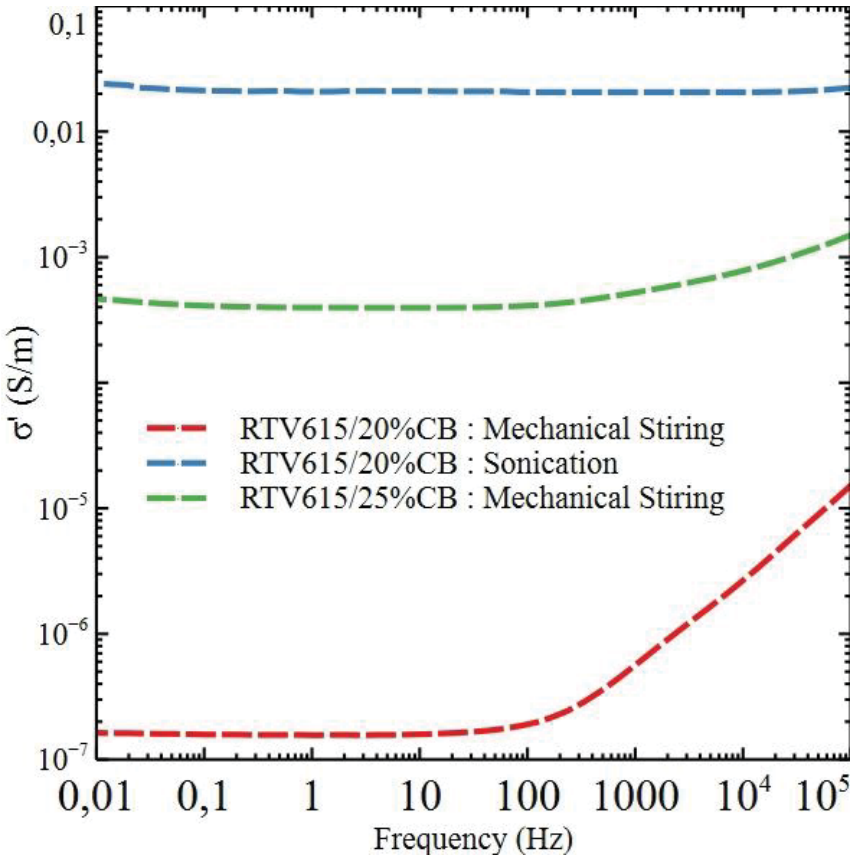


Figure 6.15: Real part of the complex conductivity as a function of frequency for RTV615/CB composites manufactured according to different dispersion processes: mechanical mixing and sonication.

The images presented in Tables 6.2 and 6.3 show, respectively, the electrical resistance measurements taken with a multimeter on different areas of the mechanically blended RTV615/20% CB and RTV615/25% CB composites. The measurements were taken on the top, bottom, and side of each sample.

The results indicate that the electrical resistance is not uniform across the entire surface of the composite. The resistance measured on the underside of the sample is higher than that measured on the sides, while the measurement taken on the top side shows a very high value (OL – Over Limit), indicating a resistance outside the multimeter's measurement range.

This spatial variation in strength suggests a non-homogeneous distribution of carbon black within the PDMS matrix, likely due to limitations in the mechanical mixing process used during composite manufacturing. Insufficient dispersion of the conductive reinforcement can lead to the formation of locally deficient areas of conductive particles, thus preventing the formation of a continuous conductive network within the material.

Furthermore, the use of an autoclave in the manufacturing process reduced the presence of air bubbles on the surface of the samples, which tended to solidify during PDMS crosslinking. This observation highlights the improvement brought about by the introduction of the autoclave in the manufacturing process, particularly in terms of the quality and homogeneity of the samples obtained.

These observations are consistent with the electrical conductivity results as a function of frequency shown in Figure 6.15, where the composites made by mechanical mixing exhibit behavior characteristic of a semi-insulating material, indicating that the percolation threshold is not reached homogeneously throughout the material.

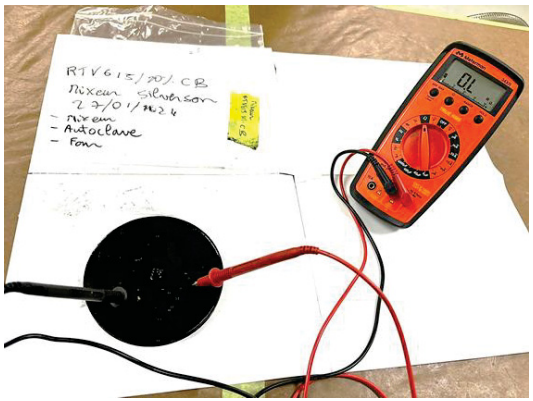
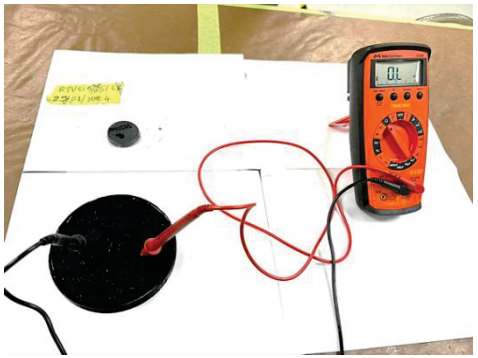
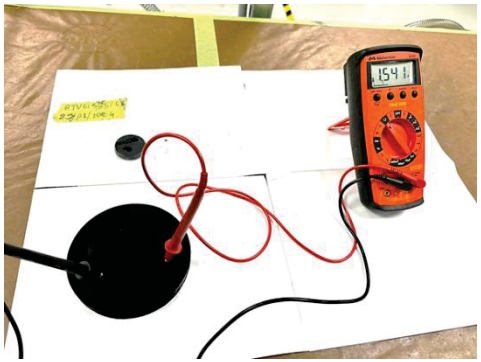
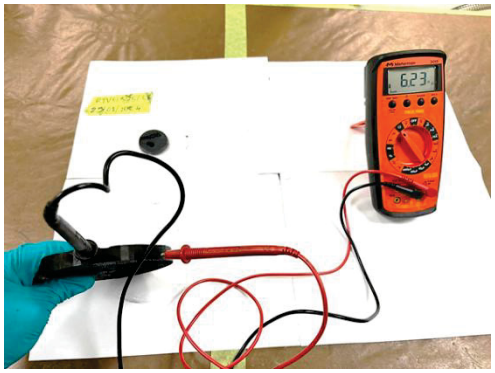
Table 6-2 Mechanical blending (RTV615/20%CB)		
		
On the top face	On the bottom face	On the side

Table 6-3 Mechanical blend (RTV615/25%CB)

		
On the top face	On the bottom face	On the side
		
In the autoclave	Without autoclave	

The images presented in Table 6.4 show electrical resistance measurements taken with a multimeter on different areas of the RTV615/20%CB composite produced by sonication dispersion. The measurements were taken on the top, bottom, and side surfaces of the sample.

The results show that sonication allows for the measurement of electrical resistance across all surfaces of the composite, unlike samples produced by mechanical mixing, where some areas exhibit resistance outside the multimeter's measurement range. However, the measured values vary from one surface to another, indicating that the carbon black distribution within the PDMS matrix, while improved, remains partially heterogeneous.

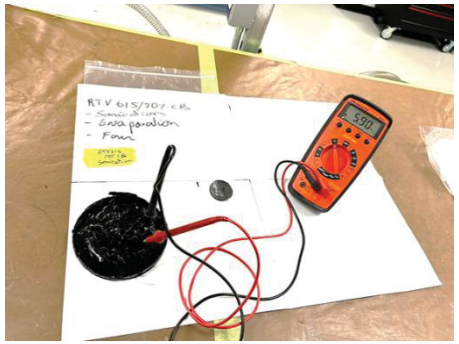
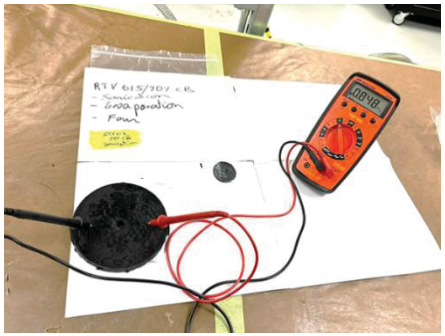
This improvement in electrical conductivity is consistent with the conductivity-frequency results shown in Figure 6.15, where the sonicated composites exhibit significantly higher conductivity values than those obtained by mechanical mixing. These observations suggest that sonication promotes better dispersion of the carbon black particles, thus facilitating the formation of a more efficient conductive network within the polymer matrix.

However, two problems were observed after the silicone cured. First, cracks were observed on the surface of the samples. These cracks appear to be related to the evaporation of the solvent (toluene) used to disperse the carbon black, which can lead to the formation of internal stresses in the material during PDMS crosslinking.

Secondly, it was observed that toluene attacks the PETG mold used for shaping the samples. This phenomenon leads to mold degradation and can affect the surface quality of the resulting composite. To avoid this problem, the use of glass or metal molds would be more appropriate for this type of process involving organic solvents.

These observations highlight that, despite the improved dispersion of the conductive reinforcement achieved through sonication, optimization of the manufacturing process remains necessary, particularly to prevent crack formation and obtain a more uniform composite surface.

Table 6-4 Sonication dispersion of RTV/615 and carbon black (RTV615/20%CB)

		
On the top face	On the bottom face	On the side
		

6.3.3.2 Carbon fiber reinforced PDMS (RTV 615)

The real part of the electrical conductivity as a function of frequency of the RTV615/8%CF composites obtained according to the three manufacturing methods described above is shown in figure 6.16.

The results show that the three composites exhibit electrically conductive behavior across the entire frequency range studied. Electrical conductivity remains relatively stable with frequency, which is characteristic of materials in which a continuous conductive network is formed within the polymer matrix.

A comparison of the different manufacturing methods indicates that the composite prepared by manual mixing for 10 minutes (Method 3) exhibits the highest conductivity values. The composite obtained by mechanical mixing (Method 1) has a slightly lower conductivity, while the one prepared by manual mixing for 30 minutes (Method 2) has the lowest conductivity values among the three processes studied.

However, the conductivity values measured for the three composites remain of the same order of magnitude, approximately 1 S/m. These results suggest that, for a mass fraction of 8% carbon fibers, the three manufacturing methods allow the formation of an efficient conductive network in the PDMS matrix.

The images of the samples presented in table 6.5 illustrate the macroscopic appearance of the composites obtained by each of the manufacturing methods.

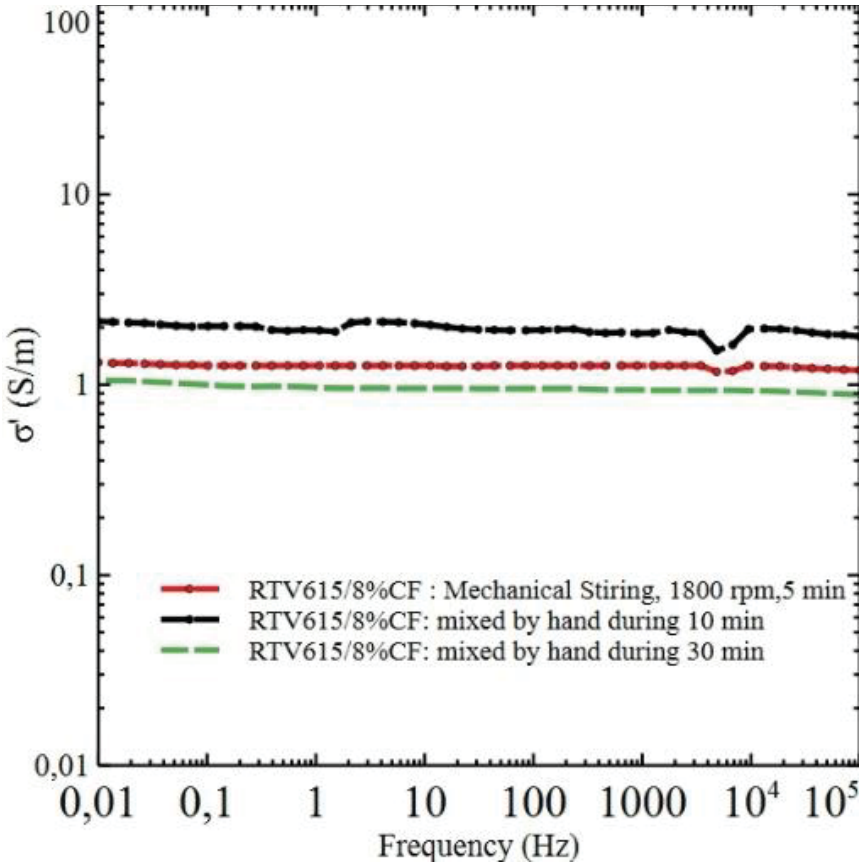


Figure 6.16**:** Real part of the complex electrical conductivity as a function of frequency for RTV615/8 % CF composites obtained according to different manufacturing processes.

Photographs of the composites presented in table 6.5, obtained using the three manufacturing methods, show notable differences in the macroscopic appearance of the samples. Although Method 3 results in relatively high electrical conductivity values, the physical appearance of the composites manufactured using Methods 2 and 3 remains less satisfactory. Indeed, visual observations indicate that the carbon fibers are not properly impregnated by the silicone matrix, leading to an irregular surface and a non-uniform distribution of the reinforcement within the material. Fiber impregnation directly influences the electrical conductivity of the composite. Good impregnation of the fibers by the polymer matrix promotes efficient contact between the conductive fibers, thus facilitating the formation of a continuous conductive network within the material. Conversely, insufficient impregnation can lead to areas rich or poor in fibers, limiting fiber-to-fiber contact and thereby reducing the efficiency of the conductive pathways

within the composite. In contrast, the composites obtained using method 1 exhibit better silicone fiber impregnation and a more homogeneous surface. These observations suggest that this method allows for better incorporation of carbon fibers into the polymer matrix, thus promoting a more uniform composite structure.

Based on the measured electrical conductivity and surface condition of the samples, Method 1 was selected for the subsequent work, particularly for studying the percolation threshold. Furthermore, this process will be optimized by using an autoclave to reduce the size of bubbles present in the composite and improve the surface quality of the samples, resulting in a more uniform and homogeneous surface.

Table 6-5 Composite made with RTV615/8wt%CF

		
Method 1	Method 2	Method 3

6.3.3.3 Percolation study of RTV615/carbon fiber composites

The percolation study carried out using RTV615/CF composites manufactured according to the modified method 1, in which the degassing step was replaced by autoclave curing, is presented in Figure 6.17. This figure shows the evolution of electrical conductivity as a function of the mass fraction of carbon fibers.

The results indicate a significant increase in electrical conductivity as the carbon fiber mass fraction increases. Analysis of the curve reveals that the percolation threshold is around approximately 1.5% carbon fiber mass fraction. Above this critical concentration, a continuous

conductive network begins to form within the PDMS matrix, leading to a rapid increase in electrical conductivity. Beyond this transition zone, the conductivity continues to increase with fiber concentration until it reaches a plateau around 6% mass fraction, at which point the electrical conductivity reaches approximately 1 S/m. In this study, the target conductivity for fabricating the artificial skin model is approximately 4.4×10^{-1} S /m. Based on the results obtained, this value corresponds to a carbon fiber mass fraction between 3% and 3.5%. These results thus allow us to identify the optimal carbon fiber concentration range for achieving the desired electrical properties for simulating the skin's electrical properties.

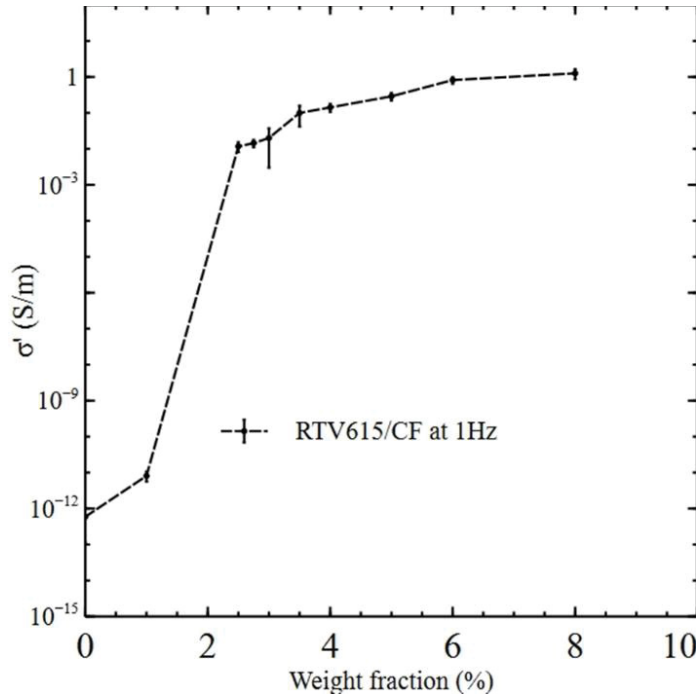


Figure 6.17**:** Real part of the complex electrical conductivity measured at 1 Hz as a function of the mass fraction of carbon fibers for RTV615/CF composites manufactured according to modified method 1 with autoclave.

Photographs of the composites and the disc-shaped artificial ear, shown in Tables 6.6 to 6.8, show that the samples obtained exhibit a uniform geometry and a relatively homogeneous dispersion of carbon fibers in the silicone matrix.

Macroscopic observations also indicate that the surface appearance of composites is improved when the manufacturing process includes the use of an autoclave. Indeed, samples obtained

using this method exhibit a more homogeneous final appearance and a more uniform surface than those manufactured without the use of an autoclave.

These results suggest that the use of the autoclave helps to improve the quality of fiber impregnation in the PDMS matrix, while reducing the presence of air bubbles and surface defects, resulting in composites with better morphological characteristics.

Table 6-6 Artificial ear made with RTV615/3%wtCF

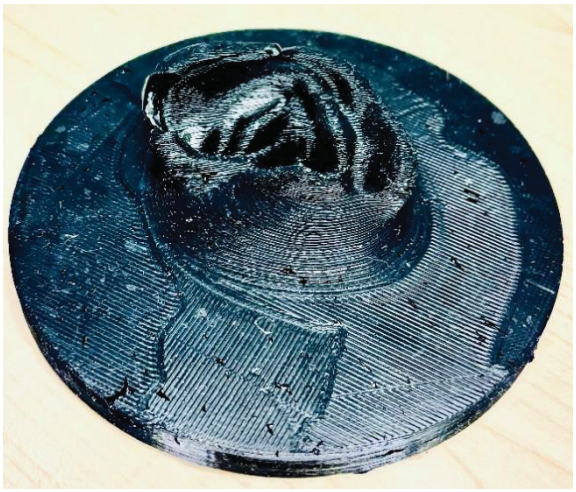
	

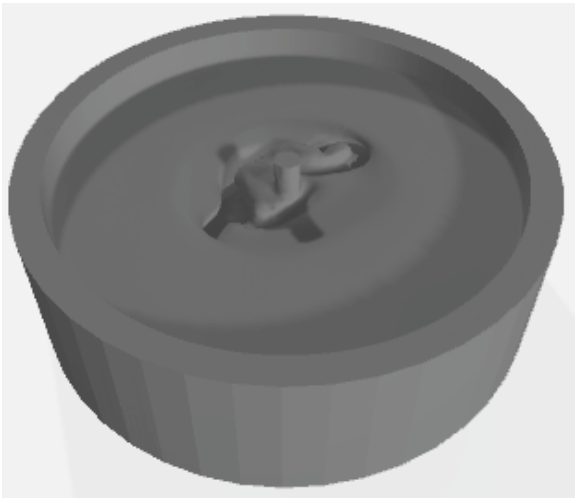
Table 6-7 Artificial ear made with 3.5wt%CF

	
Top view	Bottom view

Table 6-8 Artificial ear made with 4wt%CF	
	
Top view	Bottom view

Figure 6.18 shows, on the one hand, the image of the silicone ear containing 3.5% carbon fibers and, on the other hand, the 3D representation of the mold used for the manufacture of the artificial ear.





a) b)

Figure 6.18 : (a) Artificial ear made of silicone filled with 3.5% carbon fibers obtained after fabrication; (b) 3D model of the mold used for the production of the artificial ear.

6.3.4 Conclusion

The exploratory work carried out in this study made it possible to evaluate different approaches to manufacturing conductive composites based on PDMS reinforced with carbon black and carbon fibers, with the aim of developing a material suitable for the manufacture of an artificial ear intended for the evaluation of EEG electrodes.

The results obtained show that the dispersion method of the conductive reinforcement plays a crucial role in the electrical properties of composites. In the case of PDMS/CB composites, the use of sonication improves the dispersion of conductive particles and significantly increases electrical conductivity compared to mechanical mixing. However, the use of solvents such as toluene presents certain challenges related to solvent evaporation, which can lead to cracking in the samples.

For PDMS/CF composites, the various manufacturing methods studied yield electrically conductive materials with conductivities on the order of 1 S/m. Macroscopic analysis of the samples and electrical measurements showed that method 1, combined with the use of an autoclave, offers the best compromise between electrical conductivity, homogeneity of fiber dispersion, and surface quality of the samples.

The percolation study conducted with RTV615/CF composites identified a percolation threshold of approximately 1.5% by mass fraction of carbon fibers, while a conductivity plateau of approximately 1 S/m is reached for concentrations above 6%. For the intended application, a target conductivity of approximately 4.4×10^{-1} S /m was selected, corresponding to a mass fraction of carbon fibers between 3% and 3.5%.

Furthermore, the use of the autoclave in the manufacturing process has proven beneficial in improving the quality of composites, notably by reducing the presence of air bubbles and enabling the production of samples with more uniform geometry and better surface homogeneity.

These results enabled the identification of optimal manufacturing conditions for the conductive artificial ear, which can be used as an experimental platform for evaluating the EEG electrodes developed in this thesis. However, a significant challenge remains: verifying the uniformity of

electrical conductivity across the entire surface of the material to prevent local variations in conductivity from causing differences in EEG measurements depending on the area of contact with the electrode.

6.4 Electrodes manufactured by 3D printing

6.4.1 Objective

The objective of this exploratory study is to evaluate the potential of 3D printing manufacturing processes for the production of electrodes. This approach primarily aims to reduce manufacturing time and lower the costs associated with the production of the metal molds used in articles 1 to 3 of this thesis.

In this context, 3D printing is being explored as an alternative solution for manufacturing polymer molds that could replace conventional metal molds. The use of printed polymer molds could thus facilitate the rapid fabrication of electrode prototypes, while offering greater flexibility in geometry design and a significant reduction in manufacturing costs.

6.4.2 Methodology

Different electrode geometries were designed and manufactured using additive manufacturing processes. Initially, electrodes were printed directly from a commercially available carbon black-filled thermoplastic polyurethane (TPU/CB) conductive filament. This approach aimed to evaluate the feasibility of directly manufacturing conductive electrodes using 3D printing, as well as the quality of the resulting structures.

Furthermore, several polymer molds were designed and manufactured using 3D printing to explore their use in molding conductive polymer composites. These molds were made from different printing materials to evaluate their thermal and mechanical resistance during the molding process. The materials studied included High Temp resin, Rigid 10K resin, and nylon.

In addition, SEBS-based polymer filaments were manufactured from pellets using a 3devo Filament Maker extruder. This step aimed to produce filaments compatible with 3D printing

processes, in order to explore the fabrication of flexible polymer structures suitable for EEG electrode applications.

6.4.3 Résultats

Figure 2.18 shows multi-tip electrodes manufactured by direct 3D printing from a commercial carbon black-filled TPU-based conductive filament (TPU/CB). These electrodes were produced using a 3D printer employing an additive manufacturing process.

Macroscopic observations show that the surface quality of the obtained electrodes remains limited. Indeed, since TPU is a thermoplastic elastomer sensitive to moisture, the presence of moisture in the filament can lead to defects during printing, such as surface irregularities and uneven material extrusion. As can be seen in the figure, the surface of the electrodes thus exhibits a non-uniform morphology characterized by striations and deposition defects between the printed layers.

Furthermore, the adhesion between the different layers deposited during printing appears relatively weak. This low interlayer cohesion results in limited mechanical strength of the multi-tip structures, meaning the microstructures can be easily damaged or torn off. In some cases, the tips can even spontaneously detach from the electrode base.

These results show that, although additive manufacturing allows for the rapid production of complex electrode geometries, significant challenges remain in terms of print quality and mechanical properties. Further work will therefore be needed to optimize printing parameters, filament drying, and material formulation to improve the robustness of 3D-printed electrodes.

Thus, although promising for rapid prototyping, additive manufacturing still requires further development before it can replace the compression manufacturing process used for the electrodes presented in articles 1 to 3 of this thesis, which currently offers better structural quality and greater reliability.



Figure 6.19**:** Multipin electrodes fabricated by direct 3D printing from a commercially available carbon black 19- filled thermoplastic polyurethane (TPU/CB) conductive filament. The electrodes were produced using an additive manufacturing process. Surface irregularities and limited interlayer adhesion are observed, resulting in low mechanical robustness of the multi-tip microstructures.

Figure 6.20 shows polymer molds manufactured by additive manufacturing. The first molds made of nylon exhibited significant limitations when used in the molding process.



a) b) c)

Figure 6.20: Polymer molds manufactured by additive manufacturing from different printing materials (a) Nylon, b) High Temp resin and c) Rigid 10K resin) with the aim of exploring their use for compression molding of conductive polymer electrodes.

Indeed, when these molds were used in a hot press, they showed significant thermal deformation, accompanied by partial melting of the material (see figure 6.21).



Figure 6.21**:** Thermal deformation and partial melting observed on additively printed nylon molds after use in a heat press during the compression molding process

These observations indicate that the thermal and mechanical resistance of the printed nylon is insufficient to withstand the temperature and pressure conditions applied during the compression process used to manufacture the electrodes. Due to these limitations, the nylon molds were abandoned for further work.

Furthermore, molds made from photopolymer resins also presented certain limitations. Although they offered better dimensional stability at room temperature, these molds proved relatively fragile and brittle, leading to cracking when pressure was applied during the molding process. These results show that, despite the advantages of additive manufacturing for the rapid production of molds, the thermomechanical properties of printed polymeric materials remain insufficient to replace the metal molds used in Articles 1 to 3 of this thesis.

Figure 6.22 shows the SEBS granules used as raw material for filament manufacturing. Figure 6.23 shows the 3devo Filament Maker machine used for extruding the polymer filaments. Figure 6.24 illustrates the SEBS filament extrusion process from the granules. Finally, Figure 2.25 shows the SEBS filaments obtained after extrusion.



Figure 6.22**:** SEBS (styrene-ethylene-butylene-styrene) granules used as a raw material for the manufacture of filaments for 3D printing.



Figure 6.23**:** 3devo Filament Maker machine used for extruding polymer filaments from thermoplastic granules.

Taken from (3devo B. V., s. d.)



Figure 6.24**:** Internal view of the 3devo Filament Maker machine showing the polymer filament extrusion process from SEBS granules.



Figure 6.25**:** SEBS filaments obtained after extrusion from granules using the 3devo Filament Maker machine, intended for use in 3D printing processes.

Table 6.9 shows the printing parameters used for filament manufacturing.

Table 6-9 SEBS-MA parameters on the filament maker		
Heater 1	220˚C	230˚C
Heater 2	220˚C	240˚C
Heater 3	220˚C	240˚C
Heater 4	220˚C	230˚C
Extruder speed	4 RPM	4 RPM
Filament fan speed	30%	50%
Manual speed	1400	1400
Filament diameter	2.5 mm	2.5 mm
Spooling speed	-	4 RPM

In their current state, the filaments produced do not yet have a uniform and smooth surface, and their diameter remains relatively irregular. Further work would therefore be necessary to optimize the extrusion conditions and obtain filaments with a stable diameter compatible with commercial 3D printers.

Within the scope of this thesis, this exploratory work was not pursued further, as it deviated from the main objective of the study. Nevertheless, this approach presents interesting potential for future research. Indeed, by manufacturing conductive composites through polymer dissolution in a solvent followed by the incorporation of conductive fillers, it would be possible to produce volume-homogeneous conductive composite filaments.

These filaments could then be used directly in additive manufacturing processes, thus avoiding the use of compression molding, which requires the fabrication of metal or polymer molds. Such an approach would potentially simplify the electrode manufacturing process, reduce

manufacturing time, and lower the costs associated with the production of next-generation EEG electrodes.

6.4.4 Conclusion

The exploratory work carried out in this study evaluated the potential of additive manufacturing and polymer filament extrusion for the fabrication of EEG electrodes and molds for compression molding. Direct 3D printing of electrodes from a commercially available carbon black-filled TPU-based conductive filament (TPU/CB) demonstrated the feasibility of manufacturing complex geometries, including multi-tip electrodes. However, observations revealed certain limitations, including insufficient interlayer adhesion, a non-uniform surface, and limited mechanical strength of the microstructures, which compromise the robustness of the resulting electrodes.

Furthermore, the use of 3D-printed polymer molds was also explored as an alternative to the metal molds used in Articles 1 to 3 of this thesis. Nylon molds exhibited thermal deformation and partial melting when used in a hot press, while molds made from photopolymer resins proved relatively brittle and prone to cracking under pressure. These results indicate that the thermomechanical properties of 3D-printed polymer materials remain insufficient to replace metal molds in the compression molding process used in this study.

Finally, the extrusion of SEBS filaments from granules using the 3devo Filament Maker demonstrated the feasibility of producing polymer filaments for 3D printing. However, the resulting filaments still exhibit surface and diameter irregularities, which currently limits their use on commercial 3D printers. Further work is needed to optimize the extrusion parameters and improve the quality of the filaments produced.

Thus, although additive manufacturing approaches show promising potential for the rapid and flexible production of electrodes, the results obtained in this exploratory work demonstrate that compression molding using metal molds remains the most reliable method for manufacturing the electrodes studied in this thesis. Nevertheless, the approaches explored open up interesting prospects for the future development of additive manufacturing processes for conductive

composites, which could ultimately simplify the fabrication of EEG electrodes and reduce their associated production costs.

6.5 General conclusion

The exploratory work carried out within the framework of this thesis has made it possible to examine several complementary approaches aimed at improving the design, manufacture and evaluation of conductive polymer EEG electrodes.

The results obtained initially allowed for the exploration of developing conductive composites based on PDMS reinforced with carbon black and carbon fibers for the fabrication of an artificial ear designed to simulate the electrode-skin interface. This work highlighted the significant influence of conductive charge dispersion methods on the electrical properties of the composites. It also demonstrated that certain manufacturing methods can achieve sufficient electrical conductivities to consider using these materials in simulation devices for EEG electrode testing.

Furthermore, the implementation of an experimental EEG acquisition setup allowed for testing the developed electrodes and evaluating the limitations associated with the electronic systems used. The experimental observations highlighted the importance of shielding, signal filtering, and the use of appropriate acquisition systems to obtain stable and reliable EEG measurements.

Research on the fabrication of conductive filaments for 3D printing has also explored a promising avenue for the rapid and flexible production of polymer electrodes. Although the resulting filaments do not yet exhibit sufficient surface quality and uniformity for direct use on commercial 3D printers, these results suggest that 3D printing could be an attractive approach for reducing manufacturing steps, eliminating the use of metal molds, and lowering the production costs of EEG electrodes.

Finally, exploratory analyses of interphase and conductive charge agglomeration highlight the importance of microstructural phenomena in the formation of the conductive network within polymer nanocomposites. These aspects represent relevant avenues of research for a better understanding of the mechanisms governing the percolation threshold and the electrical properties of conductive composites.

Overall, this exploratory work complements the results obtained in the scientific articles of this thesis by providing insights into the materials, manufacturing processes, and experimental systems associated with polymer EEG electrodes. It also opens up several avenues for future research, particularly in the development of biomimetic devices for electrode evaluation, the optimization of 3D printing manufacturing processes, and the in-depth study of interfacial interactions in conductive nanocomposites.

.

RECOMMENDATIONS

This thesis investigated the development of flexible dry EEG electrodes through an integrated material–electrode–application approach, to address key limitations of conventional gel-based EEG systems in terms of comfort, stability, and suitability for long-term and wearable applications. By combining conductive thermoplastic polymers with carbon-based fillers and systematically evaluating their electrical, mechanical, and thermo-mechanical behavior, this work demonstrates that electrode performance emerges from a complex interplay between material formulation, electrode geometry, and the electrode–skin interface.

Across the three studies, the results highlight that achieving reliable EEG acquisition without conductive gel is not solely a matter of maximizing electrical conductivity, but rather of carefully balancing conductivity, mechanical compliance, and interfacial stability. The findings collectively challenge the conventional assumption that higher filler loadings or stiffer materials necessarily lead to better EEG performance, and instead show that optimized composite design can yield low contact impedance while preserving flexibility and user comfort. Together, these results contribute to a more nuanced understanding of how material structure and electrode design govern EEG signal quality under realistic usage conditions.

Material design and structure–property relationships

The first study demonstrated that flexible polymer composites based on SEBS and EVA, filled with carbon black or carbon nanotubes, can be engineered to achieve electrical conductivity levels suitable for dry EEG applications while maintaining mechanical compliance. Systematic characterizations of electrical, mechanical, thermal, and morphological properties revealed clear structure–property relationships, highlighting the trade-offs between filler type, filler loading, flexibility, and conductivity. These results demonstrate that bulk conductive composites offer a robust alternative to coated electrodes, thereby mitigating issues related to coating delamination and long-term durability.

Electrode architecture and functional performance

The second study showed that electrode-level performance is strongly influenced not only by material composition but also by electrode geometry. By comparing SEBS/CB and SEBS/CNT

composites in flexible multipin electrode architectures, this work demonstrated that multipoint contact improves scalp conformity and reduces contact impedance under realistic pressure conditions. The results further emphasized that different conductive fillers induce distinct mechanical and thermo-mechanical responses, reinforcing the importance of jointly optimizing material formulation and electrode design rather than treating these aspects independently.

Hybrid conductive networks and EEG validation

The third study highlighted the potential of hybrid CNT/CB conductive networks within SEBS and SEBS-MA matrices to overcome limitations of single-filler systems. By leveraging the complementary roles of CNTs and CB, hybrid nanocomposites achieved low contact impedance at reduced total filler loadings while maintaining mechanical flexibility comparable to that of the unfilled polymer. In vivo EEG recordings demonstrated stable signal acquisition and clear detection of brain activity, with performance comparable to or exceeding that of commercial dry electrodes. These findings confirm that hybrid conductive architectures provide an effective strategy for balancing electrical performance and comfort in flexible EEG electrodes.

Toward flexible, comfortable, and ecologically valid EEG systems

Taken together, the three studies underscore several overarching themes relevant to next-generation EEG technology.

First, material compliance is a core functional requirement, not a secondary consideration, for ensuring stable electrode–skin contact during prolonged recordings.

Second, nonlinear trade-offs between conductivity, stiffness, and comfort must be explicitly addressed through rational composite design rather than empirical optimization alone.

Third, electrode performance must be evaluated under realistic conditions, including mechanical deformation and in vivo EEG measurements, to ensure ecological validity.

By bridging materials science, electrode engineering, and EEG validation, this work demonstrates how fundamental structure–property insights can directly inform practical electrode design. The results also illustrate the importance of aligning laboratory

characterization methods with real-world operating conditions to avoid misleading performance assessments.

Future directions

Several promising research directions naturally emerge from the results of this thesis and open perspectives for further improving the performance and applicability of flexible EEG electrodes. From a materials standpoint, future work could focus on advanced material optimization by exploring alternative hybrid conductive filler systems, such as graphene-based fillers or hierarchical combinations of nanofillers. These approaches may enable finer control over percolation behavior and interfacial interactions, thereby improving electrical conductivity while preserving or even enhancing mechanical compliance. In parallel, the development of more sophisticated dispersion strategies could reduce agglomeration effects, improve reproducibility, and further stabilize the electromechanical response of the composites under deformation.

Beyond material formulation, manufacturing considerations represent a critical step toward practical deployment. Investigating scalable and industrially relevant processing techniques, including additive manufacturing and advanced molding strategies, could significantly enhance fabrication reproducibility and allow the realization of more complex electrode geometries tailored to scalp morphology. Such approaches would also facilitate the transition from laboratory-scale prototyping to large-scale production, an aspect that is essential for the translation of flexible EEG electrodes into commercial and clinical devices.

Another important research axis concerns long-term and environmental stability. While the present work demonstrates promising electrical and mechanical performance under controlled conditions, extended testing under realistic physiological environments remains necessary. Future studies should therefore examine the effects of humidity, sweat, temperature fluctuations, and repeated motion on electrode performance over prolonged periods. This would provide a more comprehensive assessment of durability, signal stability, and potential degradation mechanisms during long-term EEG monitoring.

In addition, expanded clinical validation is required to fully establish the relevance of these electrodes in real-world applications. Larger-scale in vivo studies involving more diverse participant populations would enable systematic evaluation of comfort, ergonomics, and signal

reliability across different head shapes, hair types, and usage scenarios. Such studies would also help identify inter-subject variability and potential limitations that may not be apparent in smaller experimental cohorts.

Finally, system-level integration constitutes a key step toward practical implementation. Integrating the developed flexible electrodes into wireless, lightweight, and miniaturized EEG platforms will be essential to unlock their full potential in applications such as neuroergonomics, brain–computer interfaces, and continuous brain monitoring. Addressing challenges related to electrical interfacing, power consumption, and signal conditioning at the system level will ultimately determine the feasibility of deploying these electrodes in next-generation wearable neurotechnologies.

Concluding remarks

This thesis shows that the performance of dry EEG electrodes is governed by a dynamic interplay among material composition, electrode architecture, and the electrode–skin interface. By moving beyond traditional gel-based paradigms and embracing flexible, bulk-conductive polymer composites, this work contributes both fundamental insights and practical solutions for next-generation EEG technologies. The findings emphasize that reliable, comfortable, and scalable EEG systems require an integrated, multidisciplinary approach that accounts for materials, mechanics, and real-world use conditions. From this perspective, the present work advances the development of flexible dry EEG electrodes capable of meeting the growing demands of clinical neurology, wearable neurotechnology, and brain–computer interface applications.

APPENDIX I RESEARCH ETHICS COMMITTEE APPROVAL

Comité d'éthique de la recherche
École de technologie supérieure

Le 21 mars 2025

Titre du projet :
Conception et fabrication d'une électrode sèche, flexible, d'électroencéphalogramme (EEG) pour utilisation mobile de longue durée

Chercheur responsable :
Ilyass Tabiai, Professeur au département de génie mécanique – École de technologie supérieure (ÉTS)

Autres membres de l'équipe de recherche :
Éric David, Professeur au département de génie mécanique – ÉTS
Jérémie Voix, Professeur au département de génie mécanique – ÉTS
Mélanie Girard, stagiaire postdoctorale au département de génie mécanique – ÉTS
Olatoundji George Gnonhoue, Étudiant au doctorat au département de génie mécanique – ÉTS

Financement :
CRSNG/PROMPT/MITACS

Partenaire industriel :
EERS

Référence : H20230504 *Demande* : *Renouvellement 2025-2026*

APPROBATION FINALE

Professeur Tabiai,

Nous accusons réception de la demande de renouvellement de l'approbation éthique pour le projet de recherche mentionné en rubrique. Le document soumis est conforme aux attentes du Comité d'éthique de la recherche (CÉR) de l'École de technologie supérieure.

J'ai donc le plaisir de vous informer que **le renouvellement de l'approbation éthique de votre projet est accordé sans condition** jusqu'au **22 avril 2026**. Selon l'état d'avancement de votre projet à cette date, vous devrez fournir au CÉR un rapport de suivi annuel pour demander le renouvellement de l'approbation éthique ou la fermeture du dossier.

En acceptant la présente approbation éthique, vous vous engagez à :

- Observer une conduite responsable pendant toute la durée de réalisation de votre projet de recherche;
- Informer dès que possible le CÉR de tout changement apporté au projet ou de tout évènement imprévu qui surviendrait au cours d'une séance de collecte de données;

- Respecter les conditions de confidentialité et de protection des renseignements et des données, telles qu'énoncées dans le dossier et approuvées par le CÉR;
- Conserver cette approbation éthique valide au moins jusqu'à la publication des premiers résultats de la recherche.

Si vous avez des questions ou des préoccupations éthiques, veuillez contacter le bureau coordonnateur du CÉR par courriel à l'adresse cer@etsmtl.ca ou par téléphone au (514) 396-8800 poste 7129 ou 7807.

Veuillez agréer, Professeur Tabiai, l'expression de mes sentiments les meilleurs.



Mathias Glaus, Ing., Ph.D.
Président, Comité d'éthique de la recherche
École de technologie supérieure

Échéance de l'approbation éthique : 22 avril 2026

Comité d'éthique de la recherche
École de technologie supérieure

Le 22 avril 2024

Titre du projet :

Conception et fabrication d'une électrode sèche, flexible, d'électroencéphalogramme (EEG) pour utilisation mobile de longue durée

Chercheur responsable :

Ilyass Tabiai, Professeur au département de génie mécanique – École de technologie supérieure (ÉTS)

Autres membres de l'équipe de recherche :

Éric David, Professeur au département de génie mécanique – École de technologie supérieure (ÉTS)

Jérémie Voix, Professeur au département de génie mécanique – École de technologie supérieure (ÉTS)

Mélanie Girard, stagiaire postdoctorale au département de génie mécanique – École de technologie supérieure (ÉTS)

Olatoundji George Gnonhoue, Étudiant au doctorat au département de génie mécanique – École de technologie supérieure (ÉTS)

Financement :

CRSNG/PROMPT/MITACS

Partenaire industriel :

EERS

Référence : H20230504 *Demande* : *Nouvelle*

APPROBATION FINALE

Professeur Tabiai,

Le projet de recherche mentionné en rubrique a été approuvé conditionnellement par le Comité d'éthique de la recherche (CÉR) de l'ÉTS en date du 18 mars 2024. Le dossier modifié et les documents demandés ont été révisés à la lumière des recommandations émises par le CÉR, et le dossier a été jugé conforme aux exigences.

J'ai donc le plaisir de vous informer que **votre projet est approuvé**. Vous pouvez **débuter le recrutement** des participantes et participants à la recherche.

Vous trouverez, jointe à la présente, une version PDF du formulaire d'information et de consentement approuvé par le CÉR. Vous êtes tenu d'utiliser cette version du document pour recruter et solliciter le consentement des personnes participantes.

Vous trouverez également l'ensemble des documents en vigueur (voir liste ci-bas).

Pour rappel, l'approbation éthique de votre projet est valable jusqu'au **22 avril 2025**. Selon l'état d'avancement de votre projet à cette date, vous devrez fournir au CÉR un rapport de suivi annuel pour demander le renouvellement de l'approbation éthique ou la fermeture du dossier.

En acceptant la présente approbation éthique, vous vous engagez à :

- Observer une conduite responsable pendant toute la durée de réalisation de votre projet de recherche;
- Informer dès que possible le CÉR de tout changement apporté au projet ou de tout évènement imprévu qui surviendrait au cours d'une séance de collecte de données;
- Respecter les conditions de confidentialité et de protection des renseignements et des données, telles qu'énoncées dans le dossier et approuvées par le CÉR;
- Conserver cette approbation éthique valide au moins jusqu'à la publication des premiers résultats de la recherche.

Aussi considérant l'implication de la compagnie EERS, nous vous recommandons de contacter le Décanat de la recherche (decanat.recherche@etsmtl.ca) pour établir les ententes de collaboration qui permettent d'encadrer le partage et l'utilisation des données et assurer leur confidentialité. Veuillez noter que cette procédure est indépendante de l'évaluation éthique faite par le CÉR, il n'est donc pas nécessaire de finaliser l'entente pour nous transmettre le dossier révisé.

Pour toute question en lien avec les recommandations émises, veuillez contacter le bureau coordonnateur du CÉR par courriel à l'adresse cer@etsmtl.ca ou par téléphone au (514) 396-8800 poste 7129.

Veuillez agréer, Professeur Tabiai, l'expression de mes sentiments les meilleurs.



Sylvie Ratté, LL. Eng., Ph.D.
Présidente par intérim, Comité d'éthique de la recherche
École de technologie supérieure

Échéance de l'approbation éthique : **22 avril 2025**

Pièces jointes : *Formulaire d'information et de consentement approuvé – V1, 22 avril 2024*
Formulaire de présentation en vigueur – V1, 22 avril 2024
Matériel de sollicitation en vigueur – V1, 22 avril 2024

cc : Ghyslain Gagnon, Doyen de la recherche
Chantal Lefebvre, Coordonnatrice du CÉR

BIBLIOGRAPHY

3devo B. V. (s. d.). *Filament Maker ONE*. Consulté 20 mars 2026, à l'adresse https://www.3devo.com/filament-maker-one

Abdulhameed, Z. N., Al Mashhadany, Y., & Salman, T. M. (2025). Mathematical Modeling, Acquisition, and Preprocessing of Core Biosignals (EEG, EOG, ECG, EMG) for Smart Healthcare Applications. *2025 18th International Conference on Development in eSystem Engineering (DeSE)*, 498-504. https://doi.org/10.1109/DeSE68208.2025.11367960

Abdullah, A. D.-A., & Al-Neami, A. Q. (2021). Performance Evaluation of a New Dry-Contact Electrode for EEG Measurement. *2021 IEEE International Biomedical Instrumentation and Technology Conference (IBITeC)*, 119-123. https://doi.org/10.1109/IBITeC53045.2021.9649333

Ai, Q., Zhao, M., Chen, K., Liu, Q., He, D., Li, Z., & Ma, L. (2024). Development and Application of Graphene Sensors in Human–Computer Interaction : A Review. *IEEE Sensors Journal*, *24*(6), 7406-7419. https://doi.org/10.1109/JSEN.2024.3360457

Ajel, R. I., Shati, N. M., & Abdullatif, F. A. (2024). A Comprehensive Analysis of the Design of Brain-Computer Interface Systems Utilizing Electroencephalography as a Means of Measurement : A Survey. *Ingénierie Des Systèmes d Information*, *29*(5), 1967-1979. https://doi.org/10.18280/isi.290528

Alam, M. N., Kumar, V., Lee, D., & Park, S. (2024). Styrene–butadiene rubber-based nanocomposites toughened by carbon nanotubes for wide and linear electromechanical

sensing applications. *Polymer Composites*, *45*(3), 2485-2499. https://doi.org/10.1002/pc.27934

Alam, M. N., Kumar, V., Lee, D.-J., & Choi, J. (2021). Magnetically active response of acrylonitrile-butadiene-rubber-based magnetorheological elastomers with different types of iron fillers and their hybrid. *Composites Communications*, *24*, 100657. https://doi.org/10.1016/j.coco.2021.100657

Alavi, K., Tarashi, S., Nazockdast, H., & Rafizadeh, M. (2023). Microstructure development and mechanical performance of MWCNTs / GNPs filled SEBS with different block content. *Polymer Composites*, *44*(11), 8125-8140. https://doi.org/10.1002/pc.27693

Al-Haidari, R., Falola, B., Alhendi, M., Schadt, M. J., Poliks, M., Balder, D., Stemmermann, A., Foster, M., Balchand, V., Kao, T.-J., & Stoffel, N. (2024). Conformal Dry Electrode for ECG Monitoring. *2024 IEEE 74th Electronic Components and Technology Conference (ECTC)*, 1662-1669. https://doi.org/10.1109/ECTC51529.2024.00275

Alikhani, E., & Mohammadi, M. (2023). EVA and SEBS-MA copolymers incorporated silicone rubber/SEBS blends : Improvement of mechanical and thermal properties. *Scientific Reports*, *13*(1), 22596. https://doi.org/10.1038/s41598-023-49796-6

Allahverdieva, Kh. V., Kakhramanov, N. T., Gadzhieva, R. Sh., & Shukyurova, A. A. (2023). Physical and Mechanical Properties of Filled Nanocomposites Based on Thermoplastic Copolymers of Ethylene with α-Olefins. *Polymer Science, Series D*, *16*(1), 193-198. https://doi.org/10.1134/S1995421223010033

Aouissi, T., Hellati, A., Zerriouh, A., Cavallo, D., Kabache, F., Benayache, W., Benaniba, M. T., & Benguerba, Y. (2025). Compatibilization of Immiscible PLA/LDPE Blends Using SEBS-g-MAH : A Multiscale Approach Combining Experimental and

Computational Studies. *Macromolecular Chemistry and Physics*, *226*(18), e00137. https://doi.org/10.1002/macp.202500137

Arai, M., Nishinaka, Y., & Miki, N. (2015). Electroencephalogram measurement using polymer-based dry microneedle electrode. *Japanese Journal of Applied Physics*, *54*(6S1), 06FP14. https://doi.org/10.7567/JJAP.54.06FP14

Aravinth, V., Navaneethakrishnan, V., Vishvanathperumal, S., & Gurumoorthi, G. (2024). Effect of Modified Nanographene Oxide (mGO)/Carbon Nanotubes (CNTs) Hybrid Filler on the Cure, Mechanical and Swelling Properties of Silicone Rubber Composites. *Journal of Inorganic and Organometallic Polymers and Materials*, *34*(1), 282-301. https://doi.org/10.1007/s10904-023-02818-2

Arjmand, M., Mahmoodi, M., Park, S., & Sundararaj, U. (2014). Impact of foaming on the broadband dielectric properties of multi-walled carbon nanotube/polystyrene composites. *Journal of Cellular Plastics*, *50*(6), 551-562. https://doi.org/10.1177/0021955X14539778

Asayesh, A., Warsito, I. F., Haueisen, J., Fiedler, P., & Vanhatalo, S. (2025). Neonatal Electroencephalogram Recording with a Dry Electrode Cap : A Feasibility Study. *Sensors*, *25*(3), 966. https://doi.org/10.3390/s25030966

Atif, M., Bongiovanni, R., Giorcelli, M., Celasco, E., & Tagliaferro, A. (2013). Modification and characterization of carbon black with mercaptopropyltrimethoxysilane. *Applied Surface Science*, *286*, 142-148. https://doi.org/10.1016/j.apsusc.2013.09.037

Azeem, M., Shahid, M., Masin, I., & Petru, M. (2025). Design and development of textile-based wearable sensors for real-time biomedical monitoring; a review. *The Journal of The Textile Institute*, *116*(1), 80-95. https://doi.org/10.1080/00405000.2024.2318500

Azizi, S., David, E., Fréchette, M. F., Nguyen-Tri, P., & Ouellet-Plamondon, C. M. (2018). Electrical and thermal conductivity of ethylene vinyl acetate composite with graphene and carbon black filler. *Polymer Testing*, *72*, 24-31. https://doi.org/10.1016/j.polymertesting.2018.09.031

Babusiak, B., Borik, S., & Balogova, L. (2018). Textile electrodes in capacitive signal sensing applications. *Measurement*, *114*, 69-77. https://doi.org/10.1016/j.measurement.2017.09.024

Baek, H. J., Kim, H. S., Heo, J., Lim, Y. G., & Park, K. S. (2013). Brain–computer interfaces using capacitive measurement of visual or auditory steady-state responses. *Journal of Neural Engineering*, *10*(2), 024001. https://doi.org/10.1088/1741-2560/10/2/024001

Baek, H. J., Lee, H. J., Lim, Y. G., & Park, K. S. (2012). Conductive Polymer Foam Surface Improves the Performance of a Capacitive EEG Electrode. *IEEE Transactions on Biomedical Engineering*, *59*(12), 3422-3431. https://doi.org/10.1109/TBME.2012.2215032

Bakytkarim, Y., Tursynbolat, S., Mukatayeva, Zh. S., Tileuberdi, Ye., Shadin, N. A., Assirbayeva, Zh. M., Wang, L. S., Zhussupova, L. A., & Toktarbay, Z. (2024). High-Sensitivity Electrochemical Detection of Chlorogenic Acid Based on Pt@r-GO@MWCNTs Ternary Nanocomposites Modified Electrodes. *Engineered Science*. https://doi.org/10.30919/es1178

Bednar, T., Babusiak, B., Smondrk, M., Cap, I., & Borik, S. (2021). The impact of active electrode guard layer in capacitive measurements of biosignals. *Measurement*, *171*, 108740. https://doi.org/10.1016/j.measurement.2020.108740

Bensalah, F., Pézard, J., Haddour, N., Erouel, M., Buret, F., & Khirouni, K. (2021). Carbon Nano-Fiber/PDMS Composite Used as Corrosion-Resistant Coating for Copper Anodes in Microbial Fuel Cells. *Nanomaterials*, *11*(11), 3144. https://doi.org/10.3390/nano11113144

Beyrouthy, T., Mostafa, N., Roshdy, A., Karar, A., & Alkork, S. (2024). Review of EEG-Based Biometrics in 5G-IoT : Current Trends and Future Prospects. *Applied Sciences*, *14*(2), 534. https://doi.org/10.3390/app14020534

Bidiyasar, R., Kumar, R., & Jakhar, N. (2024). A critical review of polymer support-based shape-stabilized phase change materials for thermal energy storage applications. *Energy Storage*, *6*(4), e639. https://doi.org/10.1002/est2.639

Bisht, N., Vishwakarma, J., Jaiswal, S., Kumar, P., Srivastava, A. K., Dhand, C., & Dwivedi, N. (2025). Synergizing chemistry : Unveiling the potential of hybrid fillers for enhanced performance in shape memory polymers. *Advanced Composites and Hybrid Materials*, *8*(1), 7. https://doi.org/10.1007/s42114-024-01059-2

Biswas, S., Biswas, A., & Sen, K. (2025). Graphene Based Hybrid Nanocomposite Materials as Sustainable Energy Resource : Synthesis to Application as Supercapacitors. *ES Chemistry and Sustainability*. https://doi.org/10.30919/escs1581

Bokobza, L. (2023). Elastomer Nanocomposites : Effect of Filler–Matrix and Filler–Filler Interactions. *Polymers*, *15*(13), 2900. https://doi.org/10.3390/polym15132900

Burgar, P. (s. d.). *Design of Flexible Dry CNT/PDMS Electrodes for In-ear EEG*.

Cabrini, F. M. (s. d.). *Auto-assemblage de bicouches de copolymères à blocs amphiphiles induit par une surface*.

Cai, Y., Chen, D., Cheng, L., Guo, S., Hu, Z., Wang, Y., Yu, H., & Zhou, Y. (2024). Preparation and sensing properties of multiscale conductive filler hybrid CNTs@Ag-MXene-TPU/TPU double-layer strain sensing materials. *Composites Part A: Applied Science and Manufacturing*, *186*, 108430. https://doi.org/10.1016/j.compositesa.2024.108430

Camarinha, A., Lopes, C., Ferreira, A., Alves, A. C., & Vaz, F. (2025). A comparative study of the corrosion behaviour of flexible dry electrodes based on Ti-Cu thin films. *Surfaces and Interfaces*, *58*, 105855. https://doi.org/10.1016/j.surfin.2025.105855

Cetin, M. S., & Karahan Toprakci, H. A. (2021a). Flexible electronics from hybrid nanocomposites and their application as piezoresistive strain sensors. *Composites Part B: Engineering*, *224*, 109199. https://doi.org/10.1016/j.compositesb.2021.109199

Cetin, M. S., & Karahan Toprakci, H. A. (2021b). Flexible electronics from hybrid nanocomposites and their application as piezoresistive strain sensors. *Composites Part B: Engineering*, *224*, 109199. https://doi.org/10.1016/j.compositesb.2021.109199

Chang, H., Zheng, M., Yu, X., Than, A., Seeni, R. Z., Kang, R., Tian, J., Khanh, D. P., Liu, L., Chen, P., & Xu, C. (2017). A Swellable Microneedle Patch to Rapidly Extract Skin Interstitial Fluid for Timely Metabolic Analysis. *Advanced Materials*, *29*(37), 1702243. https://doi.org/10.1002/adma.201702243

Chen, K., Li, Z., Guo, J., Yang, X., Guo, B., & Shen, H. (2024). A Flexible Capacitive Pressure Sensor Based on Thermoplastic Polyurethane Porous Films by Non-Solvent Induced Phase Separation. *IEEE Sensors Journal*, *24*(8), 12217-12224. https://doi.org/10.1109/JSEN.2024.3372587

Chen, K., Ren, L., Chen, Z., Pan, C., Zhou, W., & Jiang, L. (2016). Fabrication of Micro-Needle Electrodes for Bio-Signal Recording by a Magnetization-Induced Self-Assembly Method. *Sensors*, *16*(9), 1533. https://doi.org/10.3390/s16091533

Chen, T., Wu, G., Panahi-Sarmad, M., Wu, Y., Xu, R., Cao, S., & Xiao, X. (2022). A novel flexible piezoresistive sensor using superelastic fabric coated with highly durable SEBS/TPU/CB/CNF nanocomposite for detection of human motions. *Composites Science and Technology*, *227*, 109563. https://doi.org/10.1016/j.compscitech.2022.109563

Chen, Y.-H., De Beeck, M. O., Vanderheyden, L., Carrette, E., Mihajlović, V., Vanstreels, K., Grundlehner, B., Gadeyne, S., Boon, P., & Van Hoof, C. (2014). Soft, Comfortable Polymer Dry Electrodes for High Quality ECG and EEG Recording. *Sensors*, *14*(12), Article 12. https://doi.org/10.3390/s141223758

Chen, Z., Ren, L., Li, J., Yao, L., Chen, Y., Liu, B., & Jiang, L. (2018). Rapid fabrication of microneedles using magnetorheological drawing lithography. *Acta Biomaterialia*, *65*, 283-291. https://doi.org/10.1016/j.actbio.2017.10.030

Cheng, L., Li, J., Guo, A., & Zhang, J. (2023). Recent advances in flexible noninvasive electrodes for surface electromyography acquisition. *Npj Flexible Electronics*, *7*(1), 39. https://doi.org/10.1038/s41528-023-00273-0

Cheng, X., Bao, C., Wang, X., Zhang, F., & Dong, W. (2019). Soft surface electrode based on PDMS-CB conductive polymer for electrocardiogram recordings. *Applied Physics A*, *125*(12), 876. https://doi.org/10.1007/s00339-019-3124-5

Cheng, Y., Wang, J., Wu, Y., Yan, F., & Yan, L. (2025). A Novel Asynchronous Brain Computer Interface Using an Un-cued SSVEP Paradigm and Early

Electroencephalography Component. *IEEE Sensors Journal*, 1-1. https://doi.org/10.1109/JSEN.2025.3542067

Chervanyov, A. I. (2023). Effect of the Interplay between Polymer–Filler and Filler–Filler Interactions on the Conductivity of a Filled Diblock Copolymer System. *Polymers*, *16*(1), 104. https://doi.org/10.3390/polym16010104

Chervanyov, A. I. (2025). Conductivity of Filled Diblock Copolymer Systems : Identifying the Main Influencing Factors. *Polymers*, *17*(11), 1502. https://doi.org/10.3390/polym17111502

Chi, Y. M., Jung, T.-P., & Cauwenberghs, G. (2010). Dry-Contact and Noncontact Biopotential Electrodes : Methodological Review. *IEEE Reviews in Biomedical Engineering*, *3*, 106-119. https://doi.org/10.1109/RBME.2010.2084078

Chlaihawi, A. A., Narakathu, B. B., Emamian, S., Bazuin, B. J., & Atashbar, M. Z. (2018). Development of printed and flexible dry ECG electrodes. *Sensing and Bio-Sensing Research*, *20*, 9-15. https://doi.org/10.1016/j.sbsr.2018.05.001

Cioffi, E., Hutber, A., Molloy, R., Murden, S., Yurkewich, A., Kirton, A., Lin, J.-P., Gimeno, H., & McClelland, V. M. (2024). EEG-based sensorimotor neurofeedback for motor neurorehabilitation in children and adults : A scoping review. *Clinical Neurophysiology*, *167*, 143-166. https://doi.org/10.1016/j.clinph.2024.08.009

Costa, P., Ribeiro, S., Botelho, G., Machado, A. V., & Lanceros Mendez, S. (2015). Effect of butadiene/styrene ratio, block structure and carbon nanotube content on the mechanical and electrical properties of thermoplastic elastomers after UV ageing. *Polymer Testing*, *42*, 225-233. https://doi.org/10.1016/j.polymertesting.2015.02.002

Cui, N., Song, Y., Tan, C.-H., Zhang, K., Yang, X., Dong, S., Xie, B., & Huang, F. (2021). Stretchable transparent electrodes for conformable wearable organic photovoltaic devices. *Npj Flexible Electronics*, *5*(1), 31. https://doi.org/10.1038/s41528-021-00127-7

Cunha, L. T., Pedrosa, P., Tavares, C. J., Alves, E., Vaz, F., & Fonseca, C. (2009). The role of composition, morphology and crystalline structure in the electrochemical behaviour of TiNx thin films for dry electrode sensor materials. *Electrochimica Acta*, *55*(1), 59-67. https://doi.org/10.1016/j.electacta.2009.08.004

Dabbagh, S. R., Sarabi, M. R., Rahbarghazi, R., Sokullu, E., Yetisen, A. K., & Tasoglu, S. (2021). 3D-printed microneedles in biomedical applications. *iScience*, *24*(1), 102012. https://doi.org/10.1016/j.isci.2020.102012

Dadjou, M., Bakhtiyari, S., Jahanshahi, A., & Bagherzadeh, R. (2024). Towards seamless conformable and comfortable wearable electronics : Polyimide-supported dry electrodes integrated in knitted fabrics. *Sensors and Actuators A: Physical*, *376*, 115613. https://doi.org/10.1016/j.sna.2024.115613

Damalerio, R. B., Lim, R., Gao, Y., Zhang, T.-T., & Cheng, M.-Y. (2023). Development of Low-Contact-Impedance Dry Electrodes for Electroencephalogram Signal Acquisition. *Sensors*, *23*(9), 4453. https://doi.org/10.3390/s23094453

Das, P. S., Park, S. H., Baik, K. Y., Lee, J. W., & Park, J. Y. (2020a). Thermally reduced graphene oxide-nylon membrane based epidermal sensor using vacuum filtration for wearable electrophysiological signals and human motion monitoring. *Carbon*, *158*, 386-393. https://doi.org/10.1016/j.carbon.2019.11.001

Das, P. S., Park, S. H., Baik, K. Y., Lee, J. W., & Park, J. Y. (2020b). Thermally reduced graphene oxide-nylon membrane based epidermal sensor using vacuum filtration for wearable electrophysiological signals and human motion monitoring. *Carbon*, *158*, 386-393. https://doi.org/10.1016/j.carbon.2019.11.001

Davidyants, N. G., Gorbunova, I. Yu., Polunin, S. V., Kravchenko, T. P., & Khoroshilov, A. V. (2025). Effect of SEBS-g-MA on recycled PS/HDPE blend miscibility. *Colloid and Polymer Science*, *303*(6), 1139-1154. https://doi.org/10.1007/s00396-025-05407-6

de Camp, N. V., Kalinka, G., & Bergeler, J. (2018). Light-cured polymer electrodes for non-invasive EEG recordings. *Scientific Reports*, *8*(1), 14041. https://doi.org/10.1038/s41598-018-32304-6

Del Bosque, A., Fernández Sánchez-Romate, X. X., De La Llana Calvo, Á., Fernández, P. R., Borromeo, S., Sánchez, M., & Ureña, A. (2023). Highly Flexible Strain Sensors Based on CNT-Reinforced Ecoflex Silicone Rubber for Wireless Facemask Breathing Monitoring via Bluetooth. *ACS Applied Polymer Materials*, *5*(10), 8589-8599. https://doi.org/10.1021/acsapm.3c01689

Demazy, N. (s. d.-a). *Iterative self-assembly of nanostructured block copolymer thin films, toward the development of functional three-dimensional structures with nanometric periodicity*.

Demazy, N. (s. d.-b). *Iterative self-assembly of nanostructured block copolymer thin films, toward the development of functional three-dimensional structures with nanometric periodicity*.

Di Flumeri, G., Aricò, P., Borghini, G., Sciaraffa, N., Di Florio, A., & Babiloni, F. (2019). The Dry Revolution : Evaluation of Three Different EEG Dry Electrode Types in Terms of

Signal Spectral Features, Mental States Classification and Usability. *Sensors*, *19*(6), 1365. https://doi.org/10.3390/s19061365

Erickson, B., Rich, R., Shankar, S., Kim, B., Driscoll, N., Mentzelopoulos, G., Fernandez-Nuñez, G., Vitale, F., & Medaglia, J. D. (2024). Evaluating and benchmarking the EEG signal quality of high-density, dry MXene-based electrode arrays against gelled Ag/AgCl electrodes. *Journal of Neural Engineering*, *21*(1), 016005. https://doi.org/10.1088/1741-2552/ad141e

Fayyaz Shahandashti, P., Pourkheyrollah, H., Jahanshahi, A., & Ghafoorifard, H. (2019). Highly conformable stretchable dry electrodes based on inexpensive flex substrate for long-term biopotential (EMG/ECG) monitoring. *Sensors and Actuators A: Physical*, *295*, 678-686. https://doi.org/10.1016/j.sna.2019.06.041

Fiedler, P., Graichen, U., Zimmer, E., & Haueisen, J. (2023). Simultaneous Dry and Gel-Based High-Density Electroencephalography Recordings. *Sensors*, *23*(24), 9745. https://doi.org/10.3390/s23249745

Fiedler, P., Muhle, R., Griebel, S., Pedrosa, P., Fonseca, C., Vaz, F., Zanow, F., & Haueisen, J. (2018a). Contact Pressure and Flexibility of Multipin Dry EEG Electrodes. *IEEE Transactions on Neural Systems and Rehabilitation Engineering*, *26*(4), 750-757. https://doi.org/10.1109/TNSRE.2018.2811752

Fiedler, P., Muhle, R., Griebel, S., Pedrosa, P., Fonseca, C., Vaz, F., Zanow, F., & Haueisen, J. (2018b). Contact Pressure and Flexibility of Multipin Dry EEG Electrodes. *IEEE Transactions on Neural Systems and Rehabilitation Engineering*, *26*(4), 750-757. https://doi.org/10.1109/TNSRE.2018.2811752

Fiedler, P., Pedrosa, P., Griebel, S., Fonseca, C., Vaz, F., Supriyanto, E., Zanow, F., & Haueisen, J. (2015). Novel Multipin Electrode Cap System for Dry Electroencephalography. *Brain Topography*, *28*(5), 647-656. https://doi.org/10.1007/s10548-015-0435-5

Fiedler, P., Pedrosa, P., Griebel, S., Fonseca, C., Vaz, F., Zanow, F., & Haueisen, J. (2011a). Novel flexible dry PU/TiN-multipin electrodes : First application in EEG measurements. *2011 Annual International Conference of the IEEE Engineering in Medicine and Biology Society*, 55-58. https://doi.org/10.1109/IEMBS.2011.6089895

Fiedler, P., Pedrosa, P., Griebel, S., Fonseca, C., Vaz, F., Zanow, F., & Haueisen, J. (2011b). Novel flexible dry PU/TiN-multipin electrodes : First application in EEG measurements. *2011 Annual International Conference of the IEEE Engineering in Medicine and Biology Society*, 55-58. https://doi.org/10.1109/IEMBS.2011.6089895

Fiedler, P., Strohmeier, D., Hunold, A., Griebel, S., Muhle, R., Schreiber, M., Pedrosa, P., Vasconcelos, B., Fonseca, C., Vaz, F., & Haueisen, J. (2016). Modular multipin electrodes for comfortable dry EEG. *IEEE Xplore*, 4.

Forcina, G. (s. d.). *Block-copolymer nano-manufacturing via spatially controlled interface and wetting manipulations*.

Fu, Y., Zhao, J., Dong, Y., & Wang, X. (2020a). Dry Electrodes for Human Bioelectrical Signal Monitoring. *Sensors*, *20*(13), 3651. https://doi.org/10.3390/s20133651

Fu, Y., Zhao, J., Dong, Y., & Wang, X. (2020b). Dry Electrodes for Human Bioelectrical Signal Monitoring. *Sensors*, *20*(13), 3651. https://doi.org/10.3390/s20133651

Gao, K., Li, L., Ji, B., & Wu, N. (2024a). Pin-Shaped Ag/AgCl Fabric Electrode Coated With Hydrogel for EEG Recording in Hairy Areas. *IEEE Sensors Journal*, *24*(16), 25316-25327. https://doi.org/10.1109/JSEN.2024.3426268

Gao, K., Li, L., Ji, B., & Wu, N. (2024b). Pin-Shaped Ag/AgCl Fabric Electrode Coated With Hydrogel for EEG Recording in Hairy Areas. *IEEE Sensors Journal*, *24*(16), 25316-25327. https://doi.org/10.1109/JSEN.2024.3426268

Gao, K.-P., Yang, H.-J., Wang, X.-L., Yang, B., & Liu, J.-Q. (2018). Soft pin-shaped dry electrode with bristles for EEG signal measurements. *Sensors and Actuators A: Physical*, *283*, 348-361. https://doi.org/10.1016/j.sna.2018.09.045

Gao, X., Yin, L., Tian, S., Huang, Y., & Ji, Q. (2024). Wearable Technology for Signal Acquisition and Interactive Feedback in Autism Spectrum Disorder Intervention : A Review. *IEEE Sensors Journal*, *24*(9), 13797-13815. https://doi.org/10.1109/JSEN.2024.3374762

Gao, Y., Soman, V. V., Lombardi, J. P., Rajbhandari, P. P., Dhakal, T. P., Wilson, D. G., Poliks, M. D., Ghose, K., Turner, J. N., & Jin, Z. (2020). Heart Monitor Using Flexible Capacitive ECG Electrodes. *IEEE Transactions on Instrumentation and Measurement*, *69*(7), 4314-4323. https://doi.org/10.1109/TIM.2019.2949320

Ghosh, S., Ganguly, S., Das, P., Das, T. K., Bose, M., Singha, N. K., Das, A. K., & Das, N. Ch. (2019). Fabrication of Reduced Graphene Oxide/Silver Nanoparticles Decorated Conductive Cotton Fabric for High Performing Electromagnetic Interference Shielding and Antibacterial Application. *Fibers and Polymers*, *20*(6), 1161-1171. https://doi.org/10.1007/s12221-019-1001-7

Gnonhoue, O. G. (2021). *Caractérisation électrique d'un condensateur haute-tension sec* [Maîtrise en génie électrique, École de technologie supérieure]. https://etsmtl.on.worldcat.org/search/detail/1529642440?databaseList=&queryString=George%20Gnonhoue

Gómez Martín, J. C., Muñoz, O., Martikainen, J., Guirado, D., Tanarro, I., Peláez, R. J., Maté, B., Jiménez-Redondo, M., Herrero, V. J., Peiteado, M., & Jardiel, T. (2024). Experimental Phase Function and Degree of Linear Polarization of Light Scattered by Hydrogenated Amorphous Carbon Circumstellar Dust Analogs. *The Astrophysical Journal Supplement Series*, *270*(1), 2. https://doi.org/10.3847/1538-4365/ad0379

Gonçalves, B. F., Costa, P., Oliveira, J., Ribeiro, S., Correia, V., Botelho, G., & Lanceros-Mendez, S. (2016). Green solvent approach for printable large deformation thermoplastic elastomer based piezoresistive sensors and their suitability for biomedical applications. *Journal of Polymer Science Part B: Polymer Physics*, *54*(20), 2092-2103. https://doi.org/10.1002/polb.24118

Gougeh, R. A. (s. d.). *Enhancing Motor Imagery-Based Brain-Computer Interface Efficacy Using Multisensory Virtual Reality Training*.

Griffin, A., Guo, Y., Hu, Z., Zhang, J., Chen, Y., & Qiang, Z. (2022). Scalable methods for directional assembly of fillers in polymer composites : Creating pathways for improving material properties. *Polymer Composites*, *43*(9), 5747-5766. https://doi.org/10.1002/pc.26905

Grigorescu, R. M., Ciuprina, F., Ghioca, P., Ghiurea, M., Iancu, L., Spurcaciu, B., & Panaitescu, D. M. (2016). Mechanical and dielectric properties of SEBS modified by

graphite inclusion and composite interface. *Journal of Physics and Chemistry of Solids*, *89*, 97-106. https://doi.org/10.1016/j.jpcs.2015.10.008

Griss, P., Enoksson, P., Tolvanen-Laakso, H. K., Merilainen, P., Ollmar, S., & Stemme, G. (2001). Micromachined electrodes for biopotential measurements. *Journal of Microelectromechanical Systems*, *10*(1), 10-16. https://doi.org/10.1109/84.911086

Gui, H., Zhao, X., Zuo, S., Liu, W., Wang, C., Xu, P., Ding, Y., & Yao, C. (2023a). Carbonized Syndiotactic Polystyrene/Carbon Nanotube/MXene Hybrid Aerogels with Egg-Box Structure : A Platform for Electromagnetic Interference Shielding and Solar Thermal Energy Management. *ACS Applied Materials & Interfaces*, *15*(33), 39740-39751. https://doi.org/10.1021/acsami.3c08176

Gui, H., Zhao, X., Zuo, S., Liu, W., Wang, C., Xu, P., Ding, Y., & Yao, C. (2023b). Carbonized Syndiotactic Polystyrene/Carbon Nanotube/MXene Hybrid Aerogels with Egg-Box Structure : A Platform for Electromagnetic Interference Shielding and Solar Thermal Energy Management. *ACS Applied Materials & Interfaces*, *15*(33), 39740-39751. https://doi.org/10.1021/acsami.3c08176

Guo, J., Wang, H., Zhang, C., Zhang, Q., & Yang, H. (2020). MPPE/SEBS Composites with Low Dielectric Loss for High-Frequency Copper Clad Laminates Applications. *Polymers*, *12*(9), 1875. https://doi.org/10.3390/polym12091875

Guo, M. (2017). *Polyethylene/polyhedral oligomeric silsesquioxanes composites : Electrical insulation for high voltage power cables* [Thèse de doctorat en génie, École de technologie supérieure]. https://etsmtl.on.worldcat.org/search/detail/1016026909?queryString=Polyethylene%2FPolyhedral%20Oligomeric%20Silsesquioxanes%20Composites%3A%20Electrical

%20Insulation%20for%20High-Voltage%20Power%20Cables&databaseList=&idDetect=true&clusterResults=false&groupVariantRecords=false&newsArticles=off&bookReviews=off

Ha, J., Park, S., Han, Y., & Kim, L. (2025). Hybrid BCI for Meal-Assist Robot Using Dry-Type EEG and Pupillary Light Reflex. *Biomimetics*, *10*(2), 118. https://doi.org/10.3390/biomimetics10020118

Habibzadeh Tonekabony Shad, E., Molinas, M., & Ytterdal, T. (2020). Impedance and Noise of Passive and Active Dry EEG Electrodes : A Review. *IEEE Sensors Journal*, *20*(24), 14565-14577. IEEE Sensors Journal. https://doi.org/10.1109/JSEN.2020.3012394

Hajare, R., & Kadam, S. (2021). Comparative study analysis of practical EEG sensors in medical diagnoses. *Global Transitions Proceedings*, *2*(2), 467-475. https://doi.org/10.1016/j.gltp.2021.08.009

Han, C.-H., Kim, S.-U., Lim, K.-S., Jung, Y.-J., Lee, S., Kim, S. H., & Hwang, H.-J. (2025a). Evaluation of a silicone-based flexible dry electrode for measuring human bioelectrical signals. *Biomedical Engineering Letters*, *15*(3), 563-574. https://doi.org/10.1007/s13534-025-00471-x

Han, C.-H., Kim, S.-U., Lim, K.-S., Jung, Y.-J., Lee, S., Kim, S. H., & Hwang, H.-J. (2025b). Evaluation of a silicone-based flexible dry electrode for measuring human bioelectrical signals. *Biomedical Engineering Letters*, *15*(3), 563-574. https://doi.org/10.1007/s13534-025-00471-x

Harati, A., & Jahanshahi, A. (2021). A reliable stretchable dry electrode for monitoring of EEG signals. *Sensors and Actuators A: Physical*, *326*, 112727. https://doi.org/10.1016/j.sna.2021.112727

Hassan, M., Abbas, G., Li, N., Afzal, A., Haider, Z., Ahmed, S., Xu, X., Pan, C., & Peng, Z. (2022). Significance of Flexible Substrates for Wearable and Implantable Devices : Recent Advances and Perspectives. *Advanced Materials Technologies*, *7*(3), 2100773. https://doi.org/10.1002/admt.202100773

Haueisen, J., Fiedler, P., Bernhardt, A., Gonçalves, R., & Fonseca, C. (2020). Novel dry electrode EEG headbands for home use : Comparing performance and comfort. *Current Directions in Biomedical Engineering*, *6*(3), 139-142. https://doi.org/10.1515/cdbme-2020-3036

He, W., Ma, J., Kang, L., Wang, L., & Zhu, M. (2024). Highly sensitive and stretchable CB/GNPs-TPU strain sensor with porous microstructure for multifunctional strain sensing. *Materials Today Communications*, *41*, 110800. https://doi.org/10.1016/j.mtcomm.2024.110800

Heid, T. (2015). *Innovative nanostructured epoxy composites for enhanced high voltage insulation systems* [Thèse de doctorat en génie, École de technologie supérieure]. https://etsmtl.on.worldcat.org/search/detail/929134975?queryString=INNOVATIVE%20NANOSTRUCTURED%20EPOXY%20COMPOSITES%20FOR%20ENHANCED%20HIGH%20VOLTAGE%20INSULATION%20SYSTEMS&bookReviews=off&newsArticles=off&databaseList=&idDetect=true&clusterResults=false&groupVariantRecords=false

Heijs, J. J. A., Havelaar, R. J., Fiedler, P., Van Wezel, R. J. A., & Heida, T. (2021). Validation of Soft Multipin Dry EEG Electrodes. *Sensors*, *21*(20), 6827. https://doi.org/10.3390/s21206827

Helgeson, A. (2000). *Analysis of Dielectric Response Measurement Methods and Dielectric Properties of Resin-Rich Insulation During Processing* [Thèse de doctorat]. Kungl Tekniska Högskolan.

Heng, W., Solomon, S., & Gao, W. (2022). Flexible Electronics and Devices as Human–Machine Interfaces for Medical Robotics. *Advanced Materials*, *34*(16), 2107902. https://doi.org/10.1002/adma.202107902

Heo, J. S., Hossain, M. F., & Kim, I. (2020). Challenges in Design and Fabrication of Flexible/Stretchable Carbon- and Textile-Based Wearable Sensors for Health Monitoring : A Critical Review. *Sensors*, *20*(14), 3927. https://doi.org/10.3390/s20143927

Hinrichs, H., Scholz, M., Baum, A. K., Kam, J. W. Y., Knight, R. T., & Heinze, H.-J. (2020). Comparison between a wireless dry electrode EEG system with a conventional wired wet electrode EEG system for clinical applications. *Scientific Reports*, *10*(1), 5218. https://doi.org/10.1038/s41598-020-62154-0

Honda, H., & Nishiyama, K. (2025). Anti-shivering Drug Influences the Characteristics of Electroencephalographic Shivering Noise During Targeted Temperature Management : A Case Report. *Cureus*. https://doi.org/10.7759/cureus.84509

Hong, W., Guo, X., Zhang, T., Mu, S., Wu, F., Yan, Z., Zhang, H., Li, X., Zhang, A., Wang, J., Cao, Y., Li, J., Dong, H., Liu, T., Liu, Z., & Zhao, Y. (2024). Flexible Strain Sensor Based on Nickel Microparticles/Carbon Black Microspheres/Polydimethylsiloxane Conductive Composites for Human Motion Detection. *ACS Applied Materials & Interfaces*, *16*(25), 32702-32712. https://doi.org/10.1021/acsami.4c04830

Hoon Lee, J., Min Lee, S., Jin Byeon, H., Sook Hong, J., Suk Park, K., & Lee, S.-H. (2014). CNT/PDMS-based canal-typed ear electrodes for inconspicuous EEG recording. *Journal of Neural Engineering*, *11*(4), 046014. https://doi.org/10.1088/1741-2560/11/4/046014

Hossain, Md. M., Li, B. M., Sennik, B., Jur, J. S., & Bradford, P. D. (2022). Adhesive free, conformable and washable carbon nanotube fabric electrodes for biosensing. *Npj Flexible Electronics*, *6*(1), 97. https://doi.org/10.1038/s41528-022-00230-3

Huang, J., Wang, C., Zhao, W., Grau, A., Xue, X., & Zhang, F. (2024). LTDNet-EEG : A Lightweight Network of Portable/Wearable Devices for Real-Time EEG Signal Denoising. *IEEE Transactions on Consumer Electronics*, 1-1. https://doi.org/10.1109/TCE.2024.3412774

Iqbal, S. M. A., Mahgoub, I., Du, E., Leavitt, M. A., & Asghar, W. (2021). Advances in healthcare wearable devices. *Npj Flexible Electronics*, *5*(1), 9. https://doi.org/10.1038/s41528-021-00107-x

Jamatia, T., Matyas, J., Olejnik, R., Danova, R., Maloch, J., Skoda, D., Slobodian, P., & Kuritka, I. (2023). Wearable and Stretchable SEBS/CB Polymer Conductive Strand as a Piezoresistive Strain Sensor. *Polymers*, *15*(7), 1618. https://doi.org/10.3390/polym15071618

Jiang, M.-J., Dang, Z.-M., Bozlar, M., Miomandre, F., & Bai, J. (2009). Broad-frequency dielectric behaviors in multiwalled carbon nanotube/rubber nanocomposites. *Journal of Applied Physics*, *106*(8), 084902. https://doi.org/10.1063/1.3238306

Jin, L., Kim, K. J., Song, E. H., Ahn, Y. J., Jeong, Y. J., Oh, T. I., & Woo, E. J. (2016). Highly precise nanofiber web-based dry electrodes for vital signal monitoring. *RSC Advances*, *6*(46), 40045-40057. https://doi.org/10.1039/C6RA00079G

Jing, L., Li, P., Li, Z., Ma, D., & Hu, J. (2025). Influence of π–π interactions on organic photocatalytic materials and their performance. *Chemical Society Reviews*, *54*(4), 2054-2090. https://doi.org/10.1039/D4CS00029C

Kaitainen, S., Kutvonen, A., Suvanto, M., Pakkanen, T. T., Lappalainen, R., & Myllymaa, S. (2014). Liquid silicone rubber (LSR)-based dry bioelectrodes : The effect of surface micropillar structuring and silver coating on contact impedance. *Sensors and Actuators A: Physical*, *206*, 22-29. https://doi.org/10.1016/j.sna.2013.11.020

Kakhramanov, N. T., & Allahverdiyeva, Kh. V. (2023). Reactive Extrusion of Multifunctional Conducting Nanocomposites Based on Polypropylene Random Copolymer and Ethylene–Propylene Block Copolymer. *Russian Journal of Applied Chemistry*, *96*(4), 441-452. https://doi.org/10.1134/S1070427223040079

Kang, B.-C., Park, B.-S., & Ha, T.-J. (2019). Highly sensitive wearable glucose sensor systems based on functionalized single-wall carbon nanotubes with glucose oxidase-nafion composites. *Applied Surface Science*, *470*, 13-18. https://doi.org/10.1016/j.apsusc.2018.11.101

Kang, T. W., Lee, J., Kwon, Y., Lee, Y. J., & Yeo, W. (2024). Recent Progress in the Development of Flexible Wearable Electrodes for Electrocardiogram Monitoring During Exercise. *Advanced NanoBiomed Research*, *4*(8), 2300169. https://doi.org/10.1002/anbr.202300169

Kappel, S. L., Rank, M. L., Toft, H. O., Andersen, M., & Kidmose, P. (2019). Dry-Contact Electrode Ear-EEG. *IEEE Transactions on Biomedical Engineering*, *66*(1), 150-158. https://doi.org/10.1109/TBME.2018.2835778

Karacan, I., & Türker, K. S. (2025). A comparison of electromyography techniques : Surface versus intramuscular recording. *European Journal of Applied Physiology*, *125*(1), 7-23. https://doi.org/10.1007/s00421-024-05640-x

Katheria, A., Das, P., Nayak, J., Roy, B., Pal, A., Biswas, S., & Das, N. Ch. (2025). MXene and Fe3O4 decorated g-C3N4 incorporated high flexible hybrid polymer composite for enhanced electrical conductivity, EMI shielding and thermal conductivity. *Next Materials*, *6*, 100292. https://doi.org/10.1016/j.nxmate.2024.100292

Kausar, A. (2016). Poly(vinylacetate)cyanomethyl Diphenylcarbamodthioate/ Poly(vinyl acetate)/Carbon Black Composite-based Sensor. *International Journal of Instrumentation Science*. https://doi.org/DOI:%2010.5923/j.instrument.20160502.01

Kausar, A., Rafique, I., & Muhammad, B. (2017). Electromagnetic Interference Shielding of Polymer/Nanodiamond, Polymer/Carbon Nanotube, and Polymer/Nanodiamond–Carbon Nanotube Nanobifiller Composite : A Review. *Polymer-Plastics Technology and Engineering*, *56*(4), 347-363. https://doi.org/10.1080/03602559.2016.1233273

Kaveh, R., Schwendeman, C., Pu, L., Arias, A. C., & Muller, R. (2024). Wireless ear EEG to monitor drowsiness. *Nature Communications*, *15*(1), 6520. https://doi.org/10.1038/s41467-024-48682-7

Khosla, A., Shah, S., Shiblee, M. N. I., Mir, S. H., Nagahara, L. A., Thundat, T., Shekar, P. K., Kawakami, M., & Furukawa, H. (2018). Carbon fiber doped thermosetting elastomer

for flexible sensors : Physical properties and microfabrication. *Scientific Reports*, *8*(1), 12313. https://doi.org/10.1038/s41598-018-30846-3

Kim, D. Y., Ku, Y., Ahn, J. W., Kwon, C., & Kim, H. C. (2018). Electro-deposited Nanoporous Platinum Electrode for EEG Monitoring. *Journal of Korean Medical Science*, *33*(21), e154. https://doi.org/10.3346/jkms.2018.33.e154

Kim, J. H., Hwang, J.-Y., Hwang, H. R., Kim, H. S., Lee, J. H., Seo, J.-W., Shin, U. S., & Lee, S.-H. (2018). Polydimethylsiloxane composite for wearable electronics. *Scientific Reports*, 12.

Kim, J. H., Lee, S. M., & Lee, S.-H. (2014). Capacitive monitoring of bio and neuro signals. *Biomedical Engineering Letters*, *4*(2), 142-148. https://doi.org/10.1007/s13534-014-0139-x

Kim, M., Kim, T., Kim, D., & Chung, W. (2015). Curved Microneedle Array-Based sEMG Electrode for Robust Long-Term Measurements and High Selectivity. *Sensors*, *15*(7), 16265-16280. https://doi.org/10.3390/s150716265

Knight, J. F., & Baber, C. (2005). A Tool to Assess the Comfort of Wearable Computers. *Human Factors: The Journal of the Human Factors and Ergonomics Society*, *47*(1), 77-91. https://doi.org/10.1518/0018720053653875

Kouediatouka, A. N., Liu, Q., Mawignon, F. J., Wang, W., Wang, J., Ruan, C., Yeo, K. F. H., & Dong, G. (2023). Sensing characterization of an amorphous PDMS/Ecoflex blend composites with an improved interfacial bonding and rubbing performance. *Applied Surface Science*, *635*, 157675. https://doi.org/10.1016/j.apsusc.2023.157675

Krachunov, S., & Casson, A. (2016). 3D Printed Dry EEG Electrodes. *Sensors*, *16*(10), 1635. https://doi.org/10.3390/s16101635

Kremer, F., & Schönhals, A. (Éds.). (2003). *Broadband Dielectric Spectroscopy*. Springer Berlin Heidelberg. https://doi.org/10.1007/978-3-642-56120-7

Krieger, K. J., Bertollo, N., Dangol, M., Sheridan, J. T., Lowery, M. M., & O'Cearbhaill, E. D. (2019). Simple and customizable method for fabrication of high-aspect ratio microneedle molds using low-cost 3D printing. *Microsystems & Nanoengineering*, *5*(1), 42. https://doi.org/10.1038/s41378-019-0088-8

Kuester, S., Merlini, C., Barra, G. M. O., Ferreira, J. C., Lucas, A., de Souza, A. C., & Soares, B. G. (2016). Processing and characterization of conductive composites based on poly(styrene-b-ethylene-ran-butylene-b-styrene) (SEBS) and carbon additives : A comparative study of expanded graphite and carbon black. *Composites Part B: Engineering*, *84*, 236-247. https://doi.org/10.1016/j.compositesb.2015.09.001

Kumar, V., Manikkavel, A., Yewale, M. A., Alam, Md. N., & Park, S.-S. (2024). Lightweight, compressible, stretchable, ultra-soft, and mechanically stable composites for piezo-electric energy generators and strain sensing. *Materials Research Bulletin*, *179*, 112962. https://doi.org/10.1016/j.materresbull.2024.112962

Kushwah, P., Tiwari, V., Shukla, S. K., & Tiwari, A. (2025). Advancements in EEG and EMG Signals for Motor Imagery Classification and Artifact Removal : A Comprehensive Review and Analysis. *2025 IEEE International Conference on Interdisciplinary Approaches in Technology and Management for Social Innovation (IATMSI)*, 1-6. https://doi.org/10.1109/IATMSI64286.2025.10984968

Lahittete, G. (s. d.-a). *Etude de l'auto-assemblage de copolymères à blocs induit par photopolymérisation pour l'impression 3D*.

Lahittete, G. (s. d.-b). *Etude de l'auto-assemblage de copolymères à blocs induit par photopolymérisation pour l'impression 3D*.

Latko, P., Bogucka, A., & Boczkowska, A. (2015). Characterization of Thermoplastic Elastomers Based Composites Doped with Carbon Black. *International Journal of Mechanical Engineering and Automation*, *2*(4), 171-176.

Leach, S., Chung, K., Tüshaus, L., Huber, R., & Karlen, W. (2020). A Protocol for Comparing Dry and Wet EEG Electrodes During Sleep. *Frontiers in Neuroscience*, *14*. https://www.frontiersin.org/article/10.3389/fnins.2020.00586

Lee, B.-H., & Yin, K. (2024). *Towards a Network Expansion Approach for Reliable Brain-Computer Interface* (arXiv:2411.11872). arXiv. https://doi.org/10.48550/arXiv.2411.11872

Lee, E. K., Baruah, R. K., Bhamra, H., Kim, Y.-J., & Yoo, H. (2021). Recent advances in electrode development for biomedical applications. *Biomedical Engineering Letters*, *11*(2), 107-115. https://doi.org/10.1007/s13534-021-00189-6

Lee, G., Ma, Y., Lee, Y., & Jung, H. (2018). Clinical Evaluation of a Low-pain Long Microneedle for Subcutaneous Insulin Injection. *BioChip Journal*, *12*(4), 309-316. https://doi.org/10.1007/s13206-018-2411-0

Lee, J. H., Hwang, J.-Y., Zhu, J., Hwang, H. R., Lee, S. M., Cheng, H., Lee, S.-H., & Hwang, S.-W. (2018). Flexible Conductive Composite Integrated with Personal Earphone for Wireless, Real-Time Monitoring of Electrophysiological Signs. *ACS Applied Materials & Interfaces*, *10*(25), 21184-21190. https://doi.org/10.1021/acsami.8b06484

Lee, O., & Lee, H. (2024). Development and printing of three-dimensional electrodes for the high body adhesion of smart wear. *Fashion and Textiles*, *11*(1), 29. https://doi.org/10.1186/s40691-024-00392-w

Lee, S. M., Byeon, H. J., Lee, J. H., Baek, D. H., Lee, K. H., Hong, J. S., & Lee, S.-H. (2014). Self-adhesive epidermal carbon nanotube electronics for tether-free long-term continuous recording of biosignals. *Scientific Reports*, *4*(1), 6074. https://doi.org/10.1038/srep06074

Lee, S. M., Kim, J. H., Byeon, H. J., Choi, Y. Y., Park, K. S., & Lee, S.-H. (2013). A capacitive, biocompatible and adhesive electrode for long-term and cap-free monitoring of EEG signals. *Journal of Neural Engineering*, *10*(3), 036006. https://doi.org/10.1088/1741-2560/10/3/036006

Lee, S. M., Kim, J. H., Park, C., Hwang, J., Hong, J. S., Lee, K. H., & Lee, S. H. (2016a). Self-Adhesive and Capacitive Carbon Nanotube-Based Electrode to Record Electroencephalograph Signals From the Hairy Scalp. *IEEE Transactions on Biomedical Engineering*, *63*(1), 138-147. https://doi.org/10.1109/TBME.2015.2478406

Lee, S. M., Kim, J. H., Park, C., Hwang, J.-Y., Hong, J. S., Lee, K. H., & Lee, S. H. (2016b). Self-Adhesive and Capacitive Carbon Nanotube-Based Electrode to Record Electroencephalograph Signals From the Hairy Scalp. *IEEE TRANSACTIONS ON BIOMEDICAL ENGINEERING*, *63*(1), 10.

Lee, S. M., Sim, K. S., Kim, K. K., Lim, Y. G., & Park, K. S. (2010). Thin and flexible active electrodes with shield for capacitive electrocardiogram measurement. *Medical &*

Biological Engineering & Computing, *48*(5), 447-457. https://doi.org/10.1007/s11517-010-0597-y

Lee, Y.-H., Wu, C.-L., Lai, C.-W., & Huang, J.-X. (2025a). Thin, Lightweight, and Highly Efficient Electromagnetic Interference Shielding Nanocomposites Composed of a π-Conjugated Block Copolymer Nanowire/Multiwalled Carbon Nanotube Bicontinuous Interpenetrating Network. *ACS Omega*, *10*(14), 14296-14305. https://doi.org/10.1021/acsomega.5c00452

Lee, Y.-H., Wu, C.-L., Lai, C.-W., & Huang, J.-X. (2025b). Thin, Lightweight, and Highly Efficient Electromagnetic Interference Shielding Nanocomposites Composed of a π-Conjugated Block Copolymer Nanowire/Multiwalled Carbon Nanotube Bicontinuous Interpenetrating Network. *ACS Omega*, *10*(14), 14296-14305. https://doi.org/10.1021/acsomega.5c00452

Leleux, P., Badier, J., Rivnay, J., Bénar, C., Hervé, T., Chauvel, P., & Malliaras, G. G. (2014). Conducting Polymer Electrodes for Electroencephalography. *Advanced Healthcare Materials*, *3*(4), 490-493. https://doi.org/10.1002/adhm.201300311

Li, C., Ma, S., Han, X., Sun, Y., Li, C., Zheng, K., Xin, Y., & Li, R. (2025). Malleable, Self-Healing, and Highly Thermally Conductive Interface Material Enabled by Interfacial Networks for Thermal Management. *ACS Applied Materials & Interfaces*, *17*(30), 43655-43668. https://doi.org/10.1021/acsami.5c09314

Li, G., Chen, N., Xu, T., & Zhang, Y. (2025). Flexible Fe3 +-doped gelatin/poly(acrylate-co-acrylamide) conductive hydrogels for biopotential acquisition, salt recognition, and supercapacitors. *Sensors and Actuators A: Physical*, *387*, 116425. https://doi.org/10.1016/j.sna.2025.116425

Li, G., Deng, Z., Cai, M., Huang, K., Guo, M., Zhang, P., Hou, X., Zhang, Y., Wang, Y., Wang, Y., Wu, X., & Guo, C. F. (2021). A stretchable and adhesive ionic conductor based on polyacrylic acid and deep eutectic solvents. *Npj Flexible Electronics*, *5*(1), 23. https://doi.org/10.1038/s41528-021-00118-8

Li, G., Liu, Y., Chen, Y., Li, M., Song, J., Li, K., Zhang, Y., Hu, L., Qi, X., Wan, X., Liu, J., He, Q., & Zhou, H. (2023). Polyvinyl alcohol/polyacrylamide double-network hydrogel-based semi-dry electrodes for robust electroencephalography recording at hairy scalp for noninvasive brain–computer interfaces. *Journal of Neural Engineering*, *20*(2), 026017. https://doi.org/10.1088/1741-2552/acc098

Li, G., Wang, S., & Duan, Y. Y. (2018). Towards conductive-gel-free electrodes : Understanding the wet electrode, semi-dry electrode and dry electrode-skin interface impedance using electrochemical impedance spectroscopy fitting. *Sensors and Actuators B: Chemical*, *277*, 250-260. https://doi.org/10.1016/j.snb.2018.08.155

Li, G., Wang, S., Li, M., & Duan, Y. Y. (2021). Towards real-life EEG applications : Novel superporous hydrogel-based semi-dry EEG electrodes enabling automatically 'charge–discharge' electrolyte. *Journal of Neural Engineering*, *18*(4), 046016. https://doi.org/10.1088/1741-2552/abeeab

Li, G., Wu, J., Xia, Y., Wu, Y., Tian, Y., Liu, J., Chen, D., & He, Q. (2020). Towards emerging EEG applications : A novel printable flexible Ag/AgCl dry electrode array for robust recording of EEG signals at forehead sites. *Journal of Neural Engineering*, *17*(2), 026001. https://doi.org/10.1088/1741-2552/ab71ea

Li, G.-L., Wu, J.-T., Xia, Y.-H., He, Q.-G., & Jin, H.-G. (2020a). Review of semi-dry electrodes for EEG recording. *Journal of Neural Engineering*, *17*(5), 051004. https://doi.org/10.1088/1741-2552/abbd50

Li, G.-L., Wu, J.-T., Xia, Y.-H., He, Q.-G., & Jin, H.-G. (2020b). Review of semi-dry electrodes for EEG recording. *Journal of Neural Engineering*, *17*(5), 051004. https://doi.org/10.1088/1741-2552/abbd50

Li, J., Ma, Y., Huang, D., Wang, Z., Zhang, Z., Ren, Y., Hong, M., Chen, Y., Li, T., Shi, X., Cao, L., Zhang, J., Jiao, B., Liu, J., Sun, H., & Li, Z. (2022). High-Performance Flexible Microneedle Array as a Low-Impedance Surface Biopotential Dry Electrode for Wearable Electrophysiological Recording and Polysomnography. *Nano-Micro Letters*, *14*(1), 132. https://doi.org/10.1007/s40820-022-00870-0

Li, J.-W., Chen, H.-F., Liu, Y.-Z., Wang, J.-H., Lu, M.-C., & Chiu, C.-W. (2024). Photocurable 3D-printed AgNPs/Graphene/Polymer nanocomposites with high flexibility and stretchability for ECG and EMG smart clothing. *Chemical Engineering Journal*, *484*, 149452. https://doi.org/10.1016/j.cej.2024.149452

Li, P., Huang, J., Li, M., & Li, H. (2022). Evaluation of flexible multi-claw and multi-channel semi-dry electrodes for evoked electroencephalography recording. *Sensors and Actuators A: Physical*, *340*, 113547. https://doi.org/10.1016/j.sna.2022.113547

Li, P., Wang, C., Li, M., Xuan, X., Zhou, B., & Li, H. (2023). Flexible Silver/Carbon Nanotube-Graphene Oxide-Polydimethylsiloxane Electrode Patch for Electroencephalography Language. *Advanced Intelligent Systems*, *5*(8), 2300018. https://doi.org/10.1002/aisy.202300018

Li, X., Tian, C., Li, H., Liu, X., Zhang, L., Hong, S., Ning, N., & Tian, M. (2022). Combined effect of volume fractions of nanofillers and filler-polymer interactions on 3D multiscale dispersion of nanofiller and Payne effect. *Composites Part A: Applied Science and Manufacturing*, *152*, 106722. https://doi.org/10.1016/j.compositesa.2021.106722

Li, X., Wang, Z., Liu, T., Li, G., Wei, Y., & Wang, X. (2025). Mechanical and electrical properties of PP composite modified by SEBS used for high voltage cable. *Engineering Fracture Mechanics*, *315*, 110807. https://doi.org/10.1016/j.engfracmech.2025.110807

Li, Y., Wei, H., Chen, L., Xie, C., Ding, H., Fang, F., Chai, Z., & Huang, Q. (2024). Regulating the Electronic Structure of MAX Phases Based on Rare Earth Element Sc to Enhance Electromagnetic Wave Absorption. *ACS Nano*, *18*(14), 10019-10030. https://doi.org/10.1021/acsnano.3c11585

Li, Y., Zhao, M., Yan, Y., He, L., Wang, Y., Xiong, Z., Wang, S., Bai, Y., Sun, F., Lu, Q., Wang, Y., Li, T., & Zhang, T. (2022). Multifunctional biomimetic tactile system via a stick-slip sensing strategy for human–machine interactions. *Npj Flexible Electronics*, *6*(1), 46. https://doi.org/10.1038/s41528-022-00183-7

Li, Y., Zhou, W., Liu, C., Geng, D., Dai, J., Xie, Y., Chen, S., Luo, T., & Shen, Z. (2021). Fabrication and characteristic of flexible dry bioelectrodes with microstructures inspired by golden margined century plant leaf. *Sensors and Actuators A: Physical*, *321*, 112397. https://doi.org/10.1016/j.sna.2020.112397

Lim, Y. G., Kim, K. K., & Park, K. S. (2007). ECG Recording on a Bed During Sleep Without Direct Skin-Contact. *IEEE Transactions on Biomedical Engineering*, *54*(4), 718-725. https://doi.org/10.1109/TBME.2006.889194

Lim, Y. G., Lee, J. S., Lee, S. M., Lee, H. J., & Park, K. S. (2014). Capacitive Measurement of ECG for Ubiquitous Healthcare. *Annals of Biomedical Engineering*, *42*(11), 2218-2227. https://doi.org/10.1007/s10439-014-1069-6

Lin, B.-S., Wang, H.-A., Huang, Y.-K., Wang, Y.-L., & Lin, B.-S. (2021). Design of SSVEP Enhancement-Based Brain Computer Interface. *IEEE Sensors Journal*, *21*(13), 14330-14338. https://doi.org/10.1109/JSEN.2020.3033470

Lin, C.-T., Liao, L.-D., Liu, Y.-H., Wang, I.-J., Lin, B.-S., & Chang, J.-Y. (2011). Novel dry polymer foam electrodes for long-term EEG measurement. *IEEE Transactions on Bio-Medical Engineering*, *58*(5), 1200-1207. https://doi.org/10.1109/TBME.2010.2102353

Lin, H., Wang, J., Cao, W., Wang, H., Rui, K., Yan, Y., & Zhu, J. (2024). Hierarchical conducting networks constructed as resistive strain sensors for personal healthcare monitoring and robotic arm control. *Chemical Engineering Journal*, *490*, 151840. https://doi.org/10.1016/j.cej.2024.151840

Lin, S., Jiang, J., Huang, K., Li, L., He, X., Du, P., Wu, Y., Liu, J., Li, X., Huang, Z., Zhou, Z., Yu, Y., Gao, J., Lei, M., & Wu, H. (2023). Advanced Electrode Technologies for Noninvasive Brain–Computer Interfaces. *ACS Nano*, *17*(24), 24487-24513. https://doi.org/10.1021/acsnano.3c06781

Lin, S., Liu, J., Li, W., Wang, D., Huang, Y., Jia, C., Li, Z., Murtaza, M., Wang, H., Song, J., Liu, Z., Huang, K., Zu, D., Lei, M., Hong, B., & Wu, H. (2019). A Flexible, Robust, and Gel-Free Electroencephalogram Electrode for Noninvasive Brain-Computer

Interfaces. *Nano Letters*, *19*(10), 6853-6861. https://doi.org/10.1021/acs.nanolett.9b02019

Litkohi, H. R., Bahari, A., & Gatabi, M. P. (2021). Pt/Fe/Ni decorated CVD grown CNTs on carbon paper as electrocatalytic electrodes in polymer fuel cells : An investigation on H2 gas on the growth of CNTs and reduction of electrocatalysts. *Diamond and Related Materials*, *119*, 108534. https://doi.org/10.1016/j.diamond.2021.108534

Liu, C., Cai, Y., Liang, T., Zang, T., Fei, G., & Xia, H. (2025). Additive manufacturing flexible, conductive and self-healing polydimethylsiloxane carbon nanotubes composites for electromagnetic interference shielding and microwave absorption. *Chemical Engineering Journal*, *520*, 165717. https://doi.org/10.1016/j.cej.2025.165717

Liu, M., Sheng, Y., Huang, C., Zhou, Y., Jiang, L., Tian, M., Chen, S., Jerrams, S., Zhou, F., & Yu, J. (2023a). Highly stretchable and sensitive SBS/Gr/CNTs fibers with hierarchical structure for strain sensors. *Composites Part A: Applied Science and Manufacturing*, *164*, 107296. https://doi.org/10.1016/j.compositesa.2022.107296

Liu, M., Sheng, Y., Huang, C., Zhou, Y., Jiang, L., Tian, M., Chen, S., Jerrams, S., Zhou, F., & Yu, J. (2023b). Highly stretchable and sensitive SBS/Gr/CNTs fibers with hierarchical structure for strain sensors. *Composites Part A: Applied Science and Manufacturing*, *164*, 107296. https://doi.org/10.1016/j.compositesa.2022.107296

Liu, Q., Yang, L., Zhang, Z., Yang, H., Zhang, Y., & Wu, J. (2023). The Feature, Performance, and Prospect of Advanced Electrodes for Electroencephalogram. *Biosensors*, *13*(1), 101. https://doi.org/10.3390/bios13010101

Liu, S., Wang, L., & Gao, R. X. (2024). Cognitive neuroscience and robotics : Advancements and future research directions. *Robotics and Computer-Integrated Manufacturing*, *85*, 102610. https://doi.org/10.1016/j.rcim.2023.102610

Liu, W., Xie, R., Zhu, J., Wu, J., Hui, J., Zheng, X., Huo, F., & Fan, D. (2022). A temperature responsive adhesive hydrogel for fabrication of flexible electronic sensors. *Npj Flexible Electronics*, *6*(1), 68. https://doi.org/10.1038/s41528-022-00193-5

Liu, Y., Wu, X., Zhang, H., Tan, C., Sha, X., Miao, L., Xue, Y., & Li, N. (2025). Self-healing poly(siloxane-urethane) carbon nanotube composites with multi-band repairing capability and efficient recovery have significant photothermal response. *Colloid and Polymer Science*, *303*(8), 1681-1693. https://doi.org/10.1007/s00396-025-05450-3

Lopez-Gordo, M. A., Sanchez-Morillo, D., & Pelayo Valle, F. (2014). Dry EEG electrodes. *Sensors (Basel, Switzerland)*, *14*(7), 12847-12870. https://doi.org/10.3390/s140712847

Lozano, J., & Stoeber, B. (2019). Microspike Array Electrode with Flexible Backing for Biosignal Monitoring. *2019 IEEE SENSORS*, 1-4. https://doi.org/10.1109/SENSORS43011.2019.8956869

Luiz G. Ferreira, & Pimenta, T. C. (2024). Dry Electrodes for Capturing Brain Electrical Signals. *2024 31st International Conference on Mixed Design of Integrated Circuits and System (MIXDES)*, 290-293. https://doi.org/10.23919/MIXDES62605.2024.10613935

Luo, B., Wu, J., Zhang, M., Zhang, Z., Zhang, X., Fang, Z., Xu, Z., & Wu, M. (2023). Surface modification of garnet fillers with a polymeric sacrificial agent enables compatible interfaces of composite solid-state electrolytes. *Chemical Science*, *14*(45), 13067-13079. https://doi.org/10.1039/D3SC04710E

Luo, Y., Guo, H., Wan, W., Deng, P., Zhang, H., & Zhou, X. (2025). Core–shell structured Fe3O4@SnO2-reinforced self-healing polyurethane composite films with enhanced electromagnetic shielding performance. *Journal of Materials Science*, *60*(30), 12783-12802. https://doi.org/10.1007/s10853-025-11250-5

Lv, S., Cao, Z., Ying, Z., Zhang, R., Tian, Y., Gong, W., & Yuan, G. (2023). Flexible, stretchable, wearable electronic skins based on aligned carbon nanotube fiber arrays for motion detection and human–machine interaction. *Sensors and Actuators A: Physical*, *362*, 114634. https://doi.org/10.1016/j.sna.2023.114634

Ma, Z. (2024). Advances in graphene-assisted flexible substrate sensors for human motion monitoring. *International Journal of Electrochemical Science*, *19*(9), 100760. https://doi.org/10.1016/j.ijoes.2024.100760

Madden, J., O'Mahony, C., Thompson, M., O'Riordan, A., & Galvin, P. (2020). Biosensing in dermal interstitial fluid using microneedle based electrochemical devices. *Sensing and Bio-Sensing Research*, *29*, 100348. https://doi.org/10.1016/j.sbsr.2020.100348

Mahato, R., Masiul Islam, Sk., & Singh, S. (2024). Flexible piezo-resistive strain sensors based on silver nanowires and graphene nanoplatelets reinforced polydimethylsiloxane for human motion detection. *Materials Today Communications*, *40*, 110056. https://doi.org/10.1016/j.mtcomm.2024.110056

Mansor, N. H. A., Markom, M. A., Tan, E. S. M. M., & Adom, A. H. (2019). Design and Fabrication of Biodegradable Microneedle Using 3D Rapid Prototyping Printer. *Journal of Physics: Conference Series*, *1372*(1), 012053. https://doi.org/10.1088/1742-6596/1372/1/012053

Mazaheri, M., Payandehpeyman, J., & Jamasb, S. (2022). Modeling of Effective Electrical Conductivity and Percolation Behavior in Conductive-Polymer Nanocomposites Reinforced with Spherical Carbon Black. *Applied Composite Materials*, *29*(2), 695-710. https://doi.org/10.1007/s10443-021-09991-y

Mazitova, A. K., Zaripov, I. I., Aminova, G. K., Ovod, M. V., & Suntsova, N. L. (2022). Fillers for polymer composite materials. *Nanotechnologies in Construction A Scientific Internet-Journal*, *14*(4), 294-299. https://doi.org/10.15828/2075-8545-2022-14-4-294-299

McCrum, N. G., Buckley, C. P., & Bucknall, C. B. (1997). *Principles of Polymer Engineering* (2nd éd.). Oxford : Oxford University Press.

Méndez, R., Constant, B., Garzon, C., Nisar, M., Nachtigall, S. M. B., & Quijada, R. (2017). Barrier, mechanical and conductive properties of polycaprolactam nanocomposites containing carbon-based particles : Effect of the kind of particle. *Polymer*, *130*, 10-16. https://doi.org/10.1016/j.polymer.2017.09.063

Meng, Y., Li, Z., & Chen, J. (2016). A flexible dry electrode based on APTES-anchored PDMS substrate for portable ECG acquisition system. *Microsystem Technologies*, *22*(8), 2027-2034. https://doi.org/10.1007/s00542-015-2490-y

Mermi Dibek, D., & Baykan, B. (2025). Eye closure sensitivity and related EEG findings : Persistence rates and classification of epilepsy syndromes by the International League Against Epilepsy. *Epileptic Disorders*, *27*(3), 407-419. https://doi.org/10.1002/epd2.70014

Mohd Radzuan, N. A., Sulong, A. B., & Sahari, J. (2017). A review of electrical conductivity models for conductive polymer composite. *International Journal of Hydrogen Energy*, *42*(14), 9262-9273. https://doi.org/10.1016/j.ijhydene.2016.03.045

Mondal, S., Nayak, L., Rahaman, M., Aldalbahi, A., Chaki, T. K., Khastgir, D., & Das, N. C. (2017). An effective strategy to enhance mechanical, electrical, and electromagnetic shielding effectiveness of chlorinated polyethylene-carbon nanofiber nanocomposites. *Composites Part B: Engineering*, *109*, 155-169. https://doi.org/10.1016/j.compositesb.2016.10.049

Moradbeigi, N., Bahari, A., & Ghasemi, S. (2023). Effect of molybdenum doping on the catalytic activity of VS_2 /CNT for the oxygen reduction reaction in alkaline media. *New Journal of Chemistry*, *47*(3), 1291-1298. https://doi.org/10.1039/D2NJ04721G

Motiepor, K., Bakhtiyari, S., Jahanshahi, A., & Bagherzadeh, R. (2025). Stretchable clutter-free E-textile EEG cap : Advancing seamless wearable solutions for emerging neuroimaging applications. *Sensors and Actuators A: Physical*, *387*, 116454. https://doi.org/10.1016/j.sna.2025.116454

Moumane, H. (s. d.). *From Scalp to Ear : Validation and Neural Source Analysis of Dry-Contact In-Ear EEG*.

Nath, K., Ghosh, S., Ghosh, S. K., Das, P., & Das, N. Ch. (2021). Facile preparation of light-weight biodegradable and electrically conductive polymer based nanocomposites for superior electromagnetic interference shielding effectiveness. *Journal of Applied Polymer Science*, *138*(22), 50514. https://doi.org/10.1002/app.50514

Nayak, J., Choudhary, S. N., Pal, A., Biswas, S., Giri, S., Banerji, P., & Das, N. C. (2025). Synergistic effect of MWCNT and $CoFe_2O_4$ in ethylene-octene copolymer foam for

electromagnetic interference shielding and thermal management. *Journal of Alloys and Compounds*, *1038*, 182718. https://doi.org/10.1016/j.jallcom.2025.182718

Niu, X., Gao, X., Liu, Y., & Liu, H. (2021). Surface bioelectric dry Electrodes : A review. *Measurement*, *183*, 109774. https://doi.org/10.1016/j.measurement.2021.109774

Oh, J., Nam, K.-W., Kim, W.-J., Kang, B.-H., & Park, S.-H. (2024a). Flexible Dry Electrode Based on a Wrinkled Surface That Uses Carbon Nanotube/Polymer Composites for Recording Electroencephalograms. *Materials*, *17*(3), 668. https://doi.org/10.3390/ma17030668

Oh, J., Nam, K.-W., Kim, W.-J., Kang, B.-H., & Park, S.-H. (2024b). Flexible Dry Electrode Based on a Wrinkled Surface That Uses Carbon Nanotube/Polymer Composites for Recording Electroencephalograms. *Materials*, *17*(3), 668. https://doi.org/10.3390/ma17030668

Olonisakin, K., Fan, M., Xin-Xiang, Z., Ran, L., Lin, W., Zhang, W., & Wenbin, Y. (2022). Key Improvements in Interfacial Adhesion and Dispersion of Fibers/Fillers in Polymer Matrix Composites; Focus on PLA Matrix Composites. *Composite Interfaces*, *29*(10), 1071-1120. https://doi.org/10.1080/09276440.2021.1878441

OpenBCI. (s. d.-a). *Cyton Biosensing Board (8-channels)*. https://doi.org/https://shop.openbci.com/products/cyton-biosensing-board-8-channel?pr_prod_strat=e5_desc&pr_rec_id=f0dfb9db3&pr_rec_pid=10306285518&pr_ref_pid=8393516155120&pr_seq=uniform

OpenBCI. (s. d.-b). *The Complete Ultracortex*. https://doi.org/https://shop.openbci.com/products/the-complete-headset-eeg

OpenBCI. (s. d.-c). *ThinkPulse™ Active Electrode Add-on Kits*. https://doi.org/https://shop.openbci.com/products/thinkpulse-active-electrode-kit?pr_prod_strat=jac&pr_rec_id=f0dfb9db3&pr_rec_pid=5952040698014&pr_ref_pid=8393516155120&pr_seq=uniform

OpenBCI. (s. d.-d). *Ultracortex « Mark IV » EEG Headset*. https://doi.org/https://shop.openbci.com/collections/frontpage/products/ultracortex-mark-iv

Oswald, T. A., & Mendes, G. (2012a). *Materials Science of Polymers for Engineers* (3rd éd.). Hanser Verlag,.

Oswald, T. A., & Mendes, G. (2012b). Structure of Polymers. In *Materials Science of Polymers for Engineers* (3rd éd.). Hanser Verlag,.

Öztürkmen, M. B., Özkutlu Demirel, M., Ağaç, Ö., Ece, R. E., & Öz, Y. (2023). Tailored multifunctional nanocomposites obtained by integration of carbonaceous fillers in an aerospace grade epoxy resin curing at high temperatures. *Diamond and Related Materials*, *135*, 109840. https://doi.org/10.1016/j.diamond.2023.109840

P, P. (2023). Electrochemical Detection of Uropathogenic Escherichia Coli Using PVA/R-GO/PEI Modified Nanocomposite Electrode. *Engineered Science*. https://doi.org/10.30919/es903

Palumbo, A., Gramigna, V., Calabrese, B., Ielpo, N., & Demeco, A. (2024). A Wearable Device-Based System : The Potential Role in Real-time and Remote EEG Monitoring. *Frontiers in Biomedical Technologies*. https://doi.org/10.18502/fbt.v11i3.15882

Pan, C., Chen, K., Jiang, L., Chen, Z., Ren, L., Liang, L., & Yuan, W. (2016). Magnetization-induced self-assembly method : Micro-needle array fabrication. *Journal of Materials*

Processing Technology, *227*, 251-258. https://doi.org/10.1016/j.jmatprotec.2015.08.025

Park, S.-J., Kim, M.-H., & Ha, T.-J. (2023). All-printed wearable humidity sensor with hydrophilic polyvinylpyrrolidone film for mobile respiration monitoring. *Sensors and Actuators B: Chemical*, *394*, 134395. https://doi.org/10.1016/j.snb.2023.134395

Park, Y.-J., Joo, H.-S., Kim, H.-J., & Lee, Y.-K. (2006). Adhesion and rheological properties of EVA-based hot-melt adhesives. *International Journal of Adhesion and Adhesives*, *26*(8), 571-576. https://doi.org/10.1016/j.ijadhadh.2005.09.004

Paul, S. J., Srivastava, S., Tawale, J. S., & Gupta, B. K. (2023). Three-dimensional CNT-rGO/PDMS porous scaffold derived supercompressible lightweight body-mounted piezoresistive force sensor for human motion monitoring. *Colloids and Surfaces A: Physicochemical and Engineering Aspects*, *675*, 131993. https://doi.org/10.1016/j.colsurfa.2023.131993

Pavlovsky, S., & Siegmann, A. (2009). Chemical sensing materials. I. Electrically conductive SEBS copolymer systems. *Journal of Applied Polymer Science*, *113*(5), 3322-3329. https://doi.org/10.1002/app.30310

Pavlyuchkova, E. A., Malkin, A. Ya., Kornev, Y. V., & Simonov-Emel'yanov, I. D. (2024). Distribution of Filler in Polymer Composites. Role of Particle Size and Concentration. *Polymer Science, Series A*, *66*(1), 113-120. https://doi.org/10.1134/S0965545X24600236

Pedrosa, P., Fiedler, P., Lopes, C., Alves, E., Barradas, N. P., Haueisen, J., Machado, A. V., Fonseca, C., & Vaz, F. (2016). Ag:TiN-Coated Polyurethane for Dry Biopotential Electrodes : From Polymer Plasma Interface Activation to the First EEG

Measurements. *Plasma Processes and Polymers*, *13*(3), 341-354. https://doi.org/10.1002/ppap.201500063

Pedrosa, P., Machado, D., Lopes, C., Alves, E., Barradas, N. P., Martin, N., Macedo, F., Fonseca, C., & Vaz, F. (2013). Nanocomposite Ag:TiN thin films for dry biopotential electrodes. *Applied Surface Science*, *285*, 40-48. https://doi.org/10.1016/j.apsusc.2013.07.154

Peng, H.-L., Jing-Quan Liu, Tian, H.-C., Dong, Y.-Z., Yang, B., Chen, X., & Yang, C.-S. (2016). A novel passive electrode based on porous Ti for EEG recording. *Sensors and Actuators B: Chemical*, *226*, 349-356. https://doi.org/10.1016/j.snb.2015.11.141

Peng, H.-L., Liu, J.-Q., Dong, Y.-Z., Yang, B., Chen, X., & Yang, C.-S. (2016). Parylene-based flexible dry electrode for bioptential recording. *Sensors and Actuators B: Chemical*, *231*, 1-11. https://doi.org/10.1016/j.snb.2016.02.061

Peng, H.-L., Liu, J.-Q., Tian, H.-C., Xu, B., Dong, Y.-Z., Yang, B., Chen, X., & Yang, C.-S. (2015). Flexible dry electrode based on carbon nanotube/polymer hybrid micropillars for biopotential recording. *Sensors and Actuators A: Physical*, *235*, 48-56. https://doi.org/10.1016/j.sna.2015.09.024

Peng, Y., Dong, J., Zhang, Y., Zhang, Y., Long, J., Sun, J., Liu, T., & Huang, Y. (2024). Thermally comfortable epidermal bioelectrodes based on ultrastretchable and passive radiative cooling e-textiles. *Nano Energy*, *120*, 109143. https://doi.org/10.1016/j.nanoen.2023.109143

Peng, Y., Lin, Y., Fan, C., Xu, Q., Xu, D., Yi, S., Zhang, H., & Wang, K. (2022). Passenger overall comfort in high-speed railway environments based on EEG : Assessment and

degradation mechanism. *Building and Environment*, *210*, 108711. https://doi.org/10.1016/j.buildenv.2021.108711

Petrossian, G., Kateb, P., Miquet-Westphal, F., & Cicoira, F. (2023). Advances in Electrode Materials for Scalp, Forehead, and Ear EEG : A Mini-Review. *ACS Applied Bio Materials*, *6*(8), 3019-3032. https://doi.org/10.1021/acsabm.3c00322

Ponnamma, D., Sadasivuni, K. K., Strankowski, M., Kasak, P., Krupa, I., & AlMaadeed, M. A.-A. (2016). Eco-Friendly Electromagnetic Interference Shielding Materials from Flexible Reduced Graphene Oxide Filled Polycaprolactone/Polyaniline Nanocomposites. *Polymer-Plastics Technology and Engineering*, *55*(9), 920-928. https://doi.org/10.1080/03602559.2015.1132435

Portelli, A., & Nasuto, S. (2017). Design and Development of Non-Contact Bio-Potential Electrodes for Pervasive Health Monitoring Applications. *Biosensors*, *7*(4), 2. https://doi.org/10.3390/bios7010002

Promsung, R., Georgopoulou, A., Nakaramontri, Y., Kalkornsurapranee, E., & Clemens, F. (2024). Piezoresistive properties for soft structures using hybrid CCB/CNT-based natural rubber latex composites. *Applied Materials Today*, *39*, 102302. https://doi.org/10.1016/j.apmt.2024.102302

Qi, F., Li, C., Jing, Y., & Chen, F. (2025). Precision-and-flexibility optimized wearable dual-channel EEG acquisition system. *Discover Applied Sciences*, *7*(2), 102. https://doi.org/10.1007/s42452-025-06516-1

Qin, Y., Zhang, C., Wang, Y., She, P., & Wong, W. (2025). Electrostatic Attraction-Driven Assembly of Non-Noble Metallo-Supramolecular Polymers With Single-Walled

Carbon Nanotubes for Boosting Photocatalytic Hydrogen Evolution. *Carbon Energy*, *7*(6), e70003. https://doi.org/10.1002/cey2.70003

Rahman, M., Karwowski, W., Sapkota, N., Ismail, L., Alhujailli, A., Sumano, R. F., & Hancock, P. A. (2023). Isometric Arm Forces Exerted by Females at Different Levels of Physical Comfort and Their EEG Signatures. *Brain Sciences*, *13*(7), 1027. https://doi.org/10.3390/brainsci13071027

Ramon, C., Garguilo, P., Fridgeirsson, E. A., & Haueisen, J. (2014). Changes in scalp potentials and spatial smoothing effects of inclusion of dura layer in human head models for EEG simulations. *Frontiers in Neuroengineering*, *7*. https://doi.org/10.3389/fneng.2014.00032

Raspopovic, S., Valle, G., & Petrini, F. M. (2021). Sensory feedback for limb prostheses in amputees. *Nature Materials*, *20*(7), 925-939. https://doi.org/10.1038/s41563-021-00966-9

Ren, H., Zheng, Z., Zhang, J., Wang, Q., & Wang, Y. (2024). Electroencephalography (EEG)-Based Comfort Evaluation of Free-Form and Regular-Form Landscapes in Virtual Reality. *Applied Sciences*, *14*(2), 933. https://doi.org/10.3390/app14020933

Ren, L., Jiang, Q., Chen, K., Chen, Z., Pan, C., & Jiang, L. (2016). Fabrication of a Micro-Needle Array Electrode by Thermal Drawing for Bio-Signals Monitoring. *Sensors*, *16*(6), 908. https://doi.org/10.3390/s16060908

Ren, L., Jiang, Q., Chen, Z., Chen, K., Xu, S., Gao, J., & Jiang, L. (2017). Flexible microneedle array electrode using magnetorheological drawing lithography for bio-signal monitoring. *Sensors and Actuators A: Physical*, *268*, 38-45. https://doi.org/10.1016/j.sna.2017.10.042

Robertson, M., Guillen-Obando, A., Barbour, A., Smith, P., Griffin, A., & Qiang, Z. (2023). Direct synthesis of ordered mesoporous materials from thermoplastic elastomers. *Nature Communications*, *14*(1), 639. https://doi.org/10.1038/s41467-023-36362-x

Ruffini, G., Dunne, S., Farrés, E., Marco-Pallarés, J., Ray, C., Mendoza, E., Silva, R., & Grau, C. (2006). A dry electrophysiology electrode using CNT arrays. *Sensors and Actuators A: Physical*, *132*(1), 34-41. https://doi.org/10.1016/j.sna.2006.06.013

Sanguantrakul, J., Hemakom, A., Soonrach, T., & Israsena, P. (2024). PDMS/CNT electrodes with bioamplifier for practical in-the-ear and conventional biosignal recordings. *Journal of Neural Engineering*, *21*(5), 056017. https://doi.org/10.1088/1741-2552/ad7905

Sayyad, P. W., Al-Nashash, H., Al-Othman, A., & Al-Sayah, M. H. (2025a). Emerging trends in system-integrated wearable epidermal and flexible electrodes : Material design and applications in physiological monitoring. *IEEE Transactions on Components, Packaging and Manufacturing Technology*, 1-1. https://doi.org/10.1109/TCPMT.2025.3539978

Sayyad, P. W., Al-Nashash, H., Al-Othman, A., & Al-Sayah, M. H. (2025b). Emerging trends in system-integrated wearable epidermal and flexible electrodes : Material design and applications in physiological monitoring. *IEEE Transactions on Components, Packaging and Manufacturing Technology*, 1-1. https://doi.org/10.1109/TCPMT.2025.3539978

Sayyad, P. W., Park, S.-J., & Ha, T.-J. (2024). Bioinspired nanoplatforms for human-machine interfaces : Recent progress in materials and device applications. *Biotechnology Advances*, *70*, 108297. https://doi.org/10.1016/j.biotechadv.2023.108297

Shad, E. H. T., Molinas, M., & Ytterdal, T. (2020). Impedance and Noise of Passive and Active Dry EEG Electrodes : A Review. *IEEE Sensors Journal*, *20*(24), 14565-14577. https://doi.org/10.1109/JSEN.2020.3012394

Shafiee, M., & Ramazani S.A., A. (2008). Investigation of Barrier Properties of Poly(ethylene vinyl acetate)/Organoclay Nanocomposite Films Prepared by Phase Inversion Method. *Macromolecular Symposia*, *274*(1), 1-5. https://doi.org/10.1002/masy.200851401

Shahmiri, M. R., Bahari, A., Karimi-Maleh, H., Hosseinzadeh, R., & Mirnia, N. (2013). Ethynylferrocene–NiO/MWCNT nanocomposite modified carbon paste electrode as a novel voltammetric sensor for simultaneous determination of glutathione and acetaminophen. *Sensors and Actuators B: Chemical*, *177*, 70-77. https://doi.org/10.1016/j.snb.2012.10.098

Shajari, S., Ramakrishnan, S., Karan, K., Sudak, L. J., & Sundararaj, U. (2022). Ultrasensitive wearable sensor with novel hybrid structures of silver nanowires and carbon nanotubes in fluoroelastomer : Multi-directional sensing for human health monitoring and stretchable electronics. *Applied Materials Today*, *26*, 101295. https://doi.org/10.1016/j.apmt.2021.101295

Sharma, P., Baloda, S., Verma, D., Janyani, V., Sharma, R., & Gupta, N. (2024a). Multiwall Carbon Nanotube/Polydimethylsiloxane Composites-Based Dry Electrodes for Bio-Signal Detection. *IEEE Journal on Flexible Electronics*, *3*(3), 108-114. https://doi.org/10.1109/JFLEX.2024.3367648

Sharma, P., Baloda, S., Verma, D., Janyani, V., Sharma, R., & Gupta, N. (2024b). Multiwall Carbon Nanotube/Polydimethylsiloxane Composites-Based Dry Electrodes for Bio-

Signal Detection. *IEEE Journal on Flexible Electronics*, *3*(3), 108-114. https://doi.org/10.1109/JFLEX.2024.3367648

Shi, S., Ni, X., Ieong, L., Li, L., & Liu, Y. (2025). Comparison of Time–Frequency Characteristics of Lower Limb EMG Signals Among Different Foot Strike Patterns During Running Using the EEMD Algorithm. *Life*, *15*(9), 1386. https://doi.org/10.3390/life15091386

Shi, Z., Jiang, B., Liang, S., Zhang, J., Suo, D., Wu, J., Chen, D., Pei, G., & Yan, T. (2023a). Claw-shaped flexible and low-impedance conductive polymer electrodes for EEG recordings : Anemone dry electrode. *Science China Technological Sciences*, *66*(1), 255-266. https://doi.org/10.1007/s11431-022-2231-3

Shi, Z., Jiang, B., Liang, S., Zhang, J., Suo, D., Wu, J., Chen, D., Pei, G., & Yan, T. (2023b). Claw-shaped flexible and low-impedance conductive polymer electrodes for EEG recordings : Anemone dry electrode. *Science China Technological Sciences*, *66*(1), 255-266. https://doi.org/10.1007/s11431-022-2231-3

Shustak, S., Inzelberg, L., Steinberg, S., Rand, D., David Pur, M., Hillel, I., Katzav, S., Fahoum, F., De Vos, M., Mirelman, A., & Hanein, Y. (2019). Home monitoring of sleep with a temporary-tattoo EEG, EOG and EMG electrode array : A feasibility study. *Journal of Neural Engineering*, *16*(2), 026024. https://doi.org/10.1088/1741-2552/aafa05

Sidheekha, M. P., Shabeeba, A., Rajan, L., Thayyil, M. S., & Ismail, Y. A. (2023). Conducting Polymer/Hydrogel Hybrid Free-Standing Electrodes for Flexible Supercapacitors Capable of Self-Sensing Working Conditions : Large-Scale Fabrication Through Facile and Low-Cost Route. *Engineered Science*. https://doi.org/10.30919/es890

Sinha, S. R., Sullivan, L., Sabau, D., San-Juan, D., Dombrowski, K. E., Halford, J. J., Hani, A. J., Drislane, F. W., & Stecker, M. M. (2016). American Clinical Neurophysiology Society Guideline 1 : Minimum Technical Requirements for Performing Clinical Electroencephalography. *Journal of Clinical Neurophysiology*, *33*(4), 303-307. https://doi.org/10.1097/WNP.0000000000000308

Song, X., Gu, Y., Wang, S., Wang, J., & Yu, L. (2025). Nanowire-Based Flexible Sensors for Wearable Electronics, Brain–Computer Interfaces, and Artificial Skins. *Electron*, e77. https://doi.org/10.1002/elt2.77

Srivastava, A. K., Bhartia, B., Mukhopadhyay, K., & Sharma, A. (2015). Long term biopotential recording by body conformable photolithography fabricated low cost polymeric microneedle arrays. *Sensors and Actuators A: Physical*, *236*, 164-172. https://doi.org/10.1016/j.sna.2015.10.041

Stauffer, F., Thielen, M., Sauter, C., Chardonnens, S., Bachmann, S., Tybrandt, K., Peters, C., Hierold, C., & Vörös, J. (2018a). Skin Conformal Polymer Electrodes for Clinical ECG and EEG Recordings. *Advanced Healthcare Materials*, *7*(7), 1700994. https://doi.org/10.1002/adhm.201700994

Stauffer, F., Thielen, M., Sauter, C., Chardonnens, S., Bachmann, S., Tybrandt, K., Peters, C., Hierold, C., & Vörös, J. (2018b). Skin Conformal Polymer Electrodes for Clinical ECG and EEG Recordings. *Advanced Healthcare Materials*, *7*(7), 1700994. https://doi.org/10.1002/adhm.201700994

Stauffer, F., Thielen, M., Sauter, C., Chardonnens, S., Bachmann, S., Tybrandt, K., Peters, C., Hierold, C., & Vörös, J. (2018c). Skin Conformal Polymer Electrodes for Clinical ECG

and EEG Recordings. *Advanced Healthcare Materials*, *7*(7), 1700994. https://doi.org/10.1002/adhm.201700994

Subramanian, V., Hari Prasad, K., Das, H. T., Ganapathy, K., Nallani, S., & Maiyalagan, T. (2022). Novel Dispersion of 1D Nanofiber Fillers for Fast Ion-Conducting Nanocomposite Polymer Blend Quasi-Solid Electrolytes for Dye-Sensitized Solar Cells. *ACS Omega*, *7*(2), 1658-1670. https://doi.org/10.1021/acsomega.1c03644

Sullivan, T. J., Deiss, S. R., & Cauwenberghs, G. (2007). A Low-Noise, Non-Contact EEG/ECG Sensor. *2007 IEEE Biomedical Circuits and Systems Conference*, 154-157. https://doi.org/10.1109/BIOCAS.2007.4463332

Sumita, M., Sakata, K., Asai, S., Miyasaka, K., & Nakagawa, H. (1991a). Dispersion of fillers and the electrical conductivity of polymer blends filled with carbon black. *Polymer Bulletin*, *25*(2), 265-271. https://doi.org/10.1007/BF00310802

Sumita, M., Sakata, K., Asai, S., Miyasaka, K., & Nakagawa, H. (1991b). Dispersion of fillers and the electrical conductivity of polymer blends filled with carbon black. *Polymer Bulletin*, *25*(2), 265-271. https://doi.org/10.1007/BF00310802

Sun, Y., He, W., Jiang, C., Li, J., Liu, J., & Liu, M. (2025). Wearable Biodevices Based on Two-Dimensional Materials : From Flexible Sensors to Smart Integrated Systems. *Nano-Micro Letters*, *17*(1), 109. https://doi.org/10.1007/s40820-024-01597-w

Svard, D., Cichocki, A., & Alvandpour, A. (2010). Design and evaluation of a capacitively coupled sensor readout circuit, toward contact-less ECG and EEG. *2010 Biomedical Circuits and Systems Conference (BioCAS)*, 302-305. https://doi.org/10.1109/BIOCAS.2010.5709631

Symeonidou, E.-R., Nordin, A. D., Hairston, W. D., & Ferris, D. P. (2018). Effects of Cable Sway, Electrode Surface Area, and Electrode Mass on Electroencephalography Signal Quality during Motion. *Sensors*, *18*(4), Article 4. https://doi.org/10.3390/s18041073

Taji, B., Chan, A. D. C., & Shirmohammadi, S. (2018). Effect of Pressure on Skin-Electrode Impedance in Wearable Biomedical Measurement Devices. *IEEE Transactions on Instrumentation and Measurement*, *67*(8), 1900-1912. https://doi.org/10.1109/TIM.2018.2806950

Tekay, E. (2020). Preparation and characterization of electro-active shape memory PCL/SEBS-g-MA/MWCNT nanocomposites. *Polymer*, *209*, 122989. https://doi.org/10.1016/j.polymer.2020.122989

Tekay, E., Aybakan, B., & Aslan, V. U. (2023). 4D printable maleated poly(styrene-b-ethylene/butylene-b-styrene) / Poly(ethylene-co-vinyl acetate) thermoplastic elastomer blends; effects of blend composition on shape memory and mechanical properties. *Additive Manufacturing*, *78*, 103870. https://doi.org/10.1016/j.addma.2023.103870

Triggiani, A. I., Liuzzi, L., Scheman, K., & Hallett, M. (2025). A brake on the blink : EEG antecedents of movement suppression and urge to move. *Clinical Neurophysiology*, *179*, 2110997. https://doi.org/10.1016/j.clinph.2025.2110997

Ugraskan, V., Isik, B., Yazici, O., & Cakar, F. (2022). Comparative physicochemical characterization of ULTEM/SWCNT nanocomposites : Surface, thermal and electrical conductivity analyses. *Journal of Polymer Research*, *29*(7), 254. https://doi.org/10.1007/s10965-022-03111-5

Van Der Heijden, P., Gilbert, C., Jafari, S., & Lucchini, M. A. (2024). Multi-Channel Soft Dry Electrodes for Electrocardiography Acquisition in the Ear Region. *Sensors*, *24*(2), 420. https://doi.org/10.3390/s24020420

Vasconcelos, B., Fiedler, P., Machts, R., Haueisen, J., & Fonseca, C. (2021). The Arch Electrode : A Novel Dry Electrode Concept for Improved Wearing Comfort. *Frontiers in Neuroscience*, *15*, 748100. https://doi.org/10.3389/fnins.2021.748100

Veronica, A., Nyein, H. Y. Y., & Hsing, I.-M. (2024). Ionogels and eutectogels for stable and long-term EEG and EMG signal acquisition. *Materials Futures*, *3*(3), 033501. https://doi.org/10.1088/2752-5724/ad5c84

Wan, B., Yang, Y., Guo, R., & Yu, X. (2025). Functionalised Conductive Elastomers for Strain Monitoring of Seismic Isolation Bearings : Experiments and Molecular Simulations. *Engineered Science*. https://doi.org/10.30919/es1479

Wang, F., Ma, M., Fu, R., & Zhang, X. (2024). EEG-based detection of driving fatigue using a novel electrode. *Sensors and Actuators A: Physical*, *365*, 114895. https://doi.org/10.1016/j.sna.2023.114895

Wang, H., Wang, X., Li, Y., Liu, Z., Ahmed, M. F., Zhang, X., & Zeng, C. (2023). Piezoelectrets from Cyclic Olefin Copolymers with Different Mechanical and Thermomechanical Properties : A Comparative Study. *Engineered Science*. https://doi.org/10.30919/es8d810

Wang, H., Yan, R., Lin, H., Sun, J., Meng, H., Hou, R., Hao, Y., Hu, S., & Zhang, J. (2025). Improving thermal comfort and cognitive ability of manual workers by cooling garment of different temperatures based on EEG analysis. *Energy and Buildings*, *331*, 115371. https://doi.org/10.1016/j.enbuild.2025.115371

Wang, J., Li, S., Yang, L., Liu, B., Xie, S., Qi, R., Zhan, Y., & Xia, H. (2024). Graphene-Based Hybrid Fillers for Rubber Composites. *Molecules*, *29*(5), 1009. https://doi.org/10.3390/molecules29051009

Wang, J., Qu, R., Ren, B., Wang, Q., Ma, F., Zhang, Y., Li, X., Wang, Y., Sun, C., Song, X., Ma, Q., Jiang, M., & Geng, X. (2025). Lightweight, Flexible, Resilient PMIA-Based Fabric with Superior Electromagnetic Shielding Performance. *Advanced Fiber Materials*, *7*(3), 784-798. https://doi.org/10.1007/s42765-025-00520-1

Wang, J., Wang, T., Liu, H., Wang, K., Moses, K., Feng, Z., Li, P., & Huang, W. (2023). Flexible Electrodes for Brain–Computer Interface System. *Advanced Materials*, *35*(47), 2211012. https://doi.org/10.1002/adma.202211012

Wang, L.-F., Liu, J.-Q., Yang, B., & Yang, C.-S. (2012a). PDMS-Based Low Cost Flexible Dry Electrode for Long-Term EEG Measurement. *IEEE Sensors Journal*, *12*(9), 2898-2904. https://doi.org/10.1109/JSEN.2012.2204339

Wang, L.-F., Liu, J.-Q., Yang, B., & Yang, C.-S. (2012b). PDMS-Based Low Cost Flexible Dry Electrode for Long-Term EEG Measurement. *IEEE Sensors Journal*, *12*(9), 2898-2904. https://doi.org/10.1109/JSEN.2012.2204339

Wang, R., Geng, L., Zhang, X., Liang, G., Zhao, J., & Liu, C. (2025). Synthesis of flexible form stable phase change materials with in-situ formed porous TiO2 for personal thermal management. *Chemical Engineering Journal*, *505*, 159592. https://doi.org/10.1016/j.cej.2025.159592

Wang, R., Jiang, X., Wang, W., & Li, Z. (2017a). A microneedle electrode array on flexible substrate for long-term EEG monitoring. *Sensors and Actuators B: Chemical*, *244*, 750-758. https://doi.org/10.1016/j.snb.2017.01.052

Wang, R., Jiang, X., Wang, W., & Li, Z. (2017b). A microneedle electrode array on flexible substrate for long-term EEG monitoring. *Sensors and Actuators B: Chemical*, *244*, 750-758. https://doi.org/10.1016/j.snb.2017.01.052

Wang, X., Meng, S., Tebyetekerwa, M., Li, Y., Pionteck, J., Sun, B., Qin, Z., & Zhu, M. (2018). Highly sensitive and stretchable piezoresistive strain sensor based on conductive poly(styrene-butadiene-styrene)/few layer graphene composite fiber. *Composites Part A: Applied Science and Manufacturing*, *105*, 291-299. https://doi.org/10.1016/j.compositesa.2017.11.027

Wang, Y., Wang, X., Sandsjö, L., Liu, X., & Guo, L. (2025a). Deploying Partially Cross-Linked Elastomers to Optimize Adhesion for Long-Term Surface Electromyography Electrodes. *Advanced Materials Interfaces*, 2400757. https://doi.org/10.1002/admi.202400757

Wang, Y., Wang, X., Sandsjö, L., Liu, X., & Guo, L. (2025b). Deploying Partially Cross-Linked Elastomers to Optimize Adhesion for Long-Term Surface Electromyography Electrodes. *Advanced Materials Interfaces*, 2400757. https://doi.org/10.1002/admi.202400757

Wang, Z. (2025). Advancements in Materials for Flexible and Soft Brain-Computer Interface. *Highlights in Science, Engineering and Technology*, *125*, 191-196. https://doi.org/10.54097/njrz3g09

Wang, Z., Chen, C., Li, W., Yuan, W., Han, T., Sun, C., Tao, L., Zhao, Y., & Chen, W. (2018). A Multichannel EEG Acquisition System With Novel Ag NWs/PDMS Flexible Dry Electrodes. *Annual International Conference of the IEEE Engineering in Medicine and Biology Society. IEEE Engineering in Medicine and Biology Society. Annual*

International Conference, *2018*, 1299-1302. https://doi.org/10.1109/EMBC.2018.8512563

Wang, Z., Ding, Y., Yuan, W., Chen, H., Chen, W., & Chen, C. (2024a). Active Claw-Shaped Dry Electrodes for EEG Measurement in Hair Areas. *Bioengineering*, *11*(3), 276. https://doi.org/10.3390/bioengineering11030276

Wang, Z., Ding, Y., Yuan, W., Chen, H., Chen, W., & Chen, C. (2024b). Active Claw-Shaped Dry Electrodes for EEG Measurement in Hair Areas. *Bioengineering*, *11*(3), 276. https://doi.org/10.3390/bioengineering11030276

Wang, Z., Ding, Y., Yuan, W., Chen, H., Chen, W., & Chen, C. (2024c). Active Claw-Shaped Dry Electrodes for EEG Measurement in Hair Areas. *Bioengineering*, *11*(3), 276. https://doi.org/10.3390/bioengineering11030276

Wang, Z., Ding, Y., Yuan, W., Chen, H., Chen, W., & Chen, C. (2024d). Active Claw-Shaped Dry Electrodes for EEG Measurement in Hair Areas. *Bioengineering*, *11*(3), 276. https://doi.org/10.3390/bioengineering11030276

Wang, Z., Yi, H., & Li, Z. (2025). Body temperature-triggered phase change dry electrode for long-term comfort electroencephalography monitoring. *National Science Open*, *4*(2), 20240025. https://doi.org/10.1360/nso/20240025

Warsito, I. F., Komosar, M., Bernhard, M. A., Fiedler, P., & Haueisen, J. (2023a). Flower electrodes for comfortable dry electroencephalography. *Scientific Reports*, *13*(1), 16589. https://doi.org/10.1038/s41598-023-42732-8

Warsito, I. F., Komosar, M., Bernhard, M. A., Fiedler, P., & Haueisen, J. (2023b). Flower electrodes for comfortable dry electroencephalography. *Scientific Reports*, *13*(1), 16589. https://doi.org/10.1038/s41598-023-42732-8

Wartzek, T., Lammersen, T., Eilebrecht, B., Walter, M., & Leonhardt, S. (2011). Triboelectricity in Capacitive Biopotential Measurements. *IEEE Transactions on Biomedical Engineering*, *58*(5), 1268-1277. https://doi.org/10.1109/TBME.2010.2100393

Wehrmann, C., Langer, M., & Schilling, M. (2013). Motion artefact detection in capacitively coupled EEG recording. *Biomedical Engineering / Biomedizinische Technik*. https://doi.org/10.1515/bmt-2013-4165

Wei, J., Liao, M., Ma, A., Chen, Y., Duan, Z., Hou, X., Li, M., Jiang, N., & Yu, J. (2020). Enhanced thermal conductivity of polydimethylsiloxane composites with carbon fiber. *Composites Communications*, *17*, 141-146. https://doi.org/10.1016/j.coco.2019.12.004

Wen, F., Zhu, C., Li, L., Zhou, B., Zhang, L., Han, C., Li, W., Yue, Z., Wu, W., Wang, G., & Zhang, S. (2022). Enhanced energy storage performance of polymer nanocomposites using hybrid 2D ZnO@MoS2 semiconductive nano-fillers. *Chemical Engineering Journal*, *430*, 132676. https://doi.org/10.1016/j.cej.2021.132676

Wilkinson, P. J., Weaver, M. C., Kister, G., & Gill, P. P. (2022). Styrene-Ethylene/Butylene-Styrene (SEBS) Block Copolymer Binder for Solid Propellants. *Propellants, Explosives, Pyrotechnics*, *47*(1), e202100142. https://doi.org/10.1002/prep.202100142

Xiao, Y., Wang, M., Li, Y., Sun, Z., Liu, Z., He, L., & Liu, R. (2021). High-Adhesive Flexible Electrodes and Their Manufacture : A Review. *Micromachines*, *12*(12), 1505. https://doi.org/10.3390/mi12121505

Xie, R., Li, Q., Teng, L., Cao, Z., Han, F., Tian, Q., Sun, J., Zhao, Y., Yu, M., Qi, D., Guo, P., Li, G., Huo, F., & Liu, Z. (2022). Strenuous exercise-tolerance stretchable dry

electrodes for continuous multi-channel electrophysiological monitoring. *Npj Flexible Electronics*, *6*(1), 75. https://doi.org/10.1038/s41528-022-00209-0

Xie, Z., Liu, D., Xiao, Y., Wang, K., Zhang, Q., Wu, K., & Fu, Q. (2022). The effect of filler permittivity on the dielectric properties of polymer-based composites. *Composites Science and Technology*, *222*, 109342. https://doi.org/10.1016/j.compscitech.2022.109342

Xing, L., & Casson, A. J. (2022). Directly conductive, flexible, 3D printed, EEG electrodes. *2022 IEEE International Conference on Flexible and Printable Sensors and Systems (FLEPS)*, 1-4. https://doi.org/10.1109/FLEPS53764.2022.9781489

Xing, L., & Casson, A. J. (2023a). 3D-printed, directly conductive and flexible electrodes for personalized electroencephalography. *Sensors and Actuators A: Physical*, *349*, 114062. https://doi.org/10.1016/j.sna.2022.114062

Xing, L., & Casson, A. J. (2023b). 3D-printed, directly conductive and flexible electrodes for personalized electroencephalography. *Sensors and Actuators A: Physical*, *349*, 114062. https://doi.org/10.1016/j.sna.2022.114062

Xiong, L., Li, N., Luo, Y., & Chen, L. (2024). Sustainable development of electroencephalography materials and technology. *SusMat*, *4*(2), e195. https://doi.org/10.1002/sus2.195

Xu, C., Huang, X., Li, C., Chen, Y., Lin, B., & Liang, X. (2016). Design of "Zn^{2+} Salt-Bondings" Cross-Linked Carboxylated Styrene Butadiene Rubber with Reprocessing and Recycling Ability via Rearrangements of Ionic Cross-Linkings. *ACS Sustainable Chemistry & Engineering*, *4*(12), 6981-6990. https://doi.org/10.1021/acssuschemeng.6b01897

Xu, M., Li, J., Ren, J., Wang, J., Xu, L., Wang, W., Sun, S., Li, H., Zhang, J., & Wu, J. (2025). Superhydrophobic and recyclable passive daytime radiative cooling fabric prepared via electrospinning. *Chemical Engineering Journal*, *509*, 161274. https://doi.org/10.1016/j.cej.2025.161274

Xu, S., Li, X., Sui, G., Du, R., Zhang, Q., & Fu, Q. (2020). Plasma modification of PU foam for piezoresistive sensor with high sensitivity, mechanical properties and long-term stability. *Chemical Engineering Journal*, *381*, 122666. https://doi.org/10.1016/j.cej.2019.122666

Xu, S., Liu, Y., Lee, H., & Li, W. (2024). Neural interfaces : Bridging the brain to the world beyond healthcare. *Exploration*, *4*(5), 20230146. https://doi.org/10.1002/EXP.20230146

Xu, Y., Sun, B., Ling, Y., Fei, Q., Chen, Z., Li, X., Guo, P., Jeon, N., Goswami, S., Liao, Y., Ding, S., Yu, Q., Lin, J., Huang, G., & Yan, Z. (2020). Multiscale porous elastomer substrates for multifunctional on-skin electronics with passive-cooling capabilities. *Proceedings of the National Academy of Sciences*, *117*(1), 205-213. https://doi.org/10.1073/pnas.1917762116

Xue, Z., Zhang, Y., Zheng, Y., Shen, S., & Li, H. (2025). Porous Microneedle Array Electrode Using Interstitial Fluid as Conductive Fillers for Biosafe and Long-Term Biopotential Monitoring. *IEEE Transactions on Electron Devices*, 1-8. https://doi.org/10.1109/TED.2024.3525456

Yan, D., Song, L., Kang, F., Mo, X., Lv, Y., Sun, J., Tang, H., Zhou, X., & Zhang, Q. (2025). *In Situ* Growth of Covalent Organic Frameworks on Carbon Nanotubes for High-

Performance Potassium-Ion Batteries. *Angewandte Chemie*, *137*(12), e202422851. https://doi.org/10.1002/ange.202422851

Yang, D., Tian, G., Chen, J., Liu, Y., Fatima, E., Qiu, J., Malek, N. A. N. N., & Qi, D. (2025). Neural electrodes for brain-computer interface system : From rigid to soft. *BMEMat*, e12130. https://doi.org/10.1002/bmm2.12130

Yang, K., McErlain-Naylor, S. A., Isaia, B., Callaway, A., & Beeby, S. (2024). E-Textiles for Sports and Fitness Sensing : Current State, Challenges, and Future Opportunities. *Sensors*, *24*(4), 1058. https://doi.org/10.3390/s24041058

Yang, L., Gan, L., Zhang, Z., Zhang, Z., Yang, H., Zhang, Y., & Wu, J. (2022). Insight into the Contact Impedance between the Electrode and the Skin Surface for Electrophysical Recordings. *ACS Omega*, *7*(16), 13906-13912. https://doi.org/10.1021/acsomega.2c00282

Yang, L., Liu, Q., Zhang, Z., Gan, L., Zhang, Y., & Wu, J. (2021). Materials for Dry Electrodes for the Electroencephalography : Advances, Challenges, Perspectives. *Advanced Materials Technologies*, 2100612. https://doi.org/10.1002/admt.202100612

Yang, L., Liu, Q., Zhang, Z., Gan, L., Zhang, Y., & Wu, J. (2022). Materials for Dry Electrodes for the Electroencephalography : Advances, Challenges, Perspectives. *Advanced Materials Technologies*, *7*(3), 2100612. https://doi.org/10.1002/admt.202100612

Yang, N., Yin, X., Liu, H., Zhou, X., Yan, X., Zhao, Y., & Cheng, T. (2024). A Multifunctional and Waterproof Wearable Microneedle Piezoresistive Sensor Based on CNT/CB/PDMS With Wide Temperature Range. *IEEE Transactions on Instrumentation and Measurement*, *73*, 1-9. https://doi.org/10.1109/TIM.2024.3481563

Yang, X., Sun, L., Zhang, C., Huang, B., Chu, Y., & Zhan, B. (2019a). Modulating the sensing behaviors of poly(styrene-ethylene-butylene-styrene)/carbon nanotubes with low-dimensional fillers for large deformation sensors. *Composites Part B: Engineering*, *160*, 605-614. https://doi.org/10.1016/j.compositesb.2018.12.119

Yang, X., Sun, L., Zhang, C., Huang, B., Chu, Y., & Zhan, B. (2019b). Modulating the sensing behaviors of poly(styrene-ethylene-butylene-styrene)/carbon nanotubes with low-dimensional fillers for large deformation sensors. *Composites Part B: Engineering*, *160*, 605-614. https://doi.org/10.1016/j.compositesb.2018.12.119

Yang, Y., Cui, T., Li, D., Ji, S., Chen, Z., Shao, W., Liu, H., & Ren, T.-L. (2022). Breathable Electronic Skins for Daily Physiological Signal Monitoring. *Nano-Micro Letters*, *14*(1), 161. https://doi.org/10.1007/s40820-022-00911-8

Yao, B., Scalco De Vasconcelos, L., Cui, Q., Cardenas, A., Yan, Y., Du, Y., Wu, D., Wu, S., Hsiai, T. K., Lu, N., Zhu, X., & He, X. (2022). High-stability conducting polymer-based conformal electrodes for bio-/iono-electronics. *Materials Today*, *53*, 84-97. https://doi.org/10.1016/j.mattod.2021.12.002

Yao, Y., Dai, H., Ji, M., Han, Y., Jiang, B., Cheng, C., Song, X., Song, Y., & Wu, G. (2024). Flexible Strain Sensor Based on AgNWs/MXene/SEBS with High Sensitivity and Wide Strain Range. *Electronic Materials Letters*, *20*(6), 684-693. https://doi.org/10.1007/s13391-024-00514-y

Ye, Z., Fang, T., Cong, C., Chen, K., Zhang, D., Kong, X., Wang, Q., Liu, S., Li, M., Zhao, B., Xia, Z., Shang, Y., Liu, L., Shi, E., Wei, X., & Cao, A. (2024). Strong and Fatigue-Resistant Carbon Nanotube Composites Enabled by Amorphous/Crystalline

Heterophase Shell. *ACS Nano*, *18*(36), 24984-24996. https://doi.org/10.1021/acsnano.4c05966

Yoon, J. E., Chung, J., Park, S., Won, H., Kim, C., Baek, I., Koh, J., & Koo, S. H. (2024). Evaluation of Gait-Assistive Soft Wearable Robot Designs for Wear Comfort, Focusing on Electroencephalogram and Satisfaction. *IEEE Robotics and Automation Letters*, *9*(10), 8834-8841. https://doi.org/10.1109/LRA.2024.3433834

Yousefzade, O., Hemmati, F., Garmabi, H., & Mahdavi, M. (2016). Thermal behavior and electrical conductivity of ethylene vinyl acetate copolymer/expanded graphite nanocomposites : Effects of nanofiller size and loading. *Journal of Vinyl and Additive Technology*, *22*(1), 51-60. https://doi.org/10.1002/vnl.21428

Yuan, H., Li, Y., Yang, J., Li, H., Yang, Q., Guo, C., Zhu, S., & Shu, X. (2021). State of the Art of Non-Invasive Electrode Materials for Brain–Computer Interface. *Micromachines*, *12*(12), 1521. https://doi.org/10.3390/mi12121521

Yuan, J.-K., Yao, S.-H., Dang, Z.-M., Sylvestre, A., Genestoux, M., & Bai, J. (2011). Giant Dielectric Permittivity Nanocomposites : Realizing True Potential of Pristine Carbon Nanotubes in Polyvinylidene Fluoride Matrix through an Enhanced Interfacial Interaction. *The Journal of Physical Chemistry C*, *115*(13), 5515-5521. https://doi.org/10.1021/jp1117163

Yun, T., Du, J., Ji, X., Tao, Y., Cheng, Y., Lv, Y., Lu, J., & Wang, H. (2023). Waterproof and ultrasensitive paper-based wearable strain/pressure sensor from carbon black/multilayer graphene/carboxymethyl cellulose composite. *Carbohydrate Polymers*, *313*, 120898. https://doi.org/10.1016/j.carbpol.2023.120898

Zare, S., Beaber, S. I., & Sun, Y. (2025). NeuroFlex : Feasibility of EEG-Based Motor Imagery Control of a Soft Glove for Hand Rehabilitation. *Sensors*, *25*(3), 610. https://doi.org/10.3390/s25030610

Zeng, H., He, Y., Zhao, R., Li, Z., Wang, W., Yang, M., Li, P., Tao, G., Sun, J., & Hou, C. (2024). Intelligent health and sport : An interplay between flexible sensors and basketball. *iScience*, *27*(3), 109089. https://doi.org/10.1016/j.isci.2024.109089

Zeng, T., Wu, Y., & Lei, M. (2024). Review : Developments and challenges of advanced flexible electronic materials for medical monitoring applications. *Advanced Composites and Hybrid Materials*, *7*(5), 141. https://doi.org/10.1007/s42114-024-00949-9

Zeydabadinezhad, M., Jowers, J., Buhl, D., Cabaniss, B., & Mahmoudi, B. (2024). A personalized earbud for non-invasive long-term EEG monitoring. *Journal of Neural Engineering*, *21*(2), 026026. https://doi.org/10.1088/1741-2552/ad33af

Zhang, Y., Rajabi, N., Taleb, F., Matviienko, A., Ma, Y., Björkman, M., & Kragic, D. (2024). *Mind Meets Robots : A Review of EEG-Based Brain-Robot Interaction Systems* (arXiv:2403.06186). arXiv. https://doi.org/10.48550/arXiv.2403.06186

Zhao, J., Yang, Y., Bo, L., Qi, J., & Zhu, Y. (2024). Research Progress on Applying Intelligent Sensors in Sports Science. *Sensors*, *24*(22), 7338. https://doi.org/10.3390/s24227338

Zhao, X., Li, J., Jiang, M., Zhai, W., Dai, K., Liu, C., & Shen, C. (2024). Flexible strain sensor based on CNTs/CB/TPU conductive fibrous film with wide sensing range and high sensitivity for human biological signal acquisition. *Polymer*, *302*, 127049. https://doi.org/10.1016/j.polymer.2024.127049

Zhao, Y., Zhang, R., Liu, Y., Wang, F., Hu, S., Yang, F., Tao, C., Wu, Q., Zha, B., Wu, J., & Huo, F. (2025). Breathable and sweat tolerance PPy-leather dry electrode for long-term electroencephalogram monitoring. *Sensors and Actuators A: Physical*, *382*, 116145. https://doi.org/10.1016/j.sna.2024.116145

Zheng, K., Jiang, C., Xu, Q., Shao, S., Xu, M., Yang, B., & Liu, J. (2024). A Concentric Ring Microneedle Electrode with Low Contact Impedance for Close Sources Laplacian EEG Recording. *IEEE Transactions on Biomedical Engineering*, 1-10. https://doi.org/10.1109/TBME.2024.3511596

Zheng, Y., Sun, Y., Li, H., Xuan, X., Li, P., & Li, M. (2024). Wearable gold–graphene dry electrode-based headband for effective brain–computer interface applications. *Journal of Materials Chemistry C*, *12*(33), 12862-12873. https://doi.org/10.1039/D4TC00574K

Zhong, W., Chen, Y., Sun, J., Wang, X., Hu, D., & Zhao, L. (2025). Preparation of SEBS foam for new-generation sports protection and monitoring by microwave selective sintering. *Chemical Engineering Journal*, *515*, 163494. https://doi.org/10.1016/j.cej.2025.163494

Zhong, X., Li, G., Xu, C., Luo, R., Meng, J., & Schalk, G. (2026). Detection of eye movements and eye blinks using a portable two-channel EEG platform. *Journal of Neuroscience Methods*, *425*, 110616. https://doi.org/10.1016/j.jneumeth.2025.110616

Zhou, B., Liu, Z., Li, C., Li, L., Zhang, X., Sheng, Y., Zhou, Y., Jiang, L., Tian, M., & Chen, S. (2022). Fabrication of ultrasensitive and flexible strain sensor based on multi-wall carbon nanotubes coated electrospun styrene-ethylene-butylene-styrene block copolymer fibrous tubes. *European Polymer Journal*, *178*, 111501. https://doi.org/10.1016/j.eurpolymj.2022.111501

Zhou, W., Ling, W., Liu, W., Peng, Y., & Peng, J. (2015). Laser direct micromilling of copper-based bioelectrode with surface microstructure array. *Optics and Lasers in Engineering*, *73*, 7-15. https://doi.org/10.1016/j.optlaseng.2015.03.011

Zhou, W., Liu, W., Liu, S., Zhang, G., & Shen, Z. (2016). Experimental investigation on surface wettability of copper-based dry bioelectrodes. *Sensors and Actuators A: Physical*, *244*, 237-242. https://doi.org/10.1016/j.sna.2016.04.044

Zhou, W., Song, R., Pan, X., Peng, Y., Qi, X., Peng, J., Hui, K. S., & Hui, K. N. (2013). Fabrication and impedance measurement of novel metal dry bioelectrode. *Sensors and Actuators A: Physical*, *201*, 127-133. https://doi.org/10.1016/j.sna.2013.06.025

Zhu, J., Li, J., Duan, A., & Wang, H. (2025). Boosting a high-performance desalination in flow-electrode capacitive deionization (FCDI) : Unraveling the role of dynamic $\pi - \pi$ stacking between a current collector and flow-electrode on enhancing charge transfer. *Desalination*, *601*, 118568. https://doi.org/10.1016/j.desal.2025.118568

Zhuo, S., Wu, Z., Williams, C., Sundaresan, C., & Ameri, S. K. (2025). In-Ear Electronics with Mechanical Adaptability for Physiological Sensing. *Advanced Healthcare Materials*, *14*(3), 2404296. https://doi.org/10.1002/adhm.202404296